

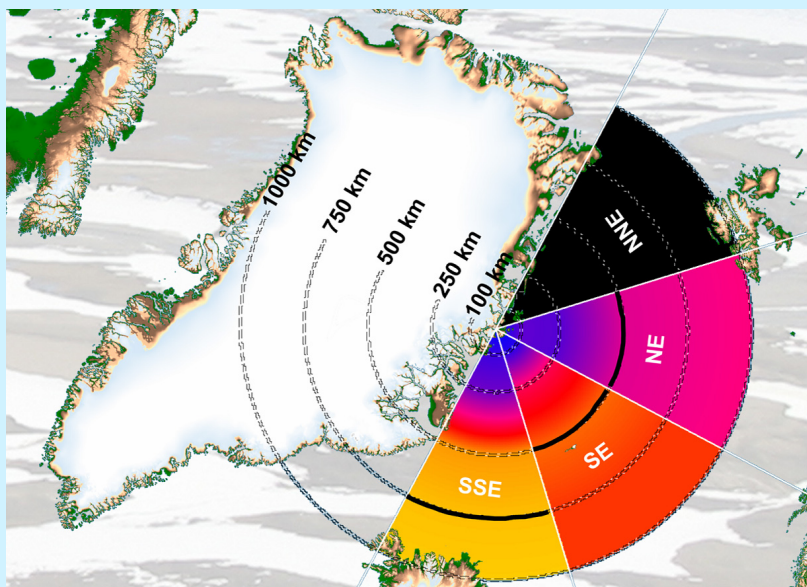


National Environmental Research Institute  
Ministry of the Environment · Denmark

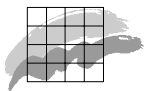
# From digital cameras to large scale sea-ice dynamics

A snow-ecosystem perspective

*PhD thesis*  
Jørgen Hinkler







**National Environmental Research Institute**  
Ministry of the Environment · Denmark

---

# From digital cameras to large scale sea-ice dynamics

A snow-ecosystem perspective

*PhD thesis*  
2005

*Jørgen Hinkler*



**ZERO**   
ZACKENBERG ECOLOGICAL RESEARCH OPERATIONS

## Data sheet

Title:	From digital cameras to large scale sea-ice dynamics
Subtitle:	A snow–ecosystem perspective. PhD thesis
Author:	Jørgen Hinkler
Department:	Department of Arctic Environment
University:	University of Copenhagen. Institute of Geography
Publisher:	National Environmental Research Institute © Ministry of the Environment
URL:	<a href="http://www.dmu.dk">http://www.dmu.dk</a>
Date of publication:	November 2005
Accepted for public defence:	October 2005 by Dr. Richard Harding, Centre for Ecology and Hydrology, Wallingford, United Kingdom; Associate Professor, Ph.D. Leif Toudal Pedersen, Technical University of Denmark; Henrik Søgaard, Institute of Geography, University of Copenhagen, Denmark.
Financial support:	Copenhagen Global Change Initiative (COGCI), University of Copenhagen, National Environmental Research Institute, and the European Commission IHP-programme (Ny-Ålesund, Large Scale Facility, contract HPRI-CT-1999-00057).
Please cite as:	Hinkler, J., 2005: From digital cameras to large-scale sea-ice dynamics. A snow–ecosystem perspective. PhD thesis. University of Copenhagen, Institute of Geography and National Environmental Research Institute (NERI). Department of Arctic Environment. 184 pp. <a href="http://afhandlinger.dmu.dk">http://afhandlinger.dmu.dk</a>
	Reproduction is permitted, provided the source is explicitly acknowledged.
Abstract:	Snow cover and vegetative conditions in the valley Zackenbergdalen (74°30'N), Northeast Greenland were mapped and analysed. For this purpose a new technique based on digital camera images was developed. The technical development has also included a pilot study on the use of multispectral camera data, performed in Ny-Ålesund (79°N), Svalbard. The mapped results for Zackenberg were used for local studies as well as for analysing relations between snow precipitation and climatic variability at larger scale. At local scale, the study demonstrates that snow cover is one of the most important mechanisms affecting the living conditions for the High Arctic flora and fauna. Analyses at larger scale show that over a 45-year period (1958–2003) snow-precipitation at Zackenberg was correlated to the North Atlantic Oscillation (NAO) in one third of the time. During 1982–2000, where this correlation was insignificant, there was a clearly significant (negative) correlation between Zackenberg snow-precipitation and annual variations in sea-ice conditions within the Greenland Sea. This indicates that sea-ice conditions might be crucial for the status of terrestrial High Arctic ecosystems in a future warmer climate.
Keywords:	Arctic, Zackenberg, Greenland, digital camera, snow, snow cover, sea-ice, NDVI, ecosystem, climate change, NAO
Layout and photos:	Jørgen Hinkler
ISBN:	87-7772-905-6
Number of pages:	184
Internet-version:	The report is available as a PDF-file from NERI's homepage <a href="http://www.dmu.dk/Pub/phd_jhi.pdf">http://www.dmu.dk/Pub/phd_jhi.pdf</a>
For sale at:	Ministry of the Environment Frontlinien Rentemestervej 8 DK-2400 Copenhagen NV Denmark Tel. +45 70 12 02 11 <a href="mailto:frontlinien@frontlinien.dk">frontlinien@frontlinien.dk</a>



# *Preface*

The research presented in this thesis was carried out within the framework of the Copenhagen Global Change Initiative (COGCI), which is a cooperation among the Faculty of Science at the University of Copenhagen and three Danish governmental research institutions: Danish Meteorological Institute (DMI), Geological Survey of Denmark and Greenland (GEUS), and National Environmental Research Institute (NERI). The two organizations involved in this work are the Institute of Geography at the University of Copenhagen and NERI, Department of Arctic Environment. The major portion of fieldwork was carried out at Zackenberg in High Arctic Northeast Greenland, and is therefore a contribution to the Zackenberg Ecological Research Operations (ZERO) (further information on ZERO is available from [www.zackenberg.dk](http://www.zackenberg.dk)). Additional fieldwork was done in collaboration with the Norwegian Polar Institute (NPI) at Ny-Ålesund, Svalbard, and was funded by the European Commission IHP-programme (Ny-Ålesund, Large Scale Facility, contract HPRI-CT-1999-00057).

During my Ph.D.-work I have participated in a number of conferences and meetings, and contributed with oral presentations, extended abstracts and a proceeding paper (Appendix 3). Finally, I also had the pleasure to visit the Atmospheric Science Department at the Colorado State University in Fort Collins, CO, USA.

## **Acknowledgements**

Throughout the work with the present thesis, I have enjoyed the support and help of many people whom I wish to thank. First and foremost, I want to thank my two supervisors and co-authors Birger Ulf Hansen and Mikkel Peter Tamstorf for their support, companionship and help both during fieldwork and for fruitful discussions throughout all stages of this work. I give my special thanks to Steen B. Pedersen for his significant contribution in laying the seeds for this dissertation through our joint work with our master thesis. Also sincere thanks to Hans Meltofte for his great interest, positive spirit and support and especially for his indispensable help regarding snow–ecosystem relations. I wish to thank Jon Børre Ørbæk at the Norwegian Polar Institute for introducing me to Ny-Ålesund, Svalbard, cooperation in fieldwork,

discussions and comments, and for great nature experiences on snow mobile. Morten Rasch has helped with fieldwork as well as comments and ideas. I thank him for this and also for his pleasant company at Zackenberg.

I also wish to thank Glen E. Liston, Department of Atmospheric Science, Colorado State University, for introducing me to his work that has inspired me greatly in relation to snow and snow-modeling.

I have also attained help from people working at the Technical University of Denmark. Thanks are given to Kim Have for developing software to perform orthographical rectification, Erik Poulsen, Ole Mærsk Møller and Keld Dueholm for technical support in relation to photogrammetry, and finally to Leif Toudal for fruitful discussions regarding sea-ice in the Greenland Sea.

Jens Hesselbjerg and Martin Stendel from the Danish Meteorological Institute are thanked for providing future scenarios of the climate in the East Greenland Region. I thank Susanne M. König for providing botanical data from Zackenberg. Are Backlund from the Norwegian Polar Institute are thanked for helping with spectroradiometer measurements.

The staff at Zackenberg Research Station is thanked for help and logistic support and also the staff at Sverdrup Station in Ny-Ålesund, Svalbard, is acknowledged.

I thank colleagues at Institute of Geography, University of Copenhagen and a special thank to Ulf P. Thomas for his tremendous work in developing a solution that made it possible to obtain digital images automatically in remote arctic areas—making this study possible. Thanks to Charlotte Sigsgaard for all her hardships climbing up the Zackenberg Mountain numerous times, both carrying field equipment and for camera inspections. Also thanks to Charlotte for comments and good spirit. Many thanks are dedicated to colleagues at the National Environmental Research Institute for their company, and a nice working environment.

Warm thanks go to my family and friends for support and patience. I look forward to spend time with them again. Finally my deepest thanks go to my wife Corna for her patience, tolerance, and work-effort—no one could have given me better support.

# Contents

Preface.....	3
Contents.....	5
<b>Synopsis.....</b>	<b>7</b>
1. Introduction .....	9
1.1 Climate change perspectives .....	9
1.2 Aim and contents of the thesis.....	12
1.3 Thesis-structure and presentation of manuscripts.....	13
2. Geographical settings and climate .....	17
2.1 Introduction to study areas.....	17
2.2 Zackenberg Research Area .....	19
2.2.1 <i>Snow</i> .....	22
2.3 NAO/AO .....	27
2.4 Ocean Currents.....	31
2.5 Sea-ice in the Greenland Sea .....	32
3. Snow–ecosystem relations & future perspectives.....	41
3.1 Snow cover, flora, and fauna.....	41
3.2 Future perspectives.....	44
4. Concluding remarks.....	49
4.1 Snow cover maps from digital camera images.....	49
4.2 Multispectral digital camera images, Svalbard .....	50
4.3 Monitoring and modeling snow–vegetation relations .....	51
4.4 Climate, sea-ice, snow, and effects on the ecosystem.....	52

References.....	55
Appendix 1. Data description.....	63
Appendix 2. Additional figures and tables.....	69
<i>A.2.1 Snow wind and temperature at Zackenberg 1997–2002</i> .....	69
<i>A.2.2 Change of spatial resolution with distance</i> .....	72
<i>A.2.3 Sea-ice types</i> .....	73
Appendix 3. Conferences and meetings.....	75
<i>A.3.1 Extended abstract—ACIA Symposium</i> .....	77
<i>A.3.2 Proceeding paper—Northern Research Basins</i> .....	81
<i>A.3.3 Extended abstract—Sixth Ny-Ålesund Int. Seminar</i> .....	89
Appendix 4. Co-author statements .....	93
<i>A.4.1 Co-author statements, Paper 1</i> .....	94
<i>A.4.2 Co-author statements, Paper 2</i> .....	97
<i>A.4.3 Co-author statements, Paper 3</i> .....	99
<i>A.4.4 Co-author statements, Paper 4</i> .....	102
<b>Papers .....</b>	<b>105</b>
Paper 1.....	107
Paper 2 .....	121
Paper 3 .....	133
Paper 4 .....	159

# Synopsis

---



# Chapter 1

## Introduction

Arctic ecosystems are particularly sensitive to disturbances, and are therefore considered to respond rapidly to climatic changes (Reynolds and Tenhunen, 1996). For these ecosystems, one of the most important variables is snow cover (Jones et al., 2001; Phoenix and Lee, 2004).

The present work is part of the Zackenberg Ecological Research Operations- (ZERO) program; which has the objective to provide knowledge about the response of a pristine High Arctic ecosystem to climatic variability, through monitoring and research (DPC, 2004). Thus, the overall objective of this study is to perform analyses of snow cover/snow-precipitation—in relation to present and possible future impacts on a High Arctic ecosystem; and to the way snow–ecosystem dynamics will respond to variations and changes in larger-scale components of the climate system.

The seeds of this work were laid already in August 1997 with the establishment of an automated digital camera at the eastern slope of the Zackenberg Mountain at 74.5°N in Northeast Greenland. This rather simple system, which consists of a standard digital camera in a weatherproof box, equipped with an electronic timer and a mechanical trigger, has provided daily images of the Zackenberg Valley since then. In June 2002, additional cameras with multispectral capability were set up at the same spot on the mountain side (see back-cover for an image of the current setup). This system of digital cameras has now turned out to be an integrated part of ZERO, and has acted as an indispensable source of data for this work.

### 1.1 Climate change perspectives

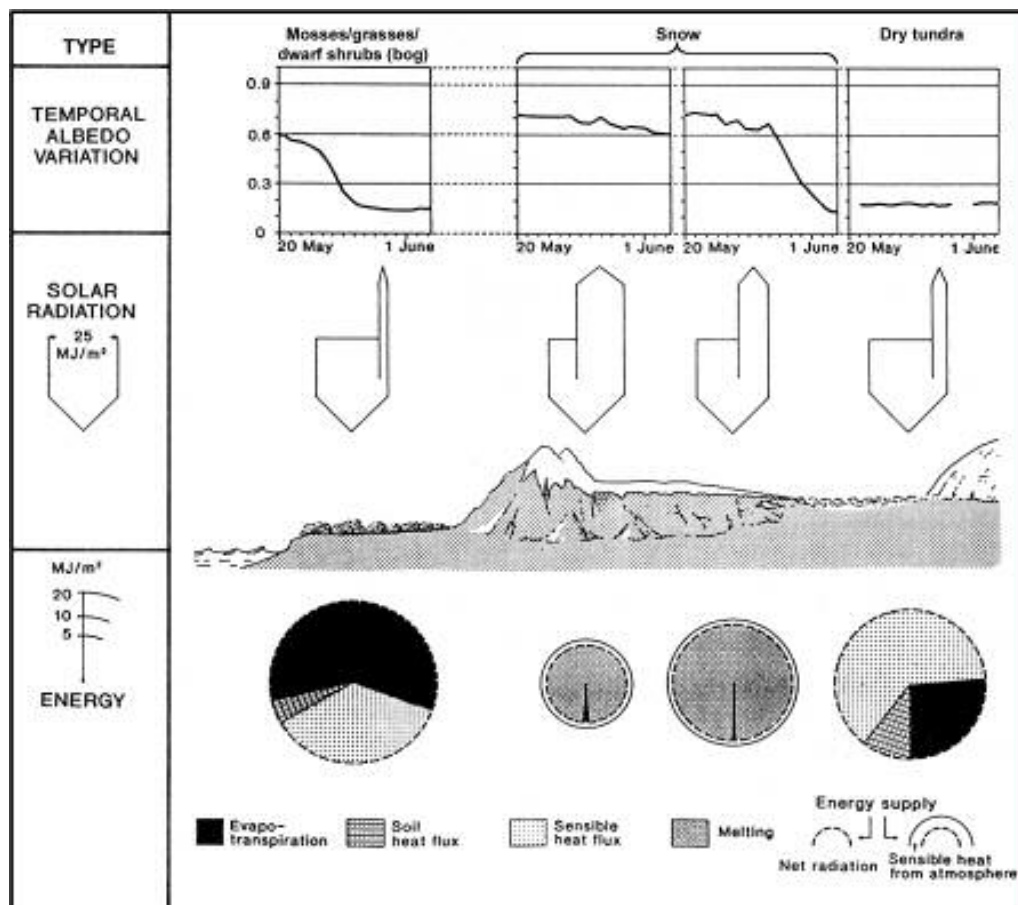
According to the latest assessment report from the Intergovernmental Panel on Climate Change (IPCC), global-mean warming from 1990 to 2100 is expected to be within a range of 1.4°C to 5.8°C in the case that no measures are taken to limit greenhouse gas emissions (IPCC, 2001). Recent research demonstrates that climate sensitivity of different General Circulation Models (GCMs) ranges as much as between 1.9°C and 11.5°C, and that most models indicate a sensitivity around 3.4°C (Stainforth et al., 2005). Although the

scatter among the individual circulation models is considerable, there is consensus that Arctic regions will undergo the greatest warming, particularly in winter, and that this may be accompanied by increasing precipitation (ACIA, 2004).

A warming Arctic is expected to alter climate system dynamics including precipitation patterns (snow cover distribution), snow-melt, and melting of sea-ice (Johannessen et al., 2004;Weltzin et al., 2003). Snow cover is an important component of the climate system, and it interacts with other components of the climate system on hemispheric-, regional-, local-, and micro-scales (Jones et al., 2001).

The most significant property of snow cover is the high albedo. This makes its presence/absence important for the surface energy budget, especially at high latitudes, where snow makes up a major part of the annual precipitation. Thus, the positive snow/ice-albedo-temperature feedback mechanism is one of the main reasons why future warming is amplified at high latitudes in GCM-simulations (ACIA, 2004).

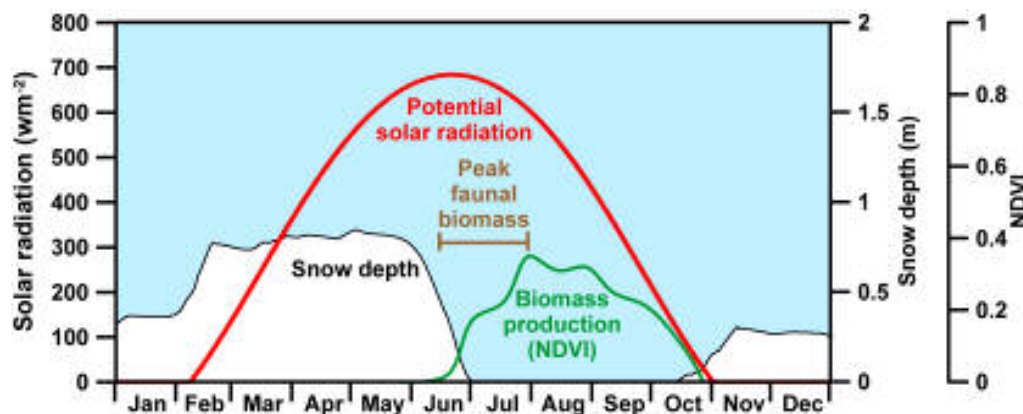
Fig. 1.1 depicts the surface energy balance for three typical Arctic surface



**Fig.1.1.** Energy balance diagram—different Arctic surface types. Source: Modified from Harding et al., 1995.



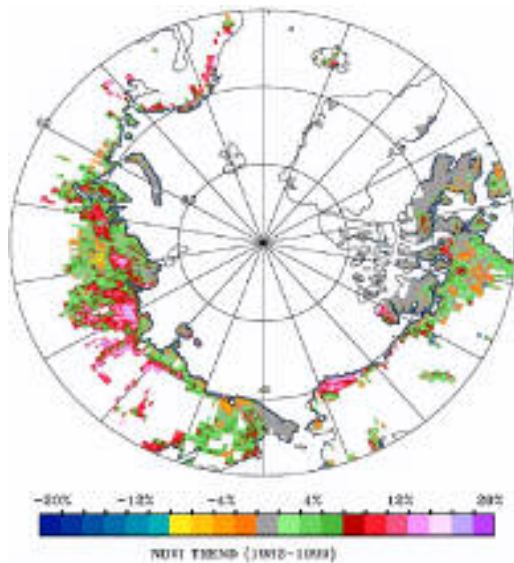
types: bog, snow covered, and dry tundra. The figure strongly emphasizes the effect of snow cover in Arctic environments. Due to the high albedo the net radiation in the snow covered areas is much lower than in areas with no snow cover, and as long as the snow cover is present during summer (where the surface air temperature generally exceeds  $0^{\circ}\text{C}$ ) by far the largest part of the energy at the surface goes to snow-melt. In the snow-free areas, on the contrary, the evapotranspiration and sensible heat fluxes are much larger in quantity. This, together with its insulative properties and ability to shield out solar radiation makes snow cover a key factor in Arctic ecosystems; and especially in the High Arctic regions, where the extreme climatic conditions leave only a small time-window for primary production and availability of food for herbivores, the role of the snow cover is critical (Meltofte, 2002). Thus, because these ecosystems are particularly sensitive to disturbances they are considered important as indicators of climate change and are topics of growing concern and scientific interest.



**Fig. 1.2.** Seasonal characteristics of a High Arctic ecosystem based on climate data (1998-season) from Zackenberg Research Station ( $74.5^{\circ}\text{N}$ ) in Northeast Greenland—Normalized Difference Vegetation Index was inferred from AVHRR satellite data provided by the National Snow and Ice Data Center, Boulder, Colorado, USA.

Fig. 1.2 is a simple sketch of the annual bio-climatic variation in a typical High Arctic ecosystem, and emphasizes the particular importance of the short snow-free summer period for the flora and fauna (e.g. vegetative activity and breeding conditions for shorebirds). However, what a future scenario of this variation will be is presently uncertain. Because warming is predicted to be accompanied by an enhanced hydrological cycle, there will be a tendency of “competition” between earlier snow-melt in spring and increased snow-precipitation in winter (Jones et al., 2001). Thus far, earlier snow-melt in spring seems to have been the more efficient of the two, at least from a circumpolar point of view. Studies based on satellite data (Myneni et al., 1997; Tucker et al., 2001; Zhou et al., 2001) have shown that in many large

regions, between 40°N and 70°N, photosynthetic activity of terrestrial vegetation inferred from Normalized Difference Vegetation Index (NDVI) has increased over the last couple of decades; and in a recent review of case studies (Stow et al., 2004) on vegetation and land-cover change in Arctic tundra systems, an upward trend in photosynthetic activity has been detected also at latitudes above 70°N (Fig. 1.3). These results are hypothesized to be in accordance with recent CO<sub>2</sub>-induced global warming and earlier snow clearance in spring.



**Fig. 1.3.** Spatial distribution of “greening” trend (1982–1999) over tundra north of 60°N during the growing season (June–September). The map is based on Normalized Difference Vegetation Index inferred from 8 km resolution NOAA AVHRR satellite data. Source: Stow et al., 2004.

However, with the prospect of increased temperatures and increased winter-snowfall, it may be reasonable also to suggest an increase in the variability in snow cover conditions with global warming, because: “it is possible that two competing factors, *X* and *Y*, that emerge with climate change can contribute to the snow cover variations and have a mean combined effect that is close to zero but, because they are independent of each other, induce a significant variance” (Jones et al., 2001). One consequence may be that future scenarios of snow–ecosystem interactions (prolonged vs. shortened growing season) may differ significantly both in time and space. Finally, as this study will show, this pattern may be further complexed by changes in other components in the climate system such as the North Atlantic Oscillation (NAO) and lake effects due to reductions in sea-ice coverage.

## 1.2 Aim and contents of the thesis

The overall objective of this work has been briefly introduced in the previous text. Below is given an explicit definition of the aim and content of the thesis.

The aim of the thesis is to analyze snow–ecosystem relations in a High Arctic ecosystem in Northeast Greenland through the development and use of

new monitoring techniques based on conventional and multispectral digital cameras. Furthermore, it is an aim to use the results in local- to large-scale (i.e. sea-ice- and atmospheric dynamics) climatic analysis; and finally to put the results in climate change perspective. The thesis is structured around four main themes:

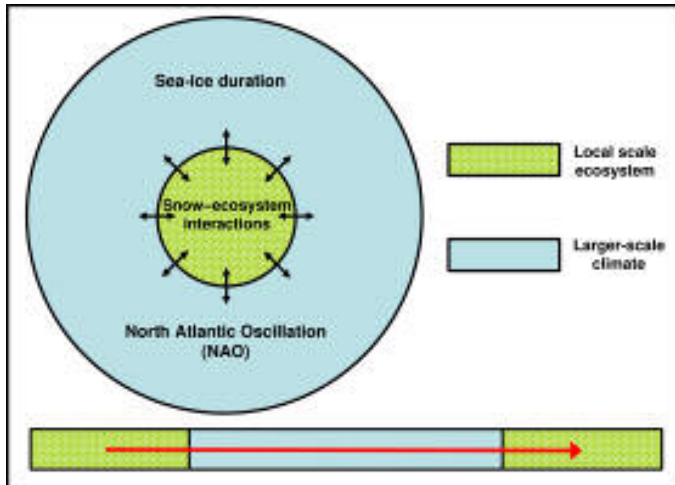
- The development of a methodology to create time series of snow cover maps from orthographically rectified digital camera images.
- The development of methodologies to perform surface classification in a High Arctic environment based on multispectral digital orthophotos; and the usage of these in an analysis of spatiotemporal variations in snow- albedo and melt.
- Modeling, and analyzing snow–vegetation relations in a High Arctic ecosystem using camera-based snow cover- and NDVI-data
- Analyzing the relations between snow-precipitation in a local-scale High Arctic ecosystem and 1) large scale climate dynamics (the NAO and sea-ice variations in the Greenland Sea) and 2) snow–ecosystem effects related to climatic change.

The core part of this work is described in four research papers, which correspond to each of the above themes in numerical order. This means that the different themes have been dealt with mainly in the paper-manuscripts and partly in the synopsis. For easy reference, the papers are named Paper 1, 2, 3, and 4.

### 1.3 Thesis-structure and presentation of manuscripts

As described above, the thesis consists of four research papers, and a synopsis. The synopsis has three main objectives: 1) to set the scene for the study in a geographical/climatological perspective, 2) to act as a supplement providing background and details, not covered in the manuscripts, and 3) to summarize the study, and its main results and conclusions. Point 1 and 2 are dealt with in chapters 2–3, and point 3 in chapter 4. The present work represents research at both local- and large spatial scales. In the thesis I move from local- to large scale in order to analyze snow cover variation and its impact on a High Arctic ecosystem, as well as climatic factors which might affect snow-precipitation.

This spatial variability is utilized in the construction of the thesis-structure. The leitmotif of the thesis is illustrated in Fig. 1.4: Although the study includes analysis at different spatial scales, the local ecosystem acts as a reference point. At the local scale, inter-annual variability of snow cover and



**Fig. 1.4.** The thesis is structured over spatial scale.

its impact on the ecosystem is analyzed, and the empirical information gathered from local-scale analyses is then used to model extended time series of snow-data (Paper 1–3). This enables me to compare local snow-variation to larger-scale climatic variables, such as the NAO or sea-ice duration; and then use linkages, found through comparisons, to discuss impacts from large-scale climatic changes on the local scale environment (Paper 4). To preserve structural consistence, the order of both the manuscripts and the chapters in the synopsis follows this path of going from local- to larger-scale, and back.

The contents of the four manuscripts included in the thesis are described briefly below. More comprehensive discussions of the results are deferred to the individual manuscripts and to Chapter 4.

**Paper 1.** The first manuscript deals with the development of methods to use oblique digital images taken by an automated digital camera for snow cover mapping and analysis. In contrast to satellite data with high spatial resolution, the digital camera images offer *both* high temporal- and high spatial resolution. The images are rectified orthographically, and a normalized snow index utilizing the red, green and blue components of the images is derived. The method is applied on images from two different melting seasons (1998 and 1999), and a small case study on snow cover depletion in the Zackenberg Valley is presented.

**Reference:**

Hinkler, J, S B Pedersen, M Rasch, B U Hansen, 2002, Automatic snow cover monitoring at high temporal and spatial resolution, using images taken by a standard digital camera: *International Journal of Remote Sensing*, v. 23, p. 4669-4682.

**Paper 2.** The second manuscript covers a pilot study on using multispectral digital camera images for surface classification and albedo mapping. The study was performed at Ny-ålesund, 79°N, Svalbard. As in Paper 1 the images are rectified orthographically. It is shown that the difference between visible and near-infrared reflectance (in addition to vegetation classification) can be used to distinguish between different types of snow. Based on spectroradiometer measurements, albedo-values characteristic for different surface types are estimated. A time series of daily surface albedo-maps are constructed and used for an analysis of the spatial distribution of snow-melt duration in the Ny-Ålesund area.

**Reference:**

Hinkler,J, J B Orbaek, B U Hansen, 2003, Detection of spatial, temporal, and spectral surface changes in the Ny-Alesund area 79 degrees N, Svalbard, using a low cost multispectral camera in combination with spectroradiometer measurements: *Physics and Chemistry of the Earth*, v. 28, p. 1229-1239.

**Paper 3.** The third manuscript deals with snow cover and vegetation interactions within the research area at Zackenberg in High Arctic Northeast Greenland. The study is based on the comprehensive amount of data, which are currently available in form of conventional- and multispectral images from Zackenberg. To reconstruct snow cover extent, snow accumulation, and NDVI back to 1988, semi-empirical models based on meteorological- and camera data are developed. As input, the models use temperature data and a limited number of satellite data (SPOT HRV and Landsat TM). The results reveal that, snow-cover-depletion and total amounts of photosynthetic activity around Zackenberg show considerable inter-annual variability. A comparison between snow cover and NDVI distribution reveals that vegetative vigor in the Zackenberg area primarily is linked to the initiation time of the snow-free period rather than to temperature.

**Reference:**

Hinkler,J, B U Hansen, M P Tamstorf, S B Pedersen, 2005, In preparation. Snow-vegetation relations in a High Arctic ecosystem: Inter-annual variability inferred from new monitoring- and modeling concepts: *To be submitted to Remote Sensing of Environment*.

**Paper 4.** The fourth paper deals with large-scale climatic variability and its impact on local snow-ecosystem dynamics in Zackenberg. End-of-winter snow depths are based on sonic snow depth measurements back to 1998

and from 1988–1997 they have been modeled at high accuracy using the approach described in Paper 3. During 1958–1975 snow depths were measured manually at Daneborg (21 km to the southeast of Zackenberg). End-of-winter snow accumulation at large scale is based on precipitation rates and surface air temperatures from the National Centers of Environmental Prediction (NCEP) assuming that the precipitation falls as snow when the air temperature is below 0°C. It is found that the NCEP based snow accumulation matches the ground based measurements fairly well, and that snow-precipitation in Northeast Greenland is correlated significantly to the NAO in one third of the time during 1959–2003. During 1982–2000, where NAO is decoupled from snow-precipitation in Northeast Greenland, sea-ice duration within the southern part of the Greenland Sea is significantly and negatively correlated to snow-precipitation amounts at Zackenberg. Furthermore, it is found that a projection of snow-precipitation over the next hundred years derived from proxy based sea-ice duration in the Southern part of the Greenland Sea is similar to what is predicted by a high resolution regional climate model. The snow cover depletion model described in Paper 3 is applied using future scenarios of temperature and snow-precipitation. Based on the modeled results, it is hypothesized that, because reduced sea-ice extent and increased snowfall in the winter is expected to be accompanied by earlier snow melt in spring and slightly increased summer temperatures, average summer snow cover (and thereby also summer ecosystem conditions) around Zackenberg will stay at a near neutral level during the current century. However, the effects of a warmer and more humid winter with larger amounts of precipitation may be more dramatic, especially for herbivores that are susceptible to changed physical properties of the snow cover, such as ice crusts in the snow pack etc.

**Reference:**

Hinkler, J, B U Hansen, M P Tamstorf, H Meltofte, 2005, in preparation. A possible linkage between sea-ice and snow-precipitation may be crucial for Arctic ecosystems in a warmer climate: *To be submitted to Journal of Climate*.

## Chapter 2

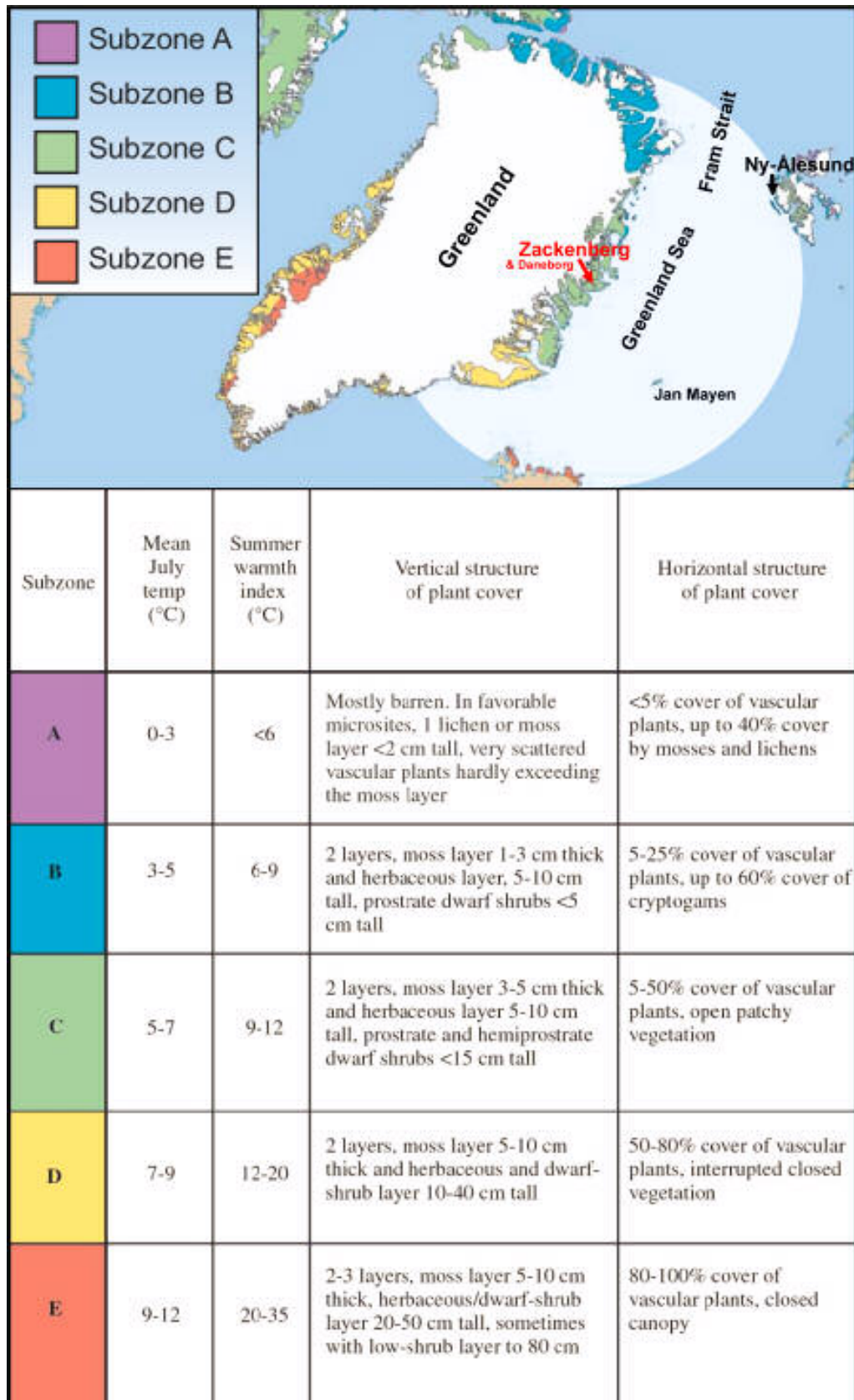
# Geographical settings and climate

Greenland is the largest island in the World (2.2 million km<sup>2</sup>) and houses the *Greenland Ice Sheet*, which is the World's second largest ice cap, next to the Antarctic. The maximum altitude of the ice cap is more than 3600 m, and it covers approximately 80% of the country leaving some 20% around the coast for the flora and fauna (Cappelen et al., 2001). As a whole the climate in Greenland is Arctic, meaning that the average temperature for the warmest month is below 10°C everywhere—except for some deep fjords in the south that fall into the Subarctic zone, where this temperature limit is just crossed (Born and Böcher, 2001). However, the differences between north and south are enormous, i.e. the distance from the southern tip (Cape Farewell, 60°N) to the northernmost point (Cape Morris Jesup, 83.4°N) is more than 2600 km. In the northern parts of the ice cap, winter temperatures can drop to below -70°C and temperatures above 25°C can occur during summer in the coastal parts of South Greenland. In some years it happens that the southern parts of Greenland receive more than 3000 mm of precipitation, while desert-like areas in the north hardly receive any precipitation at all. The majority of the coastal ice-free area is mountainous, with numerous fjords reaching into the interior, and many islands scattered directly off the coast. Thus, locally, large contrasts in the weather can be observed due to complex topography, which makes the climate vary considerably even over short distances. The northerly location of the country, the presence of the ice cap, and the cold more or less ice-filled surrounding sea are the most important factors determining the cold climate of Greenland (Cappelen et al., 2001).

### 2.1 Introduction to study areas

An excellent description of the general climate of Greenland is available from the report by Cappelen et al. (2001), and thus the following will only focus on areas of specific interest to the present work. The study has its main point of interest focused around 74.5°N, 20.5°W at Zackenberg in Northeast Greenland. The Zackenberg Research Area (ZRA) is the site where the major portion of the fieldwork was carried out, and the area has further acted as an example of a High Arctic ecosystem to be compared to local- as well as larger scale climatic variability.





**Fig. 2.1.** Overview map of the region and the sites of interest. Zackenberg is the main fieldwork site and is indicated with red. The shaded region (1000 km radius from Zackenberg) is the area considered for sea-ice analysis. Source: Modified from CAVM Team, 2003.



Fig. 2.1 sets the geographical scene for the study. Zackenberg and Daneborg are marked with red, whereas other locations (Ny-Ålesund, and the island of Jan Mayen) contributing with data at local scale are marked using black types. Because it was used for analysis of sea-ice variation in relation to snow-precipitation in ZRA, the part of the Greenland Sea confined by a radius of 1000 km from Zackenberg is highlighted.

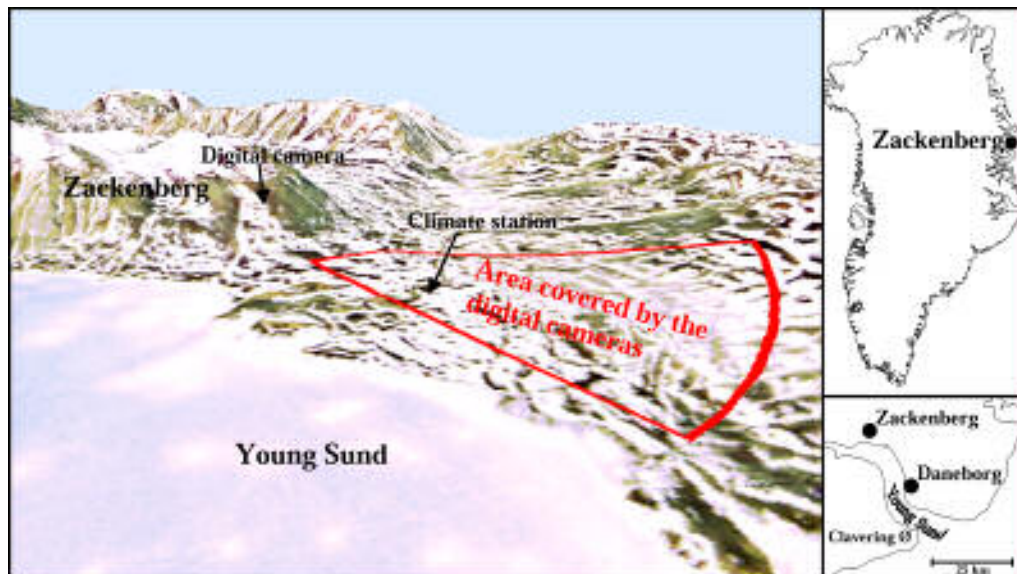
To give a visual impression of the climatic diversity in the terrestrial parts of the region, Fig. 2.1 also provides indications of different bio-climatic zones with proposed names: (A) Arctic polar desert zone, (B) Northern arctic tundra zone, (C) Middle arctic tundra zone, (D) Southern arctic tundra zone, and (E) Arctic shrub-tundra zone (CAVM Team, 2003; Elvebakk, 2000). The position of Zackenberg in this scheme is discussed in section 2.2 and in Paper 3.

At Ny-Ålesund (78.9°N, 11.9°E) Svalbard, a pilot study dealing with multispectral camera-data for surface classification and albedo mapping was carried out. In relation to this thesis, this area is thus important from a methodological- rather than from a climatological point of view. A discussion of the Ny-Ålesund area is therefore deferred to the brief description given in Paper 2.

From the geographical and climatological perspectives, the region around Zackenberg (local perspective, Papers 1 and 3), the North Atlantic Oscillation and sea-ice variations in the Greenland Sea (large scale perspective, Paper 4) are the most important geographical components of this work. Therefore, the next two sections (2.2 and 2.3) will deal with ZRA, the North Atlantic Oscillation, and sea-ice conditions in the Greenland Sea.

## 2.2 Zackenberg Research Area

Within ZRA, the Zackenberg Research Station forms the platform for the Zackenberg Ecological Research Operations (ZERO). ZERO was initiated with reconnaissance in the early 1990's and the research station together with the ZERO monitoring program was established in July 1995. Observational data from ZRA's Automatic Weather Station (AWS) is thus available from since that time, whereas longer term meteorological records (since 1958) are available from the AWS run by the Danish Meteorological Institute at Daneborg, 21 km to the southeast of Zackenberg. In August 1997 the first automatic digital camera was set up 500 m above sea level at the eastern site of the Zackenberg Mountain (Fig. 2.2) to take daily images of the Zackenberg Valley (Paper 1). Additionally in 2002, a multispectral digital camera (Paper 3) was set up at the same location, also obtaining daily images. The area covered



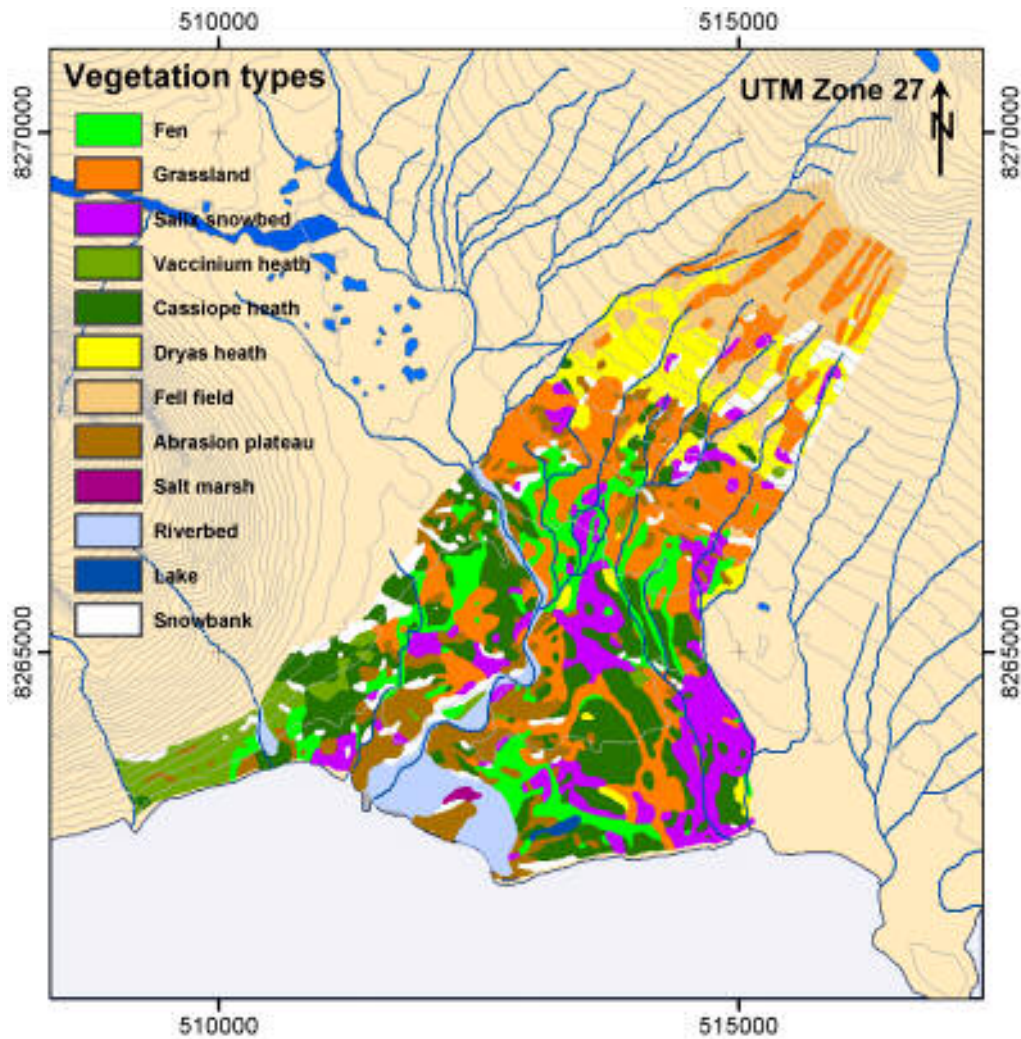
**Fig. 2.2.** Zackenberg Research Area. The area covered by digital cameras totals 17 km<sup>2</sup>.

by the cameras totals 17 km<sup>2</sup>—in Fig. 2.2 it is indicated by a red polygon (further information on camera extent and resolution of orthophotos is available in Paper 1 and Appendix 2.2). This area thus forms the basis for main analysis at local scale in this study.

ZRA is a high relief mountainous landscape, which consists of nearly horizontal valley floors below altitudes of 200 m, steep slopes between 200 and 800 m and plateaus above 800 m. The area is located in the zone of continuous permafrost and hosts a large diversity of glacial, periglacial and coastal landscape features and a great variety of biotopes like fens, heaths, fell fields, and grasslands. The mean annual air temperature (1996–2003) is slightly above -10°C, and from early June to early September, the mean daily temperature generally exceeds 0°C. Due to the huge amounts of sea-ice that are transported in the East Greenland Current, the distance from the land to the open sea is large during winter in Northeast Greenland (Cappelen et al., 2001). This combined with clear weather and strong radiation cooling makes winters become relatively cold. Thus, at ZRA the average temperature of the coldest months (December–March) is around -20°C (Table 2.1) and during short periods it can drop down close to -40°C. In East Greenland the transition zone from Low to High Arctic is located to the south of Ittoqqortoormiit (Scoresbysund) between 68°N and 70°N (Bliss and Matveyeva, 1992). The latitude of ZRA (74.5°N) thus indicate a position well into the High Arctic climate zone (definition: the average temperature of the warmest month <5°C). However, as ZRA is situated in a coastal domain inside the Young Sund and Tyroler Fjord fjord-systems, the local climate is not

**Table 2.1.** Monthly mean temps. in the Daneborg (D) Zackenberg (Z) region 1988–2004. The part of the study, which deals mainly with Zackenberg at local scale covers this period of time.

	Jan.	Feb.	Mar.	Apr.	May	Jun.	Jul.	Aug.	Sep.	Oct.	Nov.	Dec.	Mean
1988 (D)	-21.8	-16.1	-21.5	-14.0	-3.3	2.4	5.2	3.5	-1.3	-8.6	-16.3	-21.4	-9.4
1989 (D)	-20.7	-22.5	-21.3	-12.4	-4.8	1.6	5.3	2.5	-11.5	-12.3	-14.3	-18.2	-10.7
1990 (D)	-12.0	-16.8	-22.2	-13.6	-1.2	2.2	4.1	4.2	-0.8	-12.4	-18.6	-16.4	-8.6
1991 (D)	-17.8	-18.7	-17.7	-15.5	-5.2	2.6	5.8	4.8	-0.8	-10.0	-15.5	-19.4	-8.9
1992 (D)	-18.0	-19.5	-21.3	-13.9	-6.3	1.1	4.3	2.4	-1.1	-8.1	-11.4	-19.1	-9.3
1993 (D)	-23.2	-20.6	-21.5	-13.7	-6.3	0.6	4.6	2.8	-2.3	-11.9	-12.6	-20.2	-10.3
1994 (D)	-20.8	-19.7	-20.4	-11.3	-5.6	1.2	4.4	4.0	-0.8	-12.2	-16.9	-18.1	-9.7
1995 (D)	-18.6	-20.8	-17.6	-9.0	-5.2	1.9	4.7	6.8	-1.7	-11.3	-14.2	-20.1	-8.8
1996 (Z)	-18.6	-20.6	-14.9	-11.1	-5.3	1.9	5.8	4.5	-1.5	-11.4	-13.3	-22.2	-8.9
1997 (Z)	-22.4	-20.8	-19.2	-13.0	-6.3	2.3	3.7	5.0	-3.7	-11.3	-18.0	-17.4	-10.1
1998 (Z)	-21.3	-19.7	-17.5	-13.1	-6.5	0.9	4.4	4.6	-2.4	-9.6	-13.9	-22.7	-9.7
1999 (Z)	-22.1	-19.7	-18.0	-15.2	-4.1	1.5	6.2	2.9	-0.9	-10.9	-12.9	-21.8	-9.6
2000 (Z)	-17.9	-19.5	-21.1	-16.1	-5.4	1.9	5.3	4.0	-2.0	-9.6	-17.5	-23.0	-10.1
2001 (Z)	-20.5	-21.1	-23.7	-19.5	-6.3	2.1	4.9	5.8	-0.4	-9.3	-16.5	-13.2	-9.8
2002 (Z)	-21.7	-21.0	-22.7	-14.6	-4.1	2.6	5.7	4.9	0.5	-5.8	-14.5	-13.7	-8.7
2003 (Z)	-24.4	-17.0	-21.5	-13.7	-5.6	2.2	7.7	6.6	0.6	-8.9	-12.8	-23.7	-9.2
2004 (Z)	-20.1	-22.9	-17.1	-7.9	-4.5	2.5	7.2	5.4	—	—	—	—	—
Min.	-24.4	-22.9	-23.7	-19.5	-6.5	0.6	3.7	2.4	-11.5	-12.4	-18.6	-23.7	
Max.	-12.0	-16.1	-14.9	-7.9	-1.2	2.6	7.7	6.8	0.6	-5.8	-11.4	-13.2	
Mean	-20.1	-19.8	-20.0	-13.4	-5.1	1.9	5.2	4.4	-1.9	-10.2	-15.0	-19.4	



**Fig. 2.3.** Vegetation map of the central part of the Zackenberg Valley. Source: Bay, 1998.

strictly High Arctic. Since 1988, the average temperature of the warmest month has varied between 4.2°C (1990) and 7.7°C (2003). Therefore, if a more specific climatic classification is considered (CAVM Team, 2003), the inter-annual variation in ZRA's July-temperatures is within a range representing 2–3 different bio-climate zones (Fig 2.1), ranging from Northern Arctic- through Middle Arctic- to Southern Arctic tundra zones (a thorough discussion on the division of the Arctic into bio-climatic sub-zones is available from Elvebakk, 2000). ZRA thus hosts a relatively large diversity of plant species—currently 152 different species of vascular plants are known to be present in the area (Bay, 1998; Meltofte, 2002). The vegetation is mainly found in the valley bottom and on the lower part of the slopes. It is dominated by four major vegetation types: 1) Fen/Grassland, which is mostly found on organic soils with high water level (<10 cm below surface), and is dominated by sedges and grasses. 2) Dwarf-shrub heath is found on minerogen soils with low organic carbon content and low vegetation density. The dominating species are *Cassiope Tetragona* and *Dryas Octopetala*. 3) *Salix Snowbed* is dominated by *Salix Arctica* and long lasting snow patches 4) Surfaces with little or no vegetation includes abrasion flats and alluvial deposits and fell-field vegetation (Bay, 1998). A detailed vegetation map of the Zackenberg Valley is given in Fig. 2.3.

The total average annual precipitation at Daneborg is 214 mm, and about 80% of this falls as snow (1961–1974) (Ohmura and Reeh, 1991). Similar values have been found at the AWS at Zackenberg. The end-of-winter snow depth measured at the Zackenberg AWS on June 1 (1998–2004) has varied from 0.44 m (2000) to 1.11 m (1999).

### 2.2.1 Snow

A pure snow cover reflects as much as 80–90 percent of the incoming solar radiation, whereas a snow-free surface such as bare soil or vegetation may reflect only 10 to 20 percent. Besides being a strong short-wave ( $\lambda \approx 0.5 \mu\text{m}$ ) reflector, snow is a strong emitter of long wave ( $\lambda \approx 10 \mu\text{m}$ ) radiation too. Due to these radiative properties, and due to a relatively high latent heat of fusion (i.e., it takes 160 times as much energy to transform one unit of ice to water as it does to raise the temperature of the same unit of ice 1°C) snow cover represents a heat sink during melt periods. Consequently, snow generally acts as an effective cooler. On the other hand, due to its poor heat transfer characteristics, snow is a great insulator. Therefore, soil surface temperature is highly dependent on the presence or absence of snow cover (Groisman et al., 1994).

Under typical winter conditions, during the polar night in Northeast Greenland, both the emissive and the insulating properties of the snow pack are of particular importance. Because of the high emissivity, temperatures can get very low in the vicinity of the snow-surface, especially under calm and cloud-free weather conditions. Such situations will be characterized by strong temperature inversion (Cappelen et al., 2001). However, due to the insulation, the soil surface organisms (e.g. the vegetation, invertebrates and small mammals) beneath the snow pack are protected against extremely low temperatures and thereby resulting frost damage.

During melt-off in the summer, the temperature conditions at the surface are closely related to the melt energy balance of the snow pack (Gray and Male, 1981). The melt energy balance is formulated as a requirement for conservation of energy:

$$(Q_{sn} + Q_{ln} + Q_h + Q_e + Q_g + Q_p) + Q_m = 0 \quad (2.1)$$

where

$Q_{sn}$  = net short wave radiation flux absorbed by the snow

$Q_{ln}$  = net long wave radiation flux ( $Q_{l\text{ incoming}} + Q_{l\text{ emitted}}$ ) at the snow-air interface

$Q_h$  = convective or sensible heat flux from the air at the snow-air interface

$Q_e$  = flux of the latent heat (evaporation, sublimation, condensation) at the snow-air interface

$Q_g$  = flux of heat from the snow-ground interface by conduction

$Q_p$  = flux of heat from rain

$Q_m$  = melt energy

As long as the snow pack is present, equation 2.1 will prevail ( $Q_m$  balances out other terms in the equation), meaning that energy generally will be used for melt rather than for raising the temperature in areas in proximity to the snow pack; the high albedo further contributes to make the snow pack act as an effective cooling mechanism, also in the summer time.

In the High Arctic, extensive snow-melt prior to the “end-of-winter-situation” seldomly occurs (e.g. at Zackenberg temperatures are generally below  $0^\circ\text{C}$  during September–May, and above  $0^\circ\text{C}$  during June–August). This means that snow-cover-depletion virtually takes place only during the summer period (June–August). At Zackenberg, heavy snowfall seldomly occurs in the summer, and therefore, in most cases snow-melt and snow cover depletion can be calculated considering only the melt balance and not (summer)-accumulation (Paper 3). However, in practice, it is rarely possible to obtain the necessary information to derive all terms of energy-input ( $Q_{sn}$ ,  $Q_{ln}$ ,  $Q_h$ ,  $Q_e$ ,  $Q_g$ ,

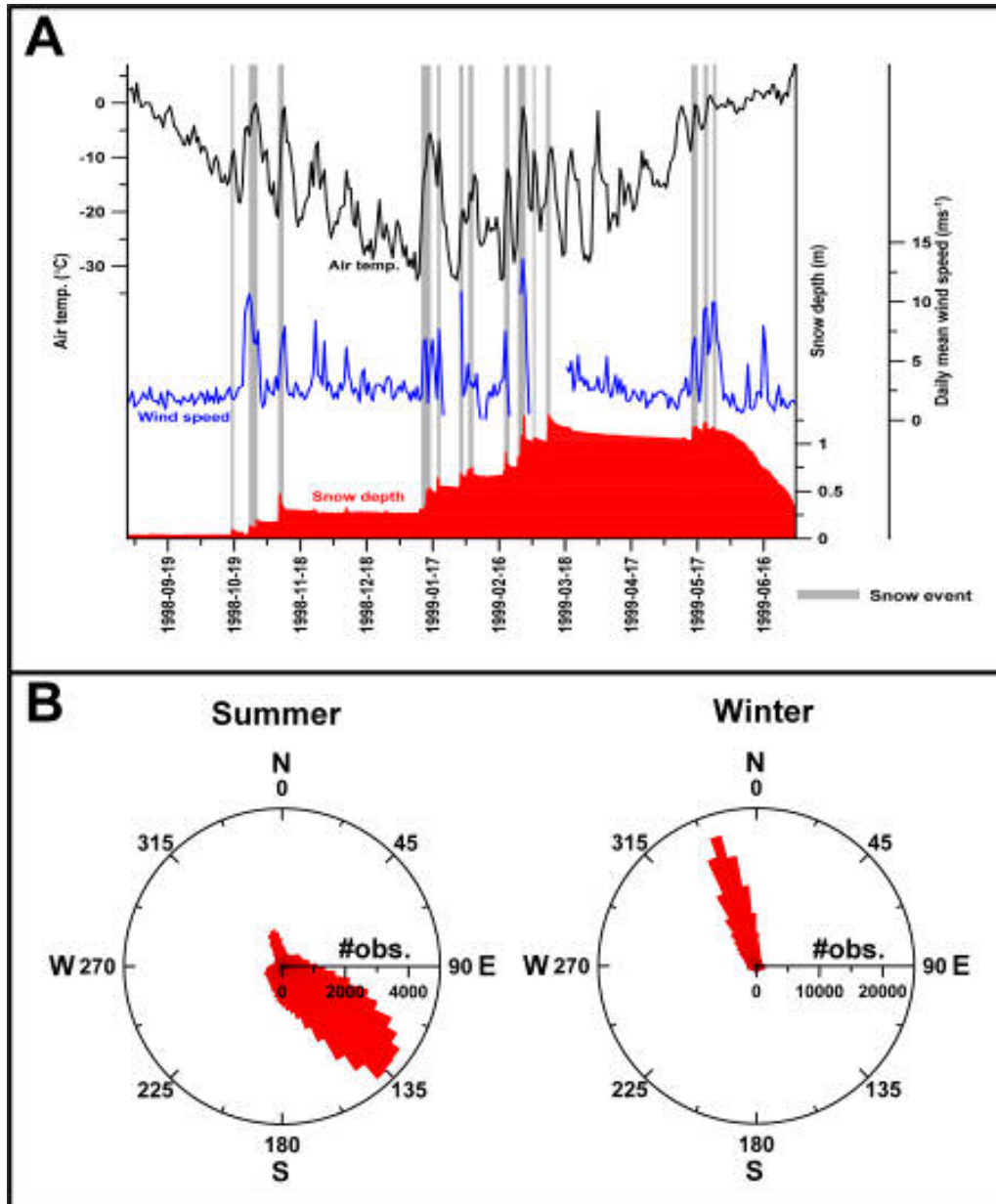


$Q_p$ ). Therefore, modeling snow melt normally requires a simplification of the energy balance. One of the most common simplifications is the degree day model, which uses the sum of temperatures above the melting point (base temperature) as a “melting potential” (Rango and Martinec, 1995).

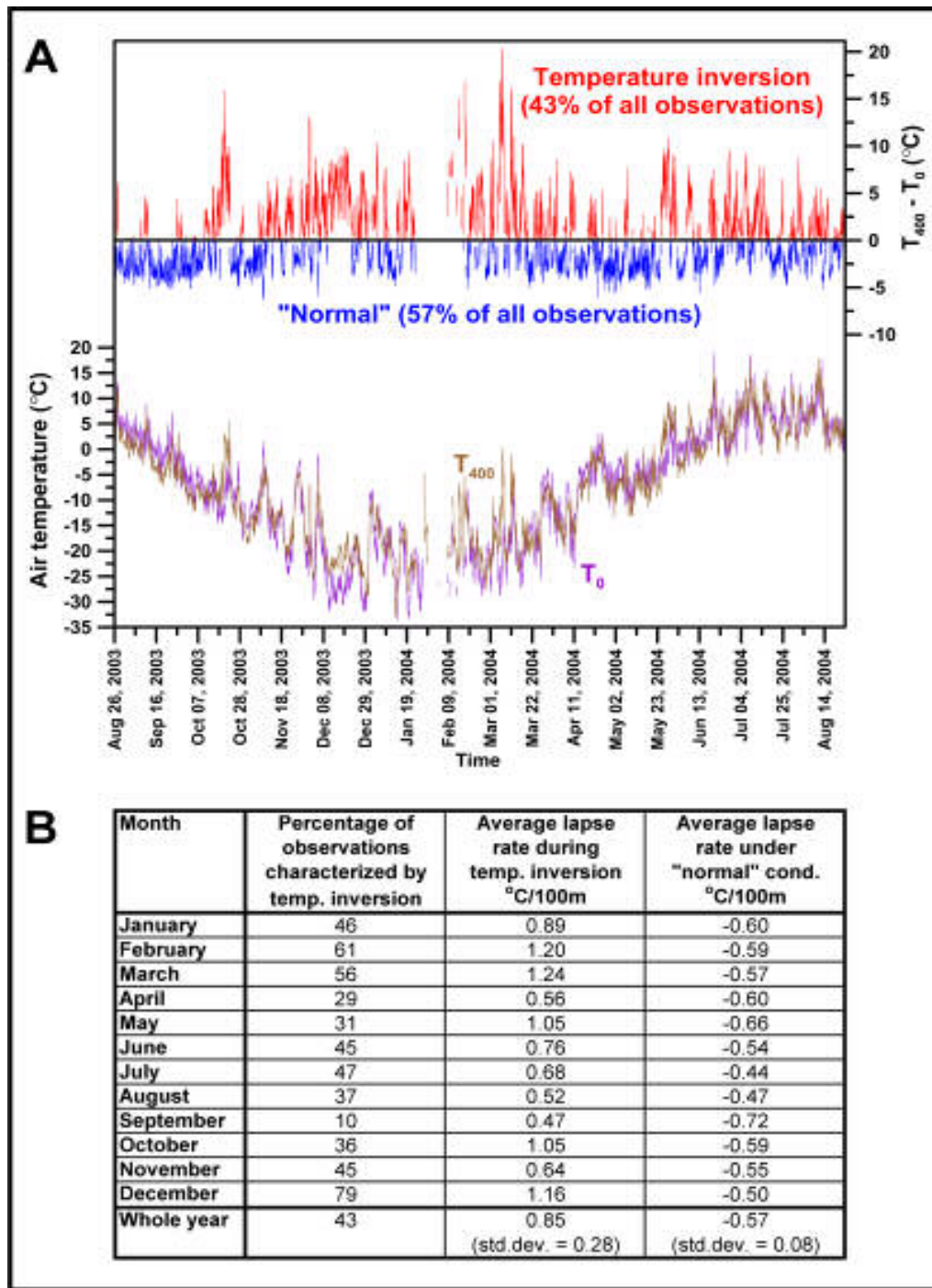
From the ecosystem perspective, the areal distribution of the snow cover is of particular importance (Jones et al., 2001). However, modeling the spatial distribution of the snow cover during melt-off is complexed by spatial variations in snow-accumulation amounts and density. These variations are generally caused by wind-drift, and metamorphosis induced by settling, wind pressure, melt etc. (comprehensive descriptions regarding formation, physical properties, and metamorphosis of snow can be found in Gray and Male, 1981). Consequently, calculating snow cover extent during melt-off requires knowledge about the spatial distribution of the snow pack’s physical characteristics. These characteristics are often related to the physical properties (mainly the prevailing wind direction and topography) of the actual area in question (Hall and Martinec, 1985; Menoes and Brubaker, 2001). In this study, the spatial distribution of “snow characteristics” specific for Zackenberg is taken into consideration using empirically derived snow cover depletion curves (Paper 3).

At Zackenberg, the snow cover might start to form already in September and usually it will start to melt by the end of May and will normally melt away before the end of August (Paper 1). In Northeast Greenland, high wind speeds and precipitation are usually connected with cyclonic activity over the Greenland Sea, and maximum winds typically occur in the coastal area, although katabatic winds from the ice cap and the mountain sides are sometimes observed in the fjords, where they may raise the temperature significantly, due to the Foehn effect (Cappelen et al., 2001). In consequence to these factors, precipitation (snow) events are usually connected with both increased air temperatures and increased wind speeds. Fig. 2.4 (A) shows that this also applies to ZRA. Here, the stronger winds are most frequent in the winter, and are often connected with snowfall and increased temperatures. Fig. 2.4 (B) shows that wind conditions in ZRA differ significantly from winter to summer. In the summer (June–August), the prevailing wind direction is from southeast, whereas north northwesterly winds (katabatic valley winds) prevail in the winter (October–April). Due to the dominance of strong northwesterly winds during winter, the snow cover within the Zackenberg Valley is distributed in a non-uniform manner over the landscape, with large snow-drifts deposited mainly on south facing slopes; and because there is no considerable inter-annual variation in the prevailing winter-wind-direction, the location of the larger snow-drifts is stable from year to year (Soegaard et

al., 2001). A consequence of this rather stable pattern of snow cover distribution (in winter) is that also the spatial course of snow-melt at ZRA during summer is relatively stable from year to year.



**Fig. 2.4.** (A) Air temperature, wind speed and snow depth measured at the Automatic Weather Station at Zackenberg during September 1<sup>st</sup>, 1998–June 30<sup>th</sup>, 1999. Major snow events are usually connected with increasing temperatures and wind speeds. (B) Frequency of wind directions at the Automatic Weather Station at Zackenberg during summer (June–August, 1996–2003) and winter (October–May, 1995–2003). Note that figures similar to A are shown for other seasons, in Appendix 2.1.



**Fig. 2.5.** (A) Temperatures ( $T_0$  and  $T_{400}$ ) at Zackenberg Research Area measured every half hour near sea level and at 400 m altitude, respectively. The upper part of the figure shows the difference between  $T_{400}$  and  $T_0$ , revealing whether there is temperature inversion. (B) Magnitude and occurrence of temperature inversion/"normal periods", September 2003–August 2004.

Sometimes during summer the fjord areas are affected by fog coming in from the ice filled sea. This leads to a temperature drop, as the mean temperature of the fog is only slightly above  $0^{\circ}\text{C}$  (Cappelen et al., 2001). Due



to this and to ice and snow-melting during summer and radiation cooling in winter, temperature inversions occur frequently in the area; and the highest temperatures are therefore often registered a few hundred meters above sea level, where also the effect of sea breezes and foggy conditions are almost absent (Cappelen et al., 2001). The spatial pattern of snow-melt in a given area depends on the initial distribution of snow cover as well as the spatial distribution of melt-energy (mainly surface air temperature and incoming solar radiation). Within ZRA melt-energy distribution is further complexed by the high frequency of temperature inversions (Fig. 2.5). Fig. 2.5 shows temperatures measured at a recently (August 2003) established AWS at 400 m altitude and at the AWS near sea level. Further, the figure displays occurrence and magnitude of temperature inversions. It is revealed that the fraction of time with inversion varies considerably over the year from as low as 10% in September to 79% in December, and that the absolute value of the lapse rate is generally higher when inversion occurs than under “normal” conditions. Sometimes in the winter, the temperature difference between 400 m and sea-level is remarkably high—in a few cases between 15°C and 20°C. In the summer, inversion can still be considerable in magnitude (occasionally in the neighborhood of 10°C), but are however generally more moderate. In June and July, where major snow melt occurs, inversion prevails in more than 45% of the time. In relation to the modeling of snow cover depletion (Paper 3) it was therefore decided not to deal with topographic correction (by including standard lapse rates) in the calculation of accumulated melt-energy (degree-days).

### 2.3 NAO/AO

The North Atlantic Oscillation (NAO) is the name for changes in the difference between the semi-permanent low pressure system centered near Iceland and a semi-permanent high pressure system centered near Azores Islands. It is most prominent during winter and forms a major source of interannual variability in the atmospheric circulation which is associated with changes in the westerlies across the North Atlantic (Hurrell, 1995).

When negative pressure anomalies over the Icelandic/Arctic region are combined with positive pressure anomalies across the subtropical Atlantic, the NAO is said to be in its positive phase. When this is the case, westerlies stronger than average are produced across middle latitudes. During winter, this leads to cold conditions over the northwest Atlantic and Greenland (further discussed below), warm and moist weather over northwestern Europe, as well as wet conditions from Iceland through Scandinavia and dry

conditions over southern Europe. During negative NAO-winters (meaning less contrast between the Icelandic Low and the Azores High), roughly opposing conditions prevail (Fig. 2.6).

There is no single way to define the NAO. However, most modern indices are derived either from the simple difference between southerly and northerly sea level pressure anomalies in the North Atlantic, or from principal component analysis on time series of gridded pressure data (Hurrell et al., 2003).

The most common way to calculate the NAO-index is, however, to use the former approach on a monthly basis as stated below:

$$\text{NAO} = \left( \frac{SLP_{Az} - \overline{SLP_{Az}}}{\delta_{Az}} \right) - \left( \frac{SLP_{Ice} - \overline{SLP_{Ice}}}{\delta_{Ice}} \right), \quad (2.2)$$

where

$SLP_{Az}$  = Monthly mean sea level pressure at the Azores

$SLP_{Ice}$  = Monthly mean sea level pressure at Iceland

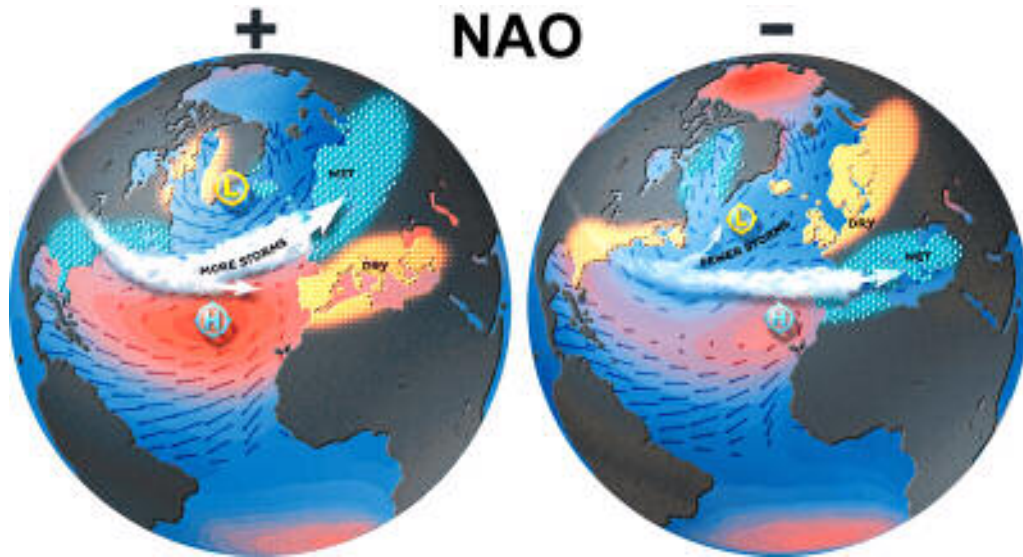
$\overline{SLP_{Az}}$  = Long term mean sea level pressure at the Azores for the month in question

$\overline{SLP_{Ice}}$  = Long term mean sea level pressure at Iceland for the month in question

$\delta_{Az}$  = Long term standard deviation of sea level pressure at the Azores for the month in question

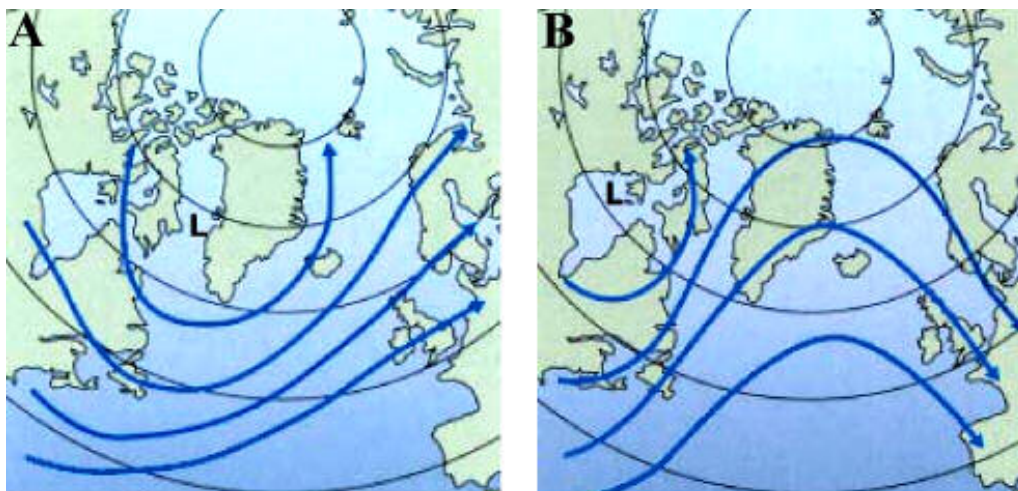
$\delta_{Ice}$  = Long term standard deviation of sea level pressure at Iceland for the month in question

The first documented observation of the NAO was actually done more than 200 years ago. In the late 1700's Hans Egede Saabye (a Danish Christian missionary stationed in Greenland) made the seemingly innocuous, observation in his diary: "When the winter in Denmark was severe, as we perceive it, the winter in Greenland in its manner was mild, and conversely" (Szalai, 2003). The explanation is illustrated in Fig. 2.7. When the Icelandic Low is deeper than normal (positive NAO) the Canadian cold vortex is displaced to the east towards the west coast of Greenland, resulting in a strong southwesterly flow of mild air from the ocean across Europe. Greenland, on the contrary, will experience a cold winter isolated from maritime Atlantic weather with an increased likelihood of polar lows to develop (Cappelen et al.,

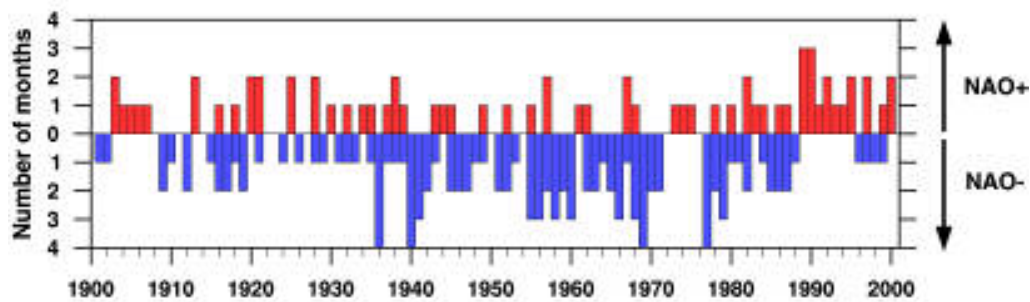


**Fig. 2.6.** The North Atlantic Oscillation is defined as the difference between the standardized pressure anomalies of the Icelandic Low and the Azores High, respectively. Source: Modified from figures by Visbeck (2004).

2001). When the NAO is in its negative phase the Icelandic and Canadian Lows are weaker and displaced to the west, and under these circumstances Atlantic cyclones will follow a northward track towards Greenland bringing in more changeable weather with frequent temperature increases. The reduced Icelandic low and the relatively higher pressure in the northeastern part of the North Atlantic will allow cold Arctic air to flow into northwestern Europe (Cappelen et al., 2001). Approximately 60% of all winters can be characterized as either statistically significant positive or negative NAO-winters (Cappelen et al., 2001). The time history of occurrence of the NAO-winters (+/-) over 1900–2000 is shown in Fig. 2.8.

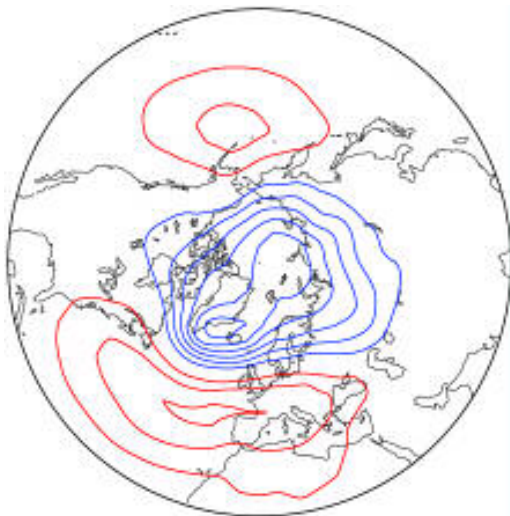


**Fig. 2.7.** Typical patterns of airflow in the North Atlantic under (A) high and (B) low winter-North Atlantic Oscillation. Source: Modified from Cappelen et al., 2002.



**Fig. 2.8.** The time history of occurrence of the North Atlantic Oscillation regimes (+/-) over 1900–2000. The vertical bars give the number of months in each winter (December–March) season that the given regime is present. The indicated year corresponds to the January of the winter season (e.g., 1990 is the winter of 1989–1990). Source: Hurrell, 2003.

Throughout the literature the oscillating modes of the northern hemisphere atmospheric circulation are sometimes described in relation to the NAO and sometimes in relation to the Arctic Oscillation (AO) (Fig 2.9). Thus, to avoid any confusion the AO is briefly discussed below: Thompson and Wallace (1998)—who were the first to describe the AO, deriving it from principal component analysis on sea level pressure data, regard the NAO as a regional (Atlantic) expression of the AO. Although the AO and the NAO share many common features, the AO has a northern center of action that covers more of the Arctic and an additional weaker center in the North Pacific, giving it a more zonally symmetric appearance (Tremblay, 2001). However, according to Wallace (2000), the NAO and AO can be viewed as manifestations of the same basic phenomenon. The time-series of the NAO and AO are thus also highly correlated. The R-squared of monthly anomalies of sea level pressure time series of NAO and AO is about 0.6 while seasonal variations have even higher correlations.



**Fig. 2.9.** The semi-permanent pressure systems of the Arctic Oscillation given as the first Principal Component contour lines of sea level pressure anomalies, 1947–1997 (red: positive, blue: negative). The Arctic Oscillation has a northern center of action that covers more of the Arctic than the North Atlantic Oscillation and it has an additional weaker center in the North Pacific, which gives it a more zonally symmetric appearance. Source: Deser, 2000.



into the Labrador Sea, where it continues as the North Atlantic Drift Current running northeastwards between Great Britain and Iceland. Here it moves further into the Nordic Seas along the Norwegian west coast as the Norwegian Current, and ends by splitting up as the western/eastern Spitsbergen Currents passing the western and eastern sides of Svalbard, respectively (Spitsbergen is the largest island of Svalbard). South of Iceland above the western slope of the Reykjanes ocean ridge, a branch of the North Atlantic current forms the Irminger Current (HYCOM Consortium, 2005).

The cold East Greenland current flows southward along the eastern coast of Greenland from the Fram Strait (between Greenland and Svalbard) via the Greenland Sea and Denmark Strait. It continues around Cape Farewell and a bit up along the west coast. It is the only major southward flowing surface ocean current in the Nordic Seas. It transports recirculating Atlantic water, Arctic Ocean water masses, and huge quantities of sea-ice (see section 2.5) from the Arctic Ocean. More than 90% of the ice exported from the Arctic Ocean (Woodgate et al., 1999) flows through the Fram Strait. Next to the Amazons, this transport represents the World's largest freshwater flux to the Oceans (Vinje, 2001; Vinje et al., 2005). The less dense Polar Surface Water follows the Greenland continental slope toward the Iceland Sea and Denmark Strait. One part—the Jan Mayen Current is, however, deflected eastward at the Jan Mayen Fracture Zone, bringing cold polar water and ice towards Jan Mayen and the eastern rim of the Greenland Sea. However, as the Atlantic mid Ocean Ridge continues from Iceland across Jan Mayen and further on to the northeast, it prevents dense and deeper water to continue into the Iceland Sea. Therefore, the deeper water circulates around the Greenland Sea Gyre<sup>1</sup>, where it interacts with the Greenland Sea waters (Rudels et al., 1999). As will be described in section 2.5 this interaction between the relatively fresh Arctic water and the warmer more dense saline Atlantic water has a marked influence on both deep water and sea-ice formation in the Greenland Sea.

## 2.5 Sea-ice in the Greenland Sea

Regarding this dissertation, sea-ice distribution within the Greenland Sea plays a central role because, as it is shown in Paper 4, sea-ice might be an important variable in relation to snow precipitation in Northeast Greenland.

---

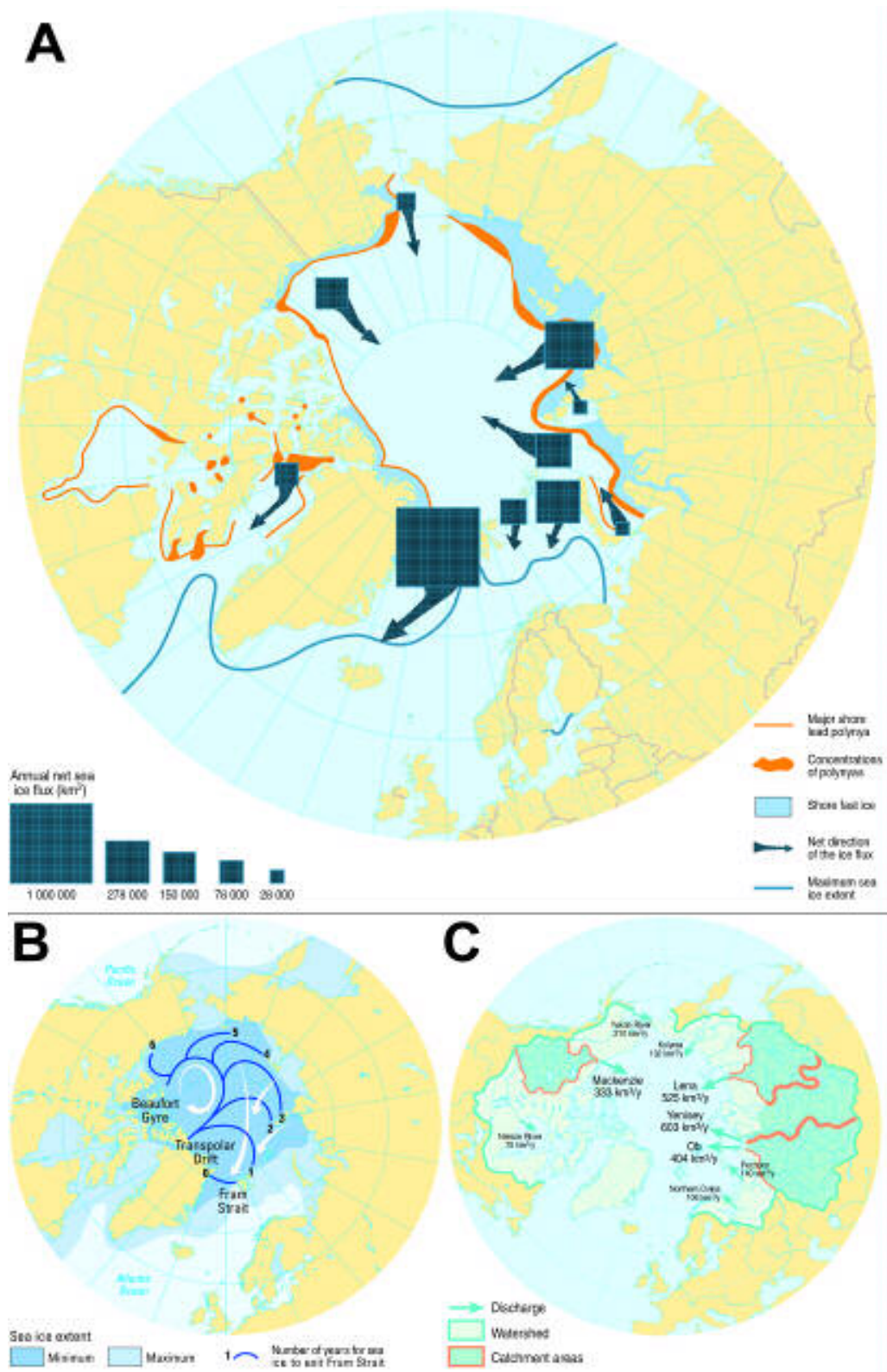
1. According to current knowledge, deep water formation in the northern North Atlantic occurs only in the Greenland Sea, the Labrador Sea, and sometimes in the Irminger Basin (Pickart et al., 2003; Vinje et al., 2002). Therefore, the waters of the Greenland Sea Gyre are considered to play a crucial role in the global thermohaline circulation in the Great Ocean Conveyor Belt (Vinje et al., 2002).



The basic definition of sea-ice is: any form of ice found at sea, which originates from the freezing of sea water. Broadly, it can be described as new ice, young ice, first-year ice, and old ice. These categories reflect the age of the ice and include different forms and thicknesses of ice at various stages of development (World Meteorological Organisation, 1970). To obtain more detail, each category is divided into a number of subcategories (Appendix 2.3). In Greenland, sea-ice is further described by its place of origin. Ice which is created in the Arctic Ocean is called Polar Ice, and ice flowing in the East Greenland Current is called Storis (“big ice” in Danish). Ice found to the west of Greenland in the Baffin Bay and the northern part of Davis Strait is called West Ice (Cappelen et al., 2001).

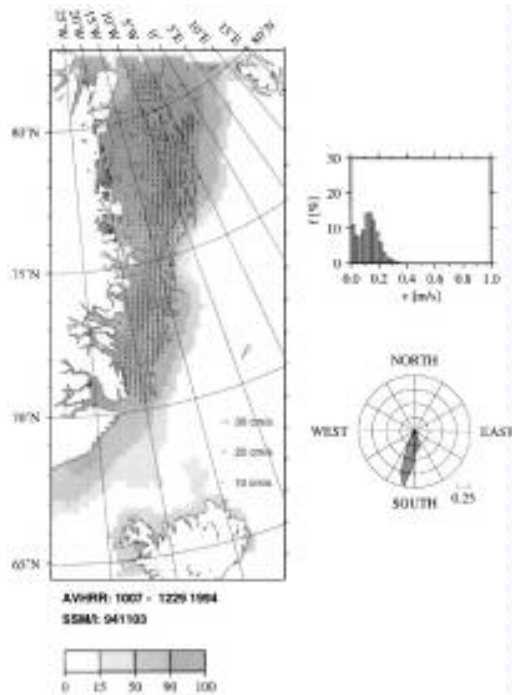
Virtually all transport of sea-ice into the Greenland Sea goes through the Fram Strait between Greenland and Svalbard (Fig. 2.11 (A)) from where it drifts along coast in the East Greenland Current (Cappelen et al., 2001). Therefore, the formation of Polar Ice in the Arctic Ocean plays a crucial role for the net balance of the sea-ice concentration in the Greenland Sea. The major part of the Arctic Ocean is covered by sea-ice throughout the year, and the two main ice circulation systems here is the Beaufort Gyre and the Transpolar Drift (Fig. 2.11 (B)). As the ice drifts in the gyre, it follows a clockwise circulation forced by the surface winds and ocean currents around the climatological Beaufort High (Vavrus and Harrison, 2003). Data inferred from drifting buoys (1979–1990) show that Polar Ice often circulates for more than five years in the gyre before it is incorporated in the Transpolar Drift where it continues towards the Fram Strait. The ice flow in the gyre accelerates, so that sea-ice tends to be thickest and most compact in the west and thinner and less compact in the east. The numbers on the blue lines in the figure indicate the time (in years) that it takes for the ice to flow to the Fram Strait from the line-positions, meaning that virtually all ice exported through Fram Strait are multi-year ice.

Due to the inflow through the Fram Strait, sea-ice distribution and formation in the Greenland Sea is much more complex and dynamic in nature than for instance the West Ice, which is mainly formed locally. Throughout the year, the ice-flux through the Fram Strait typically varies from approximately 0.09 to 0.14 Sv (1 Sv = 1,000,000 m<sup>3</sup>/s) flowing in a band which may be several hundred kilometers wide (Martin and Wadhams, 1999). A few hundred kilometers south of the Fram Strait the Greenland Sea Current accelerates, causing the Storis ice-drift to spread out (Fig. 2.12). In winter new ice is rapidly formed between the floes of Polar Ice, causing the composition of the



**Fig. 2.11.** (A) Approximate net sea-ice exchange between the Arctic Ocean and the Nordic Seas. (B) Annual max/min sea-ice extents and sea-ice motion. The numbered blue lines indicate the time it takes (in years) for the ice at the line-positions to exit the Arctic Basin through the Fram Strait. (C) Freshwater river-discharge from the major Arctic rivers. Source: AMAP, 1998.

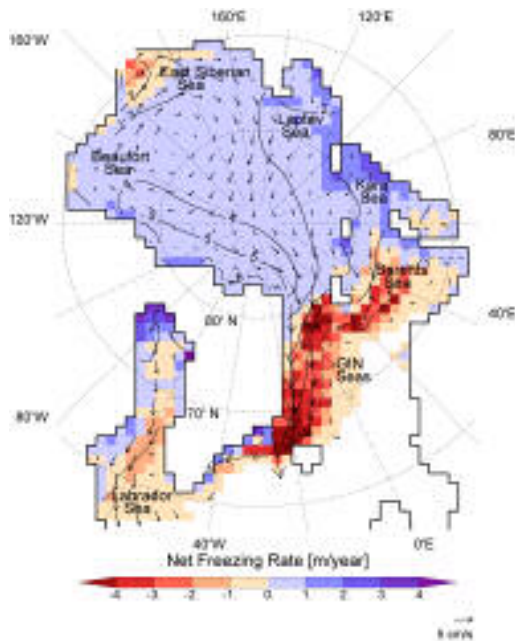




**Fig. 2.12.** Composite of sea-ice drift derived from NOAA AVHRR images, October–December 1994. The drift velocity vectors are shown on a background of sea-ice concentrations derived from SSM/I data (see Appendix 1). South of the Fram Strait the ice drift spreads out as the Greenland Sea Current accelerates. The rightmost part of the figure shows a histogram and a normalized rose diagram of the drift velocity. Source: Martin and Wadhams, 1999.

ice to be a mixture of Polar Ice and First Year Ice. Initially, the size of a single floe of Polar Ice may be more than 7000 km<sup>2</sup> (about the size of Zealand in Denmark or 120 times the area of Manhattan Island). However, as the floes are drifting southwards along the coast they are broken into smaller pieces by wind, sea swells, and collision with other floes; and around 70°N (the latitude of Scoresbysund) only a few floes are more than a hundred meters wide. To the south of this latitude there are major seasonal variations, because of the spreading and melting of the ice (Cappelen et al., 2001). This means that the ice-drift in the East Greenland Current forms a major part of the net balance of the ice-cover in the Greenland Sea, but it also means that it contributes to highly increase the complexity of the balance, especially in the southern part.

As freshwater freezes already at 0°C and sea-water (with a salinity of 34‰) freezes around -2°C, the freshwater/salinity balance plays a crucial role for the formation of sea-ice. The primary freshwater source to the Greenland Sea is the flux of low saline multi-year sea-ice and liquid freshwater from the Arctic Ocean going through the Fram Strait (Mysak et al., 1990; Pedersen, 2004). Basically, this source can be divided into two main sub-sources: the extraction of salt through freezing (Steele and Flato, 2000) and inflow from major Arctic rivers (Fig 2.11 (C))—the Yenisey, Lena, and Ob, for instance, are the three largest Arctic rivers, and represent nearly 10% of the global annually river discharge (Driscoll and Haug, 1998).



**Fig. 2.13.** Long term average (1958–1997) conditions of simulated Arctic ice cover. The color shading shows net freezing rates (growth due to freezing minus melt), and the arrows represent the ice drift vectors. Source: Hilmer et al., 1998.

Fig. 2.13 reveals that on an annual basis the net freezing rate is negative (around minus four meters per year in some places) in the Greenland Sea. Thus, in spite of the large annual export of ice through the Fram Strait, it is always more or less ice free by the end of summer. However, typically during winter the central Greenland Sea develops a local cover of pancake ice (Appendix 2.3), which occupies a tongue-shaped region called Odden (Danish/Norwegian word for headland) stretching northeast from the East Greenland Current at approximately 72–75°N (Fig. 2.14). This particular ice cover forms due to influence from the cold Jan Mayen Current, which diverts eastwards from the East Greenland Current at these latitudes (Wadhams, 1999). This current is also the south side of the Greenland Sea Gyre. The Odden ice tongue shows great year to year variations. In a severe season, at the end of November, Odden extends well east of the Greenwich meridian (National Geospatial-Intelligence Agency, 2004), and in “milder” seasons it may hardly develop.

Since ice formation involves an immediate salt flux into the surface water, the formation of ice in the “Odden area” is important for both the freshwater/salinity balance in the Greenland Sea Gyre and the region located south of the ice tongue (Wadhams et al., 2003). Considering this freshwater/salinity balance, the general picture is that salinification mainly occurs in the northern parts of Odden towards the center of the Greenland Sea Gyre, where the pancake-ice is formed; whereas melting (freshening) occurs mainly near the southeastern edge of the ice tongue. This is due to the fact that



**Fig. 2.14.** Arctic sea-ice extent in February 1989, inferred from SSM/I satellite passive microwave brightness temperatures. This year the Odden ice tongue appeared very clearly. The thick black line indicates the median ice edge, and the red circular arrow indicates the location of the Greenland Sea Gyre. Source: National Snow and Ice Data Center, Boulder, Colorado, USA.

the pancakes are blown to the southeast (where they end up melting) by the cold northwesterly winds that prevail during winter. In addition to the salt-flux from Odden, the Greenland Sea Gyre also receives a surplus of salt from the warm West Spitsbergen Current (extension of the Gulf Stream), which mixes up with the colder East Greenland-Jan Mayen Currents in this area.



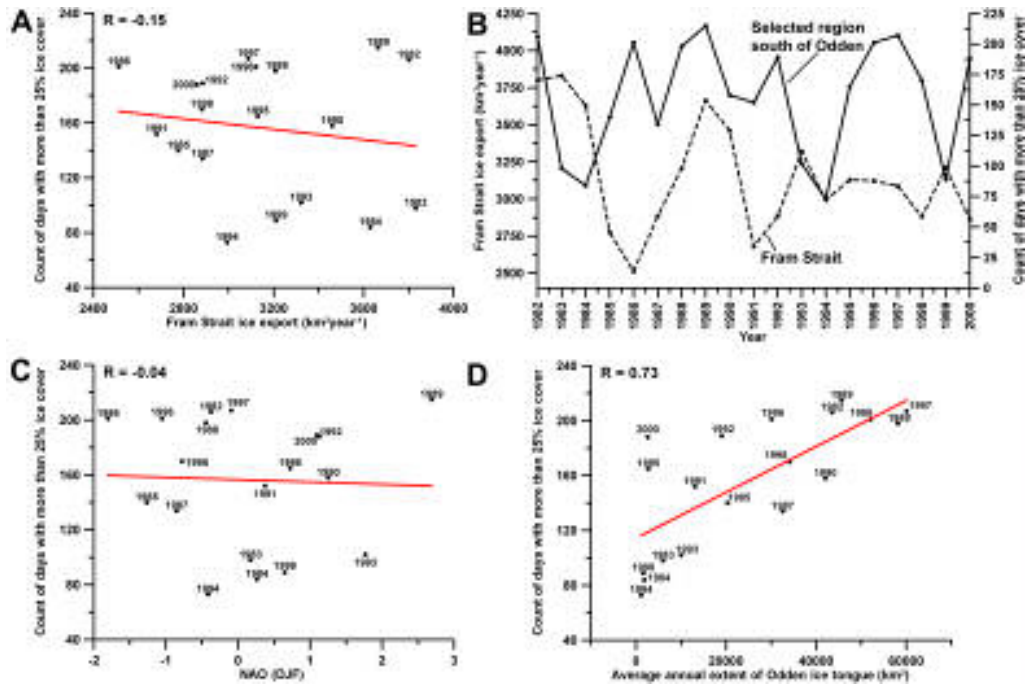
**Fig. 2.15.** Sea-ice distribution February 2<sup>nd</sup>, 1989. The rightmost polygon indicates mapping area of the Odden ice tongue, and the more or less triangular polygon indicates the area of special interest (Paper 4) south of Odden.

Concerning this dissertation the sea-ice distribution (and thereby also the freshwater-balance, which also affects local ice formation) in the Greenland Sea south of Odden (Fig. 2.15) is of particular interest, as it might be linked to winter-precipitation amounts in Northeast Greenland (Paper 4). However, the fact that the freshwater balance of this area is affected *both* by the “direct” flux of multi-year ice from the East Greenland Current and the freeze-melt processes within the Odden area, complicates the way sea-ice is distributed here, and should therefore be subjective for further studies.

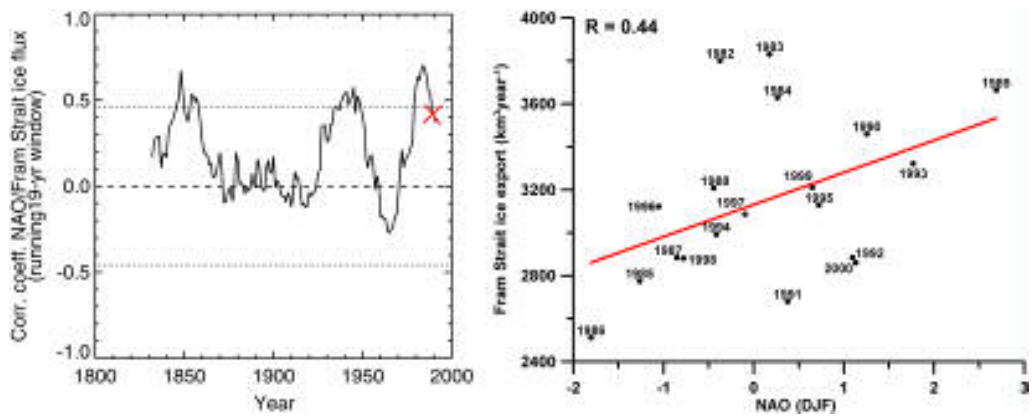
Due to the large magnitude of the ice-flux through the Fram Strait, it would be reasonable—at a first estimate, to expect this ice-flux to have

profound influence on sea-ice distribution in virtually all parts of the Greenland Sea. This is, however, not the case, and is illustrated below: Fig. 2.16 (A-B) compares annual ice-flux through the Fram Strait to durations of time with large sea-ice extents in the region south of Odden. Unexpectedly, the amounts of sea-ice registered in this area do not reflect the annual ice export through Fram Strait. The two parameters are not correlated at all ( $R = -0.15$ ) and neither are they connected in accordance with an eventual lagged correlation. Regarding teleconnection patterns (NAO/AO) over the period 1982–2000, there doesn't seem to be any correlation between the NAO and the ice distribution south of Odden either ( $R = -0.04$ ) (Fig. 2.16 (C)). As discussed previously, the pancake ice formed in the northern parts of Odden is transported southwards by the wind during winter. Apparently, this transport of ice/fresher water is a major controlling factor regarding sea-ice amounts south of Odden. Fig. 2.16 (D) shows that the average annual extent of the Odden ice tongue is highly correlated to the sea-ice amounts registered south of it ( $R = 0.73$ ). Thus, to explain sea-ice coverage in this area the variability of Odden (and thereby the Jan Mayen Current) must be considered rather than external factors such as teleconnections and/or external ice-flux into the East Greenland Current. The relation between the extent of Odden and the local conditions in the Jan Mayen region is further emphasized by findings by Comiso et al. (2001). They showed the extent of the Odden ice tongue to have a strong negative correlation with monthly surface air temperatures recorded at Jan Mayen, which suggests that it is reasonable to use the temperature at Jan Mayen as a proxy for the extent of Odden (Comiso et al., 2001; Paper 4).

It is, however, important to mention that the sea-ice data (Appendix 1) dealt with here is limited to the period 1982–2000. Thus, it is not clear whether ice extents south of Odden are correlated to e.g. NAO during other periods of time due to e.g. some decadal or multi-decadal periodicity. For instance, this seems to be the case for the ice-flux through Fram Strait: Based on historical observations of the Storis (1820–2002) Schmith and Hansen (2003) reconstructed the Fram Strait ice export almost two centuries back in time. Based on a running 19-year window they found the correlation between ice export and NAO to vary in a nearly oscillating manner over multi-decadal periods (Fig. 2.17). In accordance with other studies (Mysak et al., 1990) Schmith and Hansen note that sea-ice anomalies coincide with temperature and salinity anomalies, and that the Arctic Ocean (and thereby also runoff from major Arctic rivers) is involved in this multi-decadal variability. They



**Fig. 2.16.** (A) Time duration (days counted during December–August) with more than 25% ice cover in selected area south of Odden ice tongue versus annual ice export through Fram Strait. (B) Time plot (1982–2000) of the parameters shown in A. (C) Time duration with extensive sea-ice (as described in A) versus North Atlantic Oscillation. (D) Time duration with extensive sea-ice (as described in A) versus average annual extent of Odden ice tongue. Sources: Daily ice extents south of Odden were derived using surface masks based on satellite SSMR & SSM/I passive microwave brightness temperatures (see Appendix 1 on data types). Annual Fram Strait ice export is from Schmith and Hansen, 2003, and North Atlantic Oscillation-data are from NOAA/Climate Prediction Center, 2002.



**Fig.2.17.** Ice export through Fram Strait and the North Atlantic Oscillation. (A) Correlation coefficient between Fram Strait ice export and winter North Atlantic Oscillation-index in a running 19-year window. The red cross indicates the center of the 1982–2000 window. Dotted lines indicate the 2 std. dev. uncertainty range. (B) Fram Strait ice export against North Atlantic Oscillation during 1982–2000, which is the period covered by this dissertation with respect to sea-ice. Sources: NOAA/Climate Prediction Center, 2002 and Schmith and Hansen, 2003.

found that rather dramatic freshening of the Nordic Sea waters—the so called Great Salinity Anomalies (GSA's) generally occur when the ice export through Fram Strait is high. The latest GSA's occurred in 1968–1970 and 1980–1982, respectively, and are claimed to be the most important anomalous climatic variability in the North Atlantic related to sea-ice (Sanchezgomez et al., 2002).

Therefore, in light of the above, it can be concluded that, if we want to better understand how larger scale phenomena such as NAO/AO or GSA's affect the sea-ice distribution south of Odden ice tongue, then a longer historical record of sea-ice observations from this particular area must be considered.

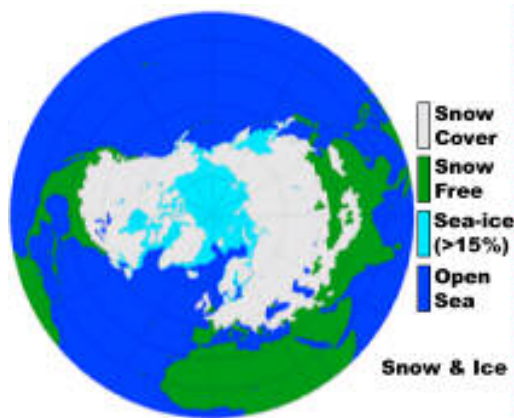
*Note: to provide an overview of the sea-ice variation within the Greenland Sea, the CD-ROM, attached to the back cover, includes a video animation of the daily sea-ice extent in the Greenland Sea during 1981–2000.*



## Chapter 3

# Snow–ecosystem relations & future perspectives

In terms of spatial extent (Fig. 3.1), seasonal snow cover is the largest single component of the cryosphere (i.e. the frozen part of the Earth's surface). With a mean winter maximum extent of 47 million square kilometers it corresponds to almost a third of the Earth's total land surface (NSIDC, 2005). Thus, due to its influence on energy and moisture budgets, snow cover is an



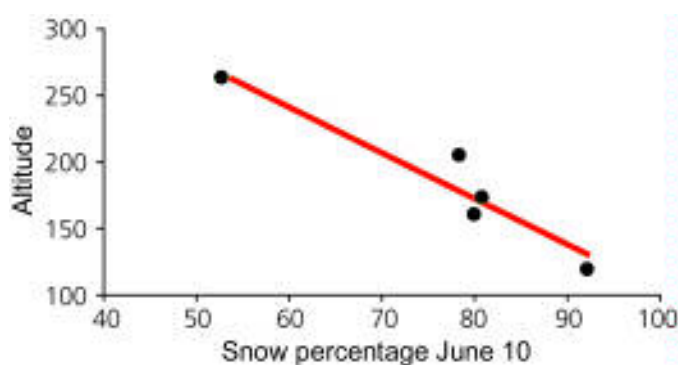
**Fig. 3.1.** Week of maximum snow extent (52,578,000 km<sup>2</sup>) for the period 1979 to 1995 (image from January 8–14, 1979). Source: National Snow and Ice Data Center, University of Colorado, Boulder, USA.

important variable at almost any spatial scale in relation to both climate change and ecosystem conditions. Especially at high latitudes, in Boreal and Arctic regions, the role of snow cover is crucial for the ecosystems. What will be the impact of possible future climatic changes on snow cover and its ecology is presently still uncertain as it may show significant variability between different regions (Jones et al., 2001). In the following sections, the importance of snow cover and its impact on a high latitude ecosystem will be illustrated mainly by examples from Zackenberg, Northeast Greenland, where it is a most crucial variable for both flora and fauna (Meltofte, 2002). Furthermore, some future perspectives for Zackenberg, inferred from this work, will be presented.

### 3.1 Snow cover, flora, and fauna

As indicated in Chapter 2, the way snow cover affects Arctic ecosystems differs from summer to winter. Studies on Arctic animals in relation to climatic

fluctuations show that especially in the winter, the state of the snow cover is crucial for the larger herbivores, such as muskoxen and caribou (Vibe, 1967). For instance, around Zackenberg (and in central Northeast Greenland in general), numerous relics from caribou in the form of antlers can be found in the terrain. At present time, however, caribou have become extinct in Northeast Greenland. Their extinction occurred at around the beginning of the 20<sup>th</sup> century and was most likely related to snow cover conditions. Because of the relatively humid winters that prevailed in the region at that time (the so called drift-ice pulsation stage, 1860–1910), increased snow-precipitation and increased frequency and intensity of thaw events during winter led to ice crust formation in the snow pack (Vibe, 1967). The consequence was difficulties for the caribou in getting access to the sparse amounts of food beneath the snow cover.

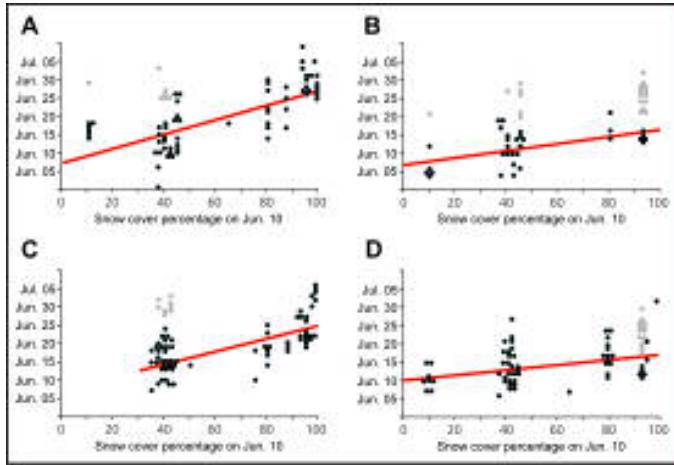


**Fig. 3.2.** Relation between the altitudinal terrain-level in Zackenberg Research Area exploited by muskoxen for grazing and snow cover extent on June 10. Source: Meltofte, 2002.

Although muskoxen are still present in Northeast Greenland, also their population dynamics have been shown to be particularly sensitive to the formation of ice crusts (Forchhammer and Boertmann, 1993; Hansen and Mosbech, 1994). Furthermore, the area which is used by muskoxen in the summer is related to snow cover extent (Fig. 3.2)—e.g. the altitudinal terrain-level in Zackenberg Research Area exploited by muskoxen for grazing is inversely proportional to snow cover extent. This relation is caused by the fact that snow accumulation increases more at higher altitudes in snow rich years (Paper 1). Therefore the snow-free (growing) season will start earlier in the lowland in such years, which gives earlier access to food for herbivores (Meltofte, 2002).

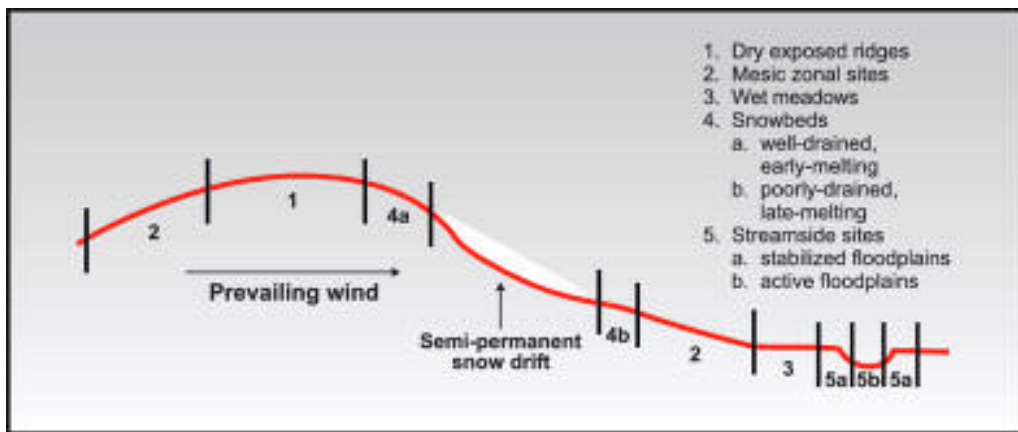
From a “bird’s perspective”, the presence/absence of snow cover is crucial for reproduction, e.g. Arctic shorebirds have to acquire resources both for egg-laying and incubation; and snow-free land is the first precondition to get this need fulfilled (Meltofte et al., 2005). This is illustrated in Fig. 3.3, which shows that egg-laying starts later in areas and years with extensive snow cover in early spring.





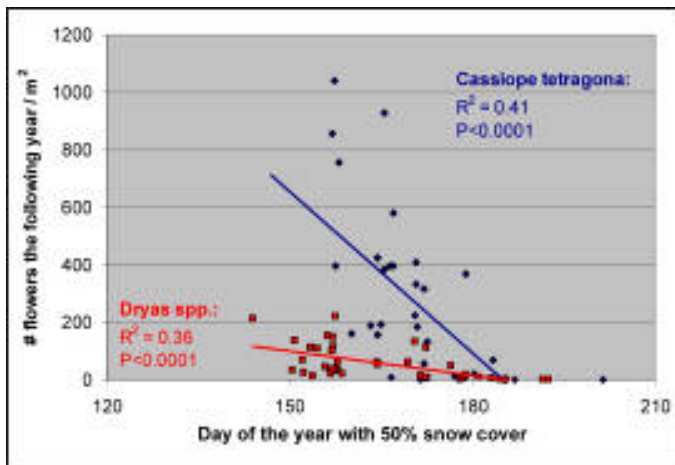
**Fig. 3.3.** First egg dates for four species of shorebirds in relation to snow coverage on June 10 in High Arctic Greenland. A) Ringed Plover, B) Turnstone, C) Dunlin, D) Sanderling. Black dots denote initial clutches, and grey dots supposed replacement clutches. Correlations for all species are statistically significant with  $p < 0.001$ . Source: Meltofte, 1985.

As opposite to the winter situation, where vegetated surfaces take advantage of the insulating properties of the snow cover, deep snow cover is a disadvantage for the vegetation in summer—except for the fact that melting snow is a source of water. Hence, the plant communities are largely distributed according to the snow cover (Böcher, 1933). This is illustrated in Fig 3.4, which is an idealized sketch of a meso-topographic gradient showing five micro-sites commonly found in arctic areas. Further information about the plant communities typically found in these micro-sites is available from the map by CAVM Team (2003) and from Walker et al. (2002).



**Fig. 3.4.** The combination of snow and small-scale topography determines distribution-patterns of plant communities. Source: CAVM Team, 2003.

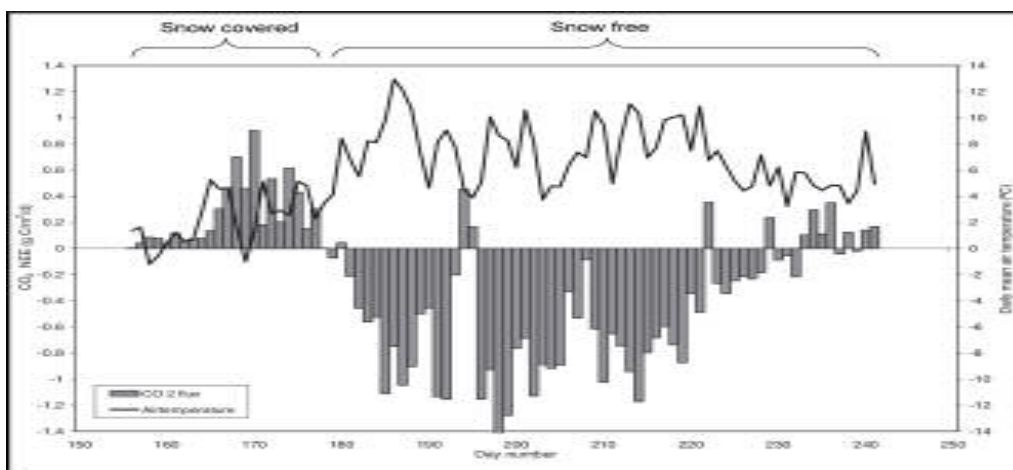
Photosynthetic activity is reliant on exposure to sunlight, and thus snow cover is decisive for the length of the growing season and thereby also for plant productivity and phenology (Paper 3). Fig. 3.5 shows the effect from snow cover on flowering for two typical species of Arctic heath vegetation at Zackenberg (*Cassiope tetragona* and *Dryas* spp.). Since flower buds are produced the previous year (Bliss and Gold, 1999; Sørensen, 1941), the number



**Fig. 3.5.** Relations between flowering and the previous year's snow melt for two typical species of Arctic heath vegetation (*Cassiope tetragona* and *Dryas* spp.).

of flowers counted one year will reflect the snow conditions in the previous growing season, i.e. the later the snow melt the previous year, the less flowers the following year.

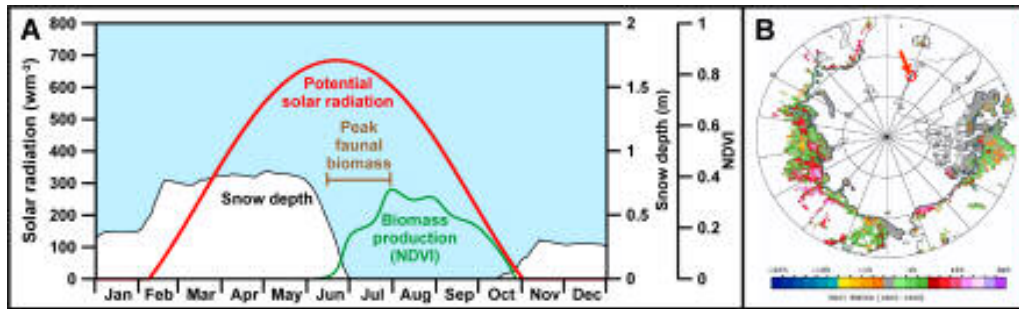
Regarding photosynthetic activity and respiration (microbial decomposition in the soil), Fig. 3.6 reveals that generally when a snow cover is present, the respiration exceeds the photosynthesis (i.e. positive Net Ecosystem Exchange), and the heath is thus a source of CO<sub>2</sub>. However during the snow-free season it is a sink. This emphasizes the importance of taking snow cover into consideration, when dealing with the carbon balance.



**Fig. 3.6.** Temporal variation in Net Ecosystem Exchange and daily mean air temperature at the heath near Zackenberg climate station in 2003. Source: Rasch and Caning, 2004.

### 3.2 Future perspectives

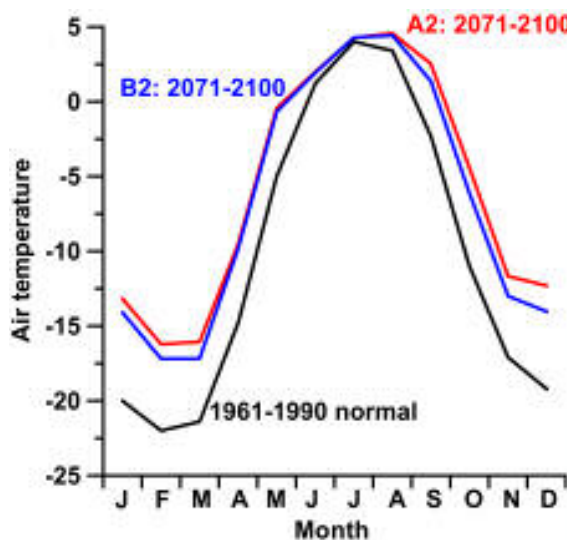
A recall of the sketch of annual bio-climatic variation the High Arctic (Fig. 3.7 (A)) and the recently observed changes in the distribution of circumpolar Normalized Difference Vegetation Index (NDVI) (Fig. 3.7 (B)) emphasizes the



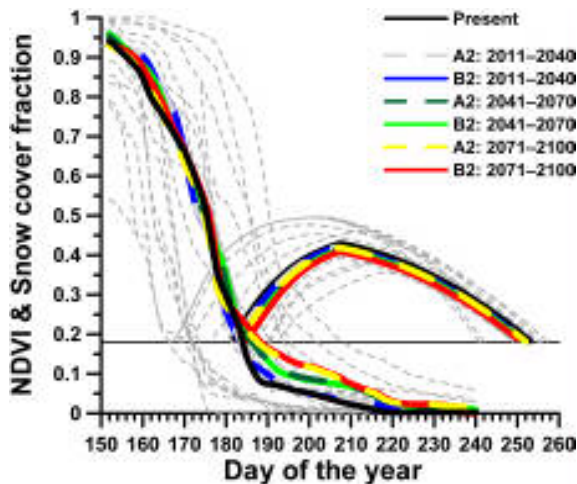
**Fig. 3.7.** (A) Seasonal characteristics of a High Arctic ecosystem. (B) Spatial distribution of “greening” trend (1982–1999) over tundra north of  $60^{\circ}\text{N}$  during the growing season (June–September). Sources: See Figs. 1.2 and 1.3.

importance of the snow-free season in High Arctic ecosystems. Especially for vegetative activity, the initiation time of this period is important (Paper 3). In the light of this and the above examples, one important question regarding the impact of possible future climatic change on snow cover and the ecology of High Arctic Northeast Greenland is: How will the snow-free season and its initiation time be affected by climate change?

Figure 3.8 shows A2 and B2 (IPCC, 2001) scenarios of monthly mean temperatures for the Zackenberg–Daneborg region in the 2071–2100 normal-period together with the observed values for 1961–1990 (Dethloff et al., 2002; Kiilsholm et al., 2003; Rysgaard et al., 2003). The model projects temperature increases between  $6.9^{\circ}\text{C}$  (A2) and  $5.9^{\circ}\text{C}$  (B2) in January and  $0.3^{\circ}\text{C}$  (A2 and B2) in July. Based on projections of future sea-ice duration, end-of-winter snow-accumulation at Zackenberg is calculated to increase by approximately 55% during the current century (Paper 4). Fig. 3.9 illustrates the expected effects of these scenarios on the snow-free period at Zackenberg in terms of snow cover depletion and NDVI, modeled on the basis of the



**Fig. 3.8.** A2 and B2 scenarios (also used in paper 4) of monthly mean air temperatures in the Zackenberg–Daneborg region for the period 2071–2100 together with the 1961–1990 temperature-climatology.



**Fig. 3.9.** Future scenarios and present state of average snow cover (also shown in Paper 4) and Normalized Difference Vegetation Index during summer at Zackenberg. Thin dashed grey lines show the observed inter-annual variability during 1988–2004 (Snow cover- and Normalized Difference Vegetation Index modeling is described in Paper 3).

methods presented in Paper 3. Temperature-input is based on A2- and B2 scenarios shown in Fig. 3.8 (periods between present time and 2071–2100 are based on interpolation, see Paper 4).

Because of increasing spring temperatures during the 21<sup>st</sup> century, snow-melt will generally start earlier at Zackenberg in the future. This combined with slightly higher summer temperatures means that spring snow clearance in large areas with uniform snow distribution will not be delayed, despite the predicted increase in winter precipitation. However, neither will it occur earlier—meaning that the combination of increased winter-precipitation and increased temperatures will have virtually no net effect on snow cover extent during the early (and for the general flora and fauna most critical) part of the melting season. However, when the later part of the season is considered, the situation is different: due to increased winter(snow)-precipitation, larger snow drifts will be formed in areas characterized by heavy snow deposition (mainly lee sides of larger features in the landscape); and these areas will thus have a prolonged melting season (Paper 4).

Due to the limited net effect on snow cover in the summer, vegetative activity (NDVI) around Zackenberg do not seem to be dramatically altered over the next 100 years (Fig. 3.9). Considering Fig. 3.7 (B) and the rather limited increase in summer temperatures, this may indicate, that in terms of NDVI Zackenberg may remain in the grey category on the figure during the next ten decades. In the winter however, significantly higher temperatures and increased precipitation amounts are expected (ACIA, 2004). It therefore seems reasonable to assume that for High Arctic ecosystems in Northeast Greenland the most dramatic effects of future climatic changes should be addressed to changes in the winter conditions (i.e. increased frequency of thaw–freeze events and thereby increased ice crust formation), rather than to changes in the summer conditions. In this context, one question of particular interest

might be: will the muskoxen in Northeast Greenland suffer the same faith over the next hundred years as did the caribou a hundred years ago?



## Chapter 4

# Concluding remarks

The aim of this thesis was to analyze snow–ecosystem relations in a High Arctic ecosystem in Northeast Greenland through the development and use of new monitoring techniques based on conventional- and multispectral digital cameras. Furthermore, it was an aim to use the results in local- to large-scale (i.e. sea-ice- and atmospheric dynamics) climatic analysis; and finally to put the results in climate change perspective. The study has been structured around four main themes:

- The development of a methodology to create time series of snow cover maps from orthographically rectified digital camera images.
- The development of methodologies to perform surface classification in a High Arctic environment based on multispectral digital orthophotos; and the usage of these in an analysis of spatiotemporal variations in snow- albedo and melt.
- Modeling, and analyzing snow–vegetation relations in a High Arctic ecosystem using camera-based snow cover- and Normalized Difference Vegetation Index-data
- Analyzing the relations between snow-precipitation in a local-scale High Arctic ecosystem and 1) large scale climate dynamics (the North Atlantic Oscillation (NAO) and sea-ice variations in the Greenland Sea) and 2) snow–ecosystem effects related to climatic change.

These four points have been dealt with mainly in the manuscripts and partly in the synopsis. The first two points mostly focus on methodological development, whereas the latter two are primarily result-oriented. To provide an overview, the main results and conclusions are summarized below.

### 4.1 Snow cover maps from digital camera images

Since 1998 digital camera images covering an area of 17 km<sup>2</sup> have been taken automatically on a daily basis from the eastern slope of the Zackenberg



Mountain. The usage of these images for snow cover mapping required the development of methods to obtain areal consistency in the images; and to detect snow-pixels in images obtained under varying conditions of illumination. To solve these tasks the images were firstly transformed into digital orthophotos at 10 m spatial resolution, and secondly, a normalized index (*RGBNDSI*) inspired by the Normalized Difference Snow Index (NDSI) was developed. This index is based on the Red, Green, and Blue components in the digital images.

Because they are obtained from 500 m altitudinal level at a distance of less than 10 km, and because they are insensitive to cloud cover above the altitude of the camera, the digital images offer both high spatial- *and* high temporal resolutions. This is a property, which cannot be achieved with satellite data, which suffer from the dilemma that temporal- and spatial resolution generally is inversely related.

The method has contributed to give a more detailed picture of snow cover depletion in the Zackenberg Research Area (ZRA) in form of snow cover depletion curves based on frequent observations of the snow cover. The shape of these curves is mainly related to the end-of-winter snow accumulation and the temperature variation during the melting season.

## 4.2 Multispectral digital camera images, Svalbard

In the summer 2002, a pilot study on using a Tetracam inc. multispectral digital camera in a High Arctic environment was performed at Ny-Ålesund, Svalbard. The introduction of this type of camera was an improvement (relative to conventional digital cameras) in relation to analysis of multiple surface types. The study showed that the normalized difference between visible and near-infrared reflectance can be used not only to classify vegetation, but also to distinguish between different types of snow (fresh, water saturated, and refrozen). Characteristic albedo values for different surface types were found from field measurements with spectroradiometer. Combining these measurements with multispectral orthophotos enabled the development of a methodology to create daily albedo maps for the Ny-Ålesund area. Based on the time series of albedo maps the duration of snow-melt was found for each pixel in the orthophotos. This duration was found to vary from around 10 days in areas close to the Ny-Ålesund settlement to more than two months in areas with heavy snow deposition or icings. Finally, as the methodology makes it possible to include the spatial distribution of both snow water equivalents (if

observations of snow-density are included) and albedo, it could be useful in future studies of hydrology and surface energy balance.

### 4.3 Monitoring and modeling snow–vegetation relations

The prevailing wind-direction in ZRA was found to be fairly constant from winter to winter; and thus also snow cover distribution in ZRA is similar in different years. Therefore, when derived as a function of melt-energy, a given snow cover depletion curve from ZRA will correspond to one, and only one end-of-winter snow accumulation. This made it possible to use digital orthophotos (obtained in six different melting seasons) to derive a data set, which reflects spatial patterns of snow cover depletion corresponding to different end-of-winter snow accumulations. On the basis of this data set, a semi-empirical modeling approach was developed to retrospectively reconstruct snow cover depletion, and snow accumulation for the period 1988–2004. The model was derived assuming that the energy available for snow melt can be expressed as the accumulation of daily mean temperatures higher than a base value. From observations of air temperature and snow melt, this value was determined to  $-2^{\circ}\text{C}$ . Because of the high frequency of temperature inversions in ZRA, it was concluded that (based on present knowledge of the area's temperature variation) model-accuracy cannot be improved by including topographic correction (using standard lapse rates) in the calculation of melt-energy. The modeled results reveal extensive inter-annual variability in both snow-precipitation amounts and snow cover extent—the accumulation has varied from less than 40 cm in some years to more than a meter in others, and the date with 50% snow coverage has varied as much as one month.

In the Arctic, vegetative activity is highly reliant on the presence/absence of snow cover. The establishment of a multispectral camera at Zackenberg gave the opportunity to analyze the relation between snow cover extent and vegetative activity (NDVI) within ZRA. The results indicated that snow cover is by far the most important parameter affecting vegetative activity in ZRA, both with respect to timing and total amount of photosynthetic activity. This enabled the usage of snow cover- and NDVI maps to interpolate a semi-empirical data set describing NDVI during green-up, as a function of snow cover and time. On the basis of this data set and the modeled snow cover, also NDVI-curves were modeled retrospectively back to 1988. Because snow cover varies extensively within ZRA, also vegetative activity varies considerably from year to year. The growing season in ZRA has varied with about four weeks

(minimum: 57 days in 1994, maximum: 89 days, 1996), and the time of maximum NDVI has varied with 20 days: from July 17 in 2004 to August 7 in 1994, whereas the mean date is July 27. The total amount of photosynthetic activity over the entire the growing season is about twice as high in growing seasons with minimum snow cover as in the seasons with the most extensive snow cover.

ZRA represents a relatively high diversity of plant-species, and in relation to summer temperatures it may be classified as representing three bio-climatic sub-zones (Northern arctic tundra zone, Middle arctic tundra zone, and Southern arctic tundra zone). This makes it reasonable to assume that some species might be adapted better to the local climate in some years, while other species might be in other years. However, there is no correlation between summer temperatures and magnitude of maximum NDVI in ZRA, and there is only a relatively limited influence from temperature on the timing of the peak vegetative activity. It was therefore concluded that the balance between summer temperatures and winter precipitation (snow cover depletion rate) may be the key parameter to predict future vegetation status in High Arctic areas like ZRA.

#### 4.4 Climate, sea-ice, snow, and effects on the ecosystem

Over the middle and high latitudes of the Northern Hemisphere the most prominent and recurrent pattern of atmospheric variability is the NAO. In the present work snow-precipitation over the North Atlantic region was derived using NCEP reanalysis precipitation rates and air temperatures in  $1.904^{\circ} \times 1.875^{\circ}$  latitude-longitude grid-cells. A running correlation analysis between the NAO and modeled snow-precipitation, using running 19-year periods, showed that end-of-winter snow accumulation in the Zackenberg region was correlated significantly to the NAO in one third of the time during 1959–2003. However, for the period 1982–2000, where the correlation was insignificant, there was a significant negative correlation between 1) sea-ice duration in the southern Greenland Sea and 2) snow-precipitation around Zackenberg. To get a more detailed picture, correlations between sea-ice duration in different sectors of the Greenland Sea and snow-precipitation around Zackenberg were calculated. This led to the identification of a “center of action” (the area with optimum correlation between sea-ice variability and terrestrial snow-precipitation), which is situated approximately 500 km north of Iceland between Greenland and the island of Jan Mayen. Sea-ice dynamics around the “center of action” are complex, and are presently not fully

understood. The complexity of ice-conditions in this region is due to several factors: inflow from external sources of ice (ice transported in the East Greenland Current, originating from the Arctic Ocean), freshwater/salinity balance, surface temperatures, and ocean currents. Due to the freezing of the cold water in the Jan Mayen Current (a branch of the East Greenland Current, passing around the southern edge of the Greenland Sea Gyre), a noteworthy feature called Odden ice tongue develops more or less significantly in different winters. It was shown that the variability in the extent of Odden is closely related to the sea-ice variation around the “center of action”, and that the sea-ice duration in the region is largely reflected in the surface air temperatures recorded at the island of Jan Mayen. It was therefore assumed that future scenarios of the surface air temperatures at Jan Mayen can be used as a proxy for the average sea-ice duration in the region in the future. For the period 2071–2100, the average end-of-winter snow accumulation at Zackenberg was calculated on the basis of the relation found between sea-ice duration and terrestrial snow-precipitation. Due to decreasing amounts of sea-ice, the result was an increase (relative to the present conditions) of 56% in winter snow-precipitation (from 68 cm to 106 cm). This corresponds well to what is predicted by a high resolution (50 km) regional climate model. It was thus concluded that sea-ice variability might play an important role in relation to snow-precipitation amounts in Northeast Greenland. The correlation analyses do not in themselves support a causal relationship between sea-ice duration and snow precipitation. However, the strikingly high correlations and the match in orders of magnitude between sea-ice based- and climate modeled snow-precipitation call for further research.

Over the 21<sup>st</sup> century, at high latitudes, GCMs predict the tendency of winter-warming to be particularly pronounced. At a first estimate, it seems reasonable to suggest that higher temperatures generally would lead to a longer growing (snow-free) season in terrestrial ecosystems. However, based on climate change scenarios (including sea-ice–snow-precipitation relations), it was shown that both temperatures and snow-precipitation can be expected to increase over the 21<sup>st</sup> century at rates, which makes the balance between melt-energy and average summer snow cover extent stay at a nearly constant level in Northeast Greenland. Due to increased spring temperatures the snow cover will start to deplete earlier, and the rather limited temperature increase in summer temperatures leaves out near neutral conditions for flora and fauna in the summer months (June–August). However, in some areas characterized by heavy snow deposition, the melting season will be prolonged. In these areas

the plant species composition may be changed in the direction of snow-bed communities.

Thus, it was concluded that the most dramatic consequences of a warmer climate on High Arctic ecosystems in Northeast Greenland will be related to changed conditions in the winter, where the most dramatic temperature increases are expected to occur. Due to increased frequency of icings and freeze-thaw events (which leads the formation of ice crusts in the snow pack); significantly warmer and more humid winters may be fatal for herbivores like lemmings and muskoxen.

## References

ACIA. Impacts of a Warming Arctic: Arctic Climate Impact Assessments. Hassol, S. J. 1-139. 2004. Canada, Cambridge University Press.

Ref Type: Report

AMAP. AMAP Assessment Report: Arctic Pollution Issues. Arctic Monitoring Assessment Programme (AMAP). xii-859. 1998. Oslo, Norway.

Ref Type: Report

Bay,C. Vegetation mapping of Zackenberg valley, Northeast Greenland. 1-29. 1998. Copenhagen, Danish Polar Center & Botanical Museum, University of Copenhagen.

Ref Type: Report

Bliss,LC, W G Gold, 1999, Vascular plant reproduction, establishment, and growth and the effects of cryptogamic crusts within a polar desert ecosystem, Devon Island, NWT, Canada: Canadian Journal of Botany-Revue Canadienne de Botanique, v. 77, p. 623-636.

Bliss,LC, N V Matveyeva, 1992, Circumpolar Arctic Vegetation, in FS Chapin, RL Jeffries, JF Reynolds, GR Shaver, J Svoboda, and EW Chu (eds), Arctic Ecosystems in a Changing Climate. And Ecophysiological Perspective.: New York, Academic Press, p. 59-89.

Böcher,TW, 1933, Studies on the vegetation of the east coast of Greenland, Meddelelser om Grønland: Copenhagen, A. Reitzels forlag , p. 1-132.

Born,EW, J Böcher, 2001, The ecology of Greenland, Atuakkiorfik Education, p. 3-429.

Cappelen,J, B V Jørgensen, E V Laursen, L S Stannius, R J Thomsen. The Observed Climate of Greenland, 1958-99 - with Climatological Standard Normals, 1961-1990. 00-18. 2001. Danish Meteorological Institute. Technical Reports.

Ref Type: Report

CAVM Team. Circumpolar Arctic Vegetation Map. Scale 1:7,500,000. [1]. 2003. Anchorage, Alaska, Conservation of Arctic Flora and Fauna (CAFF), U.S. Fish and Wildlife Service.

Ref Type: Map

Comiso, J.C., P. Wadhams, L. T. Pedersen, R. A. Gersten, 2001, Seasonal and interannual variability of the Odden ice tongue and a study of environmental effects: *Journal of Geophysical Research-Oceans*, v. 106, p. 9093-9116.

Deser, C., 2000, On the teleconnectivity of the "Arctic Oscillation": *Geophysical Research Letters*, v. 27, p. 779-782.

Dethloff, K., M. Schwager, J. H. Christensen, S. Kilsholm, A. Rinke, W. Dorn, F. Jung-Rothenhausler, H. Fischer, S. Kipfstuhl, H. Miller, 2002, Recent Greenland accumulation estimated from regional climate model simulations and ice core analysis: *Journal of Climate*, v. 15, p. 2821-2832.

DPC. ZERO annual reports 1996-2004. Meltofte, H., Thing, H., Rasch, M., and Caning, K. 2004. Danish Polar Center, Ministry of Science Technology and Innovation.

Ref Type: Report

Drange, H., 2001, Gulf Stream unlikely to shut down: *Cicero*, p. 1-6.

Driscoll, N.W., G. H. Haug, 1998, A short circuit in thermohaline circulation: A cause for northern hemisphere glaciation?: *Science*, v. 282, p. 436-438.

Elvebakk, A. Bioclimatic delimitation and Subdivision of the Arctic. <http://www.toyen.uio.no/panarctflora/papers/delimitation/delimitation.htm#Disc>. 2000.

Ref Type: Electronic Citation

Forchhammer, M., D. Boertmann, 1993, The Muskoxen *Ovibos Moschatus* in North and Northeast Greenland - Population Trends and the Influence of Abiotic Parameters on Population-Dynamics: *Ecography*, v. 16, p. 299-308.

Gray, D.M., D. H. Male, 1981, *Handbook of Snow*, Toronto, Oxford, New York, Sydney, Paris, Frankfurt, Pergamon Press.

Groisman, P.Y., T. R. Karl, R. W. Knight, 1994, Observed Impact of Snow Cover on the Heat-Balance and the Rise of Continental Spring Temperatures: *Science*, v. 263, p. 198-200.

Hall, D.K., J. Martinec, 1985, *Remote Sensing of Ice and Snow*, Cambridge: Chapman and Hall.

Hansen, B.U., A. Mosbech, 1994, Use of NOAA-AVHRR Data to Monitor Snow Cover and Spring Melt-off in the Wildlife Habitats in Jameson-Land, East Greenland: *Polar Research*, v. 13, p. 125-137.

Harding, R.J., R. C. Johnson, H. Soegaard, 1995, The Energy-Balance of Snow and Partially Snow Covered Areas in Western Greenland: *International Journal of Climatology*, v. 15, p. 1043-1058.



Hilmer,R, M Harder, P Lemke, 1998, Sea ice transport: a highly variable link between Arctic and North Atlantic: *Geophysical Research Letters*, v. 25, p. 3359-3362.

Hinkler,J, S B Pedersen, M Rasch, B U Hansen, 2002, Automatic snow cover monitoring at high temporal and spatial resolution, using images taken by a standard digital camera: *International Journal of Remote Sensing*, v. 23, p. 4669-4682.

Hurrell,JW, 1995, Decadal Trends in the North-Atlantic Oscillation - Regional Temperatures and Precipitation: *Science*, v. 269, p. 676-679.

Hurrell,JW, Y Kushnir, G Ottersen, M Visbeck, 2003, An Overview of the North Atlantic Oscillation, in JW Hurrell, Y Kushnir, G Ottersen, and M Visbeck (eds), *The North Atlantic Oscillation. Climatic Significance and Environmental impact*: Washington, DC, American Geophysical Union, p. 1-35.

HYCOM Consortium. Ocean Surface Currents. Site Index / Site Map. <http://oceancurrents.rsmas.miami.edu/site-map.html> . 2005.  
Ref Type: Electronic Citation

IPCC. *Climate Change 2001: The Scientific Basis. Contribution of Working Group I to the Third Assessment Report of the Intergovernmental Panel on Climate Change*. Houghton, J. T., Ding, Y., Griggs, D. J., Noguer, M., van der Linden, P. J., Dai, X., Maskell, K., and Johnson, C. A. 1-881. 2001. Cambridge, United Kingdom and New York, NY, USA, Cambridge University Press.  
Ref Type: Report

Johannessen,OM, L Bengtsson, M W Miles, S I Kuzmina, V A Semenov, G V Alekseev, A P Nagurnyi, V F Zakharov, L P Bobylev, L H Pettersson, K Hasselmann, H P Cattle, 2004, Arctic climate change: observed and modeled temperature and sea-ice variability: *Tellus A*, v. 56, p. 559-560.

Jones,HG, J G Pomeroy, D A Walker, D M Holland, 2001, *Snow Ecology: An Interdisciplinary Examination of Snow-covered Ecosystems*, Cambridge University Press.

Kiilsholm,S, J H Christensen, K Dethloff, A Rinke, 2003, Net accumulation of the Greenland ice sheet: High resolution modeling of climate changes: *Geophysical Research Letters*, v. 30.

Martin,T, P Wadhams, 1999, Sea-ice flux in the East Greenland Current: Deep-Sea Research Part II-Topical Studies in Oceanography, v. 46, p. 1063-1082.

Meltofte,H, 1985, Populations and breeding schedules of waders, Charadrii, in high arctic Greenland: *Meddelelser om Grønland, Bioscience*, v. 16, p. 1-44.

Meltofte,H. Sne, is og 35 graders kulde. Hvad er effekterne af klimaændringer i Nordøstgrønland? Meltofte, H. 41, 5-88. 2002. Denmark, Ministry of the

Environment, National Environmental Research Institute. TEMA-rapporter fra DMU.

Ref Type: Report

Meltofte,H, T Piersma, H Boyd, B McCaffery, B Ganter, R E Gill, V V Golovnyuk, K Graham, R I G Morrison, E Nol, H-U Rösner, D Schamel, H Schekkerman, M Y Soloviev, P S Tomkovich, D Tracy, I Tulp, L Wennerberg. Arctic shorebirds and climate: a circumpolar review of breeding conditions. *Arctic* . 2005.

Ref Type: In Press

Menoës,MC, K L Brubaker. How Similar Are Snow Depletion Curves from Year to Year? Case Study in the Upper Rio Grande Watershed. 58th EASTERN SNOW CONFERENCE, Ottawa, Ontario, Canada . 2001.

Ref Type: Abstract

Myneni,RB, C D Keeling, C J Tucker, G Asrar, R R Nemani, 1997, Increased plant growth in the northern high latitudes from 1981 to 1991: *Nature*, v. 386, p. 698-702.

Mysak,LA, D K Manak, R F Marsden, 1990, Sea-ice anomalies observed in the Greenland and Labrador seas during 1901–1984 and their relations to an interdecadal Arctic climate cycle: *Climate Dynamics*, v. 5, p. 111-113.

National Geospatial-Intelligence Agency. Sailing Directions (planning guide). Arctic Ocean. 180. 2004. Bethesda, Maryland, USA, US National Geospatial-Intelligence Agency.

Ref Type: Report

NOAA/Climate Prediction Center. North Atlantic Oscillation (NAO). <http://www.cpc.ncep.noaa.gov/data/teledoc/nao.html> . 2002.

Ref Type: Electronic Citation

NSIDC. Northern Hemisphere Snow Extent: What sensors on satellites are telling us about snow cover. The National Snow and Ice Data Center (NSIDC), University of Colorado Boulder . 2005.

Ref Type: Electronic Citation

Ohmura,A, N Reeh, 1991, New Precipitation and Accumulation Maps for Greenland: *Journal of Glaciology*, v. 37, p. 140-148.

Pedersen,LT. Sea-ice in the Greenland Sea. 2004.

Ref Type: Personal Communication

Phoenix,GK, J A Lee, 2004, Predicting impacts of Arctic climate change: Past lessons and future challenges: *Ecological Research*, v. 19, p. 65-74.

Pickart,RS, M A Spall, M H Ribergaard, G W K Moore, R F Milliff, 2003, Deep convection in the Irminger Sea forced by the Greenland tip jet: *Nature*, v. 424, p. 152-156.

- Rango,A, J Martinec, 1995, Revisiting the Degree-Day Method for Snowmelt Computations: *Water Resources Bulletin*, v. 31, p. 657-669.
- Rasch,M, K Caning. Zackenberg Ecological Research Operations, 9th Annual Report, 2003. 2004. Copenhagen, Danish Polar Center, Ministry of Science, Technology and innovation, 2004.  
Ref Type: Report
- Reynolds,JF, J D Tenhunen, 1996, Ecosystem response, resistance, resilience, and recovery in Arctic landscapes: Introduction, in JF Reynolds and JD Tenhunen (eds), *Landscape function and disturbance in Arctic Tundra*: Heidelberg, Springer, p. 3-18.
- Rudels,B, H J Friedrich, D Quadfasel, 1999, The arctic circumpolar boundary current: *Deep-Sea Research Part II-Topical Studies in Oceanography*, v. 46, p. 1023-1062.
- Rysgaard,S, T Vang, M Stjernholm, B Rasmussen, A Windelin, S Kiilsholm, 2003, Physical conditions, carbon transport, and climate change impacts in a northeast Greenland fjord: *Arctic Antarctic and Alpine Research*, v. 35, p. 301-312.
- Sanchezgomez,E, W Cabosnarvaez, M J Ortizbevia, 2002, Sea ice concentration anomalies as long range predictors of anomalous conditions in the North Atlantic basin: *Tellus Series A-Dynamic Meteorology and Oceanography*, v. 54, p. 245-259.
- Schmith,T, C Hansen, 2003, Fram Strait ice export during the nineteenth and twentieth centuries reconstructed from a multiyear sea ice index from southwestern Greenland: *Journal of Climate*, v. 16, p. 2782-2791.
- Soegaard,H, B Hasholt, T Friberg, C Nordstroem, 2001, Surface energy- and water balance in a high-arctic environment in NE Greenland: *Theoretical and Applied Climatology*, v. 70, p. 35-51.
- Sørensen,T, 1941, Temperature relations and phenology of the Northeast Greenland flowering plants, *Meddelelser om Grønland*: Copenhagen, A. Reitzels forlag.
- Stainforth,DA, T Aina, C Christensen, M Collins, N Faull, D J Frame, J A Kettleborough, S Knight, A Martin, J M Murphy, C Piani, D Sexton, L A Smith, R A Spicer, A J Thorpe, M R Allen, 2005, Uncertainty in predictions of the climate response to rising levels of greenhouse gases: *Nature*, v. 433, p. 403-406.
- Steele,M, G M Flato, 2000, Sea ice growth, melt and modeling: a survey, in EL Lewis, EP Jones, and P Lemke (eds), *The Freshwater Budget of the Arctic Ocean*: Kluwer Academic Pub, p. 533-588.

Stow,DA, A Hope, D McGuire, D Verbyla, J Gamon, F Huemmrich, S Houston, C Racine, M Sturm, K Tape, L Hinzman, K Yoshikawa, C Tweedie, B Noyle, C Silapaswan, D Douglas, B Griffith, G Jia, H Epstein, D Walker, S Daeschner, A Petersen, L M Zhou, R Myneni, 2004, Remote sensing of vegetation and land-cover change in Arctic Tundra Ecosystems: Remote Sensing of Environment, v. 89, p. 281-308.

Szalai,S. North Atlantic Oscillation (NAO).  
<http://www.atmosphere.mpg.de/enid/77d9810278d8243047762d9afacoae3b,55a304092d09/193.html> . 2003.  
Ref Type: Electronic Citation

Thompson,DWJ, J M Wallace, 1998, The Arctic Oscillation signature in the wintertime geopotential height and temperature fields: Geophysical Research Letters, v. 25, p. 1297-1300.

Tremblay,LB, 2001, Can we consider the Arctic Oscillation independently from the Barents Oscillation?: Geophysical Research Letters, v. 28, p. 4227-4230.

Tucker,CJ, D A Slayback, J E Pinzon, S O Los, R B Myneni, M G Taylor, 2001, Higher northern latitude normalized difference vegetation index and growing season trends from 1982 to 1999: International Journal of Biometeorology, v. 45, p. 184-190.

Vavrus,S, S P Harrison, 2003, The impact of sea-ice dynamics on the Arctic climate system: Climate Dynamics, v. 20, p. 741-757.

Vibe,C. Arctic Animals in Relation to Climatic Fluctuations. 1-227. 1967. The Danish Zoogeographical Investigations in Greenland.  
Ref Type: Thesis/Dissertation

Vinje,T, 2001, Fram strait ice fluxes and atmospheric circulation: 1950-2000: Journal of Climate, v. 14, p. 3508-3517.

Vinje,T, T B Loynning, I Polyakov, 2002, Effects of melting and freezing in the Greenland sea: Geophysical Research Letters, v. 29.

Vinje,T, A Rudberg, S Østerhus. Ice fluxes through Fram Strait.  
<http://www.gfi.uib.no/~svein/esop2tv.html> . 2005.  
Ref Type: Electronic Citation

Visbeck,M. North Atlantic Oscillation.  
<http://www.ldeo.columbia.edu/res/pi/NAO/> . 2004.  
Ref Type: Electronic Citation

Wadhams,P, 1999, The Odden ice tongue and Greenland Sea convection: Weather, v. 54, p. 91-97.

Wadhams,P, N R Davis, M Doble, N Hughes, A Kaletsky, J Wilkinson, Y Aksenov, L Brigham, D Flocco, R Hall, I Jonsdottir, E Harker, S Vaughan, D

Barber, S Sakai. SPRI 2000 Review 2000. Sea Ice and Polar Oceanography Group. Scott Polar Research Institute, University of Cambridge . 2003.

Ref Type: Electronic Citation

Walker,DA, W A Gould, H A Maier, M K Raynolds, 2002, The Circumpolar Arctic Vegetation Map: AVHRR-derived base maps, environmental controls, and integrated mapping procedures: *International Journal of Remote Sensing*, v. 23, p. 4551-4570.

Wallace, JM, 2000, North Atlantic Oscillation/annular mode: Two paradigms - one phenomenon: *Quarterly Journal of the Royal Meteorological Society*, v. 126, p. 791-805.

Wanner,H, S Bronnimann, C Casty, D Gyalistras, J Luterbacher, C Schmutz, D B Stephenson, E Xoplaki, 2001, North Atlantic Oscillation - Concepts and studies: *Surveys in Geophysics*, v. 22, p. 321-382.

Weltzin,JF, M E Loik, S Schwinning, D G Williams, P A Fay, B M Haddad, J Harte, T E Huxman, A K Knapp, G H Lin, W T Pockman, M R Shaw, E E Small, M D Smith, S D Smith, D T Tissue, J C Zak, 2003, Assessing the response of terrestrial ecosystems to potential changes in precipitation: *Bioscience*, v. 53, p. 941-952.

Woodgate,RA, E Fahrbach, G Rohardt, 1999, Structure and transports of the East Greenland Current at 75 degrees N from moored current meters: *Journal of Geophysical Research-Oceans*, v. 104, p. 18059-18072.

World Meteorological Organisation. WMO sea-ice nomenclature, terminology, codes and illustrated glossary. [259]. 1970. Geneva, World Meteorological Organisation. WMO/OMM/BMO.

Ref Type: Serial (Book,Monograph)

Zhou,LM, C J Tucker, R K Kaufmann, D Slayback, N V Shabanov, R B Myneni, 2001, Variations in northern vegetation activity inferred from satellite data of vegetation index during 1981 to 1999: *Journal of Geophysical Research-Atmospheres*, v. 106, p. 20069-20083.



## Appendix 1

# Data description

Location	Data-type	Description
<b>Zackenberg</b>	<i>Conventional Camera Images (CDCIs)</i> <i>Digital</i>	The conventional digital camera is a Kodak DC50 (single CCD) with a resolution of 756×504 pixels. The CCD is coated with a color array (checkerboard-style) of red, green and blue photosites. Thus each photosite on the CCD is sensitive to only one color. Interpolation algorithms creating the missing R, G and B values are applied before a bitmap image is created.
	<i>Multispectral Camera (MDCIs)</i> <i>Digital Images</i>	The multispectral camera is a Tetracam inc. single-CCD camera with a resolution of 1200×1024 pixels and a color filter array (checkerboard-style) applied to it. As for the CDCI-camera, each pixel on the CCD is sensitive to only one color. After color reconstruction (demosaicing processing using raw pixel data), the green, red, and near infrared (G, R, NIR) spectral bands approximately cover the following wavelength intervals: 520–570 nm (G), 600–690 nm (R), and 750–850 nm (NIR).
	<i>Conventional Camera Images</i> <i>Reflex</i>	In 1997 reconnaissance for camera-establishment on the eastern slope of the Zackenberg Mountain was performed. In relation to this, three images were taken in the 1997 melting season at 1997-06-13, 1997-06-23, and 1997-06-30. As for the CDCIs snow mapping, from these images, was performed using orthographic rectification and the <i>RGBNDSI</i> -algorithm (Paper 1).
	<i>Satellite data with high spatial resolution</i>	<p><b>1.</b> Landsat Thematic Mapper (TM)/Enhanced Thematic Mapper (ETM+) and <b>2.</b> Système Probatoire pour l'Observation de la Terre (SPOT) High Resolution Visible (HRV).</p> <p><b>Landsat TM/ETM+:</b> The TM-sensors record energy in seven spectral channels in the visible, reflective (near) infrared, and thermal-infrared regions of the spectrum. Wavelength-intervals of the spectral channels are: <i>ch.1: 450–520 nm, ch.2: 520–600 nm, ch.3: 630–690 nm, ch.4: 760–900 nm, ch.5: 1,550–1,750 nm, ch.7: 2,080–2,350 nm, ch.6: 10,400–12,500 nm.</i></p> <p>The spatial resolution is 30×30 m for the six reflective bands, and for the thermal band (ch.6) it is 120×120 m.</p>

		<p>The Landsat satellites orbit the Earth in Sun-synchronous near-polar orbits at an altitude of 705 km altitude. The temporal resolution (repetitive coverage) is 16 days, however, due to the polar orbit, it is slightly better at high latitudes, because overlap between satellite-scanning tracks will occur in areas close to the poles.</p> <p><b>SPOT HRV:</b> The HRV sensors operate in the visible and near infrared parts of the spectrum in three spectral bands: ch.1: 500–590 nm, ch.2: 610–680 nm, ch.3: 790–890 nm. Like Landsat, the SPOT-satellites orbit the Earth in Sun-synchronous near-polar orbits—the altitude is 832 km, and the spatial resolution is 20×20 m at nadir (when the sensors are viewing directly below the spacecraft); in panchromatic mode the spatial resolution is 10×10 m. If the HRV instruments were only capable of nadir viewing the temporal resolution would be 26 days. However, through commands from the ground stations, it is possible to point the mirrors to off-nadir view angles. This can increase the temporal resolution to as good as about five days, but of course with decreased spatial resolution.</p> <p>A more comprehensive description of the TM and SPOT systems can be found in (Jensen, 1996).</p> <p><b>Atmospheric correction:</b></p> <p>In connection with this work, TM and SPOT data were atmospherically corrected with the ATCOR2 algorithm (Richter, 1996).</p>
	<p><i>Satellite data with coarse spatial resolution</i></p>	<p>Normalized Difference Vegetation Index NDVI in Fig. 1.1 is derived from bi-weekly maximum-composites based on <i>AVHRR Polar Pathfinder data</i> with 1.25 km spatial resolution (Scambos et al., 2000). The Pathfinder data are provided by the National Snow and Ice Data Center (NSIDC), Boulder, Colorado, USA, and are derived from Advanced Very High Resolution Radiometer (AVHRR) satellite data from the National Oceanic and Atmospheric Administration (NOAA). NDVI are calculated using AVHRR ch.1: 580–680 nm (visible) and ch.2: 725–1,050 nm (near infrared): <math>(ch.2 - ch.1) / (ch.2 + ch.1)</math></p> <p>The 1.25 km pathfinder data are thoroughly documented at <a href="http://nsidc.org/data/docs/daac/nsidco065_avhrr_1.25km.gd.html">http://nsidc.org/data/docs/daac/nsidco065_avhrr_1.25km.gd.html</a></p>
	<p><i>Air temperatures</i></p>	<p>Since July 1995, air temperatures have been recorded hourly at the main Automatic Weather Station (AWS) at Zackenberg. The sensor is placed 2 m above the surface, and the position of the AWS is about 30 m above sea-level. In August 2003 an additional AWS was established approximately 400 m above sea level, also measuring at 2 m above the</p>



		terrain. A technical description of the temperature sensors can be found in (Misissueqqaarnerit, 1995).
	<i>Measured snow depths</i>	Snow depths have been measured automatically with a sonic range sensor at the main AWS since August 1997. With sound it measures the distance between the sensor head and the snow-surface. The decreasing/increasing distance between the surface and the sensor head during accumulation/melt can then easily be converted to snow-depths.
	<i>Wind speed and wind direction.</i>	Wind speed and direction have been measured since July 1995 at 2 m/7.5 m and 7.5 m above the terrain, respectively. Technical descriptions of the sensors can be found in (Misissueqqaarnerit, 1995).
	<i>Field measurements of Normalized Difference Vegetation Index (NDVI)</i>	<p>Since 1999 NDVI has been measured regularly in 26 different plots, which represent the 4 main types of vegetation present in the Zackenberg Valley (Cassiope, Dryas, Salix, and Eriophorum). The measurements were performed using a Skye 110 instrument with a 660–730 nm sensor. The sensor measures RVI which is defined: near infrared / red.</p> <p>NDVI is defined: <math>(\text{near infrared} - \text{red}) / (\text{near infrared} + \text{red})</math>.</p> <p>Thus, <math>\text{NDVI} = (1 - \text{RVI}) / (1 + \text{RVI})</math>.</p> <p>Further information about the Skye sensors are available at: <a href="http://www.skyeinstruments.com/2Channel.htm">http://www.skyeinstruments.com/2Channel.htm</a>.</p>
<b>Daneborg</b>	<i>Air temperatures</i>	<p>Daily mean air temperatures for the period 1988–1998, and monthly means for 1958–1999 were provided by the Danish Meteorological Institute. The weather station is situated 44 m above sea level.</p> <p>The monthly data are part of the data set used in Cappelen et al., (2001), and is available from <a href="http://www.dmi.dk/dmi/troo-18-data_files.zip">http://www.dmi.dk/dmi/troo-18-data_files.zip</a>. The report is available from <a href="http://www.dmi.dk/dmi/troo-18.pdf">http://www.dmi.dk/dmi/troo-18.pdf</a>.</p>
	<i>Measured snow depths</i>	Snow depths have been measured at Daneborg during 1958–1975. The monthly means and maxima are available from Cappelen et al., (2001), see description above.
<b>Jan Mayen</b>	<i>Air temperatures</i>	Air temperatures from Jan Mayen were provided by the Norwegian Meteorological Institute—Det Norske Meteorologiske Institut (DNMI). Observations are recorded 2 m above the terrain, and the weather station is located 10 m above sea level.

<p><b><i>Ny-Ålesund</i></b></p>	<p><i>Multispectral Camera (MDCIs)</i>      <i>Digital Images</i></p>	<p>Properties of the RDCIs obtained at Ny-Ålesund, Svalbard May 22–August 14, 2002 are equivalent to what is described above for MDCIs taken at Zackenberg.</p>
	<p><i>Spectral reflectance</i>      <i>surface</i></p>	<p>Spectral field data were collected during May–August, 2002. Measurements were performed with a Fieldspec FR spectroradiometer (analytical spectral devices) measuring from 350 to 2500 nm. It consists of three built-in separate spectrometers. The first one measures from 350 to 1000 nm using a 512 element photodiode array, and has a spectral resolution of about 3 nm. The second and third ones are of scanning types and measure from 900 to 1850 nm and 1700 to 2500 nm, respectively sampling every 2 nm, with a spectral resolution of about 10 ±11 nm. Results presented here primarily use data from the first spectrometer covering the visible/near-infrared (VNIR) wavelength range from 350 to 1050 nm. The optical detector (which simply consists of the bare optical fiber with an adapter limiting the field of view to 18) was fastened to a standard camera tripod to avoid movements during the less than one-second integration time of the measurement, and measurements were acquired 50 cm above the surface of interest. The spectral albedo was determined as the ratio of incident solar radiation reflected from the surface target and the incident radiation reflected from a calibrated white reference Spectralon plate (about 30×30 cm). Both the spectroradiometer and the reference Spectralon were calibrated at the optical calibration lab in Ny-Ålesund to “NIST traceable reference lamps and spectralons”.</p>
<p><b><i>Greenland Sea</i></b></p>	<p><i>Satellite-based sea-ice concentrations</i></p>	<p>Daily sea-ice concentrations (1981–2000) are extracted from the surface maps that comes along with the 5 km AVHRR Polar Pathfinder data (Fowler et al., 2000), that are available the NSIDC at <a href="http://nsidc.org/data/nsidc-0066.html">http://nsidc.org/data/nsidc-0066.html</a>. The ice concentrations are derived from the 25 km spatial resolution Scanning Multichannel Microwave Radiometer (SMMR) (before 1987) and Special Sensor Microwave/Imager (SSM/I) (1987 and after) using the NASA Team algorithm (Cavalieri, 2005). This algorithm is designed to provide a consistent time series of sea ice concentrations (the fraction of ocean area covered by sea ice) spanning the coverage of several passive microwave instruments.</p> <p><b>Main sources of error:</b></p> <p>Errors in the derived sea ice concentrations arise from several sources. In order of importance, these are 1) the inability of the algorithm to discriminate among more than two radiometrically different sea ice types, 2) seasonal variations in sea ice</p>

		<p>emissivity, 3) non-seasonal variations in sea ice emissivity, and 4) weather effects at concentrations greater than about 15%, and 5) random and systematic instrument error.</p> <p>A comprehensive description of the algorithm and sources of error can be obtained from (Cavalieri, 2005).</p>
<b>North Atlantic region</b>	<i>NCEP reanalysis data: surface air temperatures &amp; precipitation rates</i>	<p>Daily values (1958–2003) of surface level temperature and precipitation rates modeled in 1.904°×1.875° latitude-longitude grid-cells were from NCEP reanalysis project at the NOAA-CIRES Climate Diagnostics Center. The data used in this study is obtained in pure ASCII form through <a href="http://www.cru.uea.ac.uk/cru/data/ncep/">http://www.cru.uea.ac.uk/cru/data/ncep/</a>.</p> <p>Comprehensive descriptions of the NCEP reanalysis forecasting models can be found through <a href="http://www.cdc.noaa.gov/cdc/reanalysis/">http://www.cdc.noaa.gov/cdc/reanalysis/</a></p>

## References

Cappelen,J, B V Jørgensen, E V Laursen, L S Stannius, R J Thomsen. The Observed Climate of Greenland, 1958-99 - with Climatological Standard Normals, 1961-1990. 00-18. 2001. Danish Meteorological Institute. Technical Reports.

Ref Type: Report

Cavalieri,DJ. NASA Team Sea Ice Algorithm.

<http://nsidc.org/data/docs/daac/nasateam/> . 2005. National Snow and Ice Data Center (NSIDC).

Ref Type: Electronic Citation

Fowler,C, J Maslanik, T Haran, T Scambos, J Key, W Emery. AVHRR Polar Pathfinder twice-daily 5 km EASE-Grid composites. 2000. Boulder, CO, USA, National Snow and Ice Data Center.

Ref Type: Data File

Jensen,JR, 1996, Remote Sensing Data Acquisition Alternatives, in JR Jensen (ed), Introductory Digital Image Processing. A Remote Sensing Perspective: Upper Saddle River, NJ, USA, Prentice-Hall, Inc., p. 17-64.

Misissueqqaarnerit. Klimastation Zackenberg. Teknisk beskrivelse. A1782. 1995. Nuuk, Greenland, Misissueqqaarnerit.

Ref Type: Report

Richter,R. A Spatially—Adaptive Fast Atmosperic Correction Algorithm—Aacor2 User Manual. 1996. Wessling, Germany, Institute for Optoelectronics.

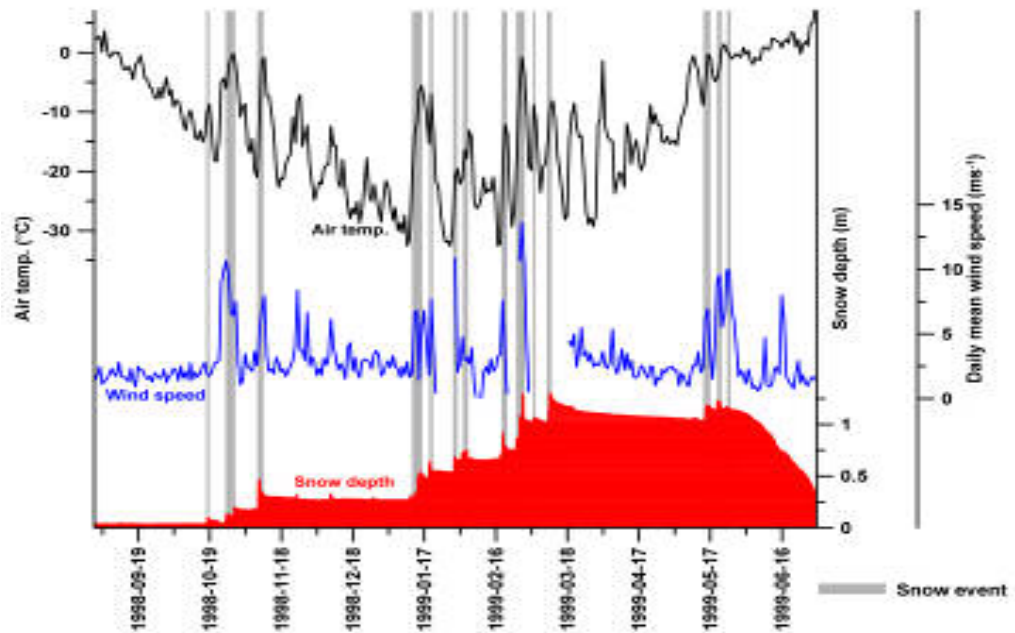
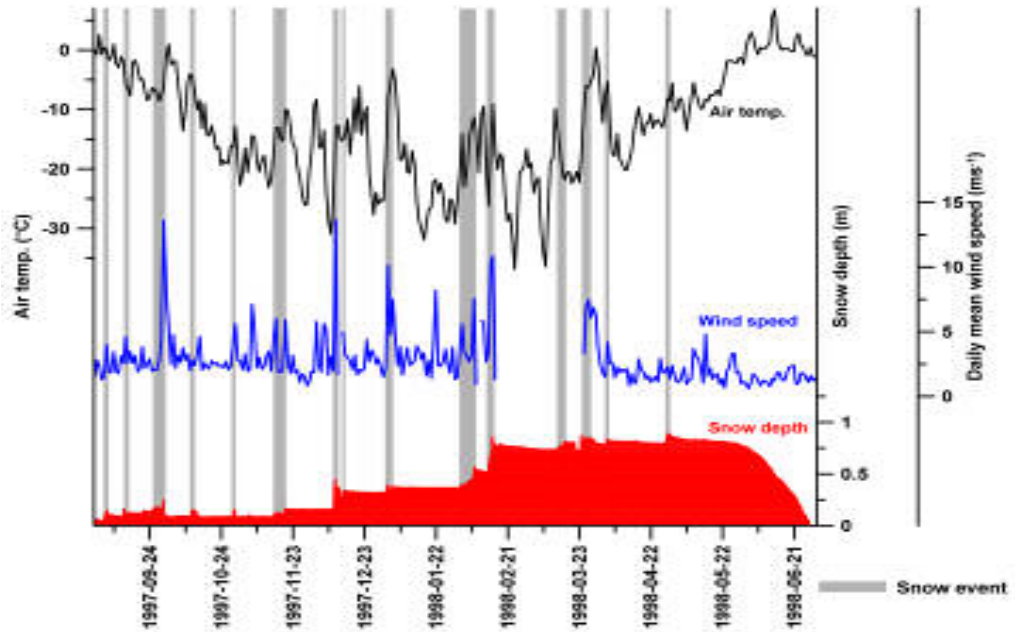
Ref Type: Report

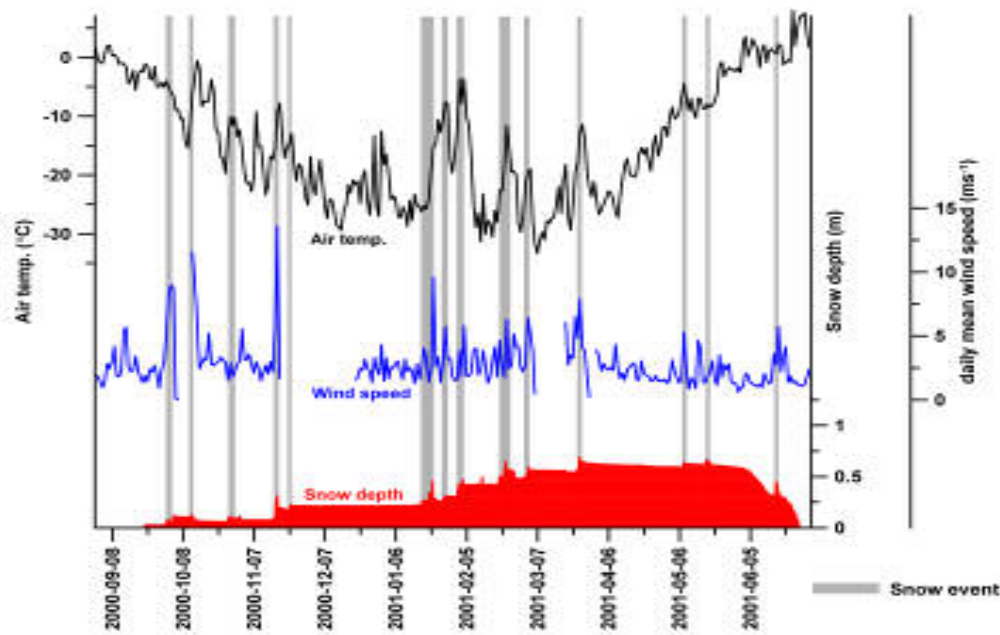
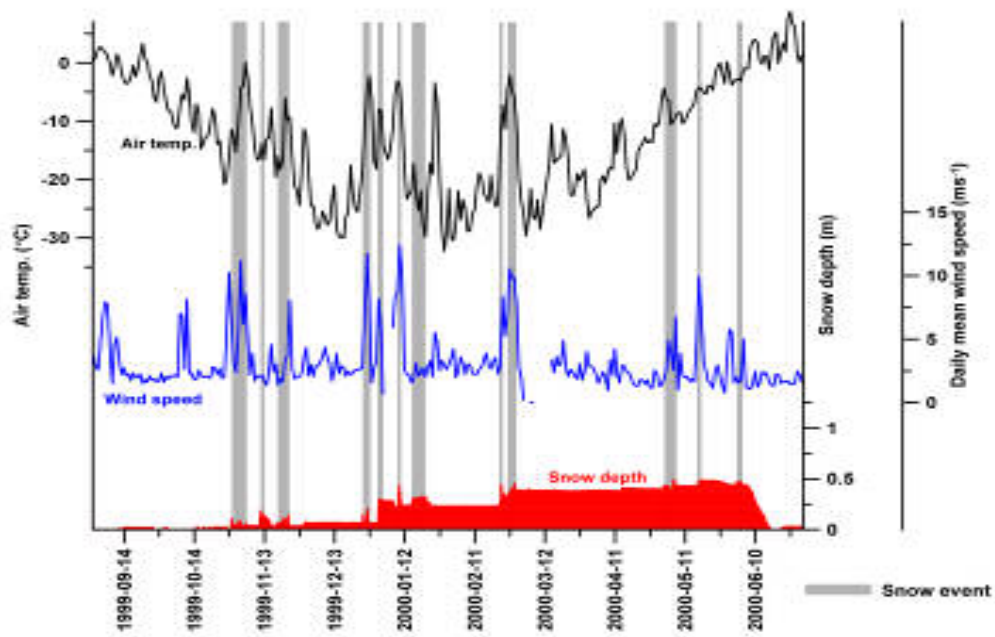
Scambos, T, T Haran, C Fowler, J Maslanik, J Key, W Emery. AVHRR Polar Pathfinder twice-daily 1.25 km EASE-Grid composites. 2000. Boulder, Colorado, USA, National Snow and Ice Data Center (NSIDC).  
Ref Type: Data File

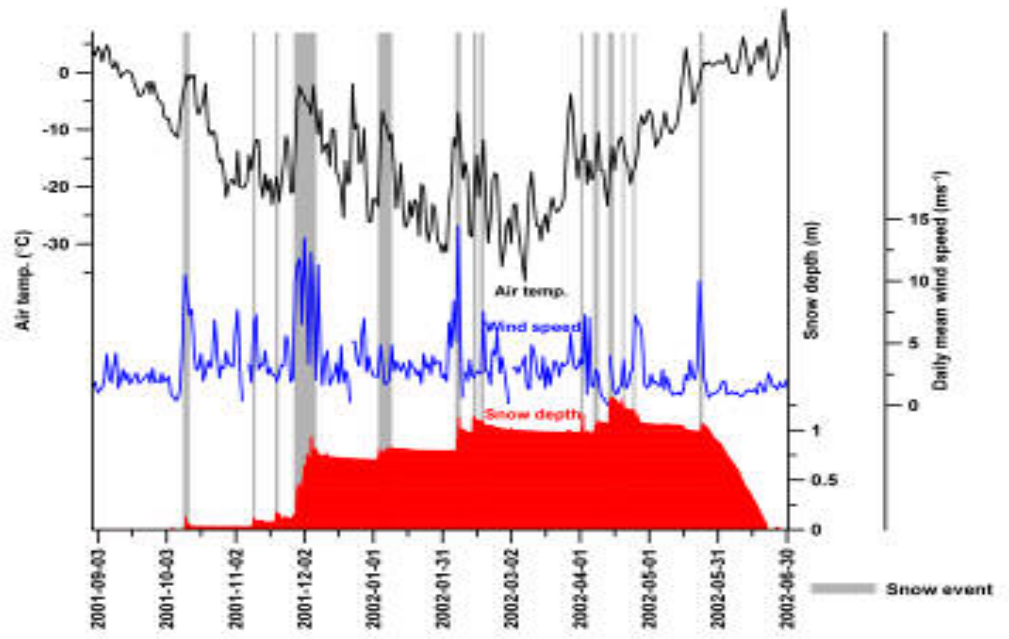
## Appendix 2

# Additional figures & tables

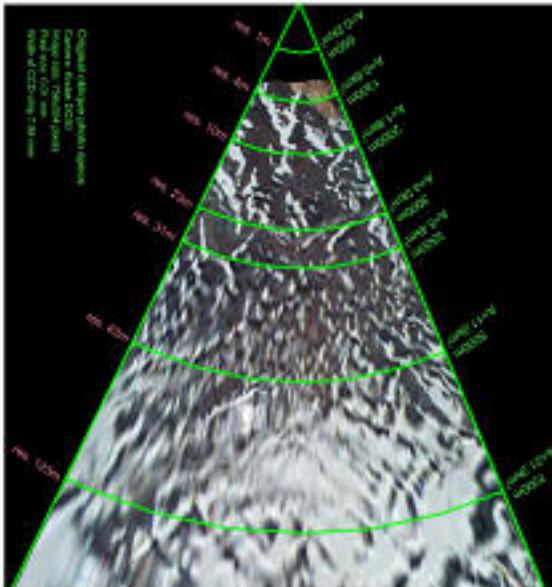
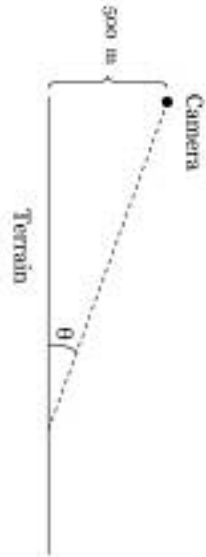
### A.2.1 Snow wind and temperature at Zackenberg 1997–2002







A.2.2 Change of spatial resolution with distance—conventional digital orthophotos based on oblique images taken with a Kodak DC50



Maximum theoretical "true" pixel sizes along and across line of sight, assuming a flat horizontal terrain.	Maximum theoretical "true" pixel sizes along and across line of sight, assuming a flat horizontal terrain.	Maximum theoretical "true" pixel sizes along and across line of sight, assuming a flat horizontal terrain.	Maximum theoretical "true" pixel sizes along and across line of sight, assuming a flat horizontal terrain.	Maximum theoretical "true" pixel sizes along and across line of sight, assuming a flat horizontal terrain.	Maximum theoretical "true" pixel sizes along and across line of sight, assuming a flat horizontal terrain.	Maximum theoretical "true" pixel sizes along and across line of sight, assuming a flat horizontal terrain.	Maximum theoretical "true" pixel sizes along and across line of sight, assuming a flat horizontal terrain.	Maximum theoretical "true" pixel sizes along and across line of sight, assuming a flat horizontal terrain.	Maximum theoretical "true" pixel sizes along and across line of sight, assuming a flat horizontal terrain.
Altitude position of camera (m)	Focal length of lens (m)	width of CCD chip (m)	Image Scan (pixels)	750x504					
500	0.009	0.00756							
500	0.63	0.63	korvus - panoramic	45.00	0.79				
600	0.81	1.46	korvus - panoramic	37.57	0.66				
1000	1.25	2.50		26.57	0.45				
1200	1.63	4.23	korvus - multiplex	21.04	0.37				
2000	2.50	16.88	SPOT - panoramic	14.04	0.24				
2600	3.75	22.50	SPOT - multiplex	8.46	0.17				
2800	4.38	26.83	Landisec TM (ch. 1-5 & 7)	8.33	0.16				
4000	5.00	40.00		7.43	0.12				
5600	6.25	62.50	Landisec 7 ch. 6	5.71	0.10				
6000	7.50	90.00		4.76	0.08				
7000	8.75	122.50	Landisec TM (ch. 6)	4.09	0.07				
18000	12.50	250.00	Mosaic	2.86	0.05				
26000	25.00	5950.00	NOAA AVHRR	1.43	0.02				



## A.2.3 Sea-ice types

	<b>Subtype</b>	<b>Description</b>
<b>New ice</b> (thickness < 10 cm)	<i>Frazil ice</i>	Fine spicules or plates of ice, suspended in water.
	<i>Grease ice</i>	A later stage of freezing than frazil ice when the crystals have coagulated to form a soupy layer on the surface. Grease ice reflects little light, giving the surface a matt appearance.
	<i>Slush</i>	Snow which is saturated and mixed with water on land or ice surfaces, or as a viscous floating mass in water after heavy snowfall.
	<i>Shuga</i>	An accumulation of spongy white lumps, a few centimeters across; they are formed from grease ice or slush and sometimes from anchor ice rising to the surface.
	<i>Nilas</i>	A thin elastic crust of ice, easily bending on waves and swell and under pressure, thrusting in a pattern of interlocking "fingers" (finger rafting). Has a matt surface and is up to 10 cm in thickness. May be subdivided into dark nilas and light nilas.
	<i>Pancake ice</i>	Predominantly circular pieces of ice from 30 cm–3 m in diameter, and up to 10 cm in thickness (unrafted), with raised rims due to the pieces striking against one another. It may be formed on a slight swell from grease ice, shuga or slush or as the result of the breaking of ice rind, nilas or, under severe conditions of swell or waves, of grey ice.
<b>Young ice</b> (10 cm < thickness < 30 cm)	<i>Grey ice</i>	Young ice 10–15 cm thick. Less elastic than nilas and breaks on swell. Usually rafts under pressure.
	<i>Grey-white ice</i>	Young ice 15–30 cm thick. Under pressure more likely to ridge than to raft.
<b>First-year ice</b>	<i>Thin first-year or white ice</i>	30–70 cm thick
	<i>Medium first-year ice</i>	70–120 cm thick
	<i>Thick first-year ice</i>	More than 120 cm thick
<b>Old ice</b>	<i>Second-year ice</i>	Old ice which has survived only one summer's melt. Because it is thicker and less dense than first-year ice, it stands higher out of the water. In contrast to multi-year ice, summer melting produces a regular pattern of puddles. Bare patches and puddles are usually greenish-blue.
	<i>Multi-year ice</i>	Old ice up to 3 m or more thick which has survived at least two summers' melt. Hummocks (hillocks of broken ice that have been forced up by pressure) even smoother than in second-year ice, and the ice is almost salt-free. Color, where bare, is usually blue. Melt pattern consists of large interconnecting irregular puddles and a well-developed drainage system.
<b>Fast ice</b>	<i>Various</i>	Sea-ice which forms and remains fast along the coast, where it is attached to the shore, to an ice wall, to an ice front, between shoals or grounded icebergs. Vertical fluctuations may be observed during changes of sea-level. Fast ice may be formed in situ from sea water or by freezing of pack ice of any age to the shore, and it may extend a few meters or several hundred kilometers from the coast. Fast ice may be more than one year old and may then be prefixed with the appropriate age category (old, second-year, or multi-year).

World Meteorological Organization. *WMO sea-ice nomenclature, terminology, codes and illustrated glossary*. [259]. 1970. Geneva, World meteorological Organization.

WMO/OMM/BMO. Ref Type: Serial (Book, Monograph)



## Appendix 3

### Conferences and meetings

- Hinkler, J., Hansen, B. U., Tamstorf, M. P., Meltofte, H., *Linkage between sea-ice distribution and snow-precipitation may considerably affect terrestrial ecosystems in future High Arctic climates*. Presented at: The ACIA International Scientific Symposium on Climate Change in the Arctic, Reykjavik, Iceland. November 9-12, 2004. Extended abstract available in section A.3.1.
- Hinkler, J., *Snow-precipitation at Zackenberg and climatic relations—with special emphasis on regional sea-ice variations*. Presented at: Zackenberg Ecological Research Operations' Workshop, Raadvad, Copenhagen, Denmark. April 17-18, 2004.
- Hinkler, J., *Snow cover monitoring in Northeast Greenland—based on orthophotos derived from standard digital camera images*. Presented at: The North Park Snow Workshop, NCAR Mesa Lab, Boulder Colorado, USA. November 6-7, 2003.
- Hinkler, J., Hansen, B. U., Tamstorf, M. P., *Sea ice and snow accumulation modelling in High Arctic Greenland*. Presented at: Northern research basins, 14<sup>th</sup> International Symposium and Workshop, Kangerlussuaq/Sdr. Strømfjord, Greenland. August 25-29, 2003. Proceeding paper available in section A.3.2. Also available from: <http://www.geogr.ku.dk/projects/nrb14/abstracts/HinklerJ.doc>.
- Hinkler, J., *Digital snow monitoring in a high arctic ecosystem in Northeast Greenland*. Presented at: Temadag om Grønlands klima at Danish Meteorological Institute, Copenhagen, Denmark. December 16, 2002.
- Hinkler, J., Ørbæk, J.B., Hansen, B.U., *Detection of spatial, temporal, and spectral surface changes in the Ny-Ålesund area 79° N*,

*Svalbard—using a low cost multispectral camera in combination with spectroradiometer measurements.* Presented at: Sixth Ny Ålesund International Scientific Seminar, Tromsø, Norway. October 8-10, 2002. Extended abstract available in section A.3.3.

- Hinkler, J., Pedersen, S.B., Hansen, B.U., Tamstorf, M.P, *A spatiotemporal analysis of the snow cover in a High Arctic environment, Zackenbergdalen Northeast Greenland.* Presented at: The Seventh Circumpolar Symposium on Remote Sensing of Polar Environments, Longyearbyen, Svalbard, Norway. June 24-27, 2002.
- Hinkler, J., *Digital snow monitoring in a high arctic ecosystem in Northeast Greenland.* Presented at: Arktisk Biologisk Forskermøde IX, Århus, Denmark. March 15, 2002.
- Hinkler, J., *Snow mapping - using Remote Digital Cameras (RDC).* Presented at: SCANNET's first annual meeting, Torshavn, Faeroe Islands. November 14-18 , 2001.
- Hinkler, J., Pedersen, S.B, *Automatic snow cover monitoring at high temporal and spatial resolution - using images taken by a standard digital camera.* Presented at: The Sixth Circumpolar Symposium on Remote Sensing of Polar Environments, Yellowknife, Canada. June 12-14, 2000. Paper 1, published in International Journal of Remote Sensing, vol. 23, 21, November 10, 2002.

*A.3.1 Extended abstract—ACIA Symposium, Reykjavik, Iceland, 2004***Linkage between sea-ice distribution and snow-precipitation may considerably affect terrestrial ecosystems in future High Arctic climates**

Jørgen Hinkler, Birger U. Hansen, Mikkel P. Tamstorf & Hans Meltofte

Main author's addresses and email:

1) Øster Voldgade 10  
University of Copenhagen, Institute of Geography  
DK-1350 Copenhagen K, Denmark

2) PO Box 358  
National Environmental Research Institute, Department of Arctic Environment  
DK-4000 Roskilde, Denmark

E-mail: [jh@geogr.ku.dk](mailto:jh@geogr.ku.dk)

**1. Introduction**

The Intergovernmental Panel on Climate Change (IPCC)'s Third Assessment Report (TAR) (2001) gives projections for global-mean warming from 1990 to 2100 within a range of 1.4° to 5.8°C in the case that no measures are taken to limit climate change. Further, research demonstrates that based on this assumption, a global-mean temperature increase around 3°C by the end of the 21<sup>st</sup> century is the most likely; and that probabilities of global-mean warming values at both the high and low ends of the TAR range [1.4°C, 5.8°C] are very low (Wigley and Raper, 2001). General Circulation Models (GCM) predict global warming to be most pronounced at high latitudes, especially during winter time when temperature increases of up to 6°C can be expected by the end of the 21<sup>st</sup> century (Hadley Centre, Max Planck Institute of Meteorology).

Arctic ecosystems are strongly influenced by snow cover and temperature, and may be expected to be markedly altered by climate change (Phoenix and Lee, 2004; Stone et al., 2002; Weller, 1998). Besides increases in winter temperatures in the Arctic, decreases in sea-ice extent are expected to occur correspondingly (Johannessen et al., 2004), which may significantly influence the regional climate. Here we present an empirical analysis from Northeast Greenland, which shows that reduced amounts of sea-ice in the region will most likely lead to increased snow-precipitation. Due to a shorter snow-free season this might have consequences for High Arctic ecosystems that at a first estimate are unexpected in a future warmer climate.

**2. Methods and Analysis**

We have calculated end-of-winter snow-precipitation amounts at two different scales – local and regional, using two different modeling approaches: The first approach, which is used at local scale (covering 12 years: 1988-2000, except 1990) exploited data from Zackenberg Research Area (ZRA), Northeast Greenland (74.5°N, 21.6°W) obtained during the melting season (June-August). It is based on snow cover maps derived from remotely sensed image data, melt energy inferred from daily mean air temperatures, and measured snow depths. The image data types are digital orthophotos covering approximately 17 km<sup>2</sup> (Hinkler et al., 2002), and high resolution satellite images (Landsat Thematic Mapper (TM) & SPOT High Resolution Visible (HRV)). Daily mean temperatures are from automatic weather stations at Zackenberg and Daneborg (located 23 km southeast of Zackenberg). The second modeling approach is used at regional scale and deals with relative humidity and temperature (Liston and Sturm, 1998) during winter time (October-May). It simply assumes that snow-precipitation falls when the air temperature is below freezing and the relative humidity is greater than 80%. For this purpose we used daily values (air temperature and relative humidity) during 1981-2000 of a 2.5°×2.5° lat-long-grid-cell from the National Centre for Environmental Prediction (NCEP) reanalysis project. The spatial coverage of the grid-cell is approximately 21,000 km<sup>2</sup> (Fig. 1). The least-squares fit, reveals that the local snow-precipitation at Zackenberg is significantly correlated with what is modeled at a much larger scale. However, it also reveals that local snow-precipitation in some winters can differ significantly from regional precipitation. This is probably because the area is characterized by strong topography, which complicates the local wind patterns and thereby also precipitation distribution.

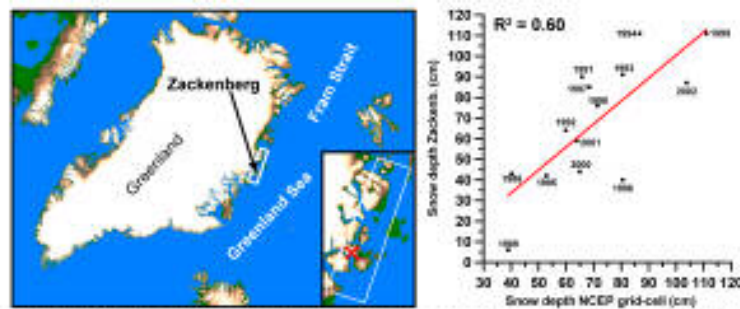


Fig. 1. (Left) Location of the Zackenberg Research Area (red cross). The rectangular area indicated by white lines corresponds to the 2.5°x2.5° lat-long grid cell (21,000 km<sup>2</sup>) from the NCEP reanalysis data, which includes the Zackenberg Research Area (ZRA). (Right) Modeled snow depths: ZRA versus entire area in NCEP grid cell (Normalized to Zackenberg, 1999).

To analyze the relation between duration of periods with extensive sea-ice within the Greenland Sea and snow-precipitation at Zackenberg we analyzed more than 8000 sea-ice maps derived from SSM/I passive microwave satellite data (Fowler et al., 2000). We divided the Greenland Sea into 4 main regions based on direction from ZRA, and each of them was further divided into 5 sub-regions based on distance from ZRA (Fig. 2). For each season (December-August), and each of the 20 regions, the time-duration (number of days with sea-ice percentage above a certain threshold) was calculated and compared to the end-of-winter snow accumulation at ZRA. To validate our results we calculated correlation-coefficients between snow accumulation and sea-ice extent using end-of-winter snow accumulations calculated from both of the above mentioned approaches. The correlation between sea-ice extent within the Greenland Sea and snow accumulation around ZRA is visualized spatially in Fig. 2. All of the regions show an inverse relationship between extensive sea-ice duration and snow accumulation (the more sea-ice the lesser the snow accumulation and vice versa), and the further one goes to the south and southeast the higher the correlation. This pattern seems to be evident (see the tables in Fig. 2) no matter which of the snow modeling approaches applied. The highest correlation occurs in the SSE region when ice-data up till a distance of 750 km from ZRA are included. This leads us to the conclusion that a “center of action”, which highly influences winter-precipitation amounts in Northeast Greenland is centered within this region – around 500 km north of Iceland between Greenland and the Island of Jan Mayen.

### 3. Discussion/perspectives

With the prospect of decreasing sea-ice off Northeast Greenland in the future, this study shows that more snow-precipitation can be expected on land. Since limited snow cover and large snow free areas today is an important precondition for the High Arctic “desert” of North and Northeast Greenland, increased snow cover in combination with increased frequency of thaw events will alter the conditions in the direction of present-day Low Arctic Southeast Greenland. For flora and fauna this would mean increased vegetation cover on presently barren lowlands, but also difficulties for herbivores from lemmings to musk oxen due to melting snow and rain in winter resulting in ice crust formation. If summer temperatures, as predicted, do not increase noteworthy, the heavier snow pack may delay spring snow clearance in High Arctic Greenland, as opposite to the predicted prolongation of the growing season in most of the Arctic. This will delay the reproductive phenology and thereby the success of many species ranging from plants to shorebirds (Meltøfte 2002). If on the contrary, summer temperatures do increase significantly, the High Arctic tundra and desert may transform into Low Arctic tundra, leaving the High Arctic habitat only as an alpine zone in mountainous areas (Meltøfte et al. 2003).

At the time of writing there are still questions that need to be clarified. Thus, more research has to be done in order to explain what mechanisms actually affect the sea-ice distribution within the regions of high correlation. Teleconnection patterns such as the Arctic and North Atlantic Oscillations (AO and NAO) do not seem to explain ice cover variations in these regions very well, and neither does modeled sea-ice fluxes through the Fram Strait (Schmith and Hansen, 2003). However, as the sea-ice distribution in the Greenland Sea is influenced by both local ice formation and a large ice-flux from the Arctic Ocean into the East Greenland Current, it cannot be generalized at a larger scale. Therefore, it might be that sea-ice formation and distribution in the southern Greenland Sea should be addressed to other (more local) factors such as the so called Odden ice tongue phenomenon (Wadhams, 1999) and/or atmosphere-ocean interactions. In this connection e.g. the position of the ice edge plays a crucial role in the formation of polar lows (Rasmussen et al., 1992).



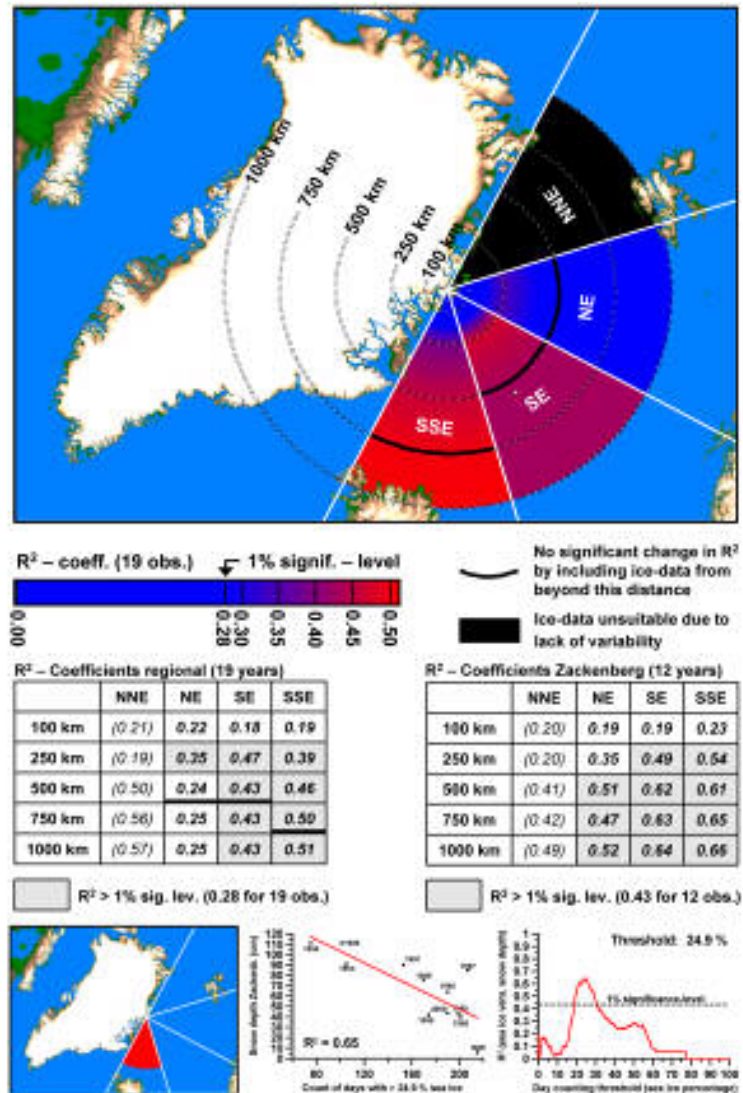


Fig. 2. Spatial distribution of the correlation between (1) end-of-winter snow-precipitation amount in the Zackenberg Region (21,000 km<sup>2</sup> – regional scale) and (2) the number of days during December to August with sea-ice percentage above a critical threshold (which differs from sub-sector to sub-sector). The Greenland Sea is divided into four sectors based on direction seen from Zackenberg Research Station (ZRA): NNE, NE, SE, SSE, and each sector is further divided into five sub-sectors based on distance from ZRA: 0-100 km, 0-250 km, 0-500 km, 0-750 km, and 0-1000 km (note that a smaller sub-sector is always included in a larger sub-sector). The tables display R<sup>2</sup> coefficients of a least squares fit between end-of-winter snow-precipitation amounts (at regional and local scales, respectively) and duration of periods with extensive sea-ice. At the bottom, the sub-region (750 km SSE) that gives the highest correlation between snow-precipitation and time-duration of extensive sea-ice is shown. The linear fit in the middle is based on local scale snow modeling over 12 years, and the diagram to the right shows that in this case a threshold of 24.9% (number of days during December-August with more than 24.9% sea-ice cover), gives the optimum correlation for the region in question (here SSE, 750 km sub-sector).

**References Cited**

- Fowler C, J Maslanik, T Haran, T Scambos, J Key, W Emery, 2000, AVHRR Polar Pathfinder twice-daily 5 km EASE-Grid composites. Boulder, CO, USA: National Snow and Ice Data Center. Digital media.
- Hinkler J, SB Pedersen, M Rasch, BU Hansen, 2002, Automatic snow cover monitoring at high temporal and spatial resolution, using images taken by a standard digital camera: *International Journal of Remote Sensing*, v. 23, p. 4669-4682.
- Johannessen OM, L Bengtsson, MW Miles, S I Kuzmina, VA Semenov, GV Alekseev, AP Nagurnyi, VF Zakharov, L Bobylev, LH Pettersson, K Hasselmann, H P Cattle, 2004, Arctic climate change: observed and modeled temperature and sea-ice variability, *Tellus*, 56A, 328-341.
- Liston GE, M Sturm, 1998, A snow-transport model for complex terrain: *Journal of Glaciology*, v. 44, p. 498-516.
- Meltofte H (ed.), 2002, sne is og 35 graders kulde – hvad er effekterne af klimaændringer i Nordostgrønland? Thematic report, National Environmental Research Institute, Ministry of the environment, Denmark, 88 pp.
- Meltofte H, S Rysgaard, SA Pedersen, 2003, Climate change in Greenland. Pp. 118-125 in: Denmark's Third National Communication on Climate Change under the United Nations Framework Convention on Climate Change. – Danish Environmental Protection Agency, Danish Ministry of the Environment.
- Phoenix GK, JA Lee, 2004, Predicting impacts of Arctic climate change: Past lessons and future challenges: *Ecological Research*, v. 19, p. 65-74.
- Rasmussen EA, TS Pedersen, LT Pedersen, J Turner, 1992, Polar Lows and Arctic Instability Lows in the Bear Island Region: *Tellus Series A-Dynamic Meteorology and Oceanography*, v. 44A, p. 133-154.
- Schmith T, C Hansen, 2003, Fram Strait ice export during the nineteenth and twentieth centuries reconstructed from a multiyear sea-ice index from southwestern Greenland: *Journal of Climate*, v. 16, p. 2782-2791.
- Stone RS, EG Dutton, JM Harris, D Longenecker, 2002, Earlier spring snowmelt in northern Alaska as an indicator of climate change: *Journal of Geophysical Research-Atmospheres*, v. 107.
- Wadhams P, 1999, The Odden ice tongue and Greenland Sea convection, *Weather* 54(3), 83-84, 91-98
- Weller G, 1998, Regional impacts of climate change in the Arctic and Antarctic: *Annals of Glaciology*, Vol 27, 1998, v. 27, p. 543-552.
- Wigley TML, SCB Raper, 2001, Interpretation of high projections for global-mean warming: *Science*, v. 293, p. 451-454.



### A.3.2 Proceeding paper—Northern Research Basins, Kangerlussuaq, Greenland, 2003

*Proceedings of the Northern Research Basins, 14<sup>th</sup> International Symposium and Workshop  
Kangerlussuaq/ Sdr. Stromfjord, Greenland, August 25-29, 2003, 59-66*

#### Sea-ice and snow accumulation modelling in High Arctic Greenland

Jørgen Hinkler  
Institute of Geography, University of Copenhagen, Denmark

Birger Ulf Hansen  
Institute of Geography, University of Copenhagen, Denmark

Mikkel Tamstorf  
Arctic Department, National Environmental Research Institute (NERI), Denmark

**ABSTRACT:** Snow cover and sea-ice affect surface radiation energy balance, and sea-ice affects both energy exchange between the atmosphere and the ocean water, and atmospheric circulation. Therefore these factors play major roles in the global climate system. Based on remote sensing at different scales the inter-annual snow accumulation at Zackenberg in Northeast Greenland (74.5 °N) was analyzed and compared to the regional sea-ice extent. Since 1998 the magnitude of the snow cover in the valley *Zackenbergdalen* has been monitored with a digital camera mounted in a weatherproof box on a mountainside approximately 450 m above the valley floor. The camera automatically obtains daily images of the valley producing a time series of images with both high spatial and temporal resolution. These oblique images were geometrically rectified into orthophotos. An algorithm - *Red Green Blue* Normalized Difference Snow Index (*RGBNDSI*) was used to identify snow pixels converting the orthophotos into snow maps. By combining these data with measures of snow depth and temperature a model to calculate local snow cover extent- and accumulation was developed. The model was used iteratively together with high-resolution satellite data (Landsat TM & SPOT HRV) to create a 14-year retrospective analysis on these parameters. The analysis reveals that due to various initial snow accumulations, and various temperature regimes during the different melting seasons, the course of the corresponding snow cover depletion curves varies from year to year. Thus, it was found that the mean date with 50 % snow cover at Zackenberg is around June 20<sup>th</sup>, deviating with more than +/- 2 weeks. Modelled snow accumulations were compared to regional sea-ice extent (inferred from 5 km resolution NOAA AVHRR data) during January-May 1988-2000. A significant correlation between snow accumulation at Zackenberg and sea-ice coverage ESE of Zackenberg was found – the lesser the number of days with huge amounts of sea-ice the larger the snow accumulation. This relationship indicates that if global warming becomes more prominent in the future (resulting in smaller amounts of sea-ice within the Greenland Sea), then larger amounts of snow can be expected in High Arctic Northeastern Greenland.

#### 1. INTRODUCTION

Polar Regions are extremely vulnerable to climate change, as they are marginal for the distribution for many species. Furthermore, Global Circulation Models (GCMs) predict that arctic areas are the ones on Earth that will experience the highest rates of temperature increase during this century (Jørgensen et al., 2001). These areas therefore play a crucial role in understanding climate change related issues.

Snow and (sea)ice coverage are key parameters in controlling the climate, both at local, regional, and global scales. Snow cover distribution determines the length of the growing season in the High Arctic, which is integral in the production of carbon dioxide and methane (Soegaard et al., 2001). Due to their high albedo snow and ice surfaces affects the surface energy balance dramatically; and they interact with the atmospheric circulation, e.g. Kwok and Rothrock (1999) found that the

*Proceedings of the Northern Research Basins, 14<sup>th</sup> International Symposium and Workshop  
Kangerlussuaq/ Sdr. Stromfjord, Greenland, August 25-29, 2003, 59-66*

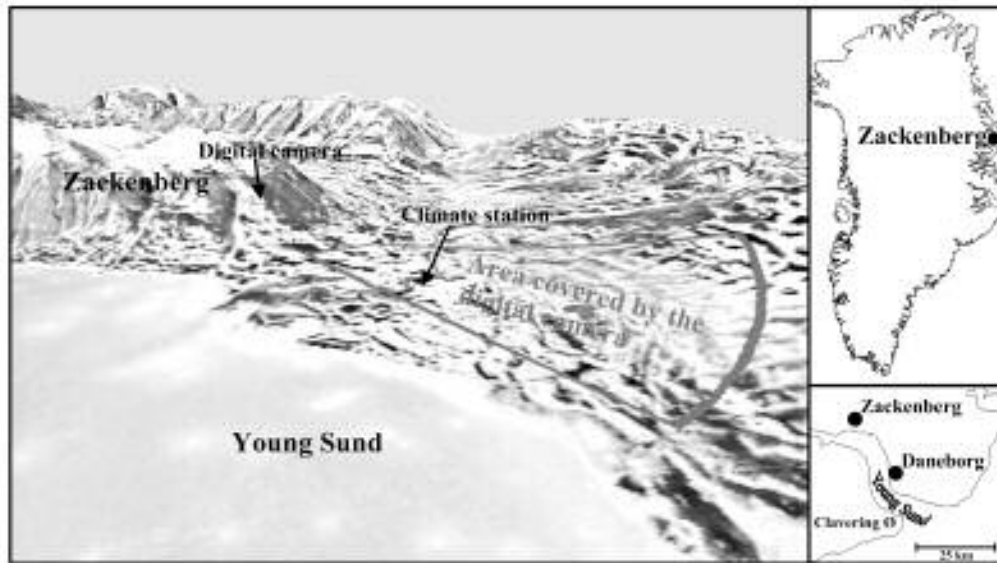


Figure 1. Zackenbergdalen study area with indication of the area covered by the digital camera (17 km<sup>2</sup>). The distance from the camera to the circular edge of the polygon is 7 km.

North Atlantic Oscillation (NAO) and the transport of sea ice between Svalbard and Greenland are correlated, and more recently Cavalieri (2002) found a very high correlation between this ice flux and the atmospheric planetary wave 1 phase. Recent studies have suggested that Northeast Greenland during a general global warming will experience higher winter temperatures and more precipitation (IPCC, 1998). This might lead to shorter summers due to a prolonged snowmelt with implications for the present habitats and animals in the region (Meltofte, 2002). Serreze et al. (2002) present a synthesis of recent change in the northern high-latitude environment. They document higher winter and spring temperatures on the northern continents with a pronounced downward tendency in sea-ice extent.

This study successfully relates regional sea-ice extent to a retrospective inter-annual analysis of the magnitude of snow accumulation at Zackenberg in High Arctic Northeast Greenland. The paper further presents a methodology to calculate inter- and intra-annual snow distribution and accumulation within the Zackenberg study area. This methodology combines temperature data and

remotely sensed image data (satellite and digital camera) to compute snow cover extent/accumulation in different melting seasons.

## 2. STUDY AREAS

All fieldwork was carried out at Zackenberg Ecological Research Station (74.5 °N, -21 °E) in Northeast Greenland (Figure 1). The Zackenberg research area is a high relief mountainous landscape consisting of nearly horizontal valley floors, steep slopes between 200 and 800 m above sea level, and plateaus above 800 m. It is located in the zone of continuous permafrost and hosts a large diversity of glacial, periglacial and coastal landscape features and a great variety of biotopes like fens, heaths, fellfield plateaus, and grasslands. Meteorological data from Zackenberg indicate a mean annual air temperature of approximately -10 °C. However from early June to early September, the mean daily temperature generally exceeds 0°C (Meltofte and Rasch, 1998; Rasch, 1999). A sub-extent of the Greenland Sea covering approximately 300.000 km<sup>2</sup> of sea-water/ice



*Proceedings of the Northern Research Basins, 14<sup>th</sup> International Symposium and Workshop  
Kangerlussuaq/ Sdr. Stromfjord, Greenland, August 25-29, 2003, 59-66*

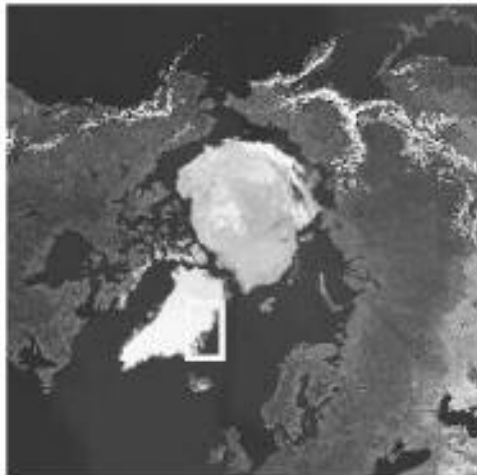


Figure 2. The sub-extent (within white rectangle) of the Greenland Sea used for sea-ice analysis.

was selected for mapping of regional sea-ice coverage (Figure 2), and a time series (1982-2000) of the sea-ice content within this area was inferred from 5 km resolution NOAA AVHRR satellite data (Fowler et al., 2000).

### 3. METHODOLOGICAL APPROACH, FIELDWORK, AND DATA

Since 1998 snow cover extent in Zackenbergdalen (dalen = "the valley") has been monitored using an automatic digital camera. The camera is situated at the slope of

Zackenbergs Mountain approximately 450 m above the valley floor, taking one image every day year round. The oblique images from the camera were rectified into digital orthophotos at 10 m spatial resolution using a software package called *Ortho* (Have, 1999). A time series of digital snow cover maps of Zackenbergdalen was then extracted from the orthophotos using the *RGBNDSI*-algorithm by Hinkler et al. (2002). To use these data for a retrospective analysis of snow coverage and snow accumulation at Zackenberg a semi-empirical model was developed to calculate these parameters in years prior to 1998. The model is based on the following assumption: If snow cover distribution in a given basin is similar from year to year, the depletion of snow covered areas during the melting season mainly depends on two factors; firstly the initial amount (depth) of snow before the snow-melt starts, and secondly: the amount of energy available for snow melt during the melting season.

The concept of the model is (for each day in the melting season) to "pick out" snow cover percentages (within the area covered by the digital camera – see Figure 1) from an interpolated dataset (interpolation method: Kriging) which holds all possible combinations of: (1) snow cover percentage (2) energy input for snow melt (given as accumulated degree days), (3) initial snow accumulation, and then produce a snow cover

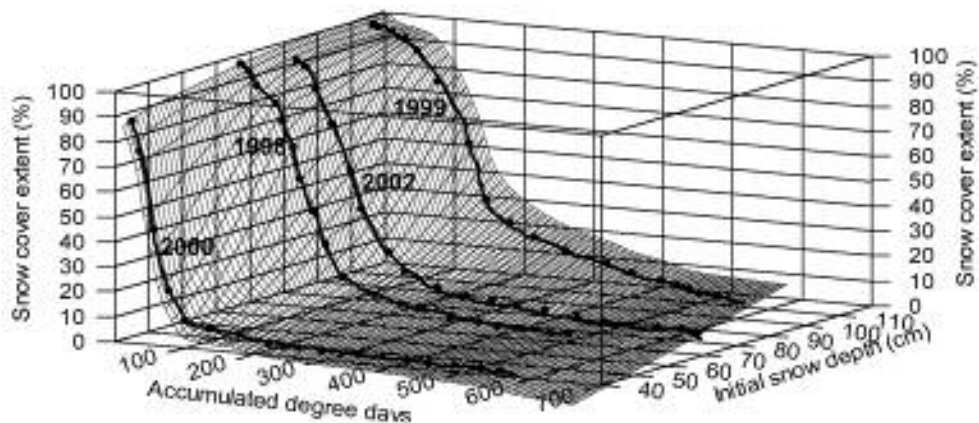


Figure 3. Visualization of the dataset containing information about snow cover depletion at Zackenberg in relation to the energy available for snowmelt (expressed as accumulated degree days) and initial snow accumulation. The thick curves display measured snow cover extent during 1998, 1999, 2000, and 2002 melting seasons.

*Proceedings of the Northern Research Basins, 14<sup>th</sup> International Symposium and Workshop  
Kangerlussuaq/ Sdr. Stromfjord, Greenland, August 25-29, 2003, 59-66*

depletion curve. The dataset was interpolated from data recorded during the 1998, 1999, 2000, and 2002 melting seasons (due to snowfall within the melting season the year 2001 was considered anomalous, and thus it was not included in the dataset). Figure 3 is a visualization of the dataset: the surface which is spanned out between the thick black curves contains all values of snow cover percentage in the entire dataset – interpolated as well as measured, and the curves themselves illustrate snow cover percentages derived from the digital camera images.

The temperature data (accumulated degree days calculated from daily means) and snow depths (means for June 1<sup>st</sup>) contained in the dataset are from the Zackenberg automatic weather station.

To derive modelled snow cover depletion a programme was written to extract snow cover data from the database. Provided that the initial snow depth at the beginning of the melting season, and the accumulated degree days for any given date(s) in the season are given, the programme finds the snow cover percentage(s) that matches this/these date(s); thereby a snow cover depletion curve is produced (Figure 7).

Prior to 1996 temperature data from the automatic weather station at Zackenberg are not available. For these years temperature data recorded at Daneborg (situated 23 km from Zackenberg) has served as input data for the model. Before 1998 no digital camera images are available and there were no measurements of snow depths at Zackenberg. Thus, the only source of image-data from Zackenberg with high spatial resolution is a limited number (14) of Landsat TM and SPOT HRV satellite images with the oldest images dating back from 1988 (Table 1). By running the model iteratively with different values of initial snow depth, snow cover depletion curves matching snow cover percentages inferred from satellite data were derived for the 1988-1996 melting seasons. During the 1997 melting season, three images of Zackenbergdalen were acquired with a standard reflex camera (Nikon F50). These images were orthographically rectified, converted to snow maps, and then used for modelling with the same iterative approach as for the satellite data.

Table 1. Dates with available satellite data.

Year	Landsat TM	SPOT HRV
1988	07-07	06-29
1989	06-17	07-16
1990	-	-
1991	06-23	-
1992	-	06-06, 07-17, 08-17
1993	07-30	-
1994	07-17	-
1995	06-25, 07-27	06-06
1996	07-15	-

Initial snow depths (found iteratively: 1988-1997; and measured: 1998-2000) were compared to the regional sea-ice content ESE of Zackenberg (Figure 2). It was found that a reasonable way to compare snow accumulation at Zackenberg to the presence of sea-ice in the Greenland Sea was to calculate the number of days during January-August with more than a certain amount of ice cover (150.000 km<sup>2</sup>) for each year. The regional sea-ice content was calculated from a time series (1982-2000) consisting of nearly 7000 5 km resolution surface maps produced by National Snow and Ice Data Center, Colorado, USA. These maps are part of the AVHRR Polar Pathfinder Twice-Daily 5 km EASE-Grid Composite dataset (Fowler et al., 2000). The data have been inferred from the NOAA AVHRR satellite sensors and contain 20 pixel-classes of sea-ice, where each class depends on ice percentage and type (multi- or first year).

#### 4. RESULTS AND DISCUSSION

This study shows that snow accumulation/ snow cover extent at Zackenberg has varied a great deal during the latest 14 years, and that this variation is significantly related to the presence of sea-ice in the Greenland Sea ESE of Zackenberg (Figure 2).



*Proceedings of the Northern Research Basins, 14<sup>th</sup> International Symposium and Workshop Kangerlussuaq/ Sdr. Stromfiord, Greenland, August 25-29, 2003, 59-66*

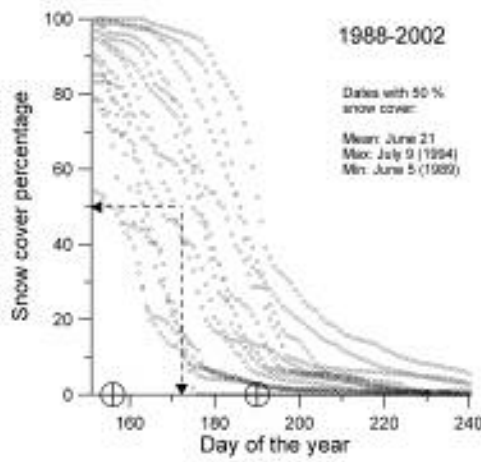


Figure 4. Variability in snow cover depletion at Zackenberg. Arrows indicate 50% snow coverage, and the date at which this occurs on average.

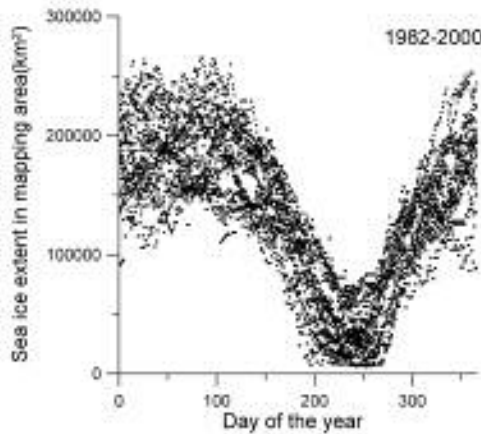


Figure 5. Variability in sea-ice coverage in the Greenland Sea ESE of Zackenberg during 1982-2000.

4.1 *Snow distribution and accumulation at Zackenberg*

Figure 7 shows modelled snow cover depletion curves during the melting seasons 1982-2002 for the area covered by the digital camera. Note that in 1982-1987 and 1990 there were no Landsat TM or SPOT data available. Thus, for these years, the initial snow depths that were used for modelling are estimates based on knowledge about sea-ice conditions. These

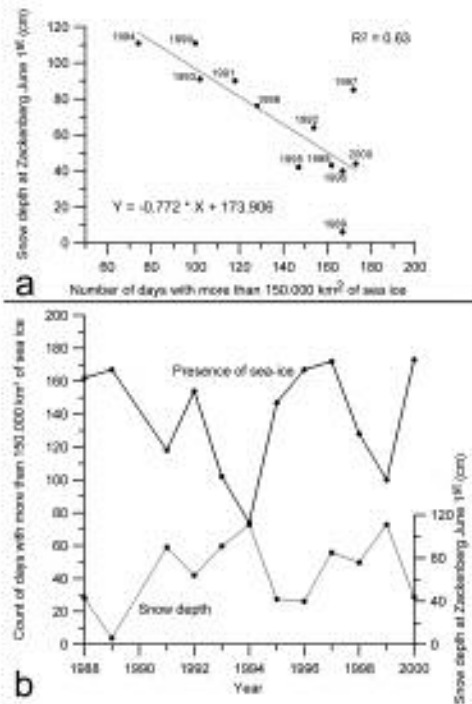


Figure 6. Relation between sea-ice in the Greenland Sea and the snow accumulation at Zackenberg. (a) Regression line, which have been used to model initial snow depths during 1982-1987. (b) Variation of snow accumulation and presence of sea-ice through time (1988-2000).

curves therefore must be looked at with criticism. For most of the years it was possible to make the modelled curves match measured snow cover percentages fairly well. However, there are some exceptions, which can be due to several factors: for instance, the mismatch in 2001 is obviously due to additional snowfall within the melting season. For years prior to 1996, temperatures measured at Daneborg, which is situated 23 km away from Zackenberg were used as input to the model. These temperatures are not necessarily a perfect substitute for the Zackenberg temperatures. Under some circumstances there is no positive correlation between air temperature and incoming solar radiation. In such situations the air temperature is not a consistent reflection of energy available for snowmelt; for example, if the air temperature is below freezing, and the sky is clear, the

*Proceedings of the Northern Research Basins, 14<sup>th</sup> International Symposium and Workshop  
Kangerlussuaq/ Sdr. Stromfjord, Greenland, August 25-29, 2003, 59-66*

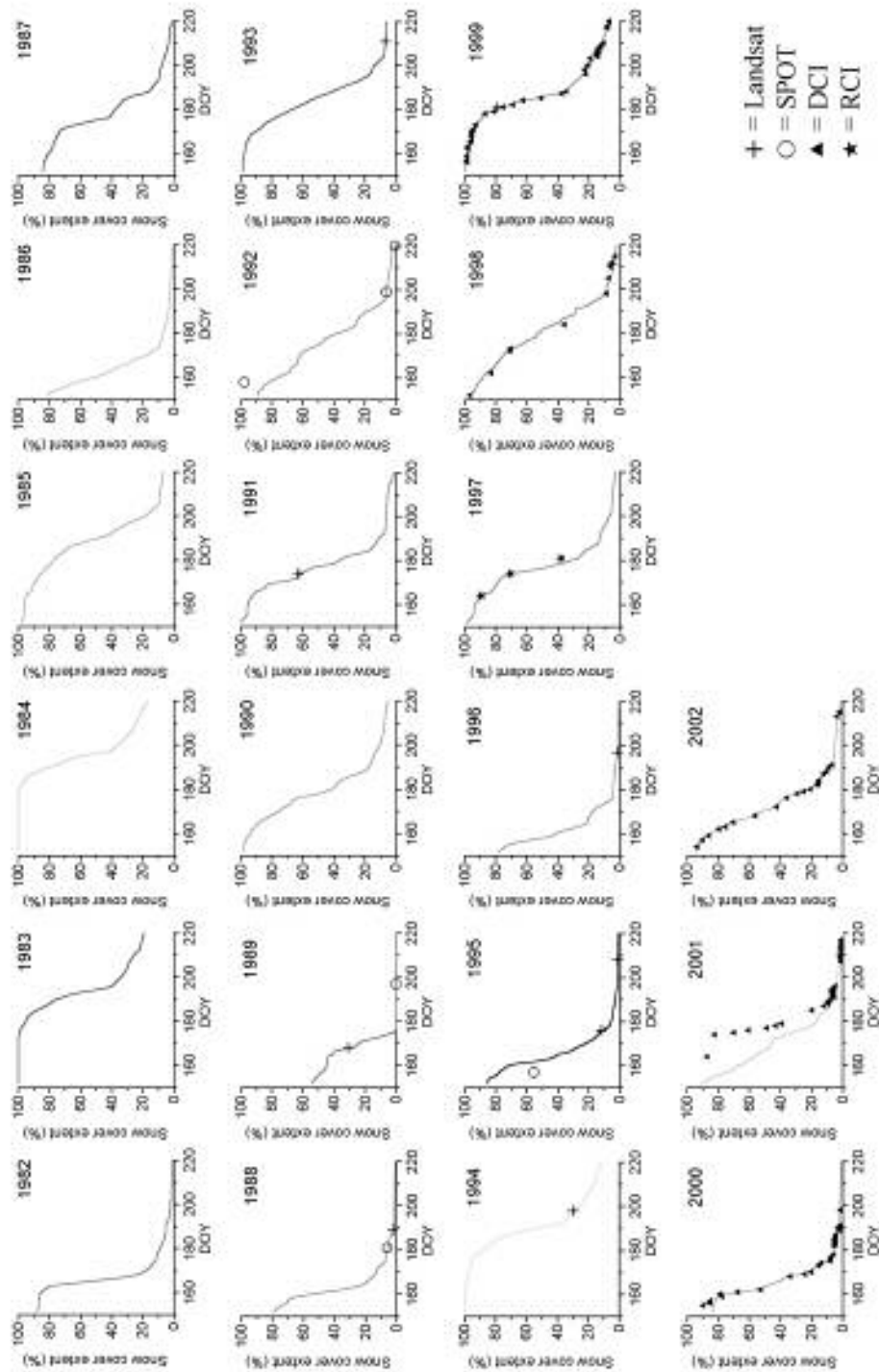


Figure 7. Modelled snow cover depletion curves for the Zaekenberg study area with indications of snow cover percentages inferred from various remotely sensed image data (satellite sensors and cameras). DCI=Digital Camera Images, RCI=Reflex Camera Images.

*Proceedings of the Northern Research Basins, 14<sup>th</sup> International Symposium and Workshop  
Kangerlussuaq/ Sdr. Stromfjord, Greenland, August 25-29, 2003, 59-66*

large amount of incoming solar radiation can raise the temperature of the snow pack to above its melting point. Finally, as the model assumes snow distribution in Zackenbergdalen to be similar every year, a winter with non-typical wind conditions can make the snow distribution take an unusual course, which will make the model fail.

The modelled results on snow cover depletion shows that the length of the melting period at Zackenberg varies a lot from year to year. Figure 4 displays the variability in snow cover depletion within the study area, and it can be observed that the date with 50% snow coverage varies with more than a month and that the mean date is around June 20<sup>th</sup>.

#### 4.2 Snow accumulation at Zackenberg in relation to ice coverage in the Greenland Sea

The amount of sea-ice within the selected mapping area (Figure 2), like the snow accumulation at Zackenberg, shows great variability (Figure 5) from year to year.

Interestingly, a comparative analysis of the EASE-grid time series of surface maps and modelled snow accumulation at Zackenberg reveals a significant correlation between snow-precipitation and number of days with large amounts of sea-ice. This is shown in Figure 6 that displays a linear fit between days with more than 150.000 km<sup>2</sup> of sea-ice and the modelled initial snow depths at Zackenberg during 1988-2000 (except 1990, where snow cover data were not available from satellite images). Even though the year 1997 seems to be an outlier, 63% of the variance can be explained by the linear fit. If this year is removed, R-squared raises to 0.83.

The result indicates that snow accumulation at Zackenberg is inversely proportional to regional sea-ice extent. Thus, in case of a future climate with increasing temperatures and less sea-ice, this study supports suggested scenarios by the IPCC with more snow-precipitation in the High Arctic. Due to the high correlation the linear relationship given in Figure 6 was used to calculate initial snow accumulation (June 1<sup>st</sup>) at Zackenberg during 1982-1987 and in 1990. Together with the accumulated temperatures from the melting seasons these snow depths were used to model snow cover depletion curves for

Zackenbergdalen (Figure 7). A high accuracy in modelling snow distribution in this way implies (of course) that the link between presence of sea-ice and precipitation found during this study are significant over more than 14 years. However, if this is the case they reflect a very interesting covariance between climatic parameters at different scales.

## 5. CONCLUSIONS AND PERSPECTIVES

This study has demonstrated methods to describe the variability of two important climatic parameters (snow-precipitation and sea-ice) at small and larger scale, respectively. The analysis of these two sets of information reveals a significant correlation between sea-ice-extent and snowfall in High Arctic Northeast Greenland – longer presence of sea ice leads to less snow accumulation, and shorter presence leads to larger snow accumulation. This is interesting in relation to future climate change as several studies as well as the majority of GCMs predict less sea-ice and increasing precipitation in High Arctic Greenland – this study is in concordance with these suggestions. Methodologically, the method presented here to model snow cover distribution could be of interest at other research locations in the North Atlantic, and the data produced would be of great value in further understanding climatic changes in the region.

## 6. ACKNOWLEDGEMENTS

The Danish Polar Center is acknowledged for providing access to ecosystem monitoring data and logistics at the research station at Zackenberg. Ulf Thomas, (former technician at Institute of Geography, University of Copenhagen) is acknowledged for developing the automatic digital camera and Kim Have (former student at the Technical University of Denmark) for developing the rectification software *Ortho*.



*Proceedings of the Northern Research Basins, 14<sup>th</sup> International Symposium and Workshop  
Kangerlussuaq/ Sdr. Stromfiord, Greenland, August 25-29, 2003, 59-66*

7. REFERENCES

Cavalieri, D.J. (2002) A link between Fram Strait sea ice export and atmospheric planetary wave phase. *Geophysical Research Letters*, Vol. 29, No. 12, 10.1029/2002GL014684.

Fowler, C., Maslanik, J., Haran, T., Scambos, T., Key, J. and Emery, W. (2000) AVHRR Polar Pathfinder Twice-Daily 5 km EASE-Grid Composites. Boulder, CO, USA: National Snow and Ice Data Center. Digital media.

Have, K. (1999) Photogrammetric image analysis for climate studies (Unpubl. master thesis). Technical University of Denmark, Department of Planning.

Hinkler, J., Pedersen, S.B., Rasch, M. and Hansen, B.U. (2002) Automatic snow cover monitoring at high temporal and spatial resolution, using images taken by a standard digital camera. *International Journal of Remote Sensing* 23, pp. 4669-4682.

Intergovernmental Panel of Climate Change (IPCC) in Watson, R.T., Zinyowera, M.C., Moss, R.H., Dokken, D.J. (1998) *The Regional Impacts of Climate Change: An Assessment of Vulnerability - IPCC Special Report*. Cambridge University Press.

Jørgensen, A.M.K., Fenger, J. and Halsnæs, K. (eds.), Danish Climate Centre (2001) *Climate Change Research: Danish Contributions*. Gads Forlag, pp. 1-22.

Kwok, R. and Rothrock, D.A. (1999) Variability of Fram Strait ice flux and North Atlantic Oscillation. *Journal of Geophysical Research* 104, pp. 5177-5189.

Meltofte, H. (ed.) (2002) Sne, is og 35 graders kulde. Hvad er effekterne af klimaændringer i Nordøstgrønland? (Thematic report). National Environmental Research Institute, Ministry of Environment No. 41, 88 pp.

Meltofte, H. and Rasch, M. (eds.) (1998) Zackenberg Ecological Research Operations, 3<sup>rd</sup> Annual Report, 1997. Danish Polar Center, Ministry of Research and Information Technology.

Rasch, M. (ed.) (1999) Zackenberg Ecological Research Operations, 4<sup>th</sup> Annual Report, 1998. Danish Polar Center, Ministry of Research and Information Technology.

Serreze M.C., Walsh J.E., Chapin F.S., Osterkamp T., Dyurgerov M., Romanovsky V., Oechel W.C., Morison J., Zhang T., Barry R.G. (2000) Observational evidence of recent

change in the northern high-latitude environment. *Climatic Change* 46, pp. 159-207.

Soegaard, H., Nordstroem C., Christensen, T.R., Friberg, T., and Hansen, B.U. (2001) Seasonal carbon dioxide balance and respiration for a high-arctic fen ecosystem in NE Greenland. *Theoretical and Applied Climatology* 70, pp. 149-166.



*A.3.3 Extended abstract—Sixth Ny Ålesund Int. Scientific Seminar, Tromsø, Norway, 2002*

**Detection of spatial, temporal, and spectral surface changes in the Ny-Ålesund area 79° N, Svalbard, using a low cost multispectral camera in combination with spectroradiometer measurements.**

Jørgen Hinkler, Jon Børre Ørbæk & Birger Ulf Hansen

Institute of Geography, University of Copenhagen, Øster Voldgade 10, 1350 Copenhagen K, Denmark. E-mail: [jh@geogr.ku.dk](mailto:jh@geogr.ku.dk), phone +45 35 32 41 68

Norwegian Polar Institute, postbox 505, N-9171 Longyearbyen, Svalbard, Norway  
E-mail: [jonbo@npolar.no](mailto:jonbo@npolar.no), phone: +47 79 02 26 00 (26 21 direct)

Institute of Geography, University of Copenhagen, Øster Voldgade 10, 1350 Copenhagen K, Denmark. E-mail: [buh@geogr.ku.dk](mailto:buh@geogr.ku.dk), phone +45 35 32 25 19

**Introduction**

This work is a pilot study on using a low cost “3 filter channel” spectral digital camera for monitoring spatiotemporal changes in surface reflectance during the melting season in the Ny-Ålesund area 79° N, Svalbard. The study is based on images taken at regular time intervals, radiation data obtained by a Fieldspec FR spectroradiometer, and solar radiation data measured at the Sverdrup Station in Ny-Ålesund.

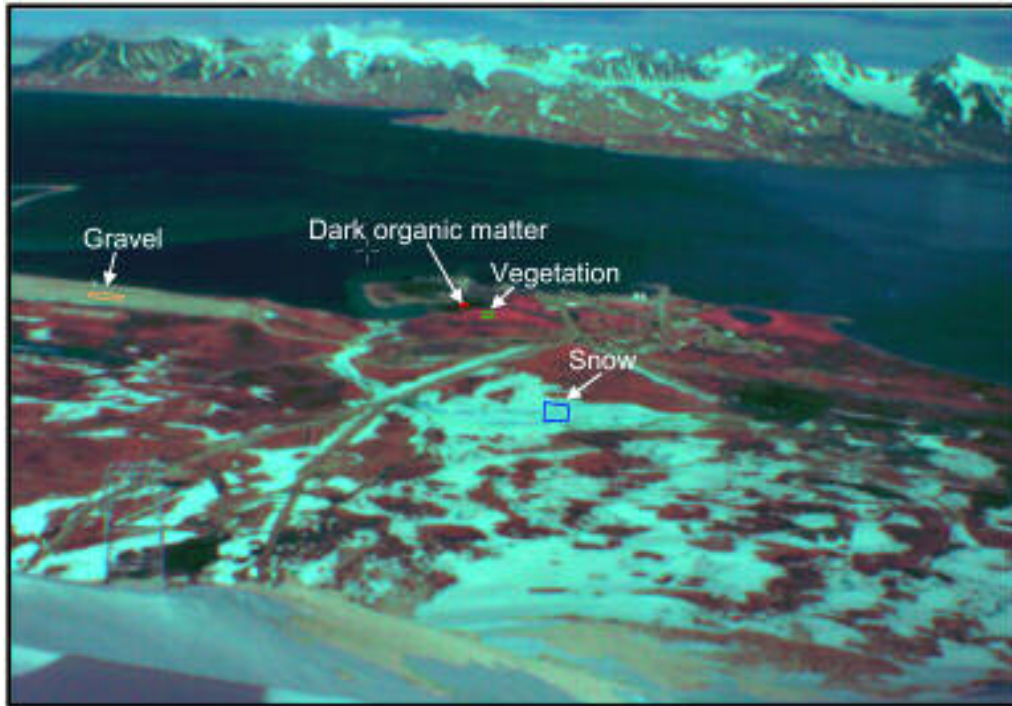
**The Study**

During the period 23/5 2002 – 30/8 2002 a Tetracam multispectral digital camera was installed 474 metres above sea level at the Zeppelin Mountain Research Station, approximately 2 km from the Ny-Ålesund settlement. The camera has been taking an image automatically every day at noon (and at 10-minute intervals on a single day), making up a time series of spectral imagery at high resolution – in both space and time. The aim of the study is to use these images for surface classification and change detection. These results can then be used for further modelling in connection with surface energy balance studies. In order to make this possible a comprehensive work of calibration experiments are being performed.

Data to be used for the experiments have been collected during two field campaigns – one in mid May before extensive snowmelt began, and one at the end of June/beginning of July, where large vegetated areas and bare-soil areas were free of snow. The first campaign was initiated as a testing phase, where the camera was set up and adjusted to the prevailing light conditions and the first measurements of spectral reflectance for snow/ice, and gravel were performed. Additionally, a number of geographical positions were measured at different locations throughout the terrain, using GPS. These data are going to be used for orthographic rectification of the images (Hinkler et al. 2002). An orthographic image has the same scale throughout the whole image, which ensures correct estimations of the size of the different surface types. During the second campaign, the spectral properties of additional surface types (vegetation, dark organic matter, and water) were measured. Furthermore, surface reflectance was tested for different view angles using both the spectroradiometer and the camera.

At the time of writing, image data have been compared to incoming global radiation, solar azimuth angle and measurements of spectral reflection for snow (Winther et al. 1999).

Figure 1 is an example of a spectral image of the Ny-Ålesund area, and it is created as a false colour composite from the red(B), green(G) and near infrared(R) channels of the camera – similar to e.g. Landsat TM ch. 2, 3, and 4. The brightness of a given image - or Digital Numbers



**Figure 1.** False colour composite of the Ny-Ålesund area obtained from the automatic spectral digital camera. Distinct surface types that have been spectrally investigated are indicated in the image.

(DN) are very sensitive to the amount of incoming solar radiation as well as the angular direction to the Sun (solar azimuth). These relationships are illustrated for red and near infrared in figures 2(a,b). The figures show the average DN's for snow and vegetation at 10 minute time intervals during a period of 26 hours (28/6 – 29/6). The figures reveal that image brightness is correlated to the global radiation and that the correlation is most significant at visible wavelengths. The camera's orientation is almost directly to the north. Consequently, when sunlight comes from northern directions during the night, image data become unusable for calculation of values related to the physical properties of the different surface types. This is due to strays of light reflected directly into the camera lens. Therefore it is important to emphasize that the camera's orientation must be in the direction away from the Sun at capture time. In figures 2(c,d) the relation between global solar radiation, red, and near infrared DN's, respectively is shown (due to azimuth problems, data obtained during the time around midnight have been excluded). Figures 2(c,d) also illustrates that the camera's response is very sensitive to the adjustment of the camera's diaphragm according to the present light conditions. During this study it has been attempted to adjust the diaphragm to cover light conditions varying from bright clear skies to overcast conditions. To avoid saturation on clear days, the diaphragm has been set at a relatively high level. Thus, on days with limited amounts of sunlight, images will be relatively dark, which reduces the dynamic range of the given image significantly. From the figures, it can be observed that at the current diaphragm-settings requires minimum 300-400  $\text{wm}^{-2}$  global radiation in order to be able to obtain different calibrations for different surface types (fitted data range: 400  $\text{wm}^{-2}$  and up).

In Figure 3 daily values (20/5 – 30/6) of the camera's red channel for the snow region are plotted against global radiation measured at the recording time. A visual examination of the images

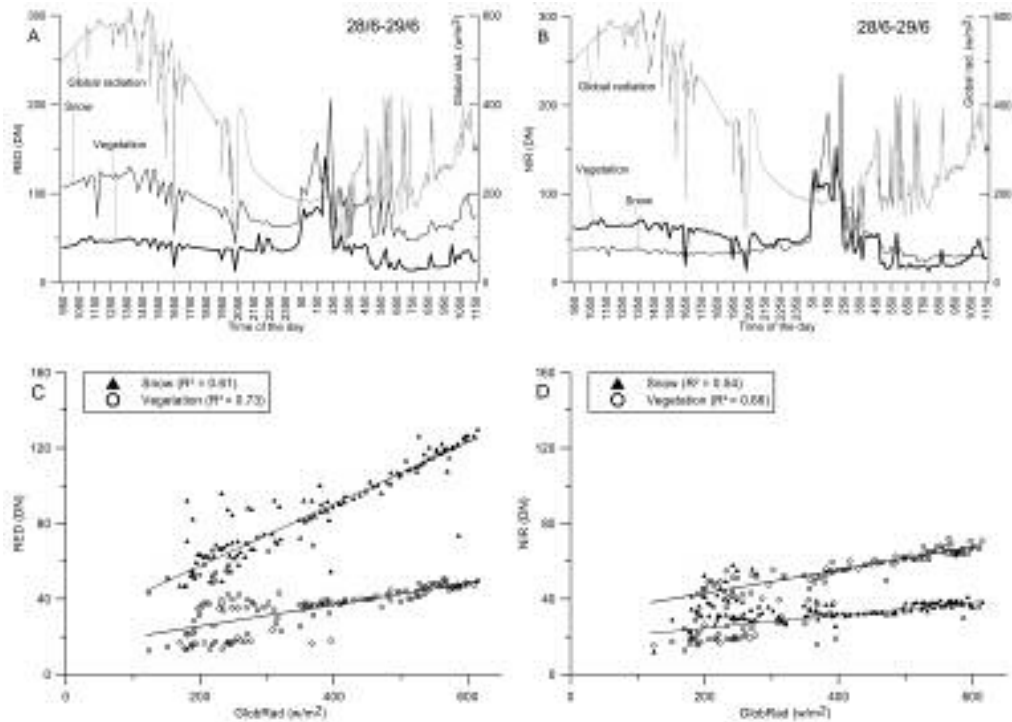


Figure 2. Image DN's for different surface types in relation to global radiation.

shows that at low levels of incident solar radiation it is possible to distinguish clouds from snow and at higher levels it is possible to separate new and old snow.

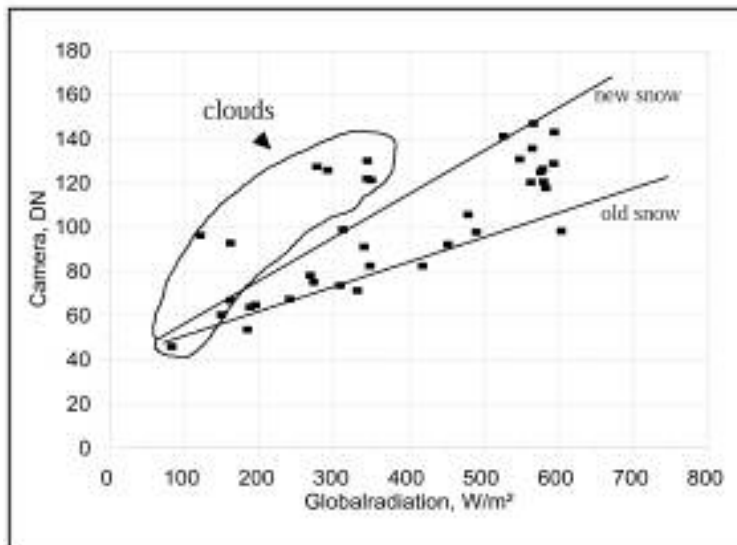


Figure 3. Camera DN's (red channel, snow region) plotted against global radiation, based on daily images captured during the period 20/5 – 30/6.

A classification test including four different surface types was performed. The test is based on red and near infrared DN's selected from a time span (28/6, 10:00-16:00) with relatively uniform radiative conditions. Figure 4 shows that for this time span the different surface types can be easily separated, however if data are obtained under more varying conditions the picture gets more complicated. To solve this task further work must be put in the development



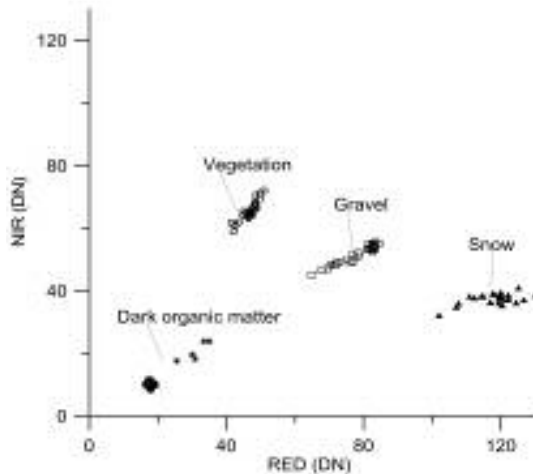


Figure 4. Nearinfrared and red channels plotted against each other for different surface types.

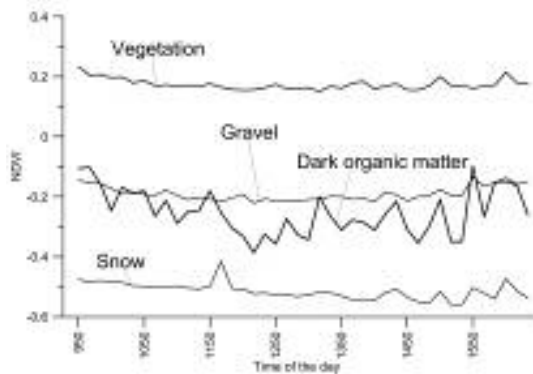


Figure 5. NDVI-index for different surface types, derived from image data obtained 28/6-2002.

of the necessary calibration routine.

The Normalized Difference Vegetation Index (NDVI) is the most commonly used remote sensing-based index for detection of the greenness of vegetation (amount of chlorophyll and development of cell-structure in plants). The index is defined:

$$NDVI = \frac{NIR - RED}{NIR + RED}$$

The values of the index range between -1 and 1. Values above approximately 0.1 usually indicate that a certain amount of chlorophyll is present. Snow has a weaker reflectance at nearinfrared wavelengths than at visible wavelengths. Therefore snow-NDVI usually is well below zero. Figure 5 indicates that data have the potential for monitoring greenness during the growing season, and that snow and vegetation can be easily separated from gravel and dark organic matter, using this index.

Gravel and dark organic matter have NDVI values of the same order of magnitude and can difficult to separate using the NDVI. To solve this other methods based on absolute DN-values must be introduced.

**Final Remarks**

The Tetracam spectral digital camera offers the possibility to monitor spectral surface changes at high temporal and spatial resolution, however some technical difficulties regarding the adjustment of the

cameras diaphragm and automatic exposure time have to be solved. Further work must be put into developing calibration routines based on solar radiation data; and a comprehensive analysis of spectral image data versus spectroradiometer data still needs to be performed.

**References**

Hinkler, J., Pedersen, S.B., Rasch, M. & Hansen, B.U. in press: Automatic snow cover monitoring at high temporal and spatial resolution, using images taken by a standard digital camera. *International Journal of Remote Sensing*.

Winther, J.-G., Gerland, S., Ørbæk, J.B., Ivanov, B., Blanco, A. & Boike, J. 1999: Spectral reflectance of melting snow in a high Arctic watershed on Svalbard: *Some implications for optical satellite remote sensing. Hydrological processes* 13, 2033.

## *Appendix 4*

### Co-author statements

A.4.1 Co-author statements, Paper 1

**Co-author Statement**

I hereby declare that I am aware that the work in the paper:

J. Hinkler, S. B. Pedersen, M. Rasch and B. U. Hansen, 2002. Automatic snow cover monitoring at high temporal and spatial resolution, using images taken by a standard digital camera. *International Journal of Remote Sensing*, 23, 4669-4682.

Of which I am a co-author, will form part of the Ph.D. dissertation by:

Jørgen Hinkler

who made a:

- major
- proportional
- minor

contribution to the work both in the research and writing phase.

Steen B. Pedersen  
Name

17/2-2005  
Date

  
Signature

## Co-author Statement

I hereby declare that I am aware that the work in the paper:

J. Hinkler, S. B. Pedersen, M. Rasch and B. U. Hansen, 2002. Automatic snow cover monitoring at high temporal and spatial resolution, using images taken by a standard digital camera. *International Journal of Remote Sensing*, 23, 4669-4682.

Of which I am a co-author, will form part of the Ph.D. dissertation by:

Jørgen Hinkler

who made a:

- major
- proportional
- minor

contribution to the work both in the research and writing phase.

Morten Rasch  
Name

20/2-05  
Date

  
Signature

## Co-author Statement

I hereby declare that I am aware that the work in the paper:

J. Hinkler, S. B. Pedersen, M. Rasch and B. U. Hansen, 2002. Automatic snow cover monitoring at high temporal and spatial resolution, using images taken by a standard digital camera. *International Journal of Remote Sensing*, 23, 4669-4682.

Of which I am a co-author, will form part of the Ph.D. dissertation by:

Jørgen Hinkler

who made a:

- major
- proportional
- minor

contribution to the work both in the research and writing phase.

Birger U. Hansen  
Name

12/1-2005  
Date

Birger Hansen  
Signature



## A.4.2 Co-author statements, Paper 2

**Co-author Statement**

I hereby declare that I am aware that the work in the paper:

Hinkler, J., Ørbæk, J. B., Hansen, B. U., 2003. Detection of spatial, temporal, and spectral surface changes in the Ny-Ålesund area 79° N, Svalbard, using a low cost multispectral camera in combination with spectroradiometer measurements. *Physics and Chemistry of the Earth*, 28, 1229-1239.

Of which I am a co-author, will form part of the Ph.D. dissertation by:

Jørgen Hinkler

who made a:

- major  
 proportional  
 minor

contribution to the work both in the research and writing phase.

Jon Børre Ørbæk  
Name

19/1-2005  
Date

Jon Børre Ørbæk  
Signature

## Co-author Statement

I hereby declare that I am aware that the work in the paper:

Hinkler, J., Ørbæk, J. B., Hansen, B. U., 2003. Detection of spatial, temporal, and spectral surface changes in the Ny-Ålesund area 79° N, Svalbard, using a low cost multispectral camera in combination with spectroradiometer measurements. *Physics and Chemistry of the Earth*, 28, 1229-1239.

Of which I am a co-author, will form part of the Ph.D. dissertation by:

Jørgen Hinkler

who made a:

major

proportional

minor

contribution to the work both in the research and writing phase.

Birger U. Hansen  
Name

12/1-2005  
Date

Birger U.  
Signature

A.4.3 Co-author statements, Paper 3

**Co-author Statement**

I hereby declare that I am aware that the work in the paper:

Snow-vegetation relations in a High Arctic ecosystem: Inter-annual variability inferred from new monitoring- and modeling concepts.

Of which I am a co-author, will form part of the Ph.D. dissertation by:

Jørgen Hinkler

who made a:

- major
- proportional
- minor

contribution to the work both in the research and writing phase.

Birger U. Hansen  
Name

21/2-05  
Date

  
Signature

## Co-author Statement

I hereby declare that I am aware that the work in the paper:

Snow–vegetation relations in a High Arctic ecosystem: Inter-annual variability inferred from new monitoring- and modeling concepts.

Of which I am a co-author, will form part of the Ph.D. dissertation by:

Jørgen Hinkler

who made a:

major

proportional

minor

contribution to the work both in the research and writing phase.

Mikkel P. Tamstorf

Name

21/2-05

Date



Signature

## Co-author Statement

I hereby declare that I am aware that the work in the paper:

J. Hinkler, B.U. Hansen, M.P. Tamstorf and S. B. Pedersen, 2005. Snow-vegetation relations in a High Arctic ecosystem: Inter-annual variability inferred from new monitoring- and modeling concepts.

Of which I am a co-author, will form part of the Ph.D. dissertation by:

Jørgen Hinkler


who made a:

- major
- proportional
- minor

contribution to the work both in the research and writing phase.

Steen B. Pedersen  
Name

17/2-2005  
Date

  
Signature

A.4.4 Co-author statements, Paper 4

**Co-author Statement**

I hereby declare that I am aware that the work in the paper:

J. Hinkler, B. U. Hansen, M. P. Tamstorf and H. Meltøfte, 2005. A possible linkage between sea-ice concentrations and snow-precipitation may be crucial for Arctic ecosystems in a warmer climate.

Of which I am a co-author, will form part of the Ph.D. dissertation by:

Jørgen Hinkler

who made a:

- major
- proportional
- minor

contribution to the work both in the research and writing phase.

Birger U. Hansen  
Name

6/9-05  
Date

Birger U. Hansen  
Signature

## Co-author Statement

I hereby declare that I am aware that the work in the paper:

J. Hinkler, B. U. Hansen, M. P. Tamstorf and H. Meltofte, 2005. A possible linkage between sea-ice concentrations and snow-precipitation may be crucial for Arctic ecosystems in a warmer climate.

Of which I am a co-author, will form part of the Ph.D. dissertation by:

Jørgen Hinkler

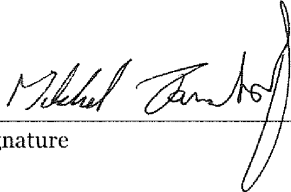
who made a:

- major
- proportional
- minor

contribution to the work both in the research and writing phase.

Mikkel P. Tamstorf  
Name

7/9-05  
Date

  
Signature

## Co-author Statement

I hereby declare that I am aware that the work in the paper:

J. Hinkler, B. U. Hansen, M. P. Tamstorf and H. Meltofte, 2005. A possible linkage between sea-ice concentrations and snow-precipitation may be crucial for Arctic ecosystems in a warmer climate.

Of which I am a co-author, will form part of the Ph.D. dissertation by:

Jørgen Hinkler

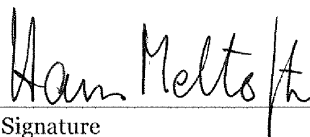
who made a:

- major
- proportional
- minor

contribution to the work both in the research and writing phase.

Hans Meltofte  
Name

7/9-05  
Date

  
Signature



# Papers

---



## Automatic snow cover monitoring at high temporal and spatial resolution, using images taken by a standard digital camera

J. HINKLER\*, S. B. PEDERSEN, M. RASCH and B. U. HANSEN  
Institute of Geography, University of Copenhagen, Øster Voldgade 10,  
1350 Copenhagen K, Denmark

**Abstract.** The inter- and intra-annual snow cover distribution in the Zackenberg-dalen valley, north-east Greenland, was monitored using images from a digital camera. The Digital Camera Images (DCIs) provide—in contrast to satellite images—data with a high temporal and spatial resolution at low cost. The digital camera, positioned on a rock 500 m above sea level (asl), automatically takes oblique photographs of the valley. To obtain the necessary area consistency for mapping purposes, the DCIs are transformed into digital orthophotos. Snow cover mapping is performed using these orthophotos. In order to suppress errors due to illumination effects, a normalized index based on red, green and blue (RGB) values was developed. The index can be used as an analogue to the Normalized Difference Snow Index (NDSI), commonly used in combination with Landsat Thematic Mapper (TM) images. During the melt-off season, a maximum of 10–15 Landsat TM passes occur over the Zackenberg area. For the 1999 melt-off season only three cloud-free TM images were usable for snow-mapping, while 46 DCIs were suitable for this purpose. Analysis of 1998 and 1999 data shows that the snow cover in Zackenbergdalen decreases gradually during the melt-off season. The resulting depletion curves have a 'laterally reversed S-shaped' form, which depends on the initial amount of snow in the area, the temperature during the melt-off season and altitudinal level.

### 1. Introduction

Snow cover is a very important component of the Earth's climate system (Brun *et al.* 1994). It is a key component of the global hydrological cycle, as it is the largest contributor to rivers over major portions of the middle and high latitudes. Water derived from snow melt is being used for generation of hydropower. Hence, the quantitative estimation of the extent of snow cover is of prime importance to hydrologists and managers of water resources (Søgaard and Thomsen 1988, Swami and Brivio 1996). Furthermore, snow cover highly affects the living conditions for plants and animals (Gray and Male 1981, Hall *et al.* 1990, Plüss and Mazzoni 1994). For instance, snow cover is considered to be a very important factor affecting musk ox mortality, reproduction and distribution in Arctic environments (Hansen and Mosbech 1994). Thus, an increasing effort has been put into snow mapping at different scales during the last decades.

---

\*Corresponding author; e-mail [jh@geogr.ku.dk](mailto:jh@geogr.ku.dk)

This paper was presented at the 6th Circumpolar Symposium on Remote Sensing of Polar Environments held in Yellowknife, Northwest Territories, Canada, from 12–14 June 2000.

Traditionally, determination of snow cover has been based on point measurements. However, such measurements will not always detect significant areal snow cover variations (Gray and Male 1981). Especially over larger areas, satellite remote sensing techniques have improved the possibility of data acquisition at regular intervals. However, over a small area, the availability of satellite data of sufficiently high resolution in space and time is still limited. The snow cover monitoring discussed in this paper was carried out as a part of Zackenberg Ecological Research Operation (ZERO), Zackenberg Station (74°30' N; 21°00' W) in north-east Greenland (figure 1).

The snow cover depletion of the Zackenberg area has previously been investigated using high resolution satellite data [Landsat Thematic Mapper (TM) and Système Probatoire pour l'Observation de la Terre (SPOT) High Resolution Visual (HRV)] (Tamstorf 1997). However, a great deal of the research in the area depends on a description of the snow cover, which is more detailed than that which can be achieved by various high resolution satellite sensors.

The purpose of this study therefore is to develop a low cost technique to produce high resolution snow cover maps of the Zackenbergdalen valley (figure 1) and use these for a case study of snow cover depletion in a High Arctic ecosystem.

To be able to use a low cost standard digital camera for automated snow cover monitoring a simple mechanical device was developed. The device consists of an automatic trigger controlled by an electronic timer, and the energy supply is from a 12 V rechargeable battery and a solar panel. The system requires energy only when the images are captured; this, together with a flash memory card, ensures that the images have to be collected only at the end of the melt-off season. All of the



Figure 1. A Landsat TM5 satellite image superimposed on the DEM of the Zackenberg area. The area where the snow cover is mapped from the DCIs are within the red polygon. The site where the digital camera is located is indicated by the black cross, and the research station is situated at the blue tower.



*Sixth Circumpolar Symposium on Remote Sensing of Polar Environments* 4671

equipment (including the camera) is sheltered in a waterproofed box with a small window (figure 2). To reduce the probability of riming inside the box, the moisture content is kept at a low level by absorbent material within the box.

The system is placed on a rock approximately 500 m above the valley, taking oblique photographs of Zackenbergdalen once every day at solar noon. The pictures are 24 bit red, green and blue (RGB) images and, to suppress illumination effects, the spectral information represented by the RGB values was used to develop a normalized snow index. A computer program for transformation of the digital images into orthophotos also was developed in cooperation with the Institute of Planning, Surveying Section, the Technical University of Denmark (Have 1999).

## 2. Theory and methods

### 2.1. Spectral reflectance of snow

The difference of reflective properties between snow and other surfaces is normally quite large, making it possible to distinguish snow from other surface types (Winther and Hall 1999). In figure 3(a) it can be observed that the reflectance of vegetation and bare soil is relatively low in the visible (VIS) part of the electromagnetic spectrum, while it is high for snow covered surfaces. In contrast to vegetation and bare soil, the reflectance of snow decreases rapidly in the near- and mid-infrared (NIR and MIR) parts of the spectrum (Duguay and LeDrew 1991).

The reflectance of snow can vary considerably, depending on several factors. As the snow ages, the reflectance generally decreases [figure 3(b)]. In NIR and MIR the decrease is mainly due to grain size growth, while in VIS it is mostly due to a higher concentration of impurities in the snow pack. Furthermore, snow to a certain extent can be regarded as transparent for short wavelengths. Therefore the reflectance will decrease in VIS and NIR for snow thicknesses less than 20–30 cm (Dozier 1989, Winther 1993, Winther and Hall 1999).

### 2.2. Digital Camera Images (DCIs)

The camera obtaining the DCIs is a Kodak DC50 digital camera containing a charge coupled device (CCD) with a dimension of  $756 \times 504$  pixels. It is coated with

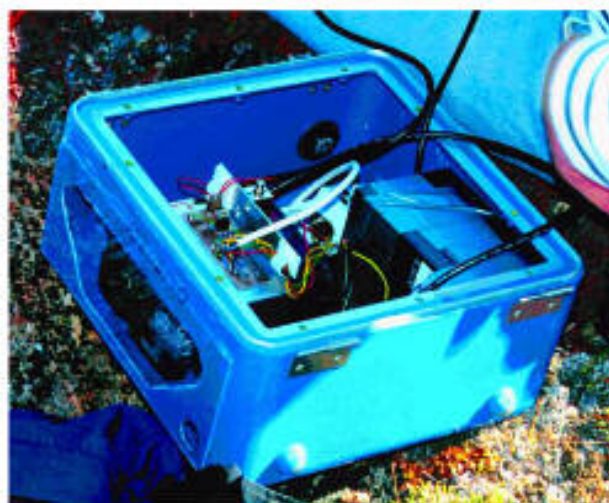


Figure 2. The automatized digital camera in the protection box.

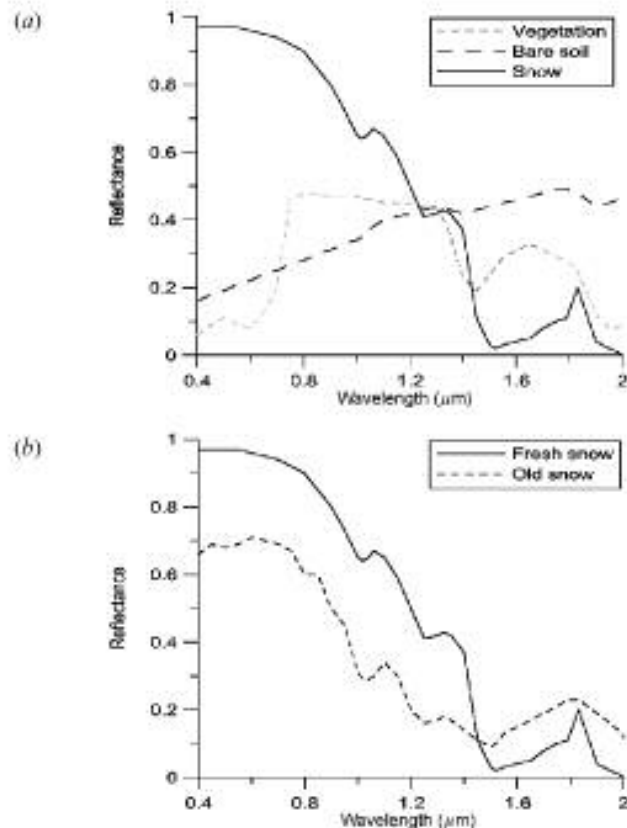


Figure 3 (a) Reflectance of vegetation, bare soil and snow (modified from Duguay and LeDrew 1991). (b) Reflectance of fresh and old snow (modified from Hall and Martinec 1985).

a colour array of red, green and blue photosites. Thus each photosite on the CCD is sensitive to only one colour.

When the image is captured, wavelengths larger than  $0.7 \mu\text{m}$  are excluded by a prefilter. This prefilter is used because the CCD is very sensitive to infrared (IR) light (Kodak, personal communication 1998). In order to obtain the maximum amount of information and increase the sharpness of the images according to the nature of the human eye, the green filters outnumber the blue and red at a ratio of two to one.

In order to compress and store the image, a specially designed algorithm, Run Adaptive Differential Compression (RADDC), is applied. After the images have been transferred to a computer they must be decompressed. Because each photosite is sensitive to only one colour, interpolation algorithms creating the 'missing' red, green and blue values are applied (Kodak 1998). Then the final result comes in the form of a 24 bit bitmap image.

### 2.3. Orthophotos

When the images are captured by the camera, they are created as a central projection of the object space. The central projection introduces some displacements, which makes it impossible to measure the size of objects represented in the images. These displacements can be removed by performing a differential rectification of the



images. The outcome of such a differential rectification is known as an orthophoto-graph or orthophoto.

An orthophoto is basically an orthogonal projection of the objects in an image. Thus, all pixels in an orthophoto will cover exactly the same area on the objectplane. This fact makes orthophotos very suitable for measuring the size of objects represented in the images.

To create orthophotos from the images a Digital Elevation Model (DEM) is required. Furthermore, the relation between the ground coordinate system and the image coordinate system must be known. A DEM can be created by a number of different methods. However, it is never an exact representation of the surface, and due to this fact errors will arise in the orthophoto.

Considering that the scale between the ground coordinate system and the image coordinate system (the focal length of the camera lens) is known, the relation between the two coordinate systems can be determined from six parameters  $(x_0, y_0, z_0, \omega_0, \phi_0, \kappa_0)$ . The first three parameters state the position of the camera in the ground coordinate system and the last three parameters describe the orientation of the CCD image plane relative to the ground coordinate system. The precision of these parameters will, of course, influence the accuracy of the orthophoto. In the case that the computation of the orthophotos is based on several images in a time-series (where the coordinates for the projection centre are equal for all images), the error introduced from these parameters will be consistent. This means that using orthophotos for measuring objects over a large area requires:

- that the coordinates for the projection centre are precise;
- that the DEM has been developed with high precision; and
- that the image has a high resolution.

Finally, the camera calibration must be determined. Errors are introduced by the lenses and the camera itself. However, by determining the camera calibration these errors can be corrected (Have 1999).

When creating the orthophotos, the pixel values are calculated by interpolation based on the pixel values from the original images. A number of methods exists, e.g. nearest neighbour, bilinear and bicubic. While the nearest neighbour and the bilinear methods use the closest and the four closest pixels, respectively, to interpolate pixel values in the orthophotos, the bicubic method uses the 16 closest pixels. Additionally the bicubic method also takes into account the gradient of the intensities of the 16 closest pixels (Press *et al.* 1992). Of the three methods mentioned the bicubic method has led to the best results, and thus this method was used here.

#### 2.4. RGB Normalized Difference Snow Index (RGBNDSI)

Due to the fact that the camera is located 500 m above sea level (asl), many of the digital images are usable even though they are obtained on days with cloudy conditions. However, the illumination of the pictures differs from image to image. Under partial cloud cover the area will be non-homogeneously illuminated, and on days where the sky is clear the images are brighter than under cloudy conditions. Therefore, automatic snow cover detection from a large series of orthophotos cannot be performed by simply introducing a threshold value in order to determine whether or not a given pixel can be classified as snow. Consequently it was necessary to develop the RGB Normalized Difference Snow Index (RGBNDSI). The index is empirically derived, but fundamentally it is based on the same principles as the



Normalized Difference Snow Index (NDSI) used for Landsat TM images. For TM data the NDSI is given by:

$$\text{NDSI} = \frac{\text{TM}_{\text{Band2}} - \text{TM}_{\text{Band5}}}{\text{TM}_{\text{Band2}} + \text{TM}_{\text{Band5}}} \quad (1)$$

where  $\text{TM}_{\text{Band2}}$ ,  $\text{TM}_{\text{Band5}}$  represent VIS and MIR, respectively (Dozier 1989).

As shown in figure 3(a), snow reflectance is very high in VIS and extremely low in MIR. Consequently, snow covered surfaces become very significant compared to other surfaces when the NDSI is applied. The MIR part of the spectrum cannot be represented directly by the RGB values, as they are a reflection of VIS. In the *RGBNDSI*, MIR therefore is replaced by a fictitious band, which is related to MIR. The new index is defined as:

$$\text{RGBNDSI} = \frac{\text{RGB} - \text{MIR}_{\text{Replacement}}}{\text{RGB} + \text{MIR}_{\text{Replacement}}} \quad (2)$$

where  $\text{RGB} = (\text{R} + \text{G} + \text{B})/3$ .

The challenge in the development of the *RGBNDSI* was to find a method to calculate the fictitious MIR replacement. The first step was to empirically evaluate an expression that led to extraordinary low brightness values for high RGB values (snow). This was done by assuming that the MIR replacement can be expressed by an inverse power function of RGB intensities [equation (5)].

In order to optimize the level of detail in the images, the camera automatically adjusts the sensitivity of the CCD sensor system relative to the total amount of brightness in the images. Consequently, in images with a high mean RGB value, low reflectance surfaces will appear darker than in images with a low mean RGB value and vice versa. Thus, the next step in the process was to find an expression which is proportional to the overall level of brightness in a given orthophoto, and use this as a threshold function  $\tau$  [equation (4)], that indirectly determines whether RGB values in an orthophoto are at a relatively high (or low) level. Under most circumstances  $\tau$  can be expressed directly as a function of the mean RGB value of the orthophoto as the number of pixels with high brightness values normally is proportional to this value. However, where a large amount of the image is darkened due to, for example, a partial cloud cover, the number of pixels with high brightness will be underestimated if  $\tau$  is related only to the mean RGB value of the orthophoto. Therefore, the amount of brightness in the orthophoto is expressed by the mean value of a recalculated orthophoto, which empirically has been determined as:

$$\text{RGB}_{\text{high}} = \frac{\text{B}^3}{\text{R}^3} \cdot \text{G} \quad (3)$$

Normally the term  $\frac{\text{B}^3}{\text{R}^3}$  is close to 1 for 'snow pixels'; however, in the case of darkening due to clouds, the blue component is higher than the red component, and in such cases an orthophoto which is recalculated using equation (3) will therefore have a higher mean RGB value than the original orthophoto.

The function  $\tau$  was evaluated empirically, determining the optimum value of  $\tau$  when calculating snow cover extents in images with high and low overall levels of

brightness, respectively. This evaluation was performed using a careful visual examination of the images in question. It was found that automatic determination of  $\tau$  led to results of high accuracy when the following linear relationship was used:

$$\tau = 200(a(\text{RGB}_{\text{High}})_{\text{Mean}} + b) \quad (4)$$

where  $a$  and  $b$  are empirically derived constants, specific for the particular camera. (For the DC50 used in 1999,  $a$  and  $b$  were found to be  $-0.0125$  and  $1.2875$ , respectively.)

Using the relationships mentioned above the MIR replacement is defined as:

$$\text{MIR}_{\text{Replacement}} = \frac{\tau^4 \cdot \text{RGB}_{\text{Max}}}{\text{RGB}^4} \quad (5)$$

where  $\text{RGB}_{\text{Max}}$  = the maximum RGB value in the digital orthophoto.

Figure 4 shows that shadow effects from clouds can be compensated for, if the  $\text{RGB}_{\text{NDSI}}$  is applied.

### 3. Case study Zackenberg

#### 3.1. Study area

The Zackenberg study area is located in a high relief mountainous environment in the High Arctic zone in part of north-east Greenland. The landscape consists of nearly horizontal valley floors below 200 m asl, steep slopes between 200–800 m asl and plateaus above 800 m asl. The main objective of the research taking place in the Zackenberg area is to focus on processes in the tundra landscapes below 200 m asl. The area is located in the zone of continuous permafrost and hosts a large diversity of glacial, periglacial and coastal landscape features and a great variety of biotopes such as fens, heaths, fell-field plateaus and grasslands. Meteorological data from Zackenberg (1996–99) indicate an annual precipitation of approximately 200 mm, mainly as snow, and a mean annual air temperature of approximately  $-10^\circ\text{C}$ . The period of frequent temperatures above  $0^\circ\text{C}$  starts in late May or early June and ends around September. From September to May the dominant wind direction is from the north, causing snowdrifts on slopes facing south.

The research at Zackenberg mainly focuses on processes in the catchment of the river Zackenbergelven. The entire catchment covers approximately  $514\text{ km}^2$ , and the majority of the scientific work takes place in the lower part of the valley (approximately  $50\text{ km}^2$ ) (Meltofte and Thing 1997, Meltofte and Rasch 1998, Rasch 1999).

#### 3.2. Snow cover detection in the Zackenberg area

The process of snow detection from the DCIs is outlined in figure 5. The first step in the process was to transform the DCIs into orthophotos. This operation of geo-referencing pixels in the DCIs is very sensitive to a number of potential errors. The factors of greatest importance are the accuracy of the image orientation relative to the ground coordinate system (the outer orientation) and the accuracy of the DEM. The actual DEM covers an area of  $10.01\text{ km} \times 8.51\text{ km}$ , and the cell size is  $10\text{ m} \times 10\text{ m}$ . It is based on measurement of contour lines in a stereo model from two aerial photographs. The amount of uncertainty generated through this operation mainly depends on the outer orientation of the two images used, the interval between the contour lines, the photo scale and the skills of the operator (Kraus 1993).



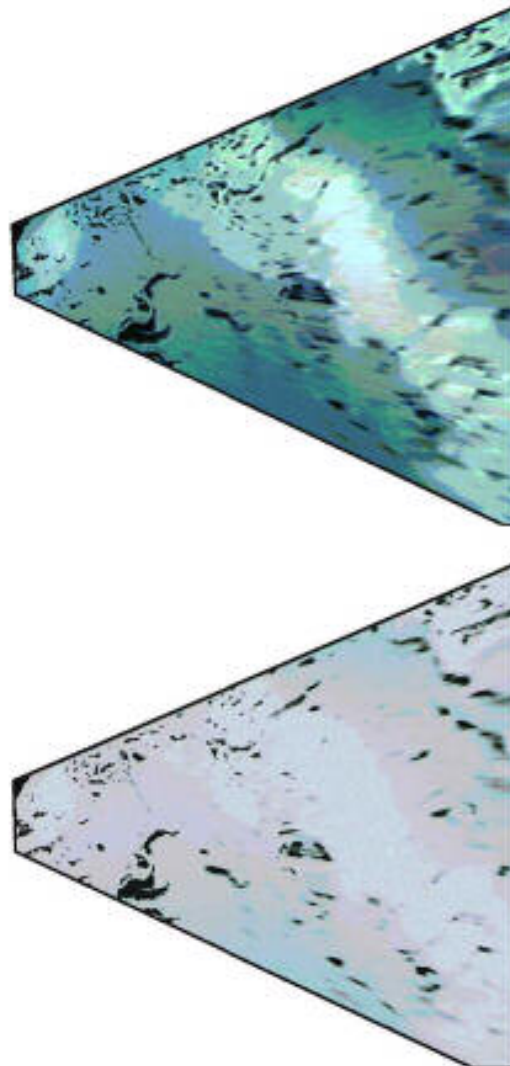


Figure 4. An *RGBNDSI* image versus the orthophoto from which it was created. The varying illumination in the original image is due to shadow effects from partial cloud cover. It can be observed that these illumination effects can be compensated for by applying the *RGBNDSI*. The original image was taken on 15 June 1999.

Due to the size of the study area and the resolution of the images, the most important source of error in this project is the outer orientation of the camera. For the outer orientation, ground control points ideally must be equally spread throughout the images. To determine these points only features of a considerable size (depending on the distance from the camera) that differ significantly from their surroundings were used.

The position of the control points was found by intersection from two known coordinates. Compared to the accuracy of the identification of the control points within the images the accuracy of this technique is high, and the largest part of the uncertainty therefore is related to the identification of the control points in the images.

The computation of the orthophotos was based on a relatively low number (not more than 10) of ground control points (GCPs). However, using these few points, it

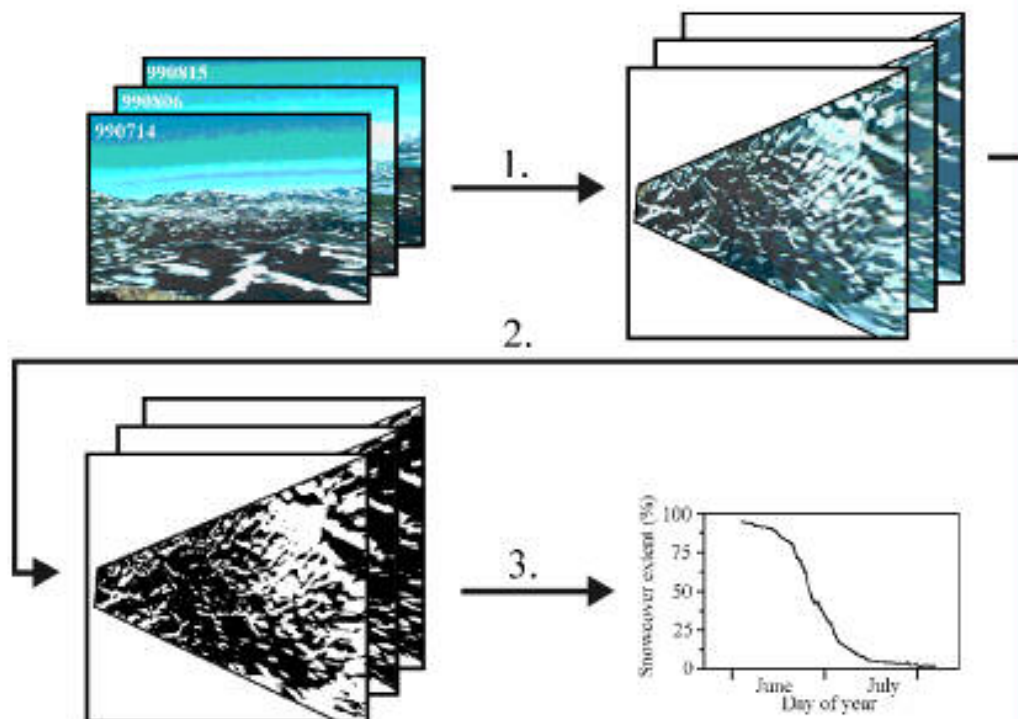


Figure 5. The steps used in the creation of snow cover depletion curves from the DCIs: 1. creating the orthophotos 2. performing snow mapping using the *RGBNDSI*; and 3. calculating snow cover extent for different dates, and creating a snow depletion curve.

has been possible to make the control points fit the rectification model (Dueholm 1989) with an rms (in camera pixels) of 0.023 and 0.013 in 1998 and 1999, respectively. From the GCPs the model calculates the position of the camera. This position is modelled with an accuracy (relative to the known position) in all directions of less than 10 m for both years. In the actual situation, where only a few control points have been measured in the field, it is a great advantage that the camera is fixed at its position during the entire melt-off season. This is due to the fact that if all the GCPs can be determined in just one image, it is possible to use them, also for rectification of images where they cannot be recognized. To eliminate errors that are due to the existence of areas invisible to the camera, these areas were calculated in concurrence with the orthophotos, and they were excluded from the calculations of the snow cover. The river running through the valley was also excluded from the calculations (figure 6), because the reflectance properties of water surfaces are difficult to deal with in oblique images. Furthermore, bright surfaces in the river bed are not necessarily snow but might be icefloes, icings, etc.

The final computation of the snow cover extent from the orthophotos was performed automatically on both the 1998 and 1999 image series using the *RGBNDSI*, with the empirically determined cut-off value of 0.6. The application to perform this operation on a whole image-series was programmed using the Chips Scripting Language (CSL) (CDT 2000). To create the regions of interest and exclude the areas mentioned above, small applications were programmed also using CSL. The regions were generated as ESRI shp-files by these applications and the DEM.

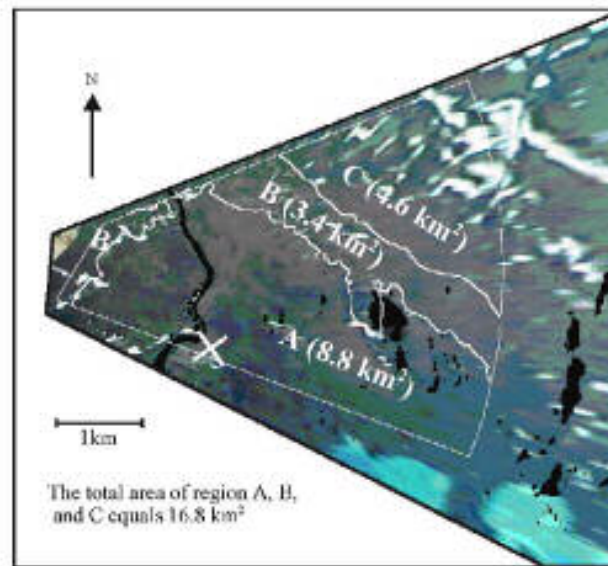


Figure 6. The three regions A, B and C and the areas excluded from calculations of the snow cover (areas invisible for the camera and Zackenbergelven) are shown. The location of the research station is indicated by the white cross.

#### 4. Results and discussion

A careful visual examination of the snow maps and the orthophotos has shown that the *RGBNSDI* leads to convincing results, when performing automatic snow detection on a large series of digital orthophotos. The snow maps produced were used to produce snow cover depletion curves as shown in figure 7. Those for 1999 are based on 46 images, while those for 1998 are based on only 17 images. The fewer images in 1998 is due to bad weather conditions and technical problems, especially at the beginning of the season. Due to the smaller number of images, potential errors in one single image will have a larger influence on the 1998 depletion curves than on the 1999 curves. The 1998 depletion curves, therefore, must be treated more critically than those for 1999. The depletion curves were produced for the following regions, all located at a distance less than 7 km within the field of view of the camera: A, 0–50 m asl; B, 50–100 m asl; C, > 100 m asl; and 'All regions' (regions A, B and C) (figure 6).

Because the accuracy of the orthophotos decreases with the distance from the camera, the 7 km limitation was chosen in order to represent the largest area that can be mapped from the orthophotos with high resolution. Region A represents the flat and rather homogeneous part of the valley, and the B and C regions represent more heterogeneous mountainous zones of intermediate and high altitudinal level, respectively.

For mountainous regions a gradual decrease in the snow cover is typical due to irregular deposition of snow, which results in variable snow depths. The gradual decrease of the snow cover results in 'laterally reversed S-shaped' depletion curves (Hall and Martinec 1985). Figure 7 shows that this is also the case for the Zackenberg area. How pronounced the S-shape of the depletion curve is, depends on the initial amount of snow and the temperature during the melt-off season.

For both 1998 and 1999, the snow cover is almost 100% at the beginning of the melt-off season. However, in 1998 the initial snow cover depletion rate was higher



## Sixth Circumpolar Symposium on Remote Sensing of Polar Environments 4679

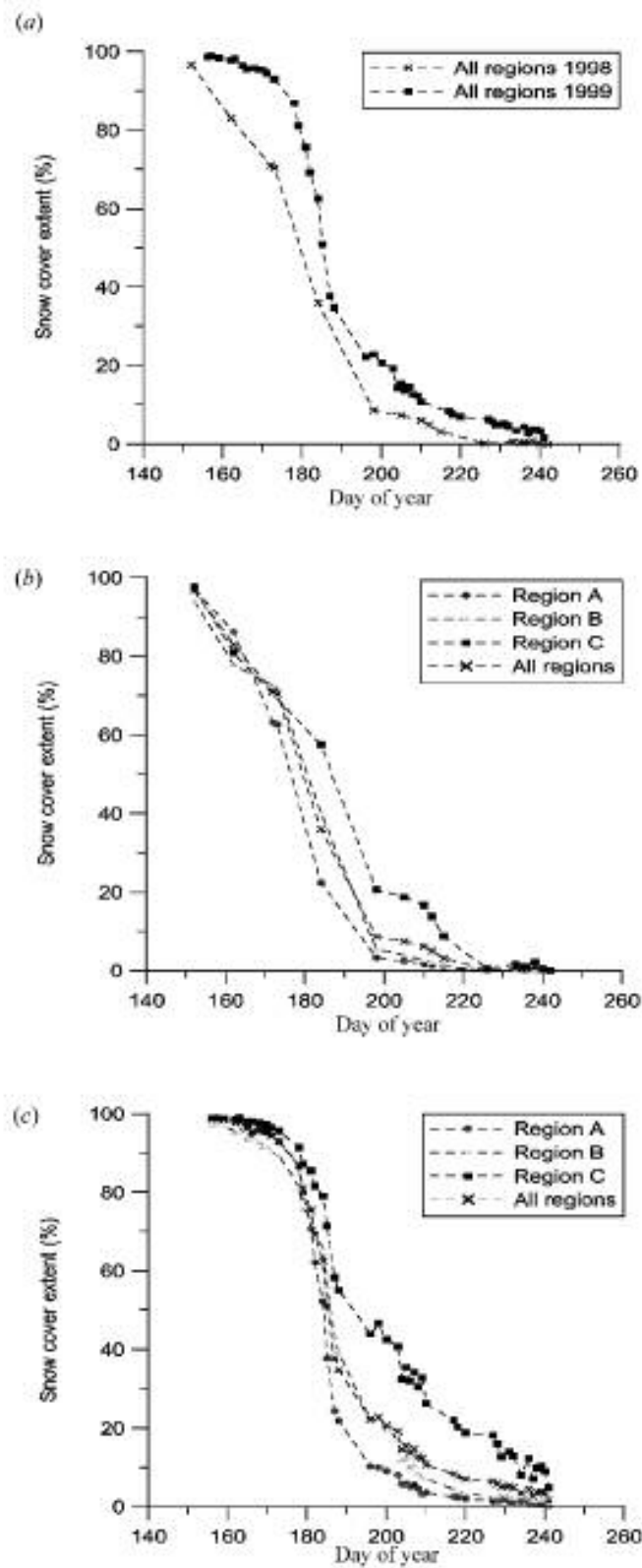


Figure 7. Snow cover depletion curves for the Zackenberg area: (a) for All regions in 1998 and 1999, respectively; (b) for region A, B, C and All regions in 1998; and (c) for region A, B, C and All regions in 1999.

than in 1999, resulting in a steeper depletion curve at the beginning of the season. Nevertheless, in 1999 the decrease from 80% to 20% happened in approximately 14 days, while in 1998 the same decrease in the snow cover took almost four weeks [figure 7(a)]. Thus, the S-shape of the depletion curves is more pronounced in 1999 than in 1998. This is due to the combination of a greater initial snow depth (figure 8) and higher temperatures (figure 9) in 1999. Furthermore, the greater initial amount of snow in 1999, has led to the fact that the day with 50% snow cover occurred one week later in 1999 than in 1998. From figure 7(b) and (c) it can be observed that the snow cover extent decreases at a higher rate in the valley than in the mountainous regions, resulting in a less pronounced S-shape of the depletion curves at higher altitudes. This is due to the fact that in the more irregular mountainous landscape large and deep snowdrifts evolve, which reduces snow cover depletion, while in the valley the disappearance of the snow cover is more abrupt due to a more uniform distribution of the snow cover thickness. Furthermore, because of the temperature

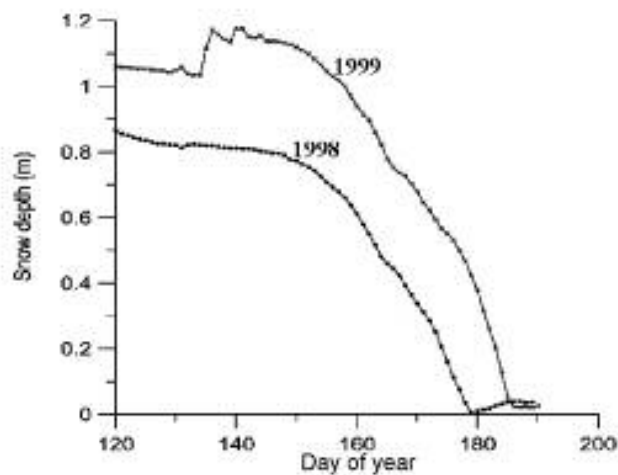


Figure 8. Snow depth measured at the research station in 1998 and 1999, respectively.

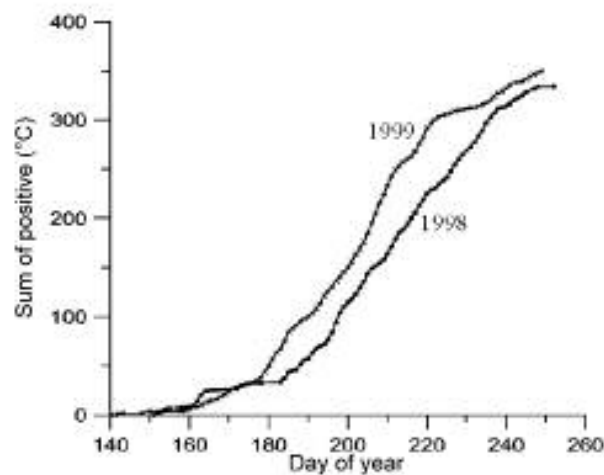


Figure 9. Sum of positive °C in the 1998 and 1999 melt-off seasons. The temperatures are measured at the research station, which is located approximately 30 m asl.



lapse rate, the snow melt is progressing from the valley floor to the higher altitudes (Hall and Martinec 1985).

### 5. Conclusions

Using DCIs transformed into orthophotos has opened the possibility of performing snow cover mapping with high temporal and spatial resolution over small areas at a very low cost. The temporal resolution of the DCIs is far beyond that which can be achieved with high resolution satellites. This is illustrated by the 1999 time series, where 46 images are usable for snow mapping purposes. To obtain a high temporal resolution, the DCIs must of course be taken frequently. However, the large number of usable images is also due to the fact that the *RGBNDSI* makes it possible to compensate for varying illumination within and between different images.

Snow cover mapping in Zackenbergdalen using the *RGBNDSI* on the orthophotos has led to convincing results. The snow depletion curves from 1998 and 1999 show that the snow cover depletion in Zackenbergdalen is characterized by a gradual decrease in the snow cover resulting in 'laterally reversed S-shaped' depletion curves. The S-shape of the depletion curves is controlled by the initial amount of snow and the temperature in the period of snow melt.

During the melt-off season, the snow cover decreases at a higher rate in the valley than at higher altitudinal levels, and thus the snow cover depletion curves turn out to have a more linear shape with increasing altitude.

### Acknowledgments

The authors want to thank Kim Have, the Technical University of Denmark, for developing the software program 'Ortho'. Without this program this work would not have been possible. The Danish Polar Center is acknowledged for providing access to ecosystem monitoring data and logistics at the research station at Zackenberg.

### References

- BRUN, E., DURAND, Y., MARTIN, E., and BRAUN, L., 1994, Snow modelling as an efficient tool to simulate snow cover evolution at different spatial scales. *Proceedings of Yokohama Symposia J2 and J5, July 1993*, IAHS Publication No. 223 (Oxfordshire: IAHS Press).
- CDT (Chips Development Team), 2000, Online user's guide. Institute of Geography, University of Copenhagen, <http://www.geogr.ku.dk/chips/index.htm>.
- DOZIER, J., 1989, Spectral signature of alpine snow cover from the Landsat Thematic Mapper. *Remote Sensing of Environment*, **28**, 9–22.
- DUEHOLM, K. S., 1989, The generic bundle adjustment US Geological Survey Open-File Report, pp. 89–185.
- DUGUAY, C. R., and LEDREW, E. F., 1991, Mapping surface albedo in the east slope of the Colorado Front Range, USA, with Landsat Thematic Mapper. *Arctic and Alpine Research*, **23**, 213–223.
- GRAY, D. M., and MALE, D. H., 1981, *Handbook of Snow* (Toronto: Pergamon).
- HALL, D. K., and MARTINEC, J., 1985, *Remote Sensing of Ice and Snow* (Cambridge: Chapman and Hall).
- HALL, D. K., KOVALICK, W. M., and CHANG, A. T. C., 1990, Satellite-derived reflectance of snow-covered surfaces in northern Minnesota. *Remote Sensing of Environment*, **33**, 87–96.
- HANSEN, B. U., and MOSBECH, A., 1994, Use of NOAA-AVHRR data to monitor snow cover and spring melt-off in the wildlife habitats in Jameson Land, East Greenland. *Polar Research*, **13**, 125–137.

4682 *Sixth Circumpolar Symposium on Remote Sensing of Polar Environment*

- HAVE, K., 1999, Photogrammetric image analysis for climate studies. Department of Planning, The Technical University of Denmark.
- KODAK, 1998, Some technical background on the Kodak digital science DC40 camera. <http://www.kodak.com/country/US/en/digital/cameras/dc40/dc40TechBkgd.shtml>.
- KRAUS, K., 1993, *Photogrammetry*, vol. 1 (Bonn: Dümmler).
- MELTOFTE, H., and RASCH, M. (eds), 1998, Zackenberg Ecological Research Operations, 3rd Annual Report 1997. Danish Polar Center, Ministry of Research and Information Technology.
- MELTOFTE, H., and THING, H. (eds), 1997, Zackenberg Ecological Research Operations, 2nd Annual Report 1996. Danish Polar Center, Ministry of Research and Information Technology.
- PLÜSS, C., and MAZZONI, R., 1994, The role of turbulent heat fluxes in the energy balance of high alpine snow cover. *Nordic Hydrology*, **25**, 25–38.
- PRESS, W. H., TEUKOLSKY, S. A., VETTERLING, W. T., and FLANNERY, B. P., 1992, *Numerical Recipes in C*, 2nd edn (Cambridge: Cambridge University Press).
- RASCH, M. (ed.), 1999, Zackenberg Ecological Research Operations, 4th Annual Report 1998. Danish Polar Center, Ministry of Research and Information Technology.
- SØGAARD, H., and THOMSEN, T., 1988, Application of satellite data to monitor snow cover and runoff in Greenland. *Nordic Hydrology*, **19**, 225–236.
- SWAMI, A. N., and BRIVIO, P. A., 1996, Hydrological modelling of snowmelt in the Italian Alps using visible and infrared remote sensing. *International Journal of Remote Sensing*, **17**, 3169–3188.
- TAMSTORF, M. P., 1997, Analyse af sne- og vegetationsdækket ved Zackenberg, NØ-Grønland. Institute of Geography, University of Copenhagen, Denmark.
- WINTHER, J.-G., 1993, Short- and long-term variability of snow albedo. *Nordic Hydrology*, **23**, 199–212.
- WINTHER, J.-G., and HALL, D. K., 1999, Satellite-derived snow coverage related to hydropower production in Norway: present and future. *International Journal of Remote Sensing*, **20**, 2991–3008.





## Detection of spatial, temporal, and spectral surface changes in the Ny-Ålesund area 79° N, Svalbard, using a low cost multispectral camera in combination with spectroradiometer measurements

Jørgen Hinkler<sup>a,\*</sup>, Jon Børre Ørbæk<sup>b,1</sup>, Birger Ulf Hansen<sup>a,2</sup>

<sup>a</sup> Institute of Geography, University of Copenhagen, Øster Voldgade 10, 1350 Copenhagen K, Denmark

<sup>b</sup> Norwegian Polar Institute, P.O. Box 505, N-9171 Longyearbyen, Svalbard, Norway

Received 30 January 2003; received in revised form 27 June 2003; accepted 5 August 2003

### Abstract

Changes in surface reflection at the arctic tundra at Ny-Ålesund, Svalbard (79° N) were monitored during the melting season 2002 using a low cost multispectral digital camera with spectral channels similar to channels 2, 3, and 4 of the Landsat Thematic Mapper satellite sensor. The camera was placed 474 m above sea level at the Zeppelin Mountain Research Station and was programmed to take an image automatically every day at solar noon. To achieve areal consistency in the images (which is necessary for mapping purposes) the images were geometrically rectified into multispectral digital orthophotos. In contrast to satellite images with high spatial resolution the orthophotos provide data with high spatial and high temporal resolution at low cost. The study area covers approximately 2 km<sup>2</sup> and when free of snow, it mainly consists of typical high arctic tundra with patchy vegetation and bare-soil in between. The spectral information in the images was used to divide the rectified images into maps representing different surface classes (including three subclasses of snow). By combining classified image data and ground measurements of spectral surface reflectance, a methodology to produce daily maps of surface albedo was developed. The method takes into account the effect of decreasing snow-albedo with ageing snow pack, and the very rapid decrease of albedo when the snow pack is shallow (<10 cm) which is due to influence from the underlying ground. The time series of modelled albedo-maps shows that the snow melt period (when the albedo decreases from 80% to 20%) varies from less than 10 days in areas near the coast or in the Ny-Ålesund settlement till more than 70 days in areas with large snow or ice accumulations. For the entire study area the mean length of the 2002 melting period was 28.3 days with a standard deviation of 15.1 days. Finally, the duration of the snowmelt season at a location where it has been measured routinely since 1980, was calculated to 23 days, which is very close to what is the average for the last two decades. © 2003 Elsevier Ltd. All rights reserved.

**Keywords:** Remote sensing; Orthophoto; Multispectral; Snow; Albedo; Reflectance; Arctic; Svalbard; Ny-Ålesund; Digital; Camera

### 1. Introduction

Surface albedo is one of the most critical variables affecting the Earth's climate. Due to an extensive snow cover, surface albedo is normally high in arctic regions. However, in the short melting season, surfaces in these regions show a significant natural variability in reflectance, both with respect to its spectral variation, and in

time and space. It is important to monitor and understand this natural variability, before using surface albedo for energy- and water balance modelling, ecological modelling of biophysical parameters and climate change research. In arctic areas the surface albedo drops from around 80% under fully snow covered conditions to bare ground levels (10–20%) within two to four weeks, and the date when the tundra becomes snow-free varies from early June till mid July (e.g. Hinkler et al., 2002; Winther et al., 1999). Thus, the changing spectral characteristics of the surface during melt-off combined with the rapid decrease in albedo call for cautious use of remote sensing-derived albedo, and a need for data recorded at frequent time intervals. Satellite remote-sensed data

\* Corresponding author. Tel.: +45-35-32-41-68.

E-mail addresses: [jh@geogr.ku.dk](mailto:jh@geogr.ku.dk) (J. Hinkler), [orbak@npolar.no](mailto:orbak@npolar.no) (J.B. Ørbæk), [buh@geogr.ku.dk](mailto:buh@geogr.ku.dk) (B.U. Hansen).

<sup>1</sup> Tel.: +47-79-02-26-00/26-21.

<sup>2</sup> Tel.: +45-35-32-25-19.

have been used in a wide variety of arctic studies for almost three decades. For example, they have been used in snow and glacier studies by Jacobsen et al. (1993), and surface energy- and water balance by Soegaard et al. (2001). Multispectral satellite data from arctic areas have also been used to monitor and model the spatio-temporal variation of biophysical parameters such as length of growing season (e.g. Tamstorf, 2000), vegetation cover fraction (e.g. Jacobsen and Hansen, 1996), leaf area index and biomass production (e.g. Hansen, 1991). However, at smaller scales image data with high spatial resolution are required to produce a detailed picture of the spatial variation of surface reflection within a given area. This need cannot be fulfilled by using high resolution satellite data like Landsat Thematic Mapper (TM) or Système Probatoire pour l'Observation de la Terre (SPOT). This is due to the fact that the temporal resolution of these satellite systems is too poor to acquire images of the same area frequently. Furthermore, satellite images are sensitive to cloud cover and data with high spatial resolution are often costly.

This study was carried out in the area around Ny-Ålesund 79° N, Svalbard and had two main purposes. The first purpose was to develop and set up a low cost system to produce a time series of orthographically rectified multispectral images of the study area (Figs. 1 and 4) offering both high spatial and temporal resolu-

tion. The second purpose was to combine these images with field measurements of surface reflectance in order to compute a time series of daily albedo-maps and then use these for calculation and description of the spatial variability of snowmelt-duration within the study area. Furthermore it was an aim to reveal peculiar albedo features that are connected to different regimes of snow melt and different surface types.

The system producing the multispectral digital orthophotos (MDOs) consists of a Tetracam multispectral three channelled (green (G), red (R), near infrared (NIR)) digital camera (MDC), and a specially developed software package—Ortho (Have, 1999). The camera was placed at the Zeppelin Mountain Station at 474 m above sea level facing Ny-Ålesund/Kongsfjorden taking daily oblique images of the Ny-Ålesund area (Fig. 4). Every image recorded under fair weather conditions from this time series were orthographically rectified. Ground truth measurements for calibration and verification of surface reflectance were performed with a Fieldspec FR spectroradiometer.

The study area (which includes the Ny-Ålesund settlement) is limited by the field of view of the camera and the coastline along Kongsfjorden (Fig. 1), and it covers approximately 2 km<sup>2</sup>. When free of snow, the surface in the area roughly consists of typical high arctic tundra with patchy vegetation and bare-soil/gravel in between. In a few spots some particularly dark surfaces, that

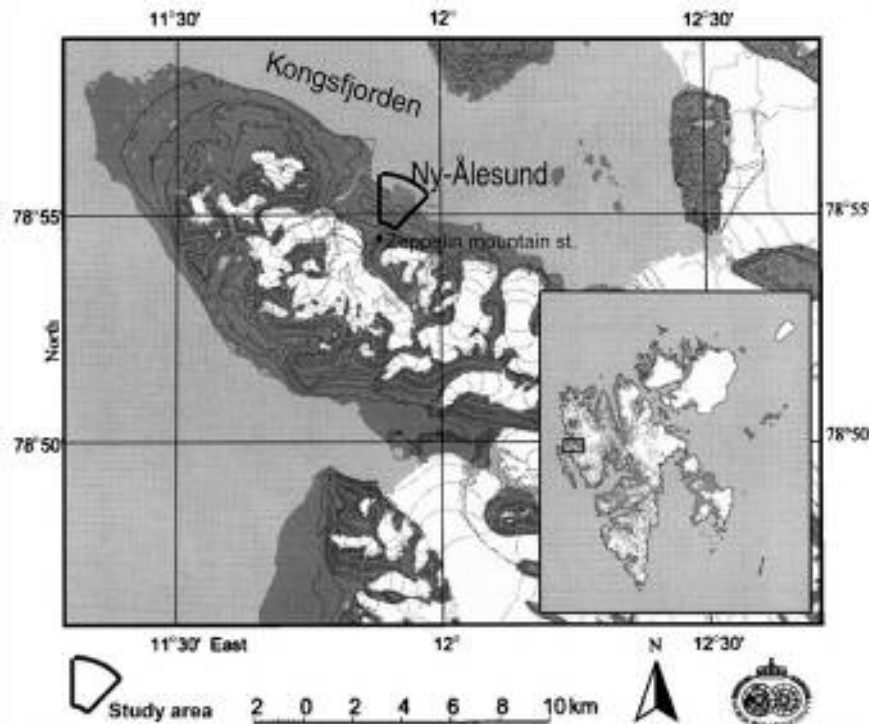


Fig. 1. Map of Kongsfjorden area, Svalbard. The study area (the area covered by the multispectral digital camera) is indicated by the black polygon.



are remnants from a former coal mining activity, are present.

## 2. Spectral properties of different surface types

In relation to remote sensing, natural surfaces can roughly be divided into four major different categories—bare-soil, vegetation, water and snow/ice. The spectral reflectance of bare-soil increases generally with wavelength, and is affected by the soil texture, moisture, and presence of organic matter. A coarse, wet and organic soil has a lower reflectance than a dry clay soil.

Vegetated surfaces have three distinct wavelength determined segments of reflectance. These can be characterized as low reflectance in the visible (400–700 nm) (VIS) part of the spectrum due to chlorophyll absorption, high reflectance in the near infrared (700–1200 nm) (NIR) part of the spectrum caused by cell structure and leaf area. In mid infrared (1200–2500 nm) vegetation has medium reflectance due to water absorption. The spectral reflectance of vegetation has a strong dependence of season as well as age and vegetation-type. The reflectance of water in VIS is a little higher than for vegetation and due to very high absorption, it declines to almost zero at higher wavelengths. The level of reflectance depends of depth and load of suspended material. Shallow water with suspended material has a high reflectance, while deep clear water has a very low reflectance.

The surface types of major interest in connection with this study are the snow covered surfaces. Snow is a matrix of ice grains, air, and water and often contains impurities like dust and plant materials. The optical properties of the snow pack in VIS and NIR depend on grain size distribution, thickness of the snow pack, occurrence of impurities and liquid water content (Warren, 1982). The reflectance from a fresh snow pack remains high in VIS, while a distinct drop occurs in NIR (Fig. 2) and finally it drops to below 10% in the mid-infrared region. The change from fresh to metamorphosed clean snow (which is due to crystal growth and increase of liquid water content) causes a reflectance decrease, especially at longer wavelengths. A further decrease in reflectance at wavelengths from 600–700 nm indicates that microscopic dust and other small particles may cover the snow surface, while macroscopic and visible dirt on the snow give a further decrease, mostly in the visible range (400–700 nm). Thinning of the snow causes a significant decrease in reflectance, as the underlying ground seems to become visible at a snow thickness of approximately 10 cm and less (Wiscombe and Warren, 1980).

Clouds highly increase the amount of diffuse radiation relative to the amount of direct radiation incident on a surface, and they also alter the spectral distribution

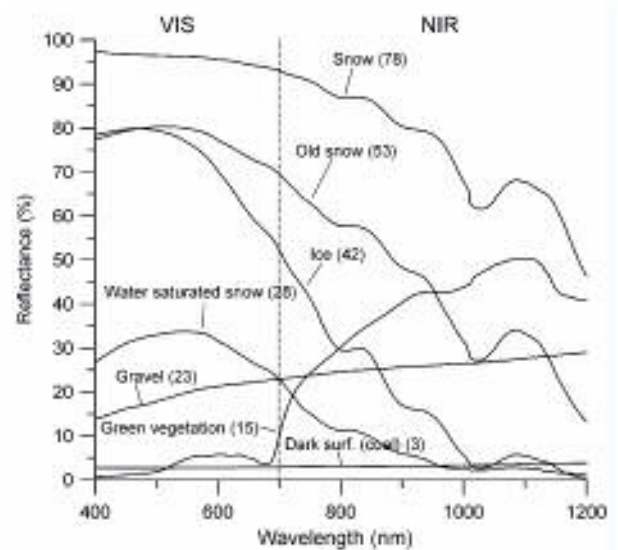


Fig. 2. Reflectance curves for seven different surface types (snow, old snow, ice, water, gravel, green vegetation, and dark surfaces—remnant from former coal deposits). All of the measurements were performed using a Fieldspec FR spectroradiometer. The numbers given in parentheses are values of numerically integrated broad band albedo.

of the radiation reaching the surface, since they absorb a higher portion of infrared than visible radiation. Thus, a relatively high portion of visible radiation reaches the surface under cloudy conditions. Work by Winther et al. (1999) has shown that the combined effect of these factors can make the integrated broad band albedo increase with up to 7% in the case of a change from clear sky to 100% overcast conditions.

As metamorphosed snow reflects radiation anisotropically (Iqbal, 1983), the sensor derived albedo strongly depends on the geometry between the sun, the sensor and the surface segment (pixel). The reflectance of snow increases with illumination angle, especially for larger grains, because snow has a tendency to be strongly forward-scattering in NIR (Dozier, 1989). The increase in albedo can be as high as 25% and the largest anisotropy is seen for metamorphosed snow in measurements facing the sun.

As mentioned, reflectance of snow decreases in the NIR part of the spectrum. When attempting to divide snow into subclasses this decrease becomes of significant importance. As snow ages or melts, the grain size increases, and especially in NIR snow reflectance is sensitive to grain size. This means that the relative proportion between VIS and NIR is larger for old snow than for fresh snow, making it possible to separate fresh and metamorphosed snow. The normalized difference snow/ice index (NDSII) (De Abreau and LeDrew, 1997) is given by

$$\text{NDSII} = \frac{\text{VIS} - \text{NIR}}{\text{VIS} + \text{NIR}} \quad (1)$$



where VIS (580–680 nm) and NIR (725–1100 nm) are integrated reflectance values. The index ranges from  $-1$  to  $1$ , with snow and ice values expected between  $0$  and  $1$ . The larger the index, the more metamorphosed the snow contained in the pixel in question. In this study the NDSII is used to distinguish between fresh and water saturated snow, and it was calculated using raw R and NIR pixel values.

### 3. Image data and field measurements

#### 3.1. Multispectral digital camera images

The MDC is a Tetracam inc. single-CCD camera with a resolution of  $1200 \times 1024$  pixels and a colour filter array applied to it. Thus each pixel on the CCD is sensitive to only one colour. After colour reconstruction (demosaicing processing using raw pixel data), the green, red, and near infrared (G, R, NIR) spectral bands approximately cover the following wavelength intervals: 520–570 nm (G), 600–690 nm (R), and 750–850 nm (NIR) (see Table 1).

The camera was set up inside the Zeppelin Mountain Research Station at 474 m above sea level facing a north to north-easterly direction towards the Ny-Ålesund settlement and Kongsfjorden (Fig. 4). The cameras internal alarm clock was programmed to trigger the camera and take a picture out through the window once a day during the period May 22–August 14. In order to obtain optimum light-conditions during image-exposure, the time of capture was set to be at solar noon. At that time of day the intensity of solar irradiation is at its maximum, and further, as the camera is pointed almost directly to the North (the same direction as the propagation of solar rays at noon) problems due to backlight and saturation can be avoided more easily. In addition to the daily images a diurnal time series was recorded at 10 min intervals at June 28–29.

This was done to investigate the cameras sensitivity to the solar azimuth angle. During the entire recording period, the local weather has varied with periods of fair weather conditions, periods with both high and low cloud cover, and periods with foggy conditions. Data were therefore recorded under a large number of different solar illuminations. Fig. 3(A)–(D) illustrate the MDCs response and dynamic range (in R and NIR) at different levels of solar illumination and at different

azimuth angles. Fig. 3(A) and (B) reveal that image brightness is correlated to the global radiation and that the correlation is most significant at visible wavelengths. Note, around midnight the Sun's position is to the north, meaning that the solar rays propagate almost directly toward the camera lens. This explains the abrupt increase in pixel values at that time of day. The MDCs response is very sensitive to the adjustment of its diaphragm. During this study it has been attempted to adjust the diaphragm to cover light conditions varying from bright clear skies to overcast conditions. To avoid saturation on clear days, the diaphragm was set at a relatively high level. Thus, under overcast conditions, images were relatively dark, reducing the dynamic range of a given image significantly. In Fig. 3(C) and (D) the relation between global solar radiation, and the R, and NIR pixel values is shown (due to azimuth problems, data recorded during the time around midnight were excluded). From the figures, it can be observed that at the current diaphragm-settings a minimum of 250 and 400  $W m^{-2}$  (for R and NIR, respectively) is required to be able to discriminate two spectrally very different surface types without ambiguity (snow and vegetation) on the basis of a single spectral channel. Therefore (see Section 4.2), surface classification was based partly on relative proportions between spectral bands. The changing weather conditions combined with the MDCs high sensitivity to different illuminations has limited the number of images from the daily time series usable for surface classification to 19 out of a total of 85.

#### 3.2. Field measurements

Spectral field data were collected during two field campaigns—the first one took place in mid May before extensive snowmelt began, and the second one at the end of June/beginning of July, where large vegetated areas and bare-soil areas were free of snow. Measurements were performed using a Fieldspec FR spectroradiometer (analytical spectral devices) measuring from 350 to 2500 nm. It consists of three built-in separate spectrometers. The first one measures from 350 to 1000 nm using a 512 element photodiode array, and has a spectral resolution of about 3 nm. The second and third ones are of scanning types and measure from 900 to 1850 nm and 1700 to 2500 nm, respectively sampling every 2 nm, with a spectral resolution of about  $10 \pm 11$  nm. Results presented here primarily use data from the first spectro-

Table 1  
The spectral channels of the Tetracam multispectral camera, the SPOT high resolution visible (HRV), and the Landsat TM satellite sensors

	MDC (nm)	SPOT (HRV) (nm)	Landsat TM (nm)
Green	520–570	Channel 1: 500–590	Channel 2: 520–600
Red	600–690	Channel 2: 610–680	Channel 3: 630–690
Near infrared	750–850	Channel 3: 790–890	Channel 4: 760–900



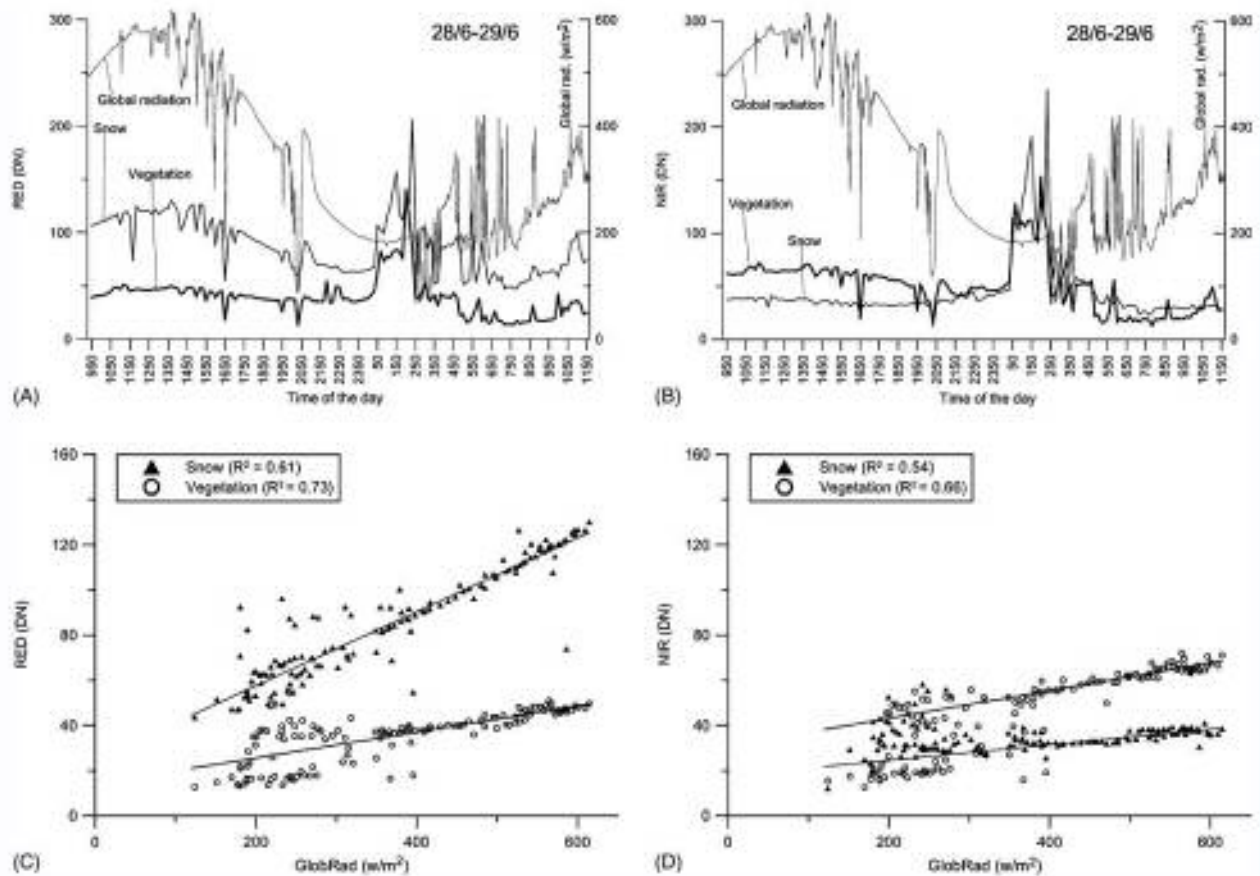


Fig. 3. Pixel values (snow and vegetation) from the diurnal (June 28–29) time series of multispectral camera images. (A, B) shows camera response (pixel values) in *R* and NIR and global radiation during the day. (C, D) shows *R* and NIR pixel values (period 21:00–04:00 excluded) plotted against global radiation.

meter covering the visible/near-infrared (VNIR) wavelength range from 350 to 1050 nm. The optical detector (which simply consists of the bare optical fibre with an adapter limiting the field of view to 18°) was fastened to a standard camera tripod to avoid movements during the less than one-second integration time of the measurement, and measurements were acquired 50 cm above the surface of interest. The spectral albedo was determined as the ratio of incident solar radiation reflected from the surface target and the incident radiation reflected from a calibrated white reference Spectralon plate (about 30 cm × 30 cm). Both the spectroradiometer and the reference Spectralon were calibrated at the optical calibration lab in Ny-Ålesund to “NIST traceable reference lamps and spectralons”.

Measurements were done on representative snow and ice surfaces as well as typical vegetation, bare-soil/gravel, and particularly dark surfaces of former coal deposits (characteristics of spectral reflectance for different surface types are displayed in Fig. 2). Spectral reflectance measurements of the selected surfaces (snow, ice/water saturated snow, gravel, and vegetation) were performed at weekly intervals.

To be able to rectify image data orthographically, 16 ground control points (GCPs) were measured at visually significant spots in the Ny-Ålesund area (Fig. 4) using global positioning system (GPS).

#### 4. Methods

##### 4.1. Creating multispectral digital orthophotos

When the images are captured by the camera, they are created as a central projection of the object space (the real world) to the image plane (the CCD-chip in the camera). The central projection introduces displacements, which makes it impossible to measure the size of objects represented in the images. These displacements can be removed by performing a differential rectification of the images. The outcome of such a rectification is known as an orthophotograph or orthophoto. An orthophoto is basically an orthogonal projection of the objects in an image, and thus, all pixels in an orthophoto will all cover areas of equal size on the object plane. However, due to lens distortion, errors will arise in the

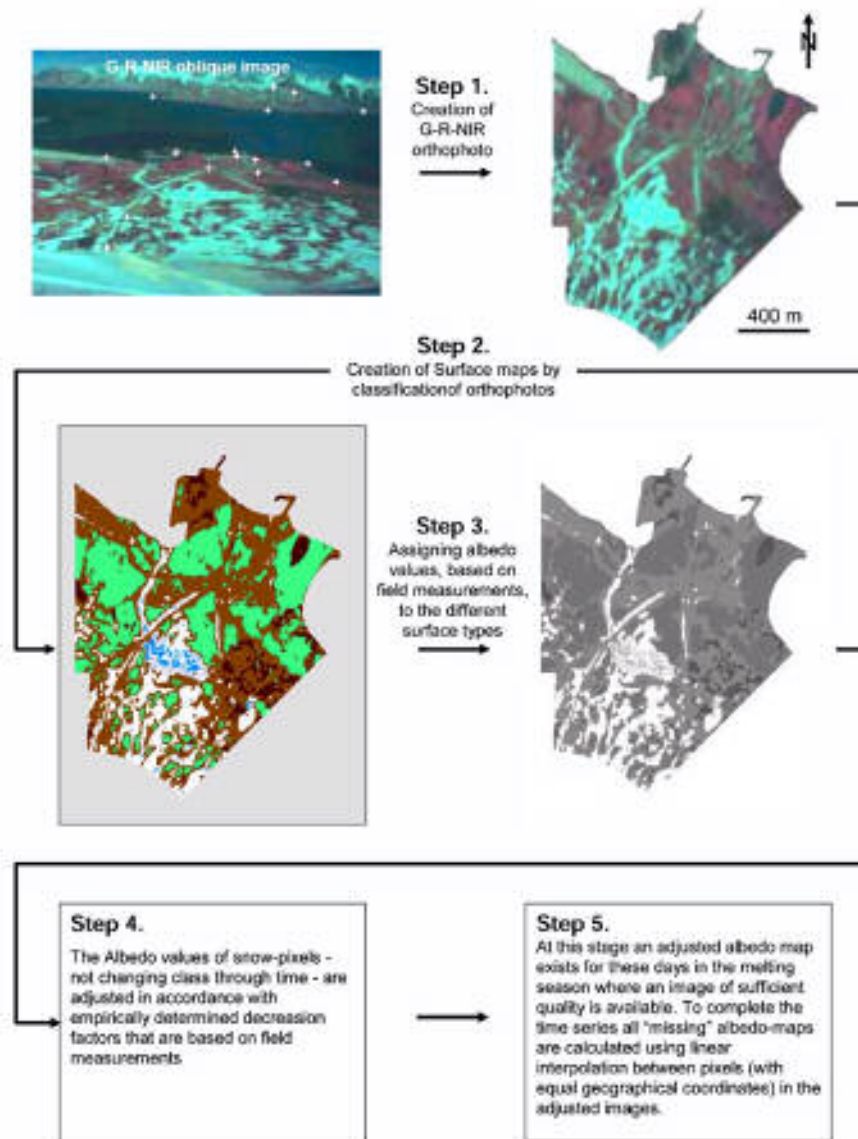


Fig. 4. Methodological sketch of the steps used in the procedure of transforming oblique image data into classified surface types and further into a full time series of albedo-maps. Ground control points (GCPs) used for geometric rectification are indicated with white crosses. On the classified map six surface types exist: snow (white), water saturated snow (blue), refrozen snow (light blue), vegetation (green), dark surfaces (dark brown), and gravel, etc. (brown).

orthophoto if distortion coefficients are not included in the rectification procedure. An exact camera calibration (Dueholm, 1989) therefore was performed in cooperation with the Technical University of Denmark (DTU).

To create the MDOs, the relation between the ground coordinate system and the image coordinate system must be known. When performing orthographic rectification using the software Ortho, this relation/transformation model is found using a digital elevation model (DEM) and a number of ground control points (GCPs). In this study orthographic rectification was based on the 16 GCPs collected during the field campaigns and a

20 m resolution DEM provided by the Norwegian Polar Institute (NPI). In order to improve the spatial resolution of the MDOs, the DEM was resampled to 4 m resolution. An example of an oblique multispectral digital image versus the corresponding MDO is illustrated in Fig. 4.

#### 4.2. Classifying multispectral digital orthophotos into different surface types

The G, R, and NIR pixel values from the MDOs were used to classify the study area into maps representing six



different surface types: fresh snow, water saturated snow, metamorphosed/refrozen snow, vegetation, very dark surfaces e.g. former coal deposits, and gravel/intermediate reflective areas such as buildings, etc.

#### 4.2.1. Classifying snow

As stated above, snow is divided into three distinct subclasses. However, in the first place all snow-pixels are selected using two empirically determined thresholds—both based on spectral reflective properties of gravel. In this study gravel is represented by the mean (raw pixel) value (in the image being processed) of the air strip situated in the upper left corner of the MDOs. The first step in the process of classifying snow involves two criteria:

$$\text{NDSII} > 1.08 \cdot \text{NDSII}_{\text{Gravel}} \quad \text{and} \quad G > 0.8 \cdot G_{\text{Gravel}}, \quad (2)$$

where  $G$  refers to raw green channel pixel values.

In order to divide snow into subclasses the following routine was introduced: The first step of the routine concerns the classification of water saturated snow. This class simply consists of pixels with an empirically determined NDSII threshold greater than 0.53. The classification of Metamorphosed/refrozen snow involves a throughput (in chronological order) of the whole time series of classified surface maps (at this stage including two snow-classes: fresh snow and water saturated snow). During the throughput it is checked whether pixels that are classified as fresh snow in the current surface map previously have been classified as water saturated snow. If this is the case, the given pixel will be assigned to the class of metamorphosed/refrozen snow.

#### 4.2.2. Classifying vegetation, very dark surfaces, and gravel/intermediate reflective areas

Due to the strong reflectivity of green vegetation in NIR, a pixel simply can be classified as vegetation if its value in NIR is large relative to its value in VIS. For the Tetracam MDC it was empirically determined that pixels containing vegetation have a NIR to  $G$  (raw pixel values) ratio larger than 1.1.

Very dark surfaces are characterized by having a very low reflectance in all parts of the shortwave-spectrum. Thus, all pixels that are *not* vegetation ( $G$  significantly higher than NIR) and have an average  $\text{GRNIR}$  value  $[(G + R + \text{NIR})/3]$  significantly lower than gravel are assigned to this class. Thus, to classify this surface type the following two selection criteria were introduced:

$$G > 1.1 \cdot \text{NIR} \quad \text{and} \quad [(G + R + \text{NIR})/3] < 0.8 \cdot [(G + R + \text{NIR})/3]_{\text{Gravel}}, \quad (3)$$

where  $G$ ,  $R$ , and NIR are raw pixel values in the red, green and near infrared channels, respectively.

Finally, if a pixel does not belong to any of the above mentioned classes, it is classified as gravel/intermediate reflective areas.

#### 4.3. Deriving daily maps of broad band albedo

The total shortwave albedo has been measured routinely at the Norwegian Polar Institute research station in Ny-Ålesund since 1980 on the same tundra location (location 1 in Fig. 6). Eppley PSP Pyranometers and during the past 10 years Kipp and Zonen Pyranometers model CM11 have been used, annually calibrated on site with reference to the station Absolute Cavity Pyrheliometer. These measurements show that the albedo normally remains above 80% until late May. Thereafter, a rapid decrease in albedo occurs until albedo levels corresponding to snow-free tundra are reached (Winther et al., 1999). Basically, this decrease in albedo is related to two main factors—firstly, when the snow cover is thick enough not to be affected by the underlying ground, the decrease in albedo is due to snow melt and metamorphosis (increasing grain size), this albedo decrease occurs less rapidly than when the albedo is affected by the underlying ground. Secondly, at shallow snow depths (<10 cm), snow-albedo starts to get influenced by the ground, and at this stage the albedo decreases very rapidly, as the snow pack is thinning and is getting increasingly transparent. By combining this knowledge with the classified surface-maps and field measurements of surface reflectance, a method to calculate a time series of albedo-maps was developed. Using this method an albedo-map of the Ny-Ålesund area was derived for each day in the entire melting season.

Fig. 5 shows measured and calculated broad band albedo for a number of different surface types (snow, ice/water saturated snow, vegetation, and gravel). Furthermore two different albedo decrease coefficients ( $0.804\% \cdot \text{day}^{-1}$  and  $0.567\% \cdot \text{day}^{-1}$ ) are visualized in the figure. These coefficients are used to calculate albedo decrease for fresh and older/metamorphosed snow, respectively (when not affected by the underlying ground). All calculation routines included in the process of deriving albedo-maps, and all routines used for image classification during this study was programmed in chips scripting language (CSL), which is an integral part of the Copenhagen Image Processing System (CHIPS) developed at the Institute of Geography, University of Copenhagen (CDT, 2002). Below is given a systematic description of the derivation of the albedo-calculation routine: During the melting season, spectral surface reflectance was measured for the six surface classes. The spectral measurements were numerically integrated to broad band albedo. In the first place a time series consisting of 19 albedo-maps (derived from the classified MDOs) was created. During this process each surface type were assigned a particular albedo value based on



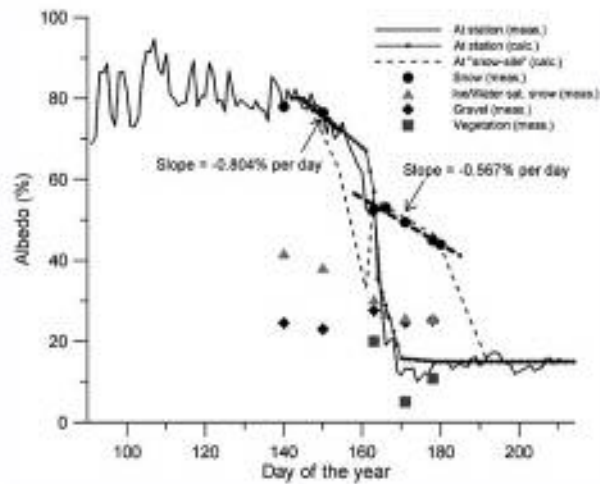


Fig. 5. Measured and modelled values of albedo at different dates. Measured data are from the NPEs research station and from spectral field measurements. Albedo decrease coefficients (fresh snow:  $-0.804\% \text{ day}^{-1}$  and metamorphosed snow:  $-0.567\% \text{ day}^{-1}$ ) are also indicated.

the numerically integrated values created from the field data: fresh snow: 80%, water saturated snow 33%, metamorphosed/refrozen snow: 55%, vegetation: 15%, very dark surfaces: 3%, and gravel/intermediate reflective areas: 23%. However, as discussed above; when the snow pack ages during the melting season, snow-albedo decreases with time; therefore snow-pixels in the 19 albedo-maps were recalculated using the above mentioned decrease factors for fresh and metamorphosed snow. The outcome of this procedure then is 19 new albedo-maps that are adjusted with respect to the age of the snow pack. The final step in calculating the time series was to fill the gaps of dates with missing albedo-maps. This was done using simple linear interpolation between pixels with equal geographical coordinates in the adjusted albedo-maps. The final output then come as a complete time series consisting of daily albedo-maps for the whole recording period/melting season (a sketch of the whole process from capturing the images to the production of daily albedo-maps is outlined in Fig. 4).

## 5. Results and analysis

In order to verify the accuracy of the derived albedo-maps, calculated and measured values of albedo were compared for the snow site where surface reflectance was measured regularly during/between the field campaigns; and for the permanent albedo monitoring station (Fig. 5). It can be observed that there is a good match between the calculated and the measured values. However, a high overall accuracy of the calculated results—spatially as well as temporally, requires, of course, that the classification of the MDOs is correct. Therefore, all classified

surface-maps were checked by a careful visual inspection, and critical pixels (pixels that have been saturated one or more times during the recording period) were excluded from statistical calculations.

Fig. 6 presents a number of selected sites where data have been extracted from the calculated albedo-maps and Fig. 8 presents the change in albedo for these sites through time. These data, reflect that in the Ny-Ålesund area, the time it takes for the albedo to decrease from its maximum around 80% till it reaches bare ground levels varies a lot. It is also interesting to note that increases after a first decrease in albedo have occurred for a number of pixels corresponding to 14% of the areas with snow cover. At site 2 for example, surface runoff makes the snow pack water saturated (lowering the albedo) and dry out/refreezing processes makes the albedo increase afterwards. At site 7, the albedo decreases rapidly down to 30–40%, and thereafter it increases again until it reaches 50–60% before a new and last decrease. This phenomena is due to the presence of “naled ice” which is an ice body being formed by the refreezing of perennial ground water flow with snow accumulation on top of it (Lefauconnier, 2003, personal communication), the spring is located in an old mine named the Ester Mine and the main recharge of the sub-permafrost groundwater aquitar is the nearby Vestre Lovénbreen glacier (Haldorsen and Heim, 1999). When snowmelt is about to end (at this location by the beginning of July) the surface

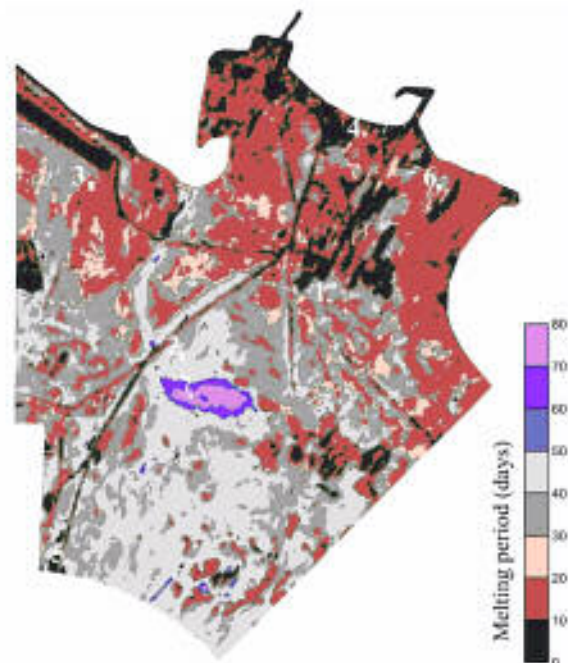


Fig. 6. Map displaying the spatial distribution of the duration of the snowmelt within the study area. Seven selected test sites are indicated on the map (corresponding curves of modelled albedo are shown in Fig. 8).



consists of ice made of a circular crystals overlapped by a layer of superimposed “dirty ice” and water saturated snow, making the albedo drop to around 35%. When the snow has disappeared, melting starts at the periphery of the crystals (especially with clear sky), and the drying of the surface and the increase of its roughness lead to an increase of the backscattering and of the albedo.

At the measurement site (close to the NPIs research station—location no. 1 in Fig. 6), the snowmelt season, defined as the period when albedo decreases from above 80% till it reaches bare ground level (<20%) has varied between 13 days in 1995 to 30 days in 1986, with an average of 23 days (Winther et al., 1999). Fig. 6 shows the spatial distribution of the length of snowmelt period in the Ny-Ålesund area (2002). The map was derived by running a throughput on the calculated albedo-maps, where the first day in the melting period is defined as the first day where the albedo gets below 80%, and the last day is defined as the day where it reaches its end value (vegetation, gravel, or dark “crust”). At the station, the derived snowmelt period lasts 23 days, indicating that with respect to the length of the snowmelt season, the year 2002 was very close to average. For the entire study area the average length of the 2002 melting season is 28.3 days with a standard deviation of 15.1 days (Fig. 7). However, from Fig. 6 it can also be observed that, spatially the length of the melting period varies a lot; from 0 days in areas where the snow is removed by human activity to between 70 and 80 days in areas with large accumulations of snow and ice. Further, it can be observed that the snow cover generally disappears most rapidly in areas close to the coast and nearby the Ny-Ålesund settlement.

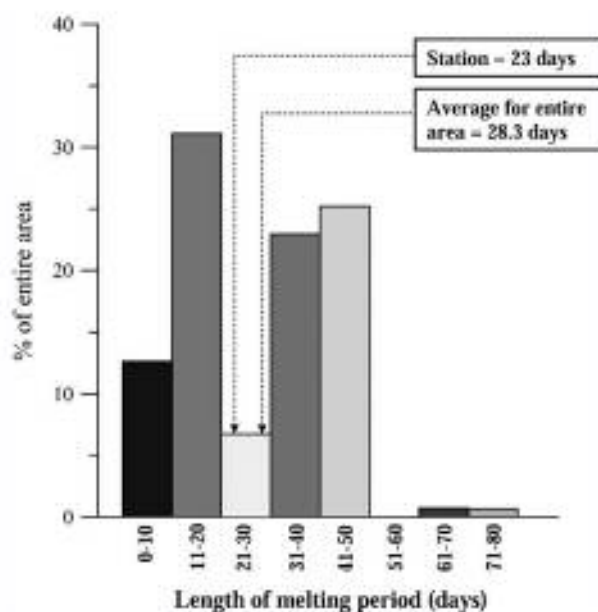


Fig. 7. The distribution of the duration of the melting period (eight temporal intervals) shown as percentages of the study area.

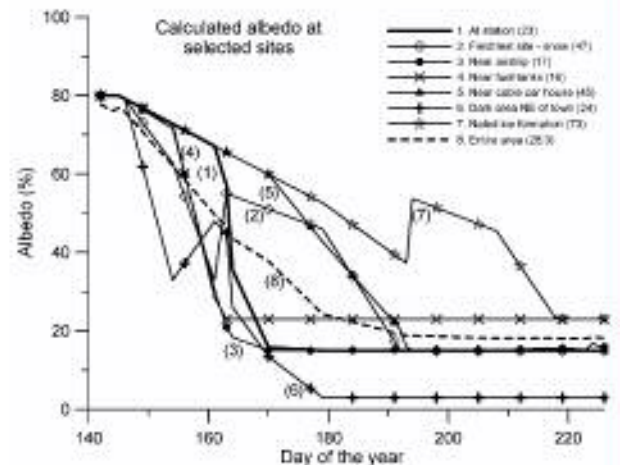


Fig. 8. Modelled surface albedo at selected test sites during the melting season. Numbers in parentheses (in legend) indicate the modelled duration of snowmelt at the selected sites.

In Fig. 7 the distribution of the length of the melting season is given as percentage of the study area. The distribution was divided into 8 segments: 0–10 days (representing 12.6% of the area), 11–20 days (31.1%), 21–30 days (6.7%), 31–50 days (23.0%), 41–50 days (25.2%), 51–60 days (0.0%), 61–70 days (0.7%), and 70–80 days (0.6%). The figure describes a bimodal distribution indicating that during the melting season bare ground surfaces within the study area become free of snow in two main steps. The first step occurs early in the melting season before the 20th day and the second occurs in the last part of the season between the 30th and the 50th day. During the first step the majority of areas becoming snow-free are situated close to the coast/near the Ny-Ålesund settlement, indicating relatively shallow snow depths in these areas and possibly a higher concentration of impurities in the snow pack. Further, it is likely that areas located close to the coast are subjected to more drift and less accumulation. The second step primarily includes areas situated closer to the Zeppelin Mountain leading to the conclusion that a large amount of the snow-precipitation is drifting towards these areas forming a thicker snow pack. After around 50 days almost all of the snow/ice cover has disappeared except at one location situated in the central part of the study area, where a reservoir of snow/ice still is present after more than 60 days, and first after 80 days the area is 100% free of snow and ice. Finally, areas that are characterized by an intermediate melting period (20–30 days) only represent a relatively small fraction of the study area and though most of them are situated nearby the coast/Ny-Ålesund-settlement they generally seem to be almost stochastically distributed. This could indicate that they are small depressions with a slightly larger snow accumulation than the adjacent areas.



## 6. Conclusion and perspectives

During the snowmelt season the surface albedo in the Ny-Ålesund area decreases continuously (starting at 80%) until bare ground levels are reached when the tundra becomes free of snow. By utilizing knowledge of the spectral properties of different surface types and spectral ground measurements in combination with spectral image data; it was possible to develop a new method to give a detailed picture of this process. By using orthographic rectification on multispectral camera images, a set of geocoded image data with high spatial and temporal resolution was produced. The temporal resolution of these image data is significantly better than what can be obtained from high spatial resolution satellite remote sensing data. Due to varying weather conditions during the recording period the number of images suitable for surface classification was limited to 19 out of a total of 85. However this number of images is still high when compared to the fact that e.g. the Landsat TM/ETM (Thematic Mapper/Enhanced Thematic Mapper) satellite sensors overpasses the same area only a couple of times per month. The orthographically rectified multispectral images were transformed into maps representing different surface classes. These classified surface maps and the values of albedo measured in the field have made us able to create a methodology to produce a complete time series of daily albedo maps. The Time series covering the 2002 melting season reveals that duration of snow melt-off in the Ny-Ålesund area varies much in space and time. It seems that the tundra becomes free of snow in two main steps—one early in the season and one late in the season. Mostly, this can be explained by different snow accumulations (smallest near the coast and largest close to the mountainside). However, due to the presence of so called naled ice at one specific site, the duration of ice/snow coverage lasts significantly longer there than at all other sites. At some sites during melt-off, the surface albedo increases and is followed by an afterwards decrease. This phenomenon is due to the presence of the naled ice, surface runoff, and small accumulations of water, which lead to the formation of ice from refrozen water or water saturated snow packs with relatively low surface albedo. Dry-out and weathering of the ice crust lead to the afterwards increase in albedo.

This great variability, combined with the fact that Ny-Ålesund offers unique facilities for research/monitoring in the Arctic, favours the idea of future use of the technique discussed in this paper in long term environmental change monitoring programs in the area.

Furthermore, time series of daily albedo-maps could contribute to improve studies of surface energy balance modelling. In that context the Ny-Ålesund area could serve as representative for a typical coastal area in the region.

Finally, if modelled lengths of the melting period were combined with temperature data, the spatial distribution of snow cover thickness could be represented in form of degree days (transformed into snow water equivalents). These data then could be used in hydrological projects, e.g. estimation of the size water reservoirs represented by the snow cover.

## Acknowledgements

This work was made possible under a grant from the European Commission IHP-programme (Ny-Ålesund Large Scale Facility, contract HPRI-CT-1999-00057). Further, the Norwegian Polar Institute is thanked for providing excellent facilities and data. Are Backlund, optical engineer at the Norwegian Polar Institutes research station (Sverdrup Station, Ny-Ålesund) is thanked for doing spectral measurements in between the field campaigns. Erik Poulsen and Ole Mærsk Møller, the Technical University of Denmark (DTU), Department of Informatics and Mathematical Modelling are thanked for doing the calibration of the camera-lens-distortion parameters. Finally, Kim Have former student at the DTU is thanked for developing the orthographic rectification software Ortho.

## References

- CDT (Chips Development Team), 2002. Online user's guide. Institute of Geography, University of Copenhagen. Available from <<http://www.geogr.ku.dk/chips/index.htm>>.
- De Abreau, R., LeDrew, E., 1997. Monitoring Snow and Ice Conditions Using a Normalized Difference Index Based On AVHRR Channels 1 and 2. Available from <[http://www.crysys.uwaterloo.ca/science/documents/ger97\\_deabreu2.pdf](http://www.crysys.uwaterloo.ca/science/documents/ger97_deabreu2.pdf)>.
- Dozier, J., 1989. Spectral signature of Alpine snow cover from the Landsat Thematic Mapper. *Remote Sensing of Environment* 28, 9–22.
- Dueholm, K.S., 1989. The generic bundle adjustment. US Geological Survey Open-File Report, pp. 89–185.
- Haldorsen, S., Heim, M., 1999. An Arctic groundwater system and its dependence upon climatic change. An example from Svalbard. *Permafrost and Periglacial Process* 10, 137–149.
- Hansen, B.U., 1991. Monitoring natural vegetation in southern Greenland using NOAA AVHRR and field measurements. *Arctic* 44 (1), 94–101.
- Have, K., 1999. Photogrammetric image analysis for climate studies. Masters thesis, Department of Planning, The Technical University of Denmark, pp. 191, unpublished.
- Hinkler, J., Pedersen, S.B., Rasch, M., Hansen, B.U., 2002. Automatic snow cover monitoring at high temporal and spatial resolution, using images taken by a standard digital camera. *International Journal of Remote Sensing* 23, 4669–4682.
- Iqbal, M., 1983. *An Introduction to Solar Radiation*. Academic Press.
- Jacobsen, A., Hansen, B.U., 1996. Estimation of the soil heat flux/net radiation ratio over high latitude natural vegetation using spectral vegetation indices. In: *Proceedings of the Fourth Circumpolar Symposium on Remote Sensing of the Polar Environments*, Lyngby 29 April–1 May 1996, pp. 33–38.



- Jacobsen, A., Carstensen, A.R., Kamper, J., 1993. Mapping of satellite derived surface albedo on the Mitdluagkat Glacier, Eastern Greenland, using a digital elevation model and SPOT HRV data. *Danish Journal of Geography* 93, 6–18.
- Lefauconnier, B., 2003. Personal communication.
- Soegaard, H., Hasbø, B., Friberg, T., Nordstroem, C., 2001. Surface energy- and water balance in a high-arctic environment in NE Greenland. *Theoretical and Applied Climatology* 70, 35–51.
- Tamstorf, M.P., 2000. Satellitbaseret vegetationskortlægning i Vestgrønland. Ph.D. thesis, pp. 177.
- Warren, S.G., 1982. Optical properties of snow. *Reviews of Geophysics and Space Physics* 20, 67–89.
- Winther, J.-G., Gerland, S., Ørbæk, J.B., Ivanov, B., Blanco, A., Boike, J., 1999. Spectral reflectance of melting snow in a high Arctic watershed on Svalbard: some implications for optical satellite remote sensing studies. *Hydrological Processes* 13, 2033–2049.
- Wiscombe, W.J., Warren, S.G., 1980. A model for the spectral albedo of snow. I: Pure snow. *Journal of the Atmospheric sciences* 37, 2712–2733.

*Note: to provide an overview of the albedo variation during melt-off, the CD-ROM, attached to the back cover, includes a video animation of surface albedo during the melting season in Ny-Ålesund, 2002.*

# **Snow–vegetation relations in a High Arctic ecosystem: Inter-annual variability inferred from new monitoring- and modeling concepts**

J. HINKLER, B. U. HANSEN, M. P. TAMSTORF, S. B. PEDERSEN

**Abstract.** For High Arctic ecosystems, snow is one of the most important climatic factors— affecting both length of the growing season, and primary plant production. To perform a retrospective analysis of inter-annual variability in snow distribution/amount and vegetative activity in a High Arctic ecosystem, these factors were investigated for the Zackenberg valley at 74.5°N in Northeast Greenland. The analysis was based on recently introduced techniques that utilize conventional and multispectral digital camera images accompanied by Landsat TM/ETM+ and SPOT HRV satellite data. Since 1998 (and since 2002 multispectral) digital cameras have been installed on the Zackenberg mountain side 500 m above the valley floor taking daily images of the valley automatically. These images were transformed into digital orthophotos, which were further used to derive surface maps for snow cover and Normalized Difference Vegetation Index (NDVI) analysis. The comprehensive amount of information represented by the snow cover- and NDVI maps was used to develop semi-empirical modeling approaches to calculate end-of-winter snow accumulation, snow-cover-depletion, and net vegetative activity (snow-free NDVI) during melt-off. These approaches are applicable if 1) at least one satellite image (or air photo) with high spatial resolution and 2) daily temperature means during the melting season are available. Currently, it has been possible to procure usable satellite data back to 1988 (except for the year 1990). Due to different end-of-winter snow accumulations, and different temperature distributions during melt-off, snow-cover-depletion around Zackenberg shows considerable inter-annual variability. A comparison between snow cover and NDVI distribution reveals that vegetative vigor in the Zackenberg area primarily is linked to the initiation time of the snow-free period rather than temperature. This indicates that in some Arctic regions increases in winter (snow)-precipitation might be as—or even more crucial for the ecosystem, than the increased temperatures projected by the majority of Global Circulation Models.

## **1. Introduction**

Arctic ecosystems are particularly sensitive to disturbances, and are therefore considered to respond rapidly to climatic changes (Reynolds and Tenhunen, 1996). Changes in vegetative distribution and activity in the Arctic are therefore important indicators of changes in the global climate.

Studies based on satellite data (Myneni et al., 1997; Tucker et al., 2001; Zhou et al., 2001) have shown that in many large regions, between 40°N and 70°N, photosynthetic activity of terrestrial vegetation inferred from Normalized Difference Vegetation Index (NDVI), has increased over the last couple of decades. These results are hypothesized to be in accordance with

recent CO<sub>2</sub>-induced global warming, indicating that bio-climatic zones generally have moved northwards. The regions exhibiting the greatest increase lie at the higher latitudes (45°N–70°N), where the snow has disappeared earlier in spring time. In a recent review of case studies on vegetation and land-cover change in Arctic tundra systems (Stow et al., 2004), an upward trend in photosynthetic activity also at latitudes beyond 70°N is similarly detected. However, at these latitudes and especially in the High Arctic climate zone, analyses of NDVI (e.g. NDVI–temperature relations) get complicated by the presence of snow cover, because the snow cover prevents the initiation of the growing season until it disappears from vegetated areas. Thus, to get a better and more detailed picture of the influence from snow cover on vegetative activity in the Arctic, there is a call for monitoring snow–NDVI relations at different spatial scales.

Most commonly, NDVI and snow observations at scales larger than plot-scales are inferred from satellite or from aircraft (Hope et al., 2004). However, these methods suffer from the dilemma that temporal- and spatial resolution generally is inversely related. Satellite sensors with high-spatial-resolution (30 m or better), such as the Landsat Thematic Mapper (TM) or Système Probatoire pour l'Observation de la Terre (SPOT) High Resolution Visible (HRV) have poor temporal resolutions of about two weeks (slightly better at high latitudes due to their polar orbits), and the images are often contaminated by cloud cover. On the contrary, high-temporal resolution systems with daily coverage, such as the Advanced Very High Resolution Radiometer (AVHRR) from the National Oceanic and Atmospheric Administration (NOAA) have poor spatial resolutions, typically at kilometer-scales; and measurements from aircraft are so costly that high temporal resolution cannot be financed through the funding available for most research projects. At local to intermediate scales, NDVI-observations from high latitude locations cannot be generalized from satellite data with high temporal/coarse spatial resolution; because each pixel contain several surface types, including snow (which has negative NDVI). Such data may therefore give an obfuscated picture of the state of the vegetation within the area in question, whereas high-spatial-resolution-data may lack the information necessary to describe the course of NDVI-curves through time.

The objective of this study is: 1) to develop a local-scale- ( $\approx 20$  km<sup>2</sup>) method for analyzing snow cover and NDVI at Zackenberg in high Arctic Northeast Greenland, which is based on Conventional- and Multispectral Digital Camera Images (CDCIs & MDCIs); and which works at both high

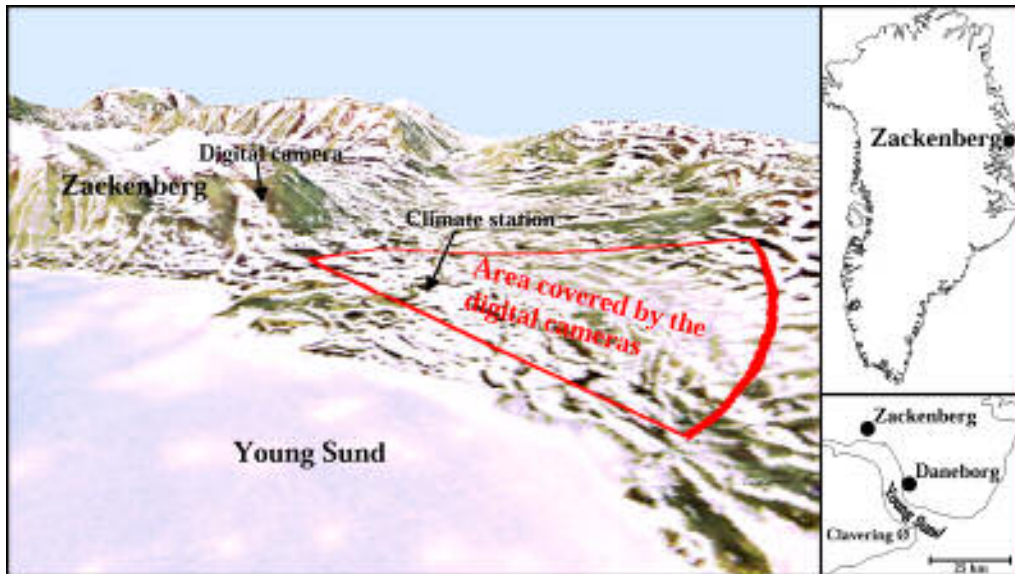
spatial- and high temporal resolution. 2) to use the comprehensive amount of data represented by the CDCIs and MDCIs to derive a semi-empirical model for calculation of snow cover extent and NDVI in years prior to the camera-installation; and to use this model for an inter-annual analysis of snow cover–NDVI relations in the Zackenberg Research Area (ZRA), retrospectively—with daily temperatures and a limited number of high-resolution satellite images as the only input-parameters.

## 2. Study area

ZRA is situated at 74.5°N, 21.6°W (Fig. 1) in Northeast Greenland. It is a high relief mountainous landscape, which consists of nearly horizontal valley floors below altitudes of 200 m, steep slopes between 200 and 800 m and plateaus above 800 m. ZRA is located in the zone of continuous permafrost and hosts a large diversity of glacial, periglacial and coastal landscape features and a great variety of biotopes like fens, heaths, fell fields, and grasslands. Continuous meteorological observations in ZRA were initiated by the Zackenberg Ecological Research Operations (ZERO) in July 1995, and indicate a mean annual air temperature (1996–2003) slightly above -10°C. From early June to early September, the mean daily temperature generally exceeds 0°C. Longer term meteorological data are available from the Automatic Weather Station (AWS) at Daneborg situated 21 km southeast of ZRA. At Daneborg the 30-year mean annual air temperature (1961–1990) is -10.3°C (Cappelen et al., 2001). According to a general climate classification (Orvig, 1970), the location of ZRA is well into the High Arctic climate zone (definition: the average temperature of the warmest month <5°C). However, as ZRA is situated in a coastal domain inside the Young Sund and Tyroler Fjord fjord-systems, the local climate is not strictly High Arctic. Since 1988 (this study deals with the period 1988–2004), the average temperature of the warmest month has varied between 4.2°C (1990) and 7.7°C (2003). Thus, if a more specific climatic classification is considered (CAVM Team, 2003), the inter-annual variation in ZRA's July-temperatures is within a range representing 2–3 different bio-climate zones—Northern arctic tundra zone, Middle arctic tundra zone, Southern arctic tundra zone (Elvebakk, 2000). ZRA therefore hosts a relatively large diversity of plant communities—currently 152 different species of vascular plants are known to be present in the area (Bay, 1998; Meltofte, 2002).

The total average annual precipitation at Daneborg is 214 mm, and about 80% of this falls as snow (1961–1974) (Ohmura and Reeh, 1991). Similar values have been found at the AWS at Zackenberg. The end-of-winter snow depth





**Fig. 1.** The Zackenberg Research Area.

measured at the Zackenberg AWS on June 1 (1998–2004) has varied from 0.44 m (2000) to 1.11 m (1999). Due to the dominance of strong winds from the NW–NE during winter, the snow cover in Zackenbergdalen is distributed unevenly over the landscape, with large snow deposited mainly on south facing slopes. The location of the larger snow-drifts is stable from year to year (Soegaard et al., 2001).

### 3. Materials and methods

The most comprehensive amount of data available for snow cover and vegetation analysis in ZRA is the CD- and MDCIs. CDCIs of the Zackenberg Valley have been obtained automatically year round on a daily basis since August 1997, and MDCIs have been obtained during June–August since June 2002 to monitor NDVI during the growing season. The NDVI is defined:

$$\text{NDVI} = \frac{\text{NIR} - \text{RED}}{\text{NIR} + \text{RED}}, \quad (1)$$

where

NIR = reflectance in the near infrared part of the spectrum

RED = reflectance in the red part of the spectrum

Due to the multispectral camera's higher power consumption, the MDCIs are only obtained in the summer-period, i.e. when the cameras can be inspected regularly, and when powering through solar panels is possible.




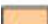


The large number of CDCIs opens the possibility of deriving a detailed description of summer snow-cover-depletion in ZRA, at both high spatial and temporal resolution. This combined with temperature data and measured snow depths (daily temperature means and end-of-winter snow depths measured at the AWS in ZRA) was used to derive a semi-empirical model for calculation of snow-cover-depletion curves in years prior to camera-installation. A snow-cover-depletion curve can be calculated if daily mean air temperatures from the melting season are available in combination with at least one of two other parameters: 1) snow coverage known for at least one day in the season or 2) the end-of-winter snow accumulation (snow depth on June 1). Like the CDCIs were used to describe snow-cover-depletion within ZRA, a detailed description of vegetative activity (NDVI) within ZRA was inferred from the MDCIs and used for derivation of another semi-empirical approach for retrospective NDVI-modeling. In this case the input parameters are derived from the modeled snow cover data, day number, temperature data, and field measurements of NDVI.

### 3.1 Data

Input- as well as output data for both the snow-cover-depletion- and NDVI models are summarized in Table 1.

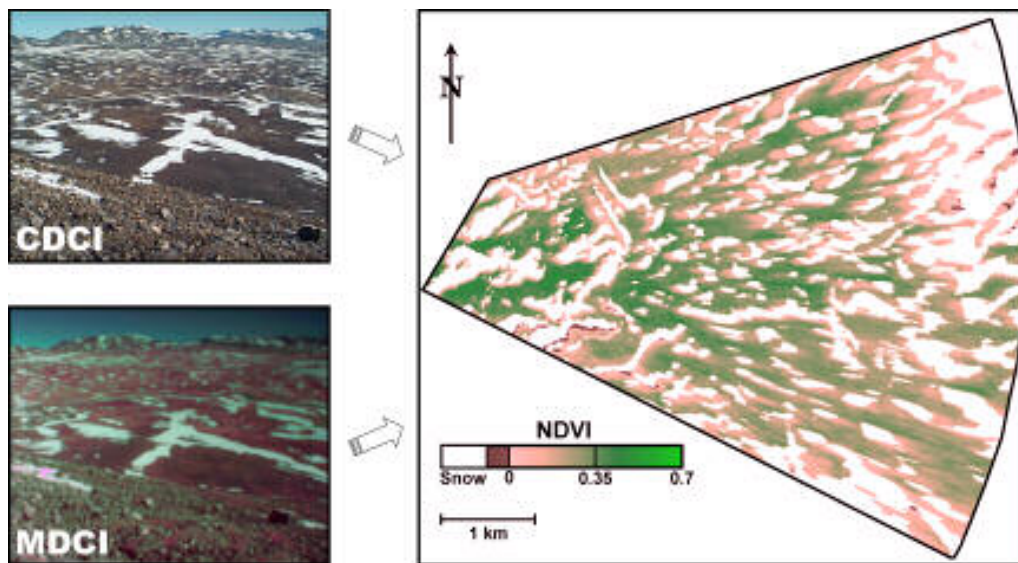
**Table 1.** In- and output data in the study.

Year	Number of camera images	Number of satellite images	Daily mean air temperature	End-of-winter snow depth	DOY of Max-NDVI	Daily snow cover	Daily NDVI
1988	—	2 (1 TM + 1 HRV)	D	MR	MR	MR	MR
1989	—	2 (1 TM + 1 HRV)	D	MR	MR	MR	MR
1990	—	—	—	—	—	—	—
1991	—	1 (1 TM)	D	MR	MR	MR	MR
1992	—	3 (3 HRV)	D	MR	MR	MR	MR
1993	—	1 (1 TM)	D	MR	MR	MR	MR
1994	—	1 (1 TM)	D	MR	MR	MR	MR
1995	—	3 (2 TM + 1 HRV)	D	MR	MR	MR	MR
1996	—	1 (1 TM)	Z	MR	MR	MR	MR
1997	3 (3 conv. reflex)	—	Z	MR	MR	MR	MR
1998	17 (17 CDCI)	—	Z	Measured	MR	Meas./MR	MR
1999	46 (46 CDCI)	1 (1 TM)	Z	Measured	Measured	Meas./MR	MR
2000	29 (29 CDCI)	—	Z	Measured	Measured	Meas./MR	MR
2001	39 (39 CDCI)	—	Z	Measured	Measured	Meas./MR	MR
2002	50 (24 CDCI + 26 MDCI)	—	Z	Measured	Measured	Meas./MR	Meas./MR
2003	85 (41 CDCI + 44 MDCI)	—	Z	Measured	Measured	Meas./MR	Meas./MR
2004	118 (43 CDCI + 75 MDCI)	—	Z	Measured	Measured	Meas./MR	Meas./MR

	Data used in derivation of snow cover depletion model
	Data used in derivation of snow cover depletion model and/or NDVI model
	Data used for derivation of snow cover depletion model and as input for NDVI model
	Data used as input for snow cover depletion model
	Data used as input for NDVI model
	Data used as input for NDVI model and snow cover depletion model
D	Daneborg
Z	Zackenbergl
MR	Modeled retrospectively

### 3.1.1 Digital camera images

The digital cameras are installed in weatherproof boxes at the side of Zackenberg Mountain at approximately 500 m above sea level, which is around 470 m above the altitude of the AWS (Fig. 1). CDCIs are captured once a day at solar noon (13:20 UTC), and MDCIs daily at the same time of the day in 2002 and bi-daily (13:20 and 14:20 UTC) in 2003–2004. To be able to quantify snow cover extents and NDVI, the oblique images were transformed into digital orthophotos (Dueholm, 1989; Have, 1999; Hinkler et al., 2002) covering approximately 17 km<sup>2</sup> (Figs. 1 and 2).



**Fig. 2.** Conventional- and Multispectral Digital Camera Images (CDCIs and MDCIs) are combined and transformed to form an orthographical snow-NDVI-map. The images in the figure were captured June 18, 2004.

Snow pixels were identified from the CDCI-orthophotos using an algorithm—*Red Green Blue* Normalized Difference Snow Index (*RGBNDSI*) by Hinkler et al. (2002), which utilizes the R, G, and B components of the digital images to compensate for varying illumination caused by shadow effects from clouds and general day to day differences in incoming solar radiation. The concept of the *RGBNDSI* is inspired by the Normalized Difference Snow Index (*NDSI*) discussed in section 3.1.3 on satellite data. In contrast to Landsat TM data the CDCIs do not contain information from the mid-infrared- (*MIR*) but only from the visible (*VIS*) part of the spectrum—in the *RGBNDSI*, *MIR*-reflectance is therefore replaced by an artificial component derived from *RGB*-values:

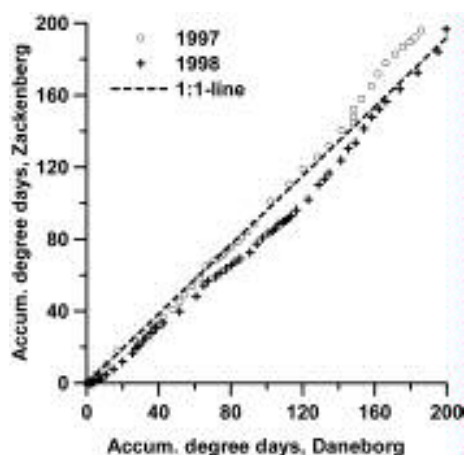
$$RGBNDSI = \frac{VIS - MIR_{\text{replacement}}}{VIS + MIR_{\text{replacement}}} \quad (2)$$

The derivation of the *RGBNDSI* is described in Hinkler et al. (2002).

The conventional digital camera is a Kodak DC50 with a resolution of 756×504 pixels. The Charge Coupled Device (CCD) is coated with a color array of red, green and blue photosites, and thus each photosite on it is sensitive to only one color. Therefore interpolation algorithms creating the missing R, G and B values are applied before a bitmap image is created. The multispectral camera is a Tetracam inc. single-CCD camera, which was used previously for surface and albedo-classification in the Ny-Ålesund Area, 79°N, Svalbard (Hinkler et al., 2003). The CCD has a resolution of 1200×1024 pixels and has a color filter array applied to it, meaning that each pixel on the CCD is sensitive to only one color. After color reconstruction (demosaiicing processing using raw pixel data), the Green, Red and Near Infrared (G, R, NIR) spectral bands approximately cover: 520–570 nm (G), 600–690 nm (R), and 750–850 nm (NIR) (see also Table 2). NDVI-maps were derived from the raw pixel values of the NIR and R spectral bands.

### 3.1.2 Meteorological data

Meteorological data (listed in column 3 and 4 in Table 1) are air temperatures measured 2 m above the surface at the AWSs at Zackenberg and Daneborg, respectively, and snow depths measured at the AWS at Zackenberg. As the Zackenberg Research Station was not established before the end of summer 1995, air temperatures covering melting seasons prior to 1996 had to be substituted by data from Daneborg. To verify whether this is reasonable, a



**Fig. 3.** Accumulated degree days, Zackenberg vs. Daneborg.

comparison between Accumulated Degree Days (ADD) at the two locations was done. Due to technical problems with the AWS at Daneborg in recent years it was possible to do the comparison only for the 1997–1998 melting seasons (Fig. 3). However, as the relation between the two is close to a 1:1 line during the major part of the melting season ( $ADD < 200$ ), a direct substitution was assessed as most reasonable.

### 3.1.3 Satellite data

Currently, it has been possible to procure cloud-free satellite data with high spatial resolution (Landsat TM, and SPOT HRV) from the melting seasons back to 1988 (see Table 1 and Fig. 7 for number and temporal coverage). The TM data cover both the visible, NIR and mid-infrared part of the spectrum (see Table 2), whereas the HRV cover the visible and NIR parts. Thus, for snow mapping based on TM-data the Normalized Difference Snow Index (NDSI) was applied (Dozier, 1989). The index is given as:

$$\text{NDSI} = \frac{\text{TM}_{\text{band2}} - \text{TM}_{\text{band5}}}{\text{TM}_{\text{band2}} + \text{TM}_{\text{band5}}} \quad (3)$$

As the HRV-data do not cover mid-infrared wavelengths, the *RGBNDSI* by Hinkler et al. (2002) was applied for snow mapping on these data with channel 3 (NIR), channel 2 (R), and channel 1 (G), and as substitutes for R, G, and B, respectively. From a careful visual inspection and from the fact that on cloud-free images, snow is relatively easy to distinguish from other surface types it was concluded that this method is of high accuracy.

	MDC (nm)	SPOT (HRV) (nm)	Landsat TM (nm)
Green	520–570	Channel 1: 500–590	Channel 2: 520–600
Red	600–690	Channel 2: 610–680	Channel 3: 630–690
Near infrared	750–850	Channel 3: 790–890	Channel 4: 760–900
Mid-infrared	—	—	Channel 5: 1550–1750

**Table 2.** Spectral channels of multispectral camera vs. satellite sensors.

### 3.1.4 Field measurements of NDVI

Since 1999 NDVI has been measured regularly in 26 different plots, which represent the 4 main types of vegetation present in ZRA (Cassiope, Dryas, Salix, and Eriophorum). The measurements were performed using a Skye 110 instrument with a 660–730 nm sensor. The Day Of the Year (DOY) at which NDVI-maximum occurs (DOY-Max-NDVI) calculated as the average peaking-time for all these plots correspond well to the DOY-Max-NDVI calculated from



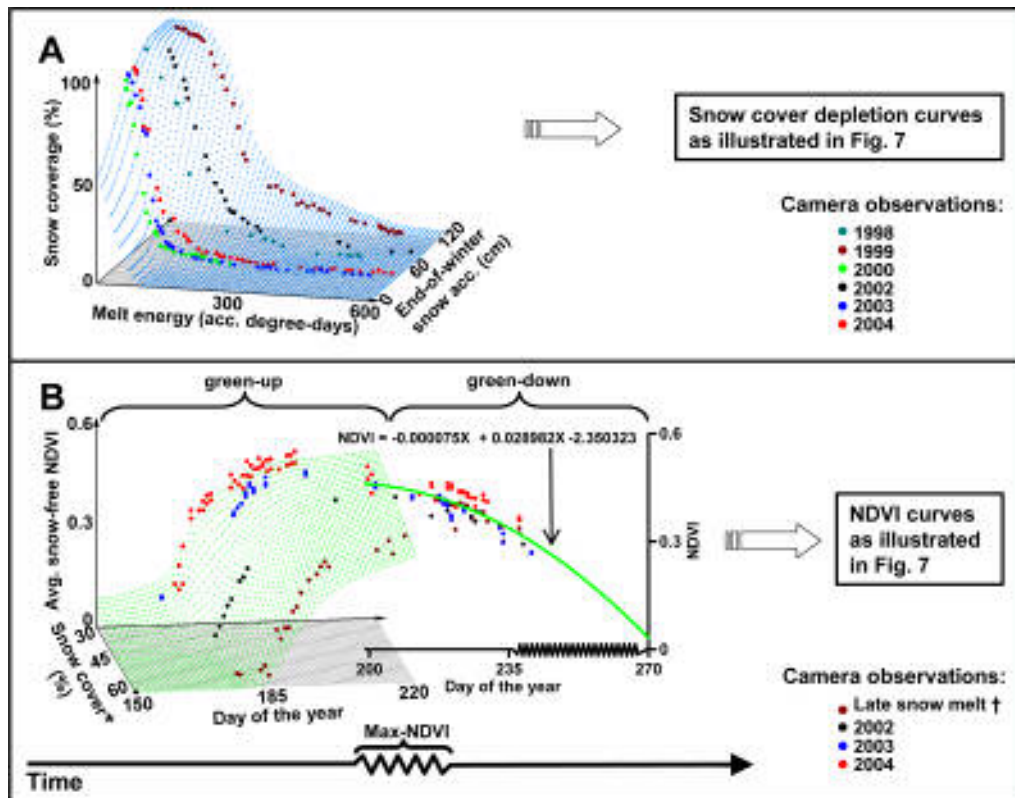
the MDCI-data in the years 2002–2004, which is calculated as the average of all snow-free pixels. It was therefore assumed that the 26 plots reflect the temporal NDVI-variation of the entire vegetation-cover at ZRA fairly well.

### 3.2 Model derivation

Ideally, modeling of any physical or biophysical parameter requires knowledge about all factors affecting it. However, due to the complexity of nature, this will rarely be possible. When considering snow cover and vegetation, local factors such as the specific climatic regime (temperature, exposure to solar radiation, wind etc.) and the terrain's topographic characteristics are particularly complex to deal with. In this study, the impact from ZRA's local characteristics on snow cover and vegetative activity is “mirrored” by a comprehensive amount of digital camera data obtained in different melting/growing seasons. The main concept of both the snow-cover-depletion- and the NDVI models is to compare this information to the primary factors (amount of precipitation, melt-energy/temperature, access to sunlight etc.) influencing the model-output (snow coverage and NDVI); and then use it to derive general data sets that represent output values corresponding to any real-world situation in ZRA. The curvatures in Fig. 4 (A) and Fig. 4 (B—green-up) is a visualization of these data sets.

#### 3.2.1 Snow-cover-depletion model

A snow-cover-depletion curve (SCDC) describes the seasonal decline in snow covered fraction as a function of time *or* cumulative melt energy (ME) (Menoès and Brubaker, 2001), which is expressed as ADD in this study. The objective of the snow-cover-depletion model is to derive an ME-based SCDC for the melting season, and then transform it to a time-based SCDC, which can be compared directly to e.g. time-based NDVI-curves. The advantage of the ME-based SCDC is that, if the spatial snow distribution (due to a prevailing wind direction during winter and location-specific topography) is assumed to be constant from year to year; then there is one, and only one, ME-based SCDC that corresponds to a specific end-of-winter snow accumulation. On the other hand, for any end-of-winter snow accumulation there is an infinite amount of time-based SCDCs (because there is an infinite amount of ways in which ME can vary with time). However, the *one* time-based SCDC which is unique for a particular melting season can be derived from a known ME-based SCDC, provided that the accumulated ME is known on a continuous (in this



**Fig. 4.** Conceptual description of (A) snow cover- and (B) NDVI models. In B, snow cover\* is defined as the average snow cover percentage (calculated from output of A) for the green-up period. Late snow melt† represents an artificial “extreme- year” with “low-NDVI/high snow cover”.

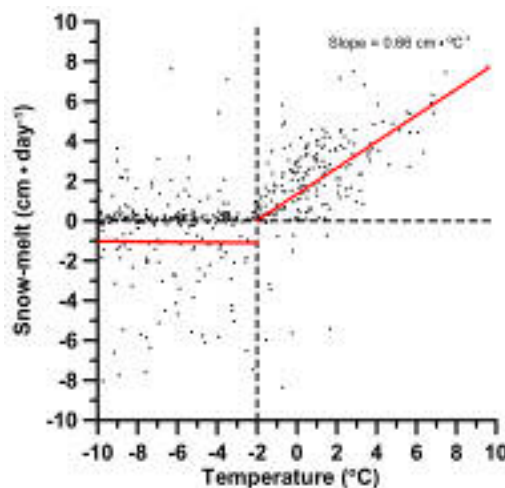
study, daily) basis through the melting season; and provided that no snowfall has occurred within the melting season.

Because the prevailing wind-direction (NNW) in ZRA is fairly constant from winter to winter, snow cover distribution in the area is assumed to be similar in different years. The basic concept of the model is thus to find *the* ME-based SCDC that corresponds to the end-of-winter snow depth for the actual year in question. To be able to do this, snow cover data represented by the CDCIs were used to interpolate a data set containing ME-based SCDCs corresponding to any end-of-winter snow accumulation at ZRA (Fig. 4 (A)). The data set is based on CDCI-data recorded during 1998–2000 and 2002–2004 and was interpolated with the Kriging method (Stein, 1999). The 2001-season was omitted due to heavy snowfall within the melting season—an event, which has only been observed once (June 15–16, 2001) since the Zackenberg Research Station was established in 1995. If the end-of winter snow accumulation is known for a given season, then its corresponding ME-based SCDC can be extracted directly from the data set. However, if it is not, it has to be found iteratively using at (least one) snow cover observation(s) from

the season in question. In practice this means that the model works by selecting snow cover percentages that match combinations of melt-energy and end-of-winter snow accumulation. This is done for each day in the melting season. The advantage of the model is that, if the end-of-winter snow accumulation is not known (in this study this concerns years prior to 1998) it can be found iteratively together with its corresponding depletion curve (provided that the ADD are available on a daily basis; and that snow coverage (here interpreted from satellite data) is known for at least one day in the melting season).

As high spatial resolution satellite data (SPOT HRV & Landsat TM) are available back to 1988 it was therefore possible also to derive snow-cover-depletion curves for the period 1988–1997, where no camera-data were available. Typically one or two cloud-free satellite images were available per melting season.

For calculation of ADD, a base-temperature below  $0^{\circ}\text{C}$  was applied. This is because the CDCIs reveal snow-melt to occur within ZRA also when the daily mean temperature is below the freezing point. An analysis based on snow depth and temperature data obtained at the AWS at Zackenberg suggests  $-2^{\circ}\text{C}$  as a plausible value for the base-temperature (Fig. 5).



**Fig. 5.** Snow melt (day-to-day differences in snow depth) vs. daily mean temperatures measured at the Automatic Weather Station (AWS) at Zackenberg.

Fig. 5 shows that above  $-2^{\circ}\text{C}$  there is a clear trend of increasing snow melt with increasing temperatures, and that the trend-line intersects the point  $(-2^{\circ}\text{C}, 0 \text{ cm} \cdot \text{day}^{-1})$ . Below  $-2^{\circ}\text{C}$  there is no up- or downward trend. The majority of the observations below  $-2^{\circ}\text{C}$  are at the “ $0 \text{ cm} \cdot \text{day}^{-1}$ ”-line, indicating that most of the time there is no snowfall. However, the fact that the trend-line is below the “ $0 \text{ cm} \cdot \text{day}^{-1}$ ”-line, indicate a net snow accumulation

during winter. The figure is based on all snow- and temperature observations recorded at the AWS within the period August 1997–August 2004, where the daily mean air temperature was between  $-10$  and  $10^{\circ}\text{C}$ .

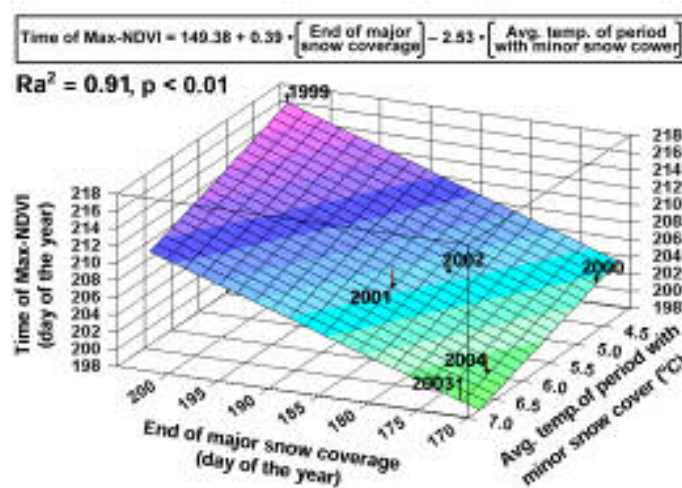
Due to the presence of permafrost in the Zackenberg Valley, which leads to poor drainage conditions and a water saturated snow pack, snow density during melt-off is generally high. Field measurements indicate mean densities around  $500 \text{ kg} \cdot \text{m}^{-3}$  (Larsen and Karlsen, 2003). The slope of the trend-line ( $0.66 \text{ cm} \cdot ^{\circ}\text{C}^{-1} \cdot \text{day}^{-1}$ ) thus indicates average snow-melt (degree-day factor) around  $3.3 \text{ mm water equivalent} \cdot \text{day}^{-1}$ . A wide range of degree-day factor for snow melt ( $0.7\text{--}9.2 \text{ mm} \cdot ^{\circ}\text{C}^{-1} \cdot \text{day}^{-1}$ ) has been reported in the literature. However, the majority of the reported values of degree-day factor range between  $3$  and  $5 \text{ mm} \cdot ^{\circ}\text{C}^{-1} \cdot \text{day}^{-1}$  (Lehr et al., 2005). This suggests that ZRA is placed in a “normal regime” of snow melt.

### 3.2.2 NDVI model

As opposite to the snow-cover-depletion model which is based solely on the approach of selecting output-data from an empirically derived data set, the NDVI model is based on a combination of 1) this approach (Fig. 4 (B)—green-up), and 2) a simple curve-fitting approach (Fig. 4 (B)—green-down). An additional input-parameter required for model application is DOY-Max-NDVI—at this DOY, calculation of NDVI changes from the first to the second approach.

The “green-up-part” of the NDVI model is based on the assumption that during “green-up-time”, (NDVI) is substantially related to snow cover extent (because virtually, photosynthetic activity occurs only in snow-free areas). Therefore, the input-parameters for this part of the model are: 1) the average snow-cover-percentage for the green-up period (derived from the output of the snow-cover-depletion model), and 2) time (expressed as DOY). The year 1999 had the most extensive snow-precipitation amount ever recorded in ZRA, while the year 2000 together with the two latest years (2003 and 2004) had some of the lowest. Regarding the snow-cover-depletion model this is an advantage, as the interpolated data set thereby covers a wide spectrum of depletion curves. When considering the NDVI-model the situation is different: Unfortunately, MDCIs were not obtained before 2002. Therefore an artificial representation of NDVI in extreme “snow-years” had to be constructed. This representation is denoted *late snow melt*<sup>†</sup> in Fig. 4 (B), and is calculated solely on the basis of pixels (2004-data) with DOY-Max-NDVI between 215 and 220

(August 2–August 7)—according to field observations, the year 1999 had maximum NDVI at DOY 218. The disadvantage of the *late snow melt*<sup>†</sup>-approach is that NDVI-values might be biased from the fact that areas characterized by late snow melt are dominated by specific vegetation types (e.g. *Salix Arctica*) (Bay, 1998). However, as there is currently no other options for an “extreme-year”-representation, the *late snow melt*<sup>†</sup>-approach is considered as the best possible approximation.



**Fig. 6.** Fit of multiple regression between 1) Time of Max-NDVI, 2) DOY where major (>18%) snow coverage ends, and 3) the average temperature within the period with minor (<18%) snow cover.

Analyses from ZRA (Meltofte, 2002) on e.g. *Dryas integrifolia* show that DOY-Max-NDVI is highly correlated to the DOY at which the major part of the snow cover has disappeared. Major snow coverage is considered to end when the snow cover percentage gets below 18%—this is because field measurements from ZRA shows that green-up starts at an approximate NDVI-value of about 0.18—and the NDVI/snow maps from the 2002–2004 seasons (see Fig. 7) indicate that “18% snow cover” and “NDVI = 0.18” occur at around the same DOY  $\pm$  a few days, in most cases. Generally, late snow melt delays DOY-Max-NDVI, however, to a certain degree the vegetation is able to compensate for late snow melt by increased plant-production-rate (Meltofte, 2002). Furthermore, vegetative growth is related to temperature; therefore it is assumed that DOY-Max-NDVI can be calculated on the basis of 1) the date at which the period with major snow cover (>18%) ends (End-DOY<sub>major</sub>), and 2) the average air temperature within the period with minor (<18%) snow cover (Avg-Temp<sub>minor</sub>). A multiple regression-fit with DOY-Max-NDVI acting as the dependent variable, is shown in Fig. 6. The adjusted R-squared of multiple determination ( $R_a^2$ ) is 0.91 ( $p < 0.01$ ). The average residual value is 1.21 days, and residuals never exceed 2 days. Between DOY-Max-NDVI and End-

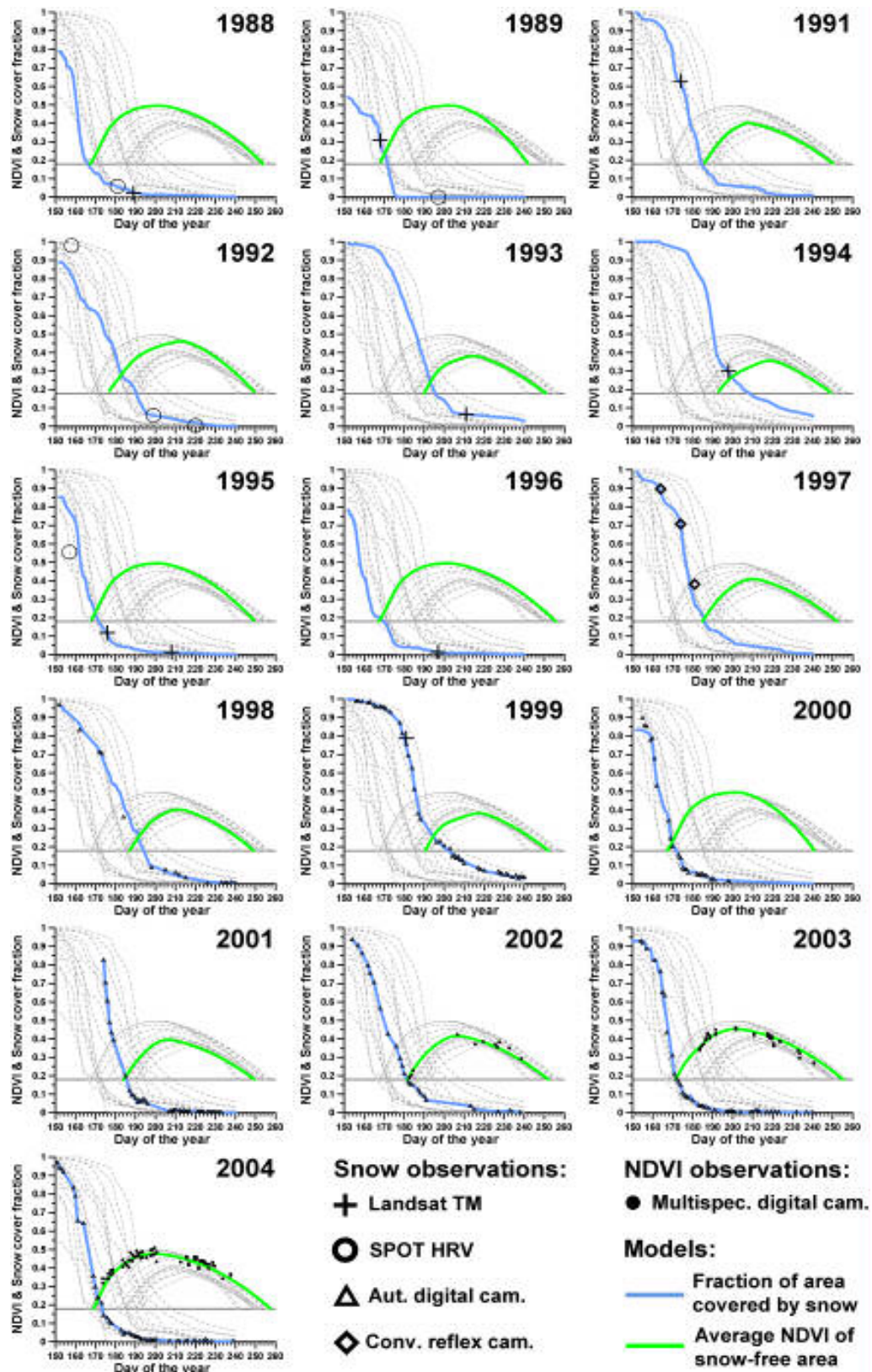


DOY<sub>major</sub> and Avg-Temp<sub>minor</sub> the R-squared is 0.86 ( $p < 0.05$ ) and 0.61 ( $0.05 < p < 0.10$ ), respectively. Between the two independents (End-DOY<sub>major</sub> and Avg-Temp<sub>minor</sub>) there is no correlation (R-squared = 0.35,  $p >> 0.10$ ). This leads to the conclusion that snow coverage is the most important parameter affecting the time of peak vegetative activity, and that the influence from temperature is less significant but is still of some importance. The “green-down-part” of the NDVI model assumes that green-down is related primarily to decreasing solar zenith angle (which is related to DOY). Furthermore, it is assumed that vegetative activity stops when the temperature gets below 0°C. Therefore, the green-down-curve is basically calculated as the equation stated in Fig. 4 (B), but is adjusted in accordance with the above assumptions: Firstly, an offset is introduced so that the curve will take its starting point at the maximum NDVI-value (which is calculated through the green-up-procedure). Secondly, if more than 3 successive days with temperatures below 0°C occur before the NDVI goes below 0.18 (see above section), the time scale of the green-down-period will be changed, meaning that this part of the NDVI-curve is “compressed in time” and will intersect 0.18, when continuous frost commences. Modeled NDVI-curves are displayed in Fig. 7.

## 4. Results

### 4.1 Snow

Fig. 7 shows that the inter-annual snow cover (and NDVI) variation in ZRA during 1988–2004 is considerable with average snow cover extent in the green-up period ranging from 15% in 1989 to 62% in 1994. Previous studies from ZRA (Meltofte, 2002) and the general monitoring programs at Zackenberg have decided to use the date with 50% snow cover as a point in time, which is generally used for inter-annual comparisons of the snow cover and factors related to it. One quantitative example of the variation is that the date with 50% snow cover varies with more than a month—the mean date is June 21 (DOY 172), whereas max- and minimum has occurred at July 9 (DOY 190, 1994) and June 6 (DOY 156, 1989), respectively. Based on the iterative modeling approach (described in section 3.2.1) end-of-winter snow depths, corresponding to the snow-accumulations at the AWS, were calculated (Table 3). The results reveal that the variation in winter-precipitation in ZRA can vary with orders of magnitude, from almost none in 1989 till more than a meter in the years 1994 and 1999. Over the last 16 years, the data indicate no significant time-trend in winter-precipitation.



**Fig. 7.** Modeled snow-cover-depletion- and NDVI curves (1988–2004), displayed together with camera- and satellite observations. The toned down curves illustrates all years, other than the actual year in question. Due to heavy snowfall within the melting season in 2001, the depletion curve starts later in this year.

**Table 3.** Snow depths (in cm) at June 1 at the Zackenberg AWS—measured (1998–2004) and modeled iteratively (1988–1997).

1988	1989	1991	1992	1993	1994	1995	1996	1997	1998	1999	2000	2001	2002	2003	2004
43	6	90	64	91	111	42	40	85	76	111	44	59	87	45	50

Snow cover depletion curves at ZRA generally tend to have a reversely S-shaped form. This indicates an uneven snow distribution, which is typical for mountainous areas, due to wind-drift and a marked topographic relief (Hall and Martinec, 1985). The steepest part of the depletion curves represents snow-depletion during the time where extensive areas, with uniform snow deposition, become free of snow. The slope of this part of the curve reflects the temperature/energy-input-flux during melt-off. This means that large slope-variations may indicate a different prevailing climatic regime (Menoès and Brubaker, 2001). Significant slope-deviations have occurred in ZRA a couple of times—e.g. the slopes were weaker than normal in 1992 and 1998, indicating temperatures markedly lower than normal.

#### 4.2 NDVI

Evidently, vegetative activity is linked to the presence/absence of snow cover. Fig. 7 gives a visual impression of this linkage. The NDVI-curves in the figure show the average NDVI of snow-free areas in ZRA (represented as the snow-free area covered by the CDCI- and MDCIs) for each day in the growing season. Due to a shortening of the growing season in areas with long lasting snow coverage, both the average length of the growing season and the average NDVI are reduced in years with extensive snow cover. Furthermore, as snow cover delays the initiation-time of the growing season, the time of NDVI-optimum is also delayed, in the case of a large snow cover extent—even though that some plant species are able to partly compensate for this (Meltofte, 2002). The inter-annual variability in NDVI and length of growing season is described for ZRA in Table 4.

The table shows that on average the length of the growing season in ZRA is 72.6 days; and that it varies with approximately  $\pm 2$  weeks (minimum: 57 days in 1994, maximum: 89 days, 1996).

DOY-Max-NDVI varies with 20 days: from 199 (July 17) in 2004 to 219 (August 7) in 1994, and the mean DOY is 207.8 ( $\approx$ July 27). The standard deviation for DOY-Max-NDVI is 6.2 days, whereas for the initiation-time of the growing season it is 10 days. This indicates that the vegetation is able to partly compensate for late snow-melt by increased plant-productivity.

**Table 4.** NDVI and growing season in ZRA. ISfNDVI—the integrated snow-free NDVI, is defined as the daily average of snow-free pixels multiplied by the snow-free fraction of the area accumulated over an entire growing season.

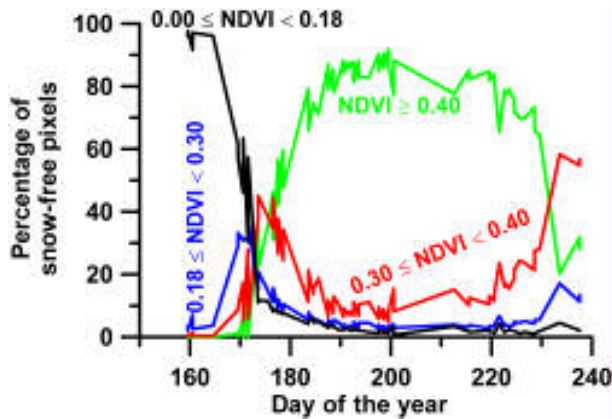
Year	Start time of growing season DOY (Date)	Time of max-NDVI DOY (Date)	End time of growing season DOY (Date)	Length of growing season Days	Max-NDVI	ISfNDVI
1988	167 (Jun.15)	203 (Jul.21)	254 (Sep.10)	87	0.50	32.97
1989	167 (Jun.16)	206 (Jul.25)	242 (Aug.30)	75	0.50	29.06
1991	186 (Jul.05)	208 (Jul.27)	250 (Sep.07)	64	0.40	19.70
1992	176 (Jun.24)	214 (Aug.01)	250 (Sep.06)	74	0.46	24.23
1993	190 (Jul.09)	215 (Aug.03)	251 (Sep.08)	61	0.38	17.09
1994	192 (Jul.11)	219 (Aug.07)	249 (Sep.06)	57	0.36	14.06
1995	167 (Jun.16)	202 (Jul.21)	250 (Sep.07)	83	0.49	31.10
1996	167 (Jun.15)	203 (Jul.21)	256 (Sep.12)	89	0.50	33.71
1997	185 (Jul.04)	210 (Jul.29)	252 (Sep.09)	67	0.41	20.85
1998	187 (Jul.06)	212 (Jul.31)	249 (Sep.06)	62	0.40	18.52
1999	191 (Jul.10)	218 (Aug.06)	252 (Sep.09)	61	0.38	17.25
2000	167 (Jun.15)	204 (Jul.22)	241 (Aug.28)	74	0.50	27.81
2001	184 (Jul.03)	205 (Jul.24)	249 (Sep.06)	65	0.39	19.88
2002	182 (Jul.01)	206 (Jul.25)	252 (Sep.09)	70	0.42	22.35
2003	171 (Jun.20)	201 (Jul.20)	255 (Sep.12)	84	0.45	29.32
2004	169 (Jun.17)	199 (Jul.17)	257 (Sep.13)	88	0.48	32.44
	Average 178.0	Average 207.8	Average 250.6	Average 72.6	Average 0.44	Avg 24.40
	St.dev. 10.0	St.dev. 6.2	St.dev. 4.3	St.dev. 10.8	St.dev. 0.05	St.dev. 6.49

The integrated snow-free NDVI (referred to in Table 4 as ISfNDVI) is defined as the daily average of snow-free pixels multiplied by the snow-free fraction of the area accumulated over an entire growing season. Thus, it reflects the total amount of photosynthetic activity that has been going on during the season, which is further related to the net primary plant production (Stow et al., 2004; Vourlitis et al., 2000). The ISfNDVI varies from below 20 in years with extensive snow coverage to well above 30 in years with limited snow cover (minimum: 14.1 in 1994, maximum: 33.7, 1996).

Maximum NDVI-values ranges from as low as 0.36 to 0.50 in years with extensive- and minor snow cover, respectively. Note that as these values are calculated as the average of all snow-free pixels, they do not reflect the peak vegetative vigor that can be found in the area, but reflects the total net peak vegetative activity in snow-free areas.

From Fig. 7 it can be observed that *on average* the growing season in ZRA started approximately at DOY 170 in 2004. However, the actual situation is (of course) more complex as some areas become snow-free sooner than others. This is illustrated by Fig. 8, which shows the variation of 4 NDVI-subdivisions through the melting/growing season. In the early part of the green-up period, the snow-free areas are a mixture of NDVI-classes, whereas in the later part,





**Fig. 8.** The temporal variation of 4 different NDVI-classes within the area covered by the cameras—expressed as each class’s relative proportion of the snow-free area during the growing season (year 2004).

the class of high NDVI-values ( $\geq 0.40$ ) predominates. At the initiation of the season, large areas become free of snow, and thus, NDVI-values belonging to  $[0.00 \leq \text{NDVI} < 0.18]$  are the most numerous, but are rapidly decreased in number as they are transformed into the higher classes. However, the situation still gets complexed by continuous melt-off (continuous “supply” of low NDVI-values). The green-down period is characterized by the transition of NDVI-values from the higher- to the lower NDVI-classes.

## 5. Discussion

### 5.1 Snow

When modeling depletion of snow cover, the spatial distribution of snow-deposition, snow density, and melt-energy (basically temperature and net radiation budgets) can be extremely complex. This study deals with these parameters by including “an empirical fingerprint of the spatial snow-melt-behavior in ZRA” using daily digital images. The accuracy of this methodology depends on, firstly, that the “fingerprint” reflects variations in real-world snow cover distribution sufficiently well, and secondly, whether the input parameters are representative for the area in question. In most cases the modeled snow coverage fits values inferred from satellite- and camera images well (Fig. 7.). However, in a few cases there are deviations of more than a couple of days (e.g. 1992 and 1995). In this study there are basically two main sources of error: 1) In the case of snowfall within the melting period (as in the year 2001), the “fingerprint-approach” breaks down, and 2) if the Daneborg-temperatures deviates significantly from ZRA-temperatures. Most likely this would occur in years where Daneborg is affected more by fog coming in from the sea than ZRA. Finally, a third source of error is that air temperatures may not necessarily reflect the melt-energy budget in a similar way in different



years, e.g. the net radiative budget at the surface may differ between days with equal temperatures due to different cloud cover etc.

## 5.2 NDVI

### *5.2.1 NDVI-characteristics as specific for this study*

Numerous sources of satellite data are available for analyses of intra-seasonal ecological variables in remote areas. Due to their high temporal resolution (daily images), the NOAA AVHRR is among the most widely used systems for analyses where short-interval time series are required. In contrast to AVHRR data, the CDCI/MDCI-method has the advantage that it combines both high spatial- and high temporal resolution. This gives the opportunity to do analyses at high temporal resolution with high precision also within the spatial domain, and to give an as precise as possible reflection of the amount of phytomass present within the study area by masking out snow-pixels. Thus, it is important to be aware that this study's output-NDVI-curves (Fig. 7) are not directly comparable to NDVI-curves based on data with coarse spatial resolution like e.g. the AVHRR.

NDVI-analyses based on AVHRR-data obtained over arctic tundra e.g. (Hope et al., 2003; Jia et al., 2004; Oechel et al., 2000) generally shows NDVI curves to be more or less symmetric (bell-shaped), whereas the curves presented here tend to be steepest during green-up. This difference is most likely related to the fact that, when only snow-free areas are considered, the dampening effect from an eventual snow cover (negative NDVI-values) is removed, i.e. in AVHRR-data each pixel may contain various surface types, including snow. However, it is important to stress that during the growing season, new pixels melts free of snow continuously as long as a snow cover is present, meaning that day to day differences in average NDVI do not refer to the same area. Therefore, when "average snow-free NDVI" is referred to in this study; it should not be mistaken as the NDVI of areas that has been snow-free during the entire growing season—but as a measure of the stage of total greenness present within snow-free areas at the actual day in question.

### *5.2.2 Climatic aspects*

Snow cover is found to be a dominating climatic parameter affecting NDVI, both with respect to timing and overall magnitude. This is not surprising, since the snow cover virtually blocks incoming Photosynthetic Active Radiation (PAR) (Belzile et al., 2001). More surprising is it that no correlation was found

between the *magnitude* of maximum NDVI measured in the field and air temperatures measured at the AWS (neither between the current nor between the previous year's temperatures). However, when it comes to the timing of maximum NDVI the influence from air temperature is of some significance (see section 3.2.2). In consequence to this, the NDVI-model does not consider temperature (except for the information that comes indirectly from the modeled snow cover) for derivation of absolute NDVI-values, but consider them only in calculating the timing of the peak-value. In the light of this, some general considerations about NDVI-temperature relations, both within and outside ZRA, requires further discussion.

Studies of NDVI-biomass relationships within single arctic vegetation types (Hope et al., 1993; Jacobsen and Hansen, 1999) have concluded that biomass is only one of several factors (Leaf Area Index, soil water content etc.) influencing the NDVI. However, Walker et al. (2003) point out that when viewed over broad regions and across major changes in vegetation biomass, there is a clear relationship between temperature, biomass, and NDVI on mesic zonal sites. Due to its limited size (about 17 km<sup>2</sup>), the part of ZRA covered by the cameras may hardly represent such a "broad region"; but because of the large diversity in plant-species, and because the area is at the boundary between climatic regimes, it might be reasonable to suggest that some species are better adapted to the local climate in some years, while other species are in others. Despite this, field measurements of NDVI (average NDVI of 26 plots) do not reveal any correlation between average summer temperatures (measured 2 m above ground at the AWS during the period with minor snow cover) and maximum NDVI-values.

The explanation may be that since germination- and growth capabilities for arctic species are often related to the climatic conditions in the previous year (Bliss and Gold, 1999), both snow cover and temperature conditions in the previous growing season (together with the conditions in the current growing season) may influence the magnitude of NDVI.

A second explanation might be inferred from the Summer Warmth Index (SWI) used e.g. by Walker et al. (2003), which is defined as the sum of mean monthly temperatures greater than 0°C. Based on temperature- and NDVI measurements from 12 different locations with an SWI ranging as much as 28°C (9°C–37°C), Walker et al. showed that maximum NDVI is significantly correlated to the SWI. In ZRA, the average SWI (1988-2004) is 12°C with minimum and maximum values of 8°C and 16°C, respectively. However, the relation found by Walker et al., shows that the SWI-range for ZRA corresponds to a

variation in maximum NDVI-values ranging from 0.39–0.42, which is too small a range to be detected with significant accuracy by the spectral sensor (the instrument used in this study is a handheld Skye 110, 660–730 nm sensor).

### **5.3 Climate change perspectives**

Findings from this study suggest that, under the present climatic conditions, ISfNDVI differs by as much as a factor of two between growing seasons with extensive and limited snow cover, respectively. It is therefore concluded that for High Arctic ecosystems like ZRA, snow cover is by far the most important climatic parameter affecting vegetative activity. The majority of General Circulation Models (GCMs) predict climatic effects of global change to be most pronounced in the Arctic, and that increases in temperature and precipitation will be particularly pronounced during winter in these regions (ACIA, 2004). As the timing of the snow-free period i.e. the growing season is basically determined by the balance between end-of-winter snow accumulation and the melt energy available for snow melt (i.e. summer temperatures), future scenarios for vegetative activity in present High Arctic regions may differ significantly:

If summer temperatures, as predicted, do not increase noteworthy, the heavier snow pack may (as opposite to the predicted prolongation of the growing season in most of the Arctic) prevent spring snow clearance in some High Arctic regions to occur earlier (Hinkler et al., 2005). If on the contrary, summer temperatures do increase significantly, the High Arctic tundra and desert may transform into Low Arctic tundra, leaving the High Arctic habitat only as an alpine zone in mountainous areas (Meltofte et al., 2003).

## **6. Conclusions**

The new methodology (based on digital camera images) presented in this study enable us to analyze snow–NDVI biomass relations at high spatiotemporal accuracy, and to mask out snow cover from NDVI data.

Measured and modeled snow cover- and NDVI data demonstrate that snow cover under present climatic conditions is by far the most important parameter affecting vegetative activity in ZRA, both with respect to timing and total amount of photosynthetic activity (ISfNDVI).

In spite of the fact that ZRA represents a relatively high diversity of plant-species (meaning that some species might be adapted better to the local climate in some years, while other species might be in other years) there is no correlation between summer temperatures and magnitude of maximum NDVI

in ZRA. On the contrary, there are some correlation between temperature and the timing of maximum NDVI, when considered in combination with snow cover.

The lack of correlation between NDVI-magnitude and summer temperatures in ZRA may be due to the fact that the inter-annual variability in SWI is not sufficiently high to cause detectable year to year differences—differences may rather be due to other factors—primarily snow cover variations and maybe other factors (limited accuracy of the spectral measurements or relations between current- and previous year's temperatures).

As snow cover is the major factor affecting NDVI in ZRA, it may be a more important parameter to take into account when predicting future scenarios of vegetation status in High Arctic areas than temperature—e.g. in Arctic areas most GCMs predict increased winter precipitation and only a limited increase in summer temperatures, and therefore, increased temperatures may not necessarily lead to reduced snow cover.

Consequently the balance between summer temperatures and winter precipitation (snow cover depletion rate) may be the key parameter to predict future vegetation status in High Arctic areas.

**Acknowledgements** The Danish Polar Center is thanked for providing access to ecosystem monitoring, data, and logistics at the research station at Zackenberg. We also thank Ulf Pierre Thomas, technician at the Institute of Geography—University of Copenhagen, for indispensable technical support. We thank Kim Have, Technical University of Denmark, for software development. Finally Charlotte Sigsgaard is thanked for valuable assistance and efforts.

## References

ACIA. Impacts of a Warming Arctic: Arctic Climate Impact Assessments. Hassol, S. J. 1-139. 2004. Canada, Cambridge University Press.

Ref Type: Report

Bay,C. Vegetation mapping of Zackenberg valley, Northeast Greenland. 1-29. 1998. Copenhagen, Danish Polar Center & Botanical Museum, University of Copenhagen.

Ref Type: Report

Belzile,C, W F Vincent, J A E Gibson, P Van Hove, 2001, Bio-optical characteristics of the snow, ice, and water column of a perennially ice-covered

lake in the High Arctic: Canadian Journal of Fisheries and Aquatic Sciences, v. 58, p. 2405-2418.

Bliss, LC, W G Gold, 1999, Vascular plant reproduction, establishment, and growth and the effects of cryptogamic crusts within a polar desert ecosystem, Devon Island, NWT, Canada: Canadian Journal of Botany-Revue Canadienne de Botanique, v. 77, p. 623-636.

Cappelen, J, B V Jørgensen, E V Laursen, L S Stannius, R J Thomsen. The Observed Climate of Greenland, 1958-99 - with Climatological Standard Normals, 1961-1990. 00-18. 2001. Danish Meteorological Institute. Technical Reports.

Ref Type: Report

CAVM Team. Circumpolar Arctic Vegetation Map. Scale 1:7,500,000. [1]. 2003. Anchorage, Alaska, Conservation of Arctic Flora and Fauna (CAFF), U.S. Fish and Wildlife Service.

Ref Type: Map

Dozier, J, 1989, Spectral Signature of Alpine Snow Cover from the Landsat Thematic Mapper: Remote Sensing of Environment, v. 28, p. 9-&.

Dueholm, KS. The generic bundle adjustment. 89-185. 1989. US Geological Survey. Open-File Report.

Ref Type: Report

Elvebakk, A. Bioclimatic delimitation and Subdivision of the Arctic. <http://www.toyen.uio.no/panarctflora/papers/delimitation/delimitation.htm#Disc>. 2000.

Ref Type: Electronic Citation

Hall, DK, J Martinec, 1985, Remote Sensing of Ice and Snow, Cambridge: Chapman and Hall.

Have, K. Photogrammetric image analysis for climate studies. 1-191. 1999. Technical University of Denmark.

Ref Type: Thesis/Dissertation

Hinkler, J, B U Hansen, M Tamstorf, H Meltofte. Linkage between sea-ice distribution and snow-precipitation might prevent the extinction of High Arctic ecosystems in a future warmer climate. 2005.

Ref Type: Unpublished Work

Hinkler, J, J B Orbaek, B U Hansen, 2003, Detection of spatial, temporal, and spectral surface changes in the Ny-Alesund area 79 degrees N, Svalbard, using a low cost multispectral camera in combination with spectroradiometer measurements: Physics and Chemistry of the Earth, v. 28, p. 1229-1239.

Hinkler, J, S B Pedersen, M Rasch, B U Hansen, 2002, Automatic snow cover monitoring at high temporal and spatial resolution, using images taken by a



standard digital camera: *International Journal of Remote Sensing*, v. 23, p. 4669-4682.

Hope,AS, W L Boynton, D A Stow, D C Douglas, 2003, Interannual growth dynamics of vegetation in the Kuparuk River watershed, Alaska based on the Normalized Difference Vegetation Index: *International Journal of Remote Sensing*, v. 24, p. 3413-3425.

Hope,AS, J S Kimball, D A Stow, 1993, The Relationship Between Tussock Tundra Spectral Reflectance Properties and Biomass and Vegetation Composition: *International Journal of Remote Sensing*, v. 14, p. 1861-1874.

Hope,AS, K R Pence, D A Stow, 2004, NDVI from low altitude aircraft and composited NOAA AVHRR data for scaling Arctic ecosystem fluxes: *International Journal of Remote Sensing*, v. 25, p. 4237-4250.

Jacobsen,A, B U Hansen, 1999, Estimation of the soil heat flux net radiation ratio based on spectral vegetation indexes in high-latitude Arctic areas: *International Journal of Remote Sensing*, v. 20, p. 445-461.

Jia,GJ, H E Epstein, D A Walker, 2004, Controls over intra-seasonal dynamics of AVHRR NDVI for the Arctic tundra in northern Alaska: *International Journal of Remote Sensing*, v. 25, p. 1547-1564.

Larsen,JN, H G Karlsen. Zackenberg Ecological research Operations, 8th Annual Report, 2002. Rasch, M. and Caning, K. 53-54. 2003. Copenhagen, Danish Polar Center, Ministry of Science, Technology and Innovation.  
Ref Type: Report

Lehr,JH, J Keeley, J Lehr. *The Encyclopedia of Water*. Lehr, J. H., Keeley, J., and Lehr, J. [http://www.wileywater.com/Contributor/Sample\\_3.htm](http://www.wileywater.com/Contributor/Sample_3.htm) . 2005. John Wiley and Sons Publishing.  
Ref Type: Electronic Citation

Meltofte,H. Sne, is og 35 graders kulde. Hvad er effekterne af klimaændringer i Nordøstgrønland? Meltofte, H. 41, 5-88. 2002. Denmark, Ministry of the Environment, National Environmental Research Institute. TEMA-rapporter fra DMU.  
Ref Type: Report

Meltofte,H, S Rysgaard, S A Pedersen, 2003, Climate change in Greenland, Denmark's third national communication on climate change. Under the United Nations Framework Convention on climate change: Danish ministry of the Environment, p. 118-123.

Menoës,MC, K L Brubaker. How Similar Are Snow Depletion Curves from Year to Year? Case Study in the Upper Rio Grande Watershed. 58th EASTERN SNOW CONFERENCE, Ottawa, Ontario, Canada . 2001.  
Ref Type: Abstract

Myneni, RB, C D Keeling, C J Tucker, G Asrar, R R Nemani, 1997, Increased plant growth in the northern high latitudes from 1981 to 1991: *Nature*, v. 386, p. 698-702.

Oechel, WC, G L Vourlitis, J Verfaillie, T Crawford, S Brooks, E Dumas, A Hope, D Stow, B Boynton, V Nosov, R Zulueta, 2000, A scaling approach for quantifying the net CO<sub>2</sub> flux of the Kuparuk River Basin, Alaska: *Global Change Biology*, v. 6, p. 160-173.

Ohmura, A, N Reeh, 1991, New Precipitation and Accumulation Maps for Greenland: *Journal of Glaciology*, v. 37, p. 140-148.

Orvig, S, 1970, *Climates of the Polar Regions*, Amsterdam, London, New York, Elsevier Publishing Company, p. 1-370.

Reynolds, JF, J D Tenhunen, 1996, Ecosystem response, resistance, resilience, and recovery in Arctic landscapes: Introduction, in JF Reynolds and JD Tenhunen (eds), *Landscape function and disturbance in Arctic Tundra*: Heidelberg, Springer, p. 3-18.

Soegaard, H, B Hasholt, T Friberg, C Nordstroem, 2001, Surface energy- and water balance in a high-arctic environment in NE Greenland: *Theoretical and Applied Climatology*, v. 70, p. 35-51.

Stein, ML, 1999, *Interpolation of Spatial Data Some Theory for Kriging*, Springer Verlag.

Stow, DA, A Hope, D McGuire, D Verbyla, J Gamon, F Huemmrich, S Houston, C Racine, M Sturm, K Tape, L Hinzman, K Yoshikawa, C Tweedie, B Noyle, C Silapaswan, D Douglas, B Griffith, G Jia, H Epstein, D Walker, S Daeschner, A Petersen, L M Zhou, R Myneni, 2004, Remote sensing of vegetation and land-cover change in Arctic Tundra Ecosystems: *Remote Sensing of Environment*, v. 89, p. 281-308.

Tucker, CJ, D A Slayback, J E Pinzon, S O Los, R B Myneni, M G Taylor, 2001, Higher northern latitude normalized difference vegetation index and growing season trends from 1982 to 1999: *International Journal of Biometeorology*, v. 45, p. 184-190.

Vourlitis, GL, W C Oechel, A Hope, D Stow, B Boynton, J Verfaillie, R Zulueta, S J Hastings, 2000, Physiological models for scaling plot measurements of CO<sub>2</sub> flux across an arctic tundra landscape: *Ecological Applications*, v. 10, p. 60-72.

Walker, DA, H E Epstein, G J Jia, A Balsler, C Copass, E J Edwards, W A Gould, J Hollingsworth, J Knudson, H A Maier, A Moody, M K Reynolds, 2003, Phytomass, LAI, and NDVI in northern Alaska: Relationships to summer warmth, soil pH, plant functional types, and extrapolation to the circumpolar Arctic: *Journal of Geophysical Research-Atmospheres*, v. 108.

Zhou,LM, C J Tucker, R K Kaufmann, D Slayback, N V Shabanov, R B Myneni, 2001, Variations in northern vegetation activity inferred from satellite data of vegetation index during 1981 to 1999: Journal of Geophysical Research-Atmospheres, v. 106, p. 20069-20083.

## **A possible linkage between sea-ice concentrations and snow-precipitation may be crucial for Arctic ecosystems in a warmer climate**

Jørgen Hinkler, Birger U. Hansen, Mikkel P. Tamstorf & Hans Meltofte

**Abstract.** Snow cover and sea-ice are major players in the climate system. Because of the high albedo the surface energy balance is dramatically affected by the presence/absence of snow and ice; and due to its insulative properties and ability to shield out solar radiation, snow cover is crucial for terrestrial ecosystems—especially in the High Arctic, where the snow-free season is short. As the global temperatures increase, sea-ice cover is expected to decrease correspondingly, which, due to expanded areas of open water, may affect both the energy budget and the hydrological cycle (including snow-precipitation). The present study compares snow-precipitation over Northeast Greenland to inter-annual variations in: large scale atmospheric circulation (North Atlantic Oscillation (NAO)) and sea-ice concentrations within the Greenland Sea. During 1959–2003, the snow-precipitation was correlated with the NAO one third of the time, according to a 19-year running correlation analysis. During 1982–2000, where this correlation was insignificant, the “snow-precipitation vs. sea-ice correlation” was significant at 1% level; and the “center of action” (the area with optimum correlation) was located approximately 500 km north of Iceland. Proxy based future sea-ice conditions combined with a simple linear relation between sea-ice duration and snow-precipitation show increases in snow-precipitation similar to what is calculated in a high resolution climate model. These increases might prevent prolongation of the snow-free season, which (unexpectedly in a warmer climate) will leave the ecosystem close to present average conditions during melt-off. The results of the present study are not sufficient to support a causal relationship between sea-ice duration and snow-precipitation. However, the strikingly high correlations and the match in orders of magnitude between sea-ice based- and climate modeled snow-precipitation call for further research.

### **1. Introduction**

The Intergovernmental Panel on Climate Change (IPCC)’s Third Assessment Report (2001) gives projections for global-mean warming from 1990 to 2100 within a range of 1.4 K to 5.8 K, if no measures are taken to limit greenhouse gas emissions. Recent research (Stainforth et al., 2005) demonstrates that climate sensitivity of different General Circulation Models (GCMs) ranges as much as between 1.9 K and 11.5 K. However, the vast majority of GCMs indicate a sensitivity around 3.4 K and predict global warming to be most pronounced at high latitudes, especially during winter. Thus, in the Arctic increases of around 6 K can be expected by the end of the 21<sup>st</sup> century (ACIA, 2004; IPCC, 2001), which is almost twice the 3.4 K global average, predicted by most GCMs.

Global warming will lead to increased evaporation and in turn to increased precipitation, which may have major implications for snow cover distribution at high latitudes, where snow makes up a major part of the annual precipitation budget (ACIA, 2004; Jones et al., 2001). In terms of spatial extent seasonal snow cover is the largest single component of the cryosphere, and with a mean winter maximum extent of 47 million square kilometers it corresponds to almost a third of the Earth's total land surface (NSIDC, 2005). Thus, one of the most important feedback mechanisms in climate change, at virtually any spatial scale, is the snow cover-albedo-temperature feedback (e.g. Groisman et al., 1994; Harding et al., 1995); which leads to enhanced warming, due to decreased snow cover (lower surface albedo). Furthermore— because of its insulative properties (e.g. protecting vegetation during winter) and ability to prevent solar radiation from reaching the surface (e.g. reducing photosynthetic activity in the summer), the presence/absence of snow cover is crucial, especially for terrestrial ecosystems in Arctic areas (Jones et al., 2001; Phoenix and Lee, 2004; Stone et al., 2002; Weller, 1998). These ecosystems are therefore considered important as indicators of climate change and are topics of great scientific interest. In the High Arctic, the response of terrestrial ecosystems to climate change is expected to be particularly pronounced, because only during a short period of the year, most plants, invertebrates, birds, and mammals are able to reproduce.

Due to the pronounced warming at high latitudes, the duration of snow cover is generally expected to decrease over the course of this century (IPCC, 2001). However, the length of the snow-free period relies on the balance between precipitation amounts and melt rate. If snow-precipitation patterns and amounts change, the spatial distribution and depth of snow cover will change correspondingly. Consequently, the rate of decrease in extent will differ from location to location, and in some parts of the Arctic the extent and duration may even increase (Frei et al., 2003).

A change in general snow-precipitation rates- and distribution patterns naturally requires changes in the atmospheric circulation at synoptic scales, such as the North Atlantic Oscillation (NAO) and/or in the hydrological cycle. From middle to high latitudes in the northern hemisphere, the NAO (Hurrell, 1995) is the most prominent weather pattern and explains the major inter-annual variability of the atmospheric circulation in the North Atlantic region (Bromwich et al., 1999). It is most pronounced during winter and is related to changes in both temperature, storminess, sea-ice distribution, and precipitation patterns (Hurrell et al., 2003; Johannessen et al., 2004).



The connection between NAO and precipitation over the western and southwestern parts of Greenland is thoroughly documented in the literature (e.g. Appenzeller et al., 1998; Bromwich et al., 1999; Hurrell, 1995), whereas for High Arctic Northeast Greenland (where this study has its main focus), information on this topic is limited.

One factor which may significantly impact the hydrological cycle in the Arctic would be reductions in sea-ice coverage, which are predicted to occur during the current century (ACIA, 2004). Expanded ice-free areas in the Nordic Seas would allow greater evaporation from the ocean surface, and result in larger moisture transport onto coastal areas and larger amounts of precipitation.

The direct contribution of observed sea-ice variability to precipitation over Greenland has not yet been subject for investigation. However, previous studies (Weatherly, 2004) based on GCM-runs, using observed sea-ice concentrations, derived from passive-microwave satellite imagery, as surface boundary conditions, reveals that increased precipitation along the Antarctic coastal areas may be associated with reduced ice concentrations. Other studies (Bromwich et al., 1998; Wu et al., 1996) based on present day climatic conditions in GCMs also indicate significant precipitation-increases over coastal Antarctica in the case of reduced sea-ice coverage.

The present study has its main point of interest focused around Zackenberg Research Station (ZRS) at 74.5°N, 20.5°W in High Arctic Northeast Greenland (Fig. 1 (C)). ZRS forms the platform for the Zackenberg Ecological Research Operations (ZERO), and was established in July 1995. ZERO aims to provide knowledge on a pristine High Arctic ecosystem and its response to climatic variations, and thus includes continuous monitoring of bio- as well as climatological parameters. At ZRS snow cover and snow depths (Fig. 1(B)) have been measured continuously since August 1997; and on the basis of high spatial resolution digital imagery (Hinkler et al., 2002) end-of-winter snow accumulation was reconstructed back to 1988 at high accuracy (section 2.2.1).

To put the observed (and the high accuracy modeled) snow data from ZRS into a more generalized climatological framework, this study aims to analyze snow-precipitation variability in High Arctic Northeast Greenland, its relation to the NAO and to variations in sea-ice concentrations in the Greenland Sea, and finally to briefly discuss some possible implications for High Arctic ecosystems in a future warmer climate with higher precipitation- and melt rates.

## 2. Materials and methods

### 2.1 Data

The study includes data at various spatial scales and resolutions, ranging from point measurements of snow depths and daily mean temperatures at ZRS (74.5°N), Daneborg (74.3°N), and the island of Jan Mayen (71.0°N) through ortho-rectified digital camera images of the local snow cover extent in the Zackenberg valley (Hinkler et al., 2002), satellite data with high spatial resolution (Landsat Thematic Mapper (TM) and Système Probatoire pour l'Observation de la Terre High Resolution Visible (SPOT HRV)), sea-ice concentrations from Scanning Multichannel Microwave Radiometer (SMMR) and Special Sensor Microwave/Imager (SSM/I) passive-microwave satellite imagery, precipitation rates and air temperatures from the National Centers for Environmental Prediction (NCEP) reanalysis project to monthly indices of the NAO, and finally, climate change-scenarios of future monthly mean air temperature and precipitation in the East Greenland region. All data are summarized in Table 1.

### 2.2 End-of-winter snow accumulation

#### 2.2.1 Locally at ZRS/Daneborg

Since August 1997, snow depths have been measured automatically every third hour (averaged to daily means in this study), using a sonic snow depth sensor. Additionally (also since 1997), an automated digital camera has been installed at the Zackenberg mountain to take daily pictures of the snow cover in the Zackenberg valley. The images were transformed into digital orthophotos and were then used for snow cover mapping (Hinkler et al., 2002).

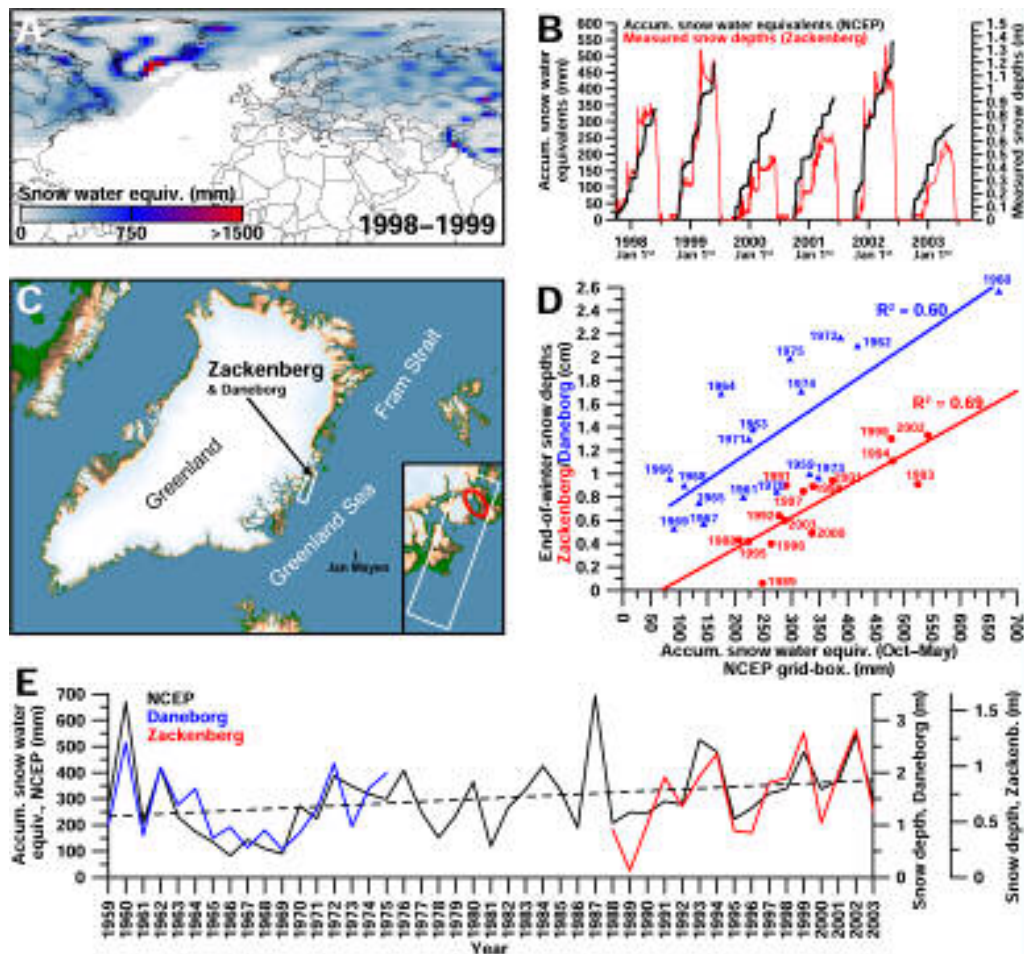
Based on a semi-empirical modeling approach (Hinkler et al., 2003; Paper 3), end-of-winter snow accumulation and summer-snow-cover-depletion in the years 1988–1997 were reconstructed: The model utilized for reconstruction was derived assuming that, for any end-of-winter snow accumulation there exists a unique relation—between the spatial progress of snow cover depletion and melt-energy accumulated over the melting season—which is specific for the study area (it is thus assumed that any particular study area has its own unique physical characteristics). The daily snow cover maps were used to construct snow cover depletion curves for seven different melting seasons (1998–2004). These data were then combined with temperature data and measured snow depths to derive a data set from which

Table 1. Data summary.

Data type	Spatial resolution	Temporal resolution	Temporal coverage (this study)	Source / citation
* Measured snow depths from ZRS and Daneborg	—	Zackenborg: Daily Daneborg: Monthly maxima	Zackenborg: 1998–2003 Daneborg: 1958–1975	ZERO & the Danish Meteorological Institute (DMI) / Cappelen et al., 2001
Measured air temp. from ZRS, Daneborg, and Jan Mayen	—	Daily	ZRS: 1996–2003 Daneborg: 1961–1995 Jan Mayen: 1961–2003	ZERO, Danish Meteorological Institute (DMI), and Norwegian Meteorological Institute (DNMI)
Digital orthophotos of Zackenberg Valley, Northeast Grl.	10 m	Daily	1998–2003	ZERO / Hinkler et al., 2002
High spatial resolution satellite images (Landsat TM & SPOT HRV)	Landsat TM: 30 m SPOT HRV: 20 m	Bi-weekly (only 1–3 images per melting season are suitable for snow mapping)	1988–1997	Landsat TM: Eurimage SPOT HRV: SPOT IMAGE
SMMR & SMM/I sea-ice concentrations	25 km (resampled to 5 km)	Daily	1981–2000	National Snow and Ice Data Center (NSIDC) / Fowler et al., 2000
National Centers for Environmental Prediction (NCEP) re-analysis project: air temp. & precip. rates	1.904°×1.875° lat-long. (grid-cell equivalent to approx. 13,500 km <sup>2</sup> at 74°N)	Daily	1958–2003	Harris, 2004 / NOAA-CIRES Climate Diagnostics Center (CDC)
North Atlantic Oscillation (NAO)	—	Monthly (only December–January–February seasonal means are utilized)	1958–2003	NOAA Climate Prediction Center
Scenarios of 30-year normal monthly mean air temp. and precipitation from a regional climate model over East Grl. & Sea (Ctrl., A2 & B2)	50 km	—	Ctrl.: 1961–1990 A2 & B2: 2071–2100	DMI / Dethloff et al., 2002; Killsholm et al., 2003; Rysgaard et al., 2003

End-of-winter snow depths at ZRS were reconstructed at high accuracy back to 1988 (see also Hinkler et al., 2003).

\*\* Sea-ice concentrations used in this study were downloaded from NSIDC as part of the 5-km Polar Pathfinder EASE-Grid composite data (Foucar et al., 2000).



**Fig. 1.** (A) Total end-of-winter accumulated snow water equivalents (1998–1999, October–May) calculated based on NCEP precipitation rates in  $1.904^{\circ} \times 1.875^{\circ}$  lat.-long. grid-cells over the North Atlantic region. The grid-cell containing Zackenbergl Research Station (ZRS) is marked with white. (B) Daily accumulated NCEP snow water equivalents ([1997-1998]–[2002-2003] winter seasons) together with corresponding snow depths measured at ZRS. (C) Location of the Zackenbergl/Danebergl-area (red ellipse). The rectangular area indicated by white lines corresponds to the NCEP  $1.904^{\circ} \times 1.875^{\circ}$  lat.-long. grid-cell (13,650 km<sup>2</sup>), which includes ZRS and Danebergl. (D) Measured/reconstructed end-of-winter snow depths at Zackenbergl/Danebergl versus the NCEP end-of-winter accumulated snow water equivalents from the grid-cell shown in C. (E) Time series (1959–2003) of NCEP end-of-winter (May 31<sup>st</sup>) accumulated snow water equivalents in the grid-cell containing ZRS together with measured/reconstructed maximum snow depths at Danebergl (1959–1975) and Zackenbergl (1988–2003), respectively. The dashed line indicate the trend in NCEP based snow-precipitation over 1959–2003.

end-of-winter snow accumulation and summer-snow-cover depletion can be found iteratively for any melting season if: 1) the snow cover extent in the study area is known for (at least) one day in the melting season and if 2) daily temperature data are available. Thus, the method is applicable if one satellite- or aerial photo with high spatial resolution and daily temperatures from the

melting season are available (if the end-of-winter snow accumulation is known, only the daily mean air temperatures are required to derive a snow cover depletion curve). Currently, it has been possible to procure usable satellite data (Landsat TM and SPOT HRV) back to 1988, whereas air temperatures from before 1995 (when ZRS was established) are available from the Danish Meteorological Institute's (DMI) automatic weather station at Daneborg 21 km southeast of Zackenberg.

At Daneborg measurements of snow depth were initiated in 1958, but were stopped in 1975 (Cappelen et al., 2001). These data as well as measured/reconstructed end-of-winter snow depths from ZRS are displayed in Fig. 1(E).

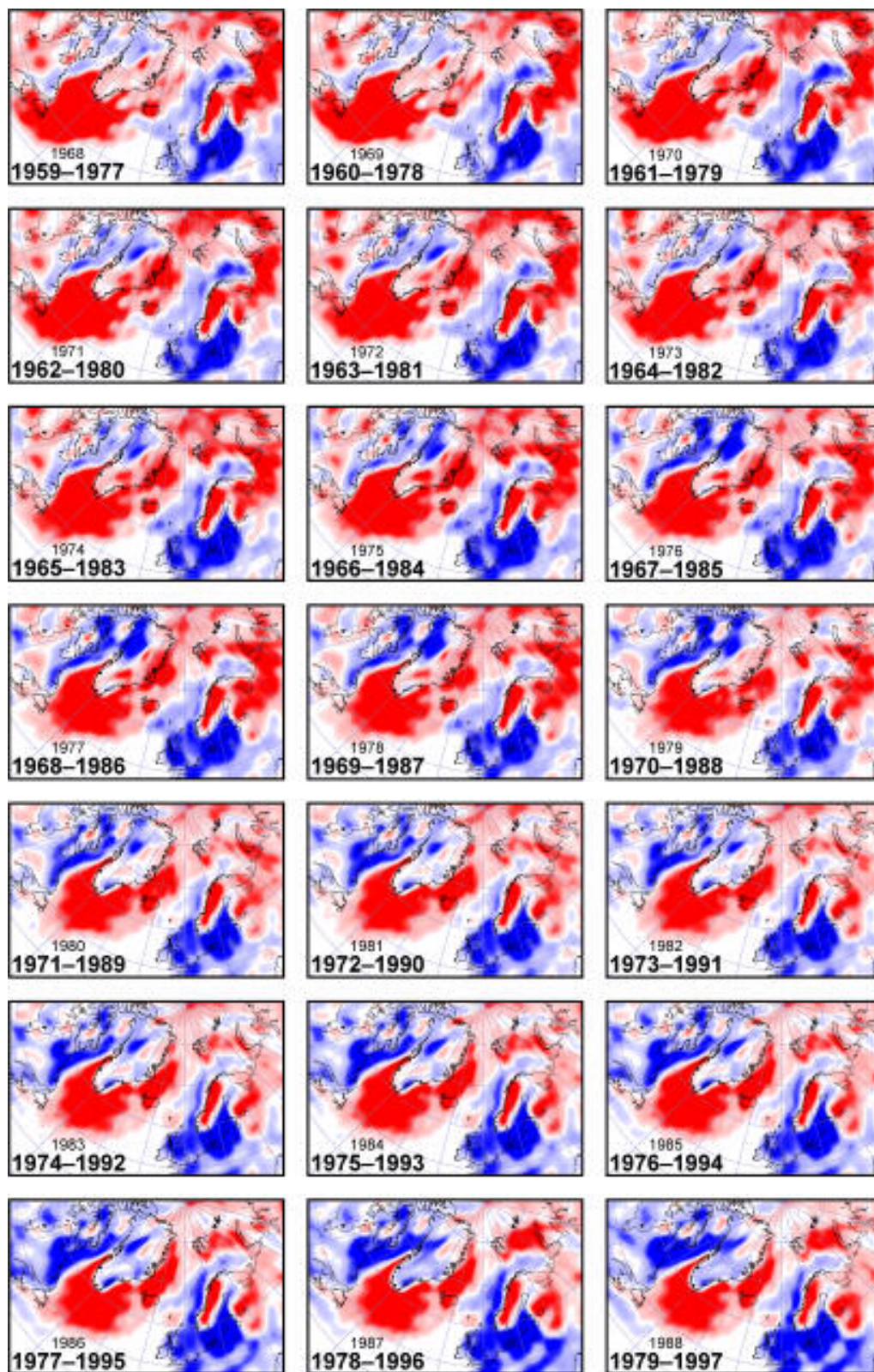
### 2.2.2 Regional to large scale in the North Atlantic region

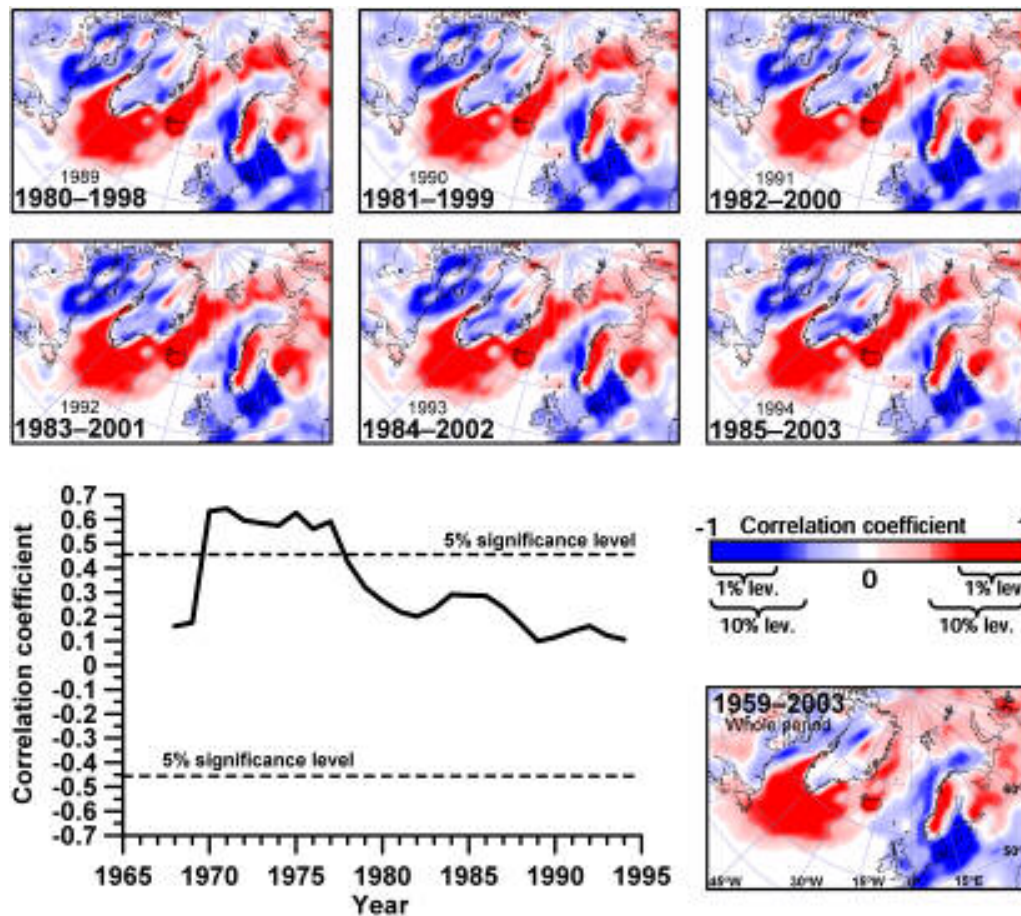
End-of-winter snow accumulation at larger scale was inferred from the NCEP reanalysis data (CDC, 2003) in  $1.904^{\circ} \times 1.875^{\circ}$  lat.-long. grid-cells, covering latitudes:  $0^{\circ}$ – $90^{\circ}$  and longitudes:  $-90^{\circ}$ – $90^{\circ}$  (Fig. 1(A)). The NCEP data utilized are daily precipitation rates and daily mean air temperatures from the period 1958–2003 (Harris, 2004). For each year (October<sub>prev. year</sub>–May<sub>year in quest.</sub>) the total accumulated amount of precipitation falling on days with mean air temperature below freezing represents the end-of-winter snow accumulation in Snow Water Equivalents (SWE). At the highest latitudes, where virtually no snow-melt occurs during winter, the end-of-winter SWE will be proportional to the end-of-winter *snow depth*. End-of-winter SWE during 1959–2003 for the grid-cell containing ZRS/Daneborg is displayed in Fig. 1(E).

## 2.3 NAO vs. snow-precipitation

NAO data were obtained from the NOAA Climate Prediction Center (CPC, 2004). To investigate how inter-annual variations in snow-precipitation and NAO are correlated in the North Atlantic region, spatially as well as over time, the correlation between accumulated snow-precipitation and winter (December-January-February) NAO-index was calculated over the period 1959–2003 (where e.g. 1959 refers to the 1958–1959 winter season). The calculation was done for each NCEP  $1.904^{\circ} \times 1.875^{\circ}$  lat.-long. grid-cell, and the time series were split into 27 sub-periods—or 19-year running windows (1959–1977, 1960–1978, .., 1985–2003). To give a better spatial impression, the results were afterwards interpolated and projected into azimuthal equal-area maps. Resulting correlation maps for each 19-year window are shown in Fig. 2. In order to put ZRS/Northeast Greenland into this framework, the running







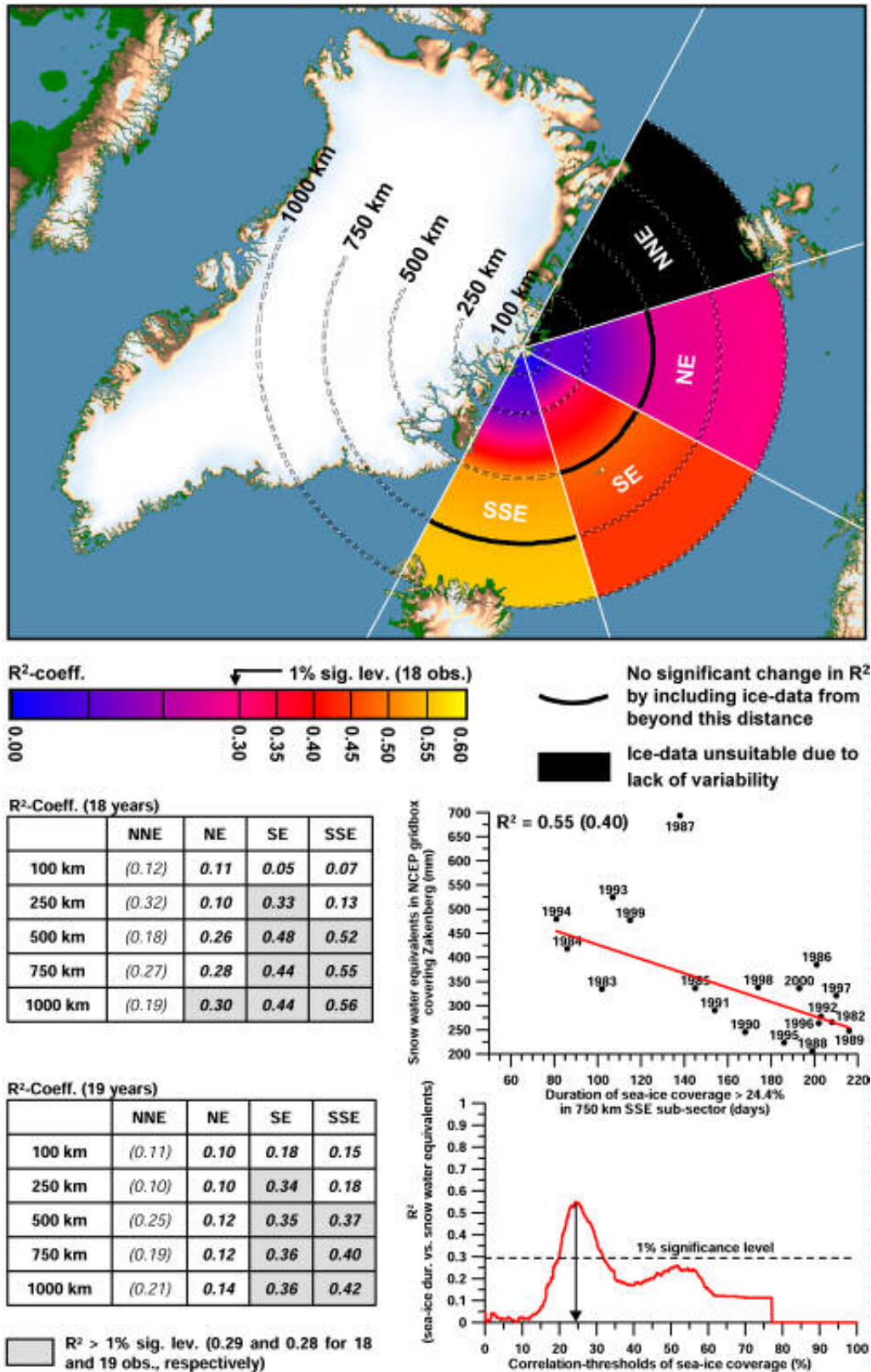
**Fig. 2.** Running correlation (1959–2003) between accumulated snow-precipitation and the North Atlantic Oscillation (NAO), spatially visualized for the North Atlantic region in 19-year windows. Densely shaded areas represent significant correlation between NAO and snow-precipitation. The years given with smaller types on the individual correlation-maps indicate the “center-year” in each 19-year window. The graph in the lower left part of the figure shows the running correlation between NCEP based end-of-winter snow water equivalents in the Zackenberg/Daneborg region and the winter NAO-index. The correlation map right to the graph shows the correlation over all 45 seasons.

correlation values for the grid-cell containing ZRS are plotted in the lower left part of the figure.

#### 2.4 Sea-ice vs. snow-precipitation

Sea-ice mapping is based on a 20-year time series (1981–2000) of gridded sea-ice concentrations (covering 19 winter seasons). Ice concentrations were derived from 25-km resolution SMMR and the SSM/I brightness temperature satellite imagery. The data were provided by the National Snow and Ice Data Center (NSIDC), Boulder, CO, USA, and was (in this study) obtained as part of the 5-km EASE-Grid composite data set (Fowler et al., 2000). In this version, the resulting 5-km data is over-sampled from the 25-km SMMR and SSM/I





**Fig. 3.** Spatial distribution of the correlation between (1) end-of-winter snow accumulation within the Zackenberg region (NCEP 1.904°×1.875° lat.-long. grid-cell covering 13,650 km<sup>2</sup> (see Fig. 1), and (2) sea-ice duration (the number of days during September–August with sea-ice concentration above a critical threshold). The Greenland Sea is divided into four sectors

based on direction from the Zackenberg Research Station (ZRS): NNE, NE, SE, SSE, and each sector is subdivided into five sub-sectors based on distance from ZRS: 0–100 km, 0–250 km, 0–500 km, 0–750 km, and 0–1000 km (note that a smaller sub-sector is always included in a larger sub-sector). The tables to the left display  $R^2$ -coefficients of least squares fits between end-of-winter snow accumulation, 1982–2000 and sea-ice duration within the individual sub-regions. The graphs in the rightmost part of the figure both concern the 750 km SSE sub-sector which is the sub-sector that shows the maximum correlation between sea-ice duration and snow precipitation. The upper graph shows a least squares fit between sea-ice duration and the Zackenberg (NCEP grid-cell) snow accumulation (if 1987 is included  $R^2=0.40$ ). The lower graph demonstrates that 24.4% is the concentration-threshold that gives the best linear correlation for this particular region.

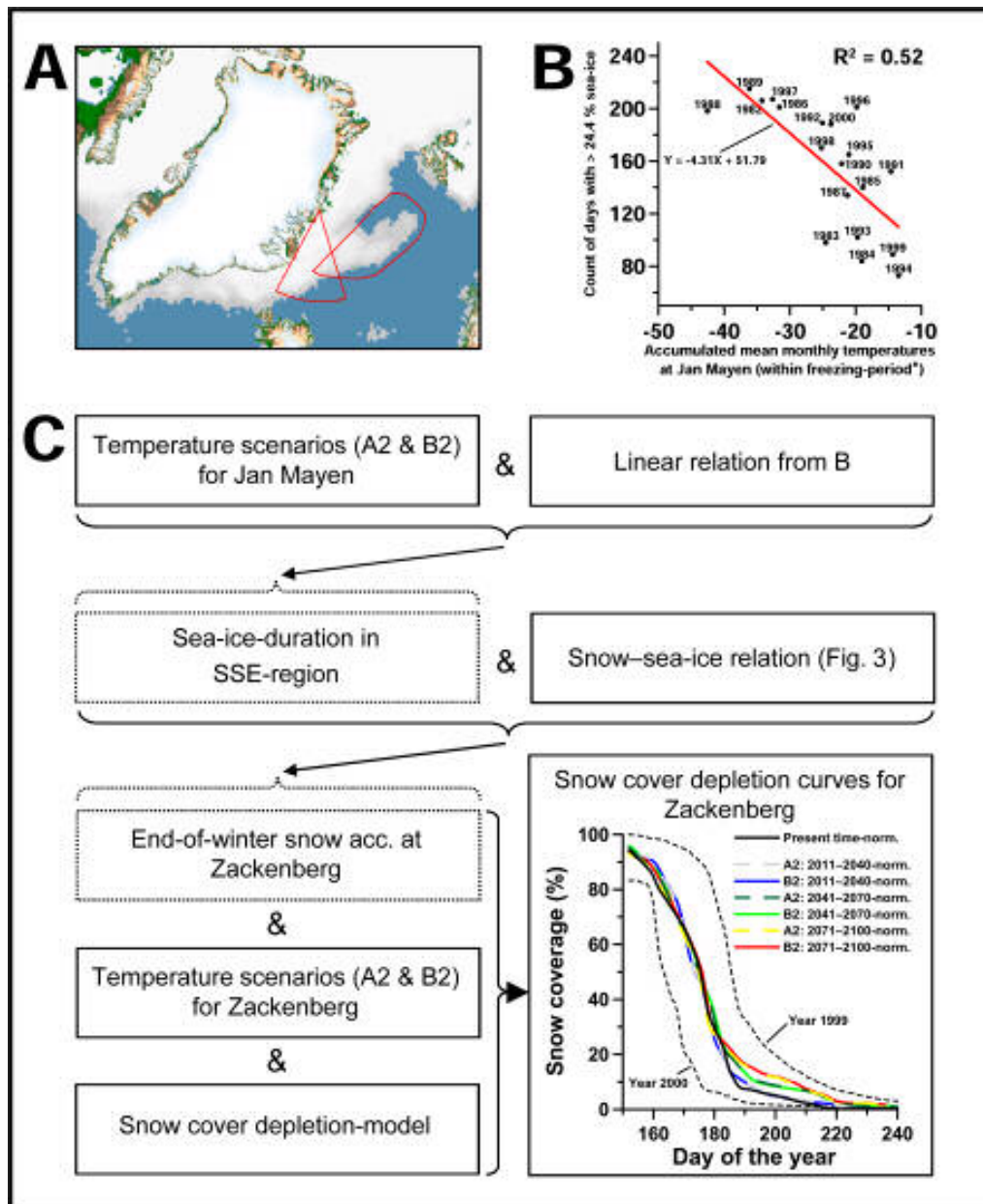
data. Because coastal areas have a jagged appearance, a 5 km land mask is applied, and the nearest appropriate sea-ice concentration is used.

To compare inter-annual variations in sea-ice concentration within the Greenland Sea to the end-of-winter snow accumulation in the Zackenberg region, the Greenland Sea was divided into four main sectors based on direction, and 20 sub-sectors (five in each main sector) based on distance from ZRS, respectively (Fig. 3). The correlation (1982–2000) between yearly sea-ice duration and Zackenberg end-of-winter snow accumulation was then calculated for each sub-sector. Sea-ice duration is defined as the number of days during December<sub>prev. year</sub>–August<sub>year in quest.</sub> with sea-ice percentage above a certain threshold. This threshold is defined as the sea-ice percentage giving the maximum correlation between sea-ice duration and end-of-winter snow accumulation, and was found iteratively by testing thresholds from 0–100% in steps by 0.1 (Fig. 3).

## 2.5 Climate change scenarios vs. sea-ice and snow cover

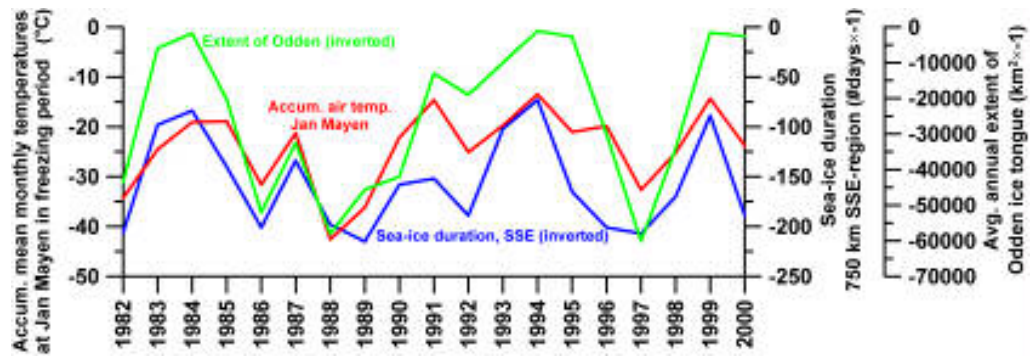
Modeled monthly mean temperatures and precipitation for two normal-periods 1961–1990 (control scenario) and 2071–2100 (A2- and B2-scenarios, according to the IPCC) were provided by the Danish Meteorological Institute (DMI). The model (Dethloff et al., 2002; Kiilsholm et al., 2003; Rysgaard et al., 2003) is a regional climate model covering East Greenland and the Greenland Sea and has a spatial resolution of 50 km.

Typically during winter, the central Greenland Sea develops a local cover of *pancake ice* (World Meteorological Organisation, 1970), which occupies a tongue-shaped region called Odden (Fig. 4(A)). During winter, where northwesterly winds prevail in this region, the pancakes are blown to the southeast (Wadhams, 1999), which makes it reasonable to assume that some inter-annual co-variation may exist between the extent of the Odden ice



**Fig. 4.** (A) Sea-ice distribution around Greenland at February 2<sup>nd</sup>, 1989 with indications (red polygons) of the Odden ice tongue mapping area and the region (750 km SSE), which shows maximum correlation between sea-ice duration and snow-precipitation at Zackenberg. (B) Sea-ice duration in 750 km SSE-region vs. accumulated monthly mean surface air temperatures at the Island of Jan Mayen within the freezing-period. (C) Conceptual description of- and results from the sea-ice based method used to derive future scenarios of summer snow-cover depletion in the Zackenberg area. \* The freezing period is defined as the period, which includes the first- and the last month with average temperature below 0°C, and all months in between.

tongue and the ice-extent in the region to the south of it (SSE-region Figs. 3 and 4(A)). Furthermore, Comiso et al. (2001) showed the extent of the Odden ice tongue to have a strong negative correlation ( $R = -0.74$ ) with monthly



**Fig. 5.** Time series (1982–2000) of: accumulated air temperatures at Jan Mayen within the freezing period\*, sea-ice duration in the 750 km SSE-region (see also Figs. 3 and 4), and average annual extent of the Odden ice tongue. Note that in order to display the co-variation more clearly, sea-ice data are multiplied by -1. \*The freezing period is defined as the period, which includes the first- and the last month with average temperature below 0°C, and all months in between.

surface air temperatures recorded at the Island of Jan Mayen (Fig. 1(C)), which further makes it reasonable to assume that winter air temperatures at Jan Mayen can be used as a proxy for the extents of the Odden ice tongue and similarly for the neighboring SSE-region. Fig. 5 shows the inter-annual variation over 19 winters (where e.g. 1982 represents the 1981–1982 winter season) of winter surface air temperatures at Jan Mayen, annual extent of the Odden ice tongue, and sea-ice duration in the SSE-region. The figure reveals that the three parameters (as expected) vary in a relatively similar manner (the correlation between annual extent of Odden and sea-ice duration in the 750 km SSE region is 0.73 and between the 750 km SSE sea-ice duration and the Jan Mayen air temperatures it is -0.72).

Thus, in the present study, proxy values of future sea-ice duration in the 750 km SSE region (which shows maximum correlation between sea-ice duration and snow-precipitation) is based on future scenarios of air temperatures at Jan Mayen (Fig. 4(B)). Furthermore, based on the assumption that sea-ice duration in the 750 km SSE region reflects end-of-winter snow accumulation in the Zackenberg/Daneborg region, the linear relation shown in Fig. 3, were used to derive future scenarios of the end-of-winter snow accumulation at ZRS.

Both East Greenland and the Island of Jan Mayen are characterized by strongly varying topography. The spatial resolution (50 km) of the topography included in the climate model is not sufficiently detailed to reflect the local topographic variation. Therefore observed temperatures may differ significantly from the control scenario. To adjust the scenarios to the observed temperatures, monthly correction coefficients were derived for



Zackenberg/Daneborg and Jan Mayen. The correction coefficients were calculated as the observed monthly means divided by the corresponding monthly means from the control scenario (using absolute temperatures in K). Since ZRS was not established before 1995, the observed temperatures representing Zackenberg during 1961–1990 are from Daneborg.

The snow cover depletion model for Zackenberg requires daily temperature input (as accumulated degree days). Thus, to derive future scenarios of daily temperatures at ZRS, daily anomalies were calculated by subtracting average observed daily means (1988–2004, Zackenberg/Daneborg) from the mean monthly temperatures (1961–1990-normal, Daneborg). These anomalies were then added to the monthly means from the A2 and B2-scenarios (2071–2100). Mean monthly temperatures for the 2011–2040 and 2041–2070 normal periods were found using simple linear interpolation between the 1961–1990 and 2071–2100 normal periods, and the average daily values for these periods were derived as described for 2071–2100.

Finally, future summer snow-cover depletion at Zackenberg was calculated using the snow-cover-depletion model (discussed in section 2.2.1) in conjunction with daily temperatures inferred from the A2 and B2 scenario data (the resulting snow cover depletion curves are shown in Fig. 4(C)).

### **3. Results and discussion**

#### **3.1 End-of-winter snow accumulation**

Snow-precipitation in the Zackenberg/Daneborg region shows high inter-annual variability. According to NCEP-data (Fig. 1(E)) the end-of-winter SWE has varied as much as from below 100 mm to almost 700 mm (in 1960 and 1987), since 1959; and viewed over the entire period (1959–2003) there has been a significant ( $p < 0.006$ , according to a Mann-Kendall trend test) positive trend in snow-precipitation of approximately 32 mm SWE per decade (Fig. 1(E)).

Generally, the variability in NCEP based SWE corresponds well with ground based snow depth data from ZRS and Daneborg ( $R^2 = 0.69$  and  $0.60$ , respectively, see Fig. 1(D–E)). The amount of scatter, which however is revealed by the least-squares-fits, may be caused by several different factors such as uncertainties in the NCEP analysis/forecast system, snow-drift/melt, complexity in local wind patterns and precipitation distribution (which is likely, because the region is characterized by strong topography), and the fact

that a 13,650 km<sup>2</sup> grid-cell may represent several different climatic conditions (e.g. Daneborg is exposed almost directly to the Greenland Sea, whereas Zackenberg is situated inside the fjord system, which may also explain the difference in the slopes of the linear fits in Fig. 1(D)). Finally, the fixed 0°C-threshold applied in the present study may be too simple for distinguishing between liquid and solid precipitation (e.g. Førland and Hanssen-Bauer, 2003).

Particularly striking for the NCEP based end-of-winter SWE is the exceptionally high values in the years 1960 and 1987. Unfortunately, no comparison to ground truth was possible for 1987, since no ground based measurements are available for that year. However, the 1960-observations from Daneborg (Fig. 1(E)) may suggest that even though this year had some of the highest amounts of snow-precipitation ever recorded, the NCEP-reanalysis might over-estimate precipitation-rates in extreme situations (such as in 1960 and 1987). Furthermore, the fact that the number of ground-stations is limited in the region might also increase uncertainty in the reanalysis data. Finally, concerning NCEP precipitation in general, Reid et al. (2001) showed that (over Europe) NCEP based precipitation is less reliable than e.g. air temperature, when compared to station based data. Annually, the precipitation correlations on a daily basis varied considerably: 0.37–0.68 and 0.30–0.61 for Central and Eastern England and 0.47–0.81 for Italy. For the air temperature the correlation coefficients were within the range: 0.96–0.98.

### 3.2 NAO vs. snow-precipitation

Fig. 2 depicts the results of the running correlation analysis. The correlation maps indicate that in the northern North Atlantic, the correlation between NAO and snow-precipitation varies considerably in time and space. In northwestern Europe and to the south and southwest of Greenland the correlation remains significant at all times during the entire period (1959–2003), but in the northernmost part of the region (the areas within and around the Arctic Ocean, the Greenland, Barents, and Kara Seas) snow-precipitation variability seems to get decoupled from the NAO from time to time. Off the East Greenland coast, snow-precipitation in major parts of the Greenland Sea and over Iceland is steadily correlated to the NAO, whereas the coastal areas, including Zackenberg/Daneborg, are decoupled in about two thirds of the time. This may suggest that, during these periods, snow-precipitation over the coastal areas may be governed by something else or simply occur stochastically. However, nine out of 27 time-windows (“center

years” 1970–1978, see graph specifically for Zackenberg/Daneborg in Fig. 2), shows significant correlation, also in the coastal areas. The reason for this is presently not known, and should be subject for further investigation. Hypothetically it may be addressed to shifts between phases where more or less continental/coastal climatic regimes predominate. These shifts could then be further addressed to multi-decadal oscillations in the large scale atmospheric circulation. Multi-decadal oscillations in climate data, ranging from global temperature to sea-ice distribution and its connection to weather patterns at synoptic scale such as the NAO has been reported by several authors, e.g.: Oscillations in global temperature proxy records over five centuries (Mann et al., 1995), global temperature anomaly data in relation to both the NAO and the El Niño-Southern Oscillation (Mann and Park, 1994), air-sea interactions in the North Pacific (Latif and Barnett, 1994), and sea-ice export through the Fram Strait vs. the NAO (Jung and Hilmer, 2001;Schmith and Hansen, 2003).

### **3.3 Sea-ice vs. snow-precipitation**

The analysis includes sea-ice data covering the period 1982–2000, in which snow-precipitation at Zackenberg/Daneborg was not correlated significantly to the NAO. Over this period of time, a significant correlation between sea-ice duration in certain regions of the Greenland Sea and snow-precipitation in the Zackenberg/Daneborg region was found. In Fig. 3 the  $R^2$ -coefficients are visualized spatially, and also shown in tabular format. Observations from Daneborg, 1960 (which had precipitation similar to 1987) indicate that the NCEP-reanalysis might over-estimate precipitation-rates in extreme situations (see section 3.1). Thus, in the calculation of the correlation coefficients visualized in the map (upper table in Fig. 3) the year 1987 was left out. However, it should be noted that the highest  $R^2$ -coefficients appear in the same sub-sectors, whether the year 1987 is included or not.

All of the regions show an inverse relationship between sea-ice duration and snow accumulation (the more sea-ice the lesser snow accumulation and *vice versa*). The further one goes to the south and southeast the higher the correlation. Most likely this is because precipitation over Northeast Greenland is usually connected with cyclonic activity over the Greenland Sea (Cappelen et al., 2001), and the warmest and most humid air masses are coming from the south. The highest (and clearly significant,  $p < 0.01$ ) correlations are found to the southeast of ZRS, and reach maximum in the SSE region, when ice-data up till a distance of 750 km from ZRS are included. This may indicate a “center of

action” to be centered within this region around 500 km north of Iceland between Greenland and the island of Jan Mayen.

Production and distribution of sea-ice in the Arctic region is generally complex and difficult to understand, because it is linked to several factors such as temperature, freshwater balance (salinity), and atmospheric- and oceanic circulation dynamics. As the latter factor (e.g. sea-ice flow through the Fram Strait) plays a dominating role within the Greenland Sea, this area is in particular complex (Martin and Wadhams, 1999; Wadhams, 1995; Wadhams and Comiso, 1999). Whether variability in sea-ice distribution within the regions of high correlation can be addressed to larger-scale climate dynamics, is still unclear. The NAO do not seem to explain ice cover variations in these regions very well over longer time spans, and neither does modeled sea-ice fluxes into the Greenland Sea through the Fram Strait (Schmith and Hansen, 2003). Therefore, it may be reasonable to suggest that as the sea-ice distribution in the Greenland Sea is influenced by both local ice formation and a large ice-flux from the Arctic Ocean into the East Greenland Current, it cannot be generalized at a larger scale. Contrarily, it might be more reasonable to suggest that sea-ice variability in the southern Greenland Sea may be stronger related to other (more local) factors such as surface air temperatures/variability of the Odden ice tongue (see also section 2.5).

Because the sea-ice duration is correlated to air temperature, the present study does not support a causal relationship between sea-ice duration and snow-precipitation: It may be possible that the air temperature controls both sea-ice duration and precipitation amounts; furthermore, for the North Atlantic as a whole, approximately 60% of all winters can be characterized as either statistically significant positive or negative NAO-winters (Cappelen et al., 2001). This means that in situations where variability in the large-scale atmospheric circulation cannot be explained by the NAO, precipitation (temperature and humidity) might be explained by other large scale atmospheric circulation phenomena.

However; the lack of correlation (in 1982–2000) between NAO and snow-precipitation, the high correlation between sea-ice duration and snow-precipitation within the same period, the fact that the NAO generally plays a dominating role in the North Atlantic region, the fact that more extensive areas of open water during winter is likely to increase atmospheric moisture content, and finally previous studies (e.g. Weatherly, 2004) on sea-ice vs. Antarctic precipitation all together makes it reasonable to assume that sea-ice duration plays a key role for the snow-precipitation budget in East Greenland.

### 3.4 Climate change perspectives

Fig. 4 gives a conceptual description of how findings of the present study were used to derive projections of future end-of-winter snow accumulation and summer snow-cover depletion at Zackenberg (see section 2.5)—the results are stated in Table 2 and in form of snow cover depletion curves in Fig. 4.

Time	End-of-winter snow accumulation A2/B2 cm	Start of snow-melt A2/B2 day of the year	99% snow cover A2/B2 day of the year	10% snow cover A2/B2 day of the year
Present	68	144 (May 24)	175 (Jun 24)	187 (Jul 06)
2011–2040	83/82	141/142 (May 21/22)	174/173 (Jun 23/22)	190/193 (Jul 09/09)
2041–2070	97/96	134/135 (May 14/15)	175/175 (Jun 24/24)	195/194 (Jul 14/13)
2071–2100	106/108	133/133 (May 13/13)	178/175 (Jun 26/25)	205/205 (Jul 24/24)

**Table 2.** Modeled end-of-winter snow accumulations at ZRS and dates which are important and descriptive for snow cover depletion.

Whether it is reasonable to use sea-ice duration in the 750 km SSE region/winter air temperature at Jan Mayen as proxy for future snow precipitation amounts at ZRS is presently still a question with no definitive answer. However, to give some verification, future end-of-winter snow accumulation based on sea-ice duration was compared to winter precipitation data from the modeled A2- and B2 scenarios provided by DMI. Both the sea-ice based approach and the A2- and B2 precipitation-scenarios reveal similar increases in snow-precipitation over the 21<sup>st</sup> century at ZRS. For 2071–2100, the A2- and B2 precipitation-scenarios show an increase of 62% and 51%, respectively (assuming that precipitation falls as snow in months with mean air temperature bellow 0°C). This corresponds to end-of-winter snow accumulations at ZRS of 110 cm (A2) and 103 cm (B2), respectively, as compared to 68 cm at present. Under both A2- and B2 conditions, the sea-ice based approach suggests 106 cm (Table 2). It cannot be excluded, however, that this match in orders of magnitude is coincidental. It is (nevertheless) concluded that the result is so striking that further research should be done; e.g. by testing the direct contribution of sea-ice variability to Arctic precipitation in climate models.

In Fig. 4(C) future summer-snow-cover-depletion curves for the Zackenberg area are shown for both the A2- and B2-scenarios, and represent the average conditions in four different periods: present time, and three modeled future scenarios (2011–2040, 2041–2070, 2071–2100). To give an impression of the current inter-annual snow-cover variability at Zackenberg, Fig. 4(C) also displays observed snow-cover depletion curves for the years 1999 and 2000, respectively. These years are representative for the most extreme snow cover conditions observed in the area, since ZRS was established.



Both scenarios (A2 and B2) show that because of increasing spring temperatures during the 21<sup>st</sup> century, snow-melt is expected to start earlier in the future (Table 2). This combined with slightly higher summer temperatures means that spring snow clearance in large areas with uniform snow distribution will not be delayed on average, despite the predicted increase in winter precipitation. Neither will it occur earlier—meaning that the combination of increased winter-precipitation and increased temperatures will have virtually no net effect on snow cover extent during the early (and for the general flora and fauna most critical) part of the melting season. However, when the later part of the season is considered, the situation is different: due to increased winter (snow)-precipitation, larger snow drifts will be formed in areas characterized by heavy snow deposition (mainly lee sides of larger features in the landscape); and these areas will thus have a prolonged melting season of about 2–3 weeks. Furthermore, with the prospect of increased inter-annual variability in precipitation (Jones et al., 2001) it is likely that the frequency of very late seasons, with reduced or no reproduction in different plants and animals, may also increase.

For Arctic ecosystems, snow cover plays almost as an important role as temperature in shaping life conditions for flora and fauna (Callaghan et al., 2005). This is particularly so for High Arctic Greenland, which has a relatively continental climate due to the dense polar drift ice in the Greenland Sea. The increasing snow-precipitation is likely to alter living conditions in the direction of present-day low Arctic Southeast Greenland (Meltofte et al., 2003; Rysgaard et al., 2003). In some regions this means up to a doubling of snow-precipitation, increased frequency and intensity of thaw events during winter and more humid and cyclonic summer weather too. For flora and fauna, this would mean increased vegetation cover on presently barren lowlands, but also difficulties for herbivores from lemmings to muskoxen due to melting snow and rain in winter resulting in ice crust formation (Forchhammer and Boertmann, 1993; Hansen and Mosbech, 1994). Opposite to the predicted prolongation of the growing season in most of the Arctic (Callaghan et al., 2005), a zero net change in early snow-melt will not alter the onset of e.g. growth and reproduction in plants in these areas (Meltofte, 2002), but the increased water supply from melting snow and summer precipitation is likely to increase plant growth on presently mesic and dry tundra. However, in snow accumulation areas, where snow-melt will be later (Fig. 4(C)) in most years, the reproductive phenology and thereby the success of many species ranging from plants to shorebirds may be delayed or even excluded (Callaghan et al.,

2005; Meltofte, 2002). Furthermore, in these areas the productivity of the vegetation will be reduced, and the plant species composition is likely to change in the direction of snow-bed communities.

#### **4. Conclusions/summary**

Over the last four decades the end-of-winter snow accumulation in the Zackenberg/Daneborg region has varied considerably, from below 100 mm SWE to almost 700 mm, according to NCEP-data. However, ground based measurements of snow depth indicate that the NCEP-reanalysis might overestimate snow-precipitation-rates in extreme situations. The precipitation data, which cover more than 40 years, show a significant trend (32 mm SWE per decade) towards increased snow-precipitation. This might indicate that general increases in winter-precipitation, which is predicted in climate models, over Northeast Greenland might already have started to occur.

The influence from the NAO on snow-precipitation within the Zackenberg/Daneborg region seems to vary over time. In contrast to e.g. Western Europe and certain areas in West Greenland (where snow-precipitation is closely correlated to the NAO), snow-precipitation over the coastal areas of Northeast Greenland seems to be significantly correlated to the NAO in some periods, and in some periods not. During the period covered by the present study (27 running 19-year periods with “center years” 1968–1994), the Zackenberg/Daneborg snow-precipitation was correlated significantly to the NAO in a third of the time (“center-year” periods 1970–1978). In accordance with previous climate-studies, this coupling/decoupling to the NAO is hypothesized to be due to decadal/multi-decadal oscillations in the climate system.

Snow-precipitation at Zackenberg/Daneborg was found to be significantly correlated to sea-ice duration in the southern Greenland Sea (SE and SSE to Zackenberg) during 1982–2000. Although this period of time represents insignificant correlation between snow-precipitation and the NAO, the high correlation between snow-precipitation and sea-ice duration does not in itself support the idea of a causal relationship between sea-ice duration and snow-precipitation. Because sea-ice duration is correlated to surface air temperature in the region it cannot be disregarded as an option that the air temperature (which may be controlled by some other large scale atmospheric circulation phenomena than the NAO) may control both sea-ice duration and precipitation. However, the fact that more extensive areas of open water should naturally be expected to increase atmospheric moisture content, the

results from this study and previous studies on sea-ice variation and its contribution to Antarctic precipitation makes it reasonable to suggest that sea-ice duration may play a key role for the snow-precipitation budget in Northeast Greenland.

In the present study it is thus hypothesized that snow-precipitation at Zackenberg may be linked to sea-ice variations in the southern Greenland Sea. It was concluded that air temperatures at the island of Jan Mayen is a reasonable proxy for sea-ice duration in this region. Therefore, to give some verification of a possible sea-ice–snow-precipitation linkage, projections of the Jan Mayen winter temperatures during the 21<sup>st</sup> century were used to derive scenarios of future sea-ice duration in the southern Greenland Sea/end-of-winter snow accumulation at Zackenberg. Because sea-ice based end-of-winter snow accumulation turned out to correspond strikingly well with snow precipitation amounts calculated in a regional climate model, further research on the topic is strongly recommended. On average, end-of-winter snow accumulations at Zackenberg are projected to increase from 68 cm at present to 106 cm by the end of the current century. When tested in a local snow cover depletion model, the combination of increased temperature/melt rate and increased snow-precipitation seems to leave summer-snow cover depletion close to status quo, however 2–3 weeks delayed in areas with pronounced snow-accumulation. From the ecosystem perspective a zero net change in early snowmelt may hardly affect the onset of e.g. vegetative growth and reproduction. However increased melt-water and summer precipitation might increase plant growth in some areas; and in areas affected by larger snow accumulation the success of many species may be delayed or even excluded. Furthermore, the prospect of increased climatic variability may also increase the frequency of seasons with late snowmelt in the future. Finally, increased snow-precipitation combined with a higher frequency of thaw/freeze events during winter may cause difficulties for mammalian herbivores, due to the formation of ice crusts.

### **Acknowledgements**

We thank Jens Hesselbjerg Christensen and Martin Stendel, Danish meteorological Institute, for providing climate scenario data for the East Greenland region. The Danish Polar Center is thanked for providing access to ecosystem monitoring, data, and logistics at the research station at Zackenberg. We also thank Ulf Pierre Thomas, technician at the Institute of Geography—University of Copenhagen, for indispensable technical support.

We thank Kim Have, Technical University of Denmark, for software development. The Norwegian meteorological Institute is thanked for providing temperature observations from Jan Mayen.

## References

ACIA. Impacts of a Warming Arctic: Arctic Climate Impact Assessments. Hassol, S. J. 1-139. 2004. Canada, Cambridge University Press.

Ref Type: Report

Appenzeller, C, T F Stocker, M Anklin, 1998, North Atlantic oscillation dynamics recorded in Greenland ice cores: *Science*, v. 282, p. 446-449.

Bromwich, D H, B Chen, K M Hines, 1998, Global atmospheric impacts induced by year-round open water adjacent to Antarctica: *Journal of Geophysical Research-Atmospheres*, v. 103, p. 11173-11189.

Bromwich, D H, Q S Chen, Y F Li, R I Cullather, 1999, Precipitation over Greenland and its relation to the North Atlantic Oscillation: *Journal of Geophysical Research-Atmospheres*, v. 104, p. 22103-22115.

Callaghan, T V, L O Björn, Y Chernov, T Christensen, B Huntley, R Ims, D Jolly, N Matveyeva, N Panikov, W Oechel, G Shaver. Tundra and Polar Desert Ecosystems. ACIA Report, Chapter 6. 2005.

Ref Type: Report

Cappelen, J, B V Jørgensen, E V Laursen, L S Stannius, R J Thomsen. The Observed Climate of Greenland, 1958-99 - with Climatological Standard Normals, 1961-1990. 00-18. 2001. Danish Meteorological Institute. Technical Reports.

Ref Type: Report

CDC. The NCEP/NCAR Reanalysis Project.  
<http://www.cdc.noaa.gov/cdc/reanalysis/>. 2003.

Ref Type: Electronic Citation

Comiso, J C, P Wadhams, L T Pedersen, R A Gersten, 2001, Seasonal and interannual variability of the Odden ice tongue and a study of environmental effects: *Journal of Geophysical Research-Oceans*, v. 106, p. 9093-9116.

CPC. North Atlantic Oscillation (NAO).

<http://www.cpc.ncep.noaa.gov/products/precip/CWlink/pna/nao.shtml>.  
2004.

Ref Type: Electronic Citation

Dethloff, K, M Schwager, J H Christensen, S Kilsholm, A Rinke, W Dorn, F Jung-Rothenhausler, H Fischer, S Kipfstuhl, H Miller, 2002, Recent

Greenland accumulation estimated from regional climate model simulations and ice core analysis: *Journal of Climate*, v. 15, p. 2821-2832.

Forchhammer, M, D Boertmann, 1993, The Muskoxen *Ovibos Moschatus* in North and Northeast Greenland - Population Trends and the Influence of Abiotic Parameters on Population-Dynamics: *Ecography*, v. 16, p. 299-308.

Førland, E J, I Hanssen-Bauer. Climate variations and implications for precipitation types in the Norwegian Arctic. 24/02. 2003. Norwegian Meteorological Institute. KLIMA.

Ref Type: Report

Fowler, C, J Maslanik, T Haran, T Scambos, J Key, W Emery. AVHRR Polar Pathfinder twice-daily 5 km EASE-Grid composites. 2000. Boulder, CO, USA, National Snow and Ice Data Center.

Ref Type: Data File

Frei, A, J A Miller, D A Robinson, 2003, Improved simulations of snow extent in the second phase of the Atmospheric Model Intercomparison Project (AMIP-2): *Journal of Geophysical Research-Atmospheres*, v. 108.

Groisman, P Y, T R Karl, R W Knight, 1994, Observed Impact of Snow Cover on the Heat-Balance and the Rise of Continental Spring Temperatures: *Science*, v. 263, p. 198-200.

Hansen, B U, A Mosbech, 1994, Use of Noaa-Avhrr Data to Monitor Snow Cover and Spring Melt-off in the Wildlife Habitats in Jameson-Land, East Greenland: *Polar Research*, v. 13, p. 125-137.

Harding, R J, R C Johnson, H Soegaard, 1995, The Energy-Balance of Snow and Partially Snow Covered Areas in Western Greenland: *International Journal of Climatology*, v. 15, p. 1043-1058.

Harris, I. NCEP/NCAR Reanalysis.

<http://www.cru.uea.ac.uk/cru/data/ncep/index.htm> . 2004.

Ref Type: Electronic Citation

Hinkler, J, B U Hansen, M Tamstorf. Sea-ice and snow accumulation modelling in High Arctic Greenland. Elberling, B., Hasholt, B., and Hansen, B. U. 59-66. 2003. Holte, Denmark, Holte Bogtrykkeri A/S. 25-8-2003.

Ref Type: Conference Proceeding

Hinkler, J, S B Pedersen, M Rasch, B U Hansen, 2002, Automatic snow cover monitoring at high temporal and spatial resolution, using images taken by a standard digital camera: *International Journal of Remote Sensing*, v. 23, p. 4669-4682.

Hurrell, J W, 1995, Decadal Trends in the North-Atlantic Oscillation - Regional Temperatures and Precipitation: *Science*, v. 269, p. 676-679.



Hurrell, JW, Y Kushnir, G Ottersen, M Visbeck, 2003, An Overview of the North Atlantic Oscillation, in JW Hurrell, Y Kushnir, G Ottersen, and M Visbeck (eds), *The North Atlantic Oscillation. Climatic Significance and Environmental impact*: Washington, DC, American Geophysical Union, p. 1-35.

IPCC. *Climate Change 2001: The Scientific Basis. Contribution of Working Group I to the Third Assessment Report of the Intergovernmental Panel on Climate Change*. Houghton, J. T., Ding, Y., Griggs, D. J., Noguer, M., van der Linden, P. J., Dai, X., Maskell, K., and Johnson, C. A. 1-881. 2001. Cambridge, United Kingdom and New York, NY, USA, Cambridge University Press.

Ref Type: Report

Johannessen, OM, L Bengtsson, M W Miles, S I Kuzmina, V A Semenov, G V Alekseev, A P Nagurnyi, V F Zakharov, L P Bobylev, L H Pettersson, K Hasselmann, H P Cattle, 2004, Arctic climate change: observed and modeled temperature and sea-ice variability: *Tellus A*, v. 56, p. 559-560.

Jones, HG, J G Pomeroy, D A Walker, D M Holland, 2001, *Snow Ecology: An Interdisciplinary Examination of Snow-covered Ecosystems*, Cambridge University Press.

Jung, T, M Hilmer, 2001, The link between the North Atlantic oscillation and Arctic Sea ice export through Fram Strait: *Journal of Climate*, v. 14, p. 3932-3943.

Kiilsholm, S, J H Christensen, K Dethloff, A Rinke, 2003, Net accumulation of the Greenland ice sheet: High resolution modeling of climate changes: *Geophysical Research Letters*, v. 30.

Latif, M, T P Barnett, 1994, Causes of Decadal Climate Variability Over the North Pacific and North-America: *Science*, v. 266, p. 634-637.

Mann, ME, J Park, 1994, Global-Scale Modes of Surface-Temperature Variability on Interannual to Century Timescales: *Journal of Geophysical Research-Atmospheres*, v. 99, p. 25819-25833.

Mann, ME, J Park, R S Bradley, 1995, Global Interdecadal and Century-Scale Climate Oscillations During the Past 5 Centuries: *Nature*, v. 378, p. 266-270.

Martin, T, P Wadhams, 1999, Sea-ice flux in the East Greenland Current: *Deep-Sea Research Part II-Topical Studies in Oceanography*, v. 46, p. 1063-1082.

Meltofte, H. Sne, is og 35 graders kulde. Hvad er effekterne af klimaændringer i Nordøstgrønland? Meltofte, H. 41, 5-88. 2002. Denmark, Ministry of the Environment, National Environmental Research Institute. TEMA-rapporter fra DMU.

Ref Type: Report

Meltofte,H, S Rysgaard, S A Pedersen, 2003, Climate change in Greenland, Denmark's third national communication on climate change. Under the United Nations Framework Convention on climate change: Danish ministry of the Environment, p. 118-123.

NSIDC. Northern Hemisphere Snow Extent: What sensors on satellites are telling us about snow cover. The National Snow and Ice Data Center (NSIDC), University of Colorado Boulder . 2005.

Ref Type: Electronic Citation

Phoenix,GK, J A Lee, 2004, Predicting impacts of Arctic climate change: Past lessons and future challenges: Ecological Research, v. 19, p. 65-74.

Reid,PA, P D Jones, O Brown, C M Goodess, T D Davies, 2001, Assessments of the reliability of NCEP circulation data and relationships with surface climate by direct comparisons with station based data: Climate Research, v. 17, p. 247-261.

Rysgaard,S, T Vang, M Stjernholm, B Rasmussen, A Windelin, S Kiilsholm, 2003, Physical conditions, carbon transport, and climate change impacts in a northeast Greenland fjord: Arctic Antarctic and Alpine Research, v. 35, p. 301-312.

Schmith,T, C Hansen, 2003, Fram Strait ice export during the nineteenth and twentieth centuries reconstructed from a multiyear sea ice index from southwestern Greenland: Journal of Climate, v. 16, p. 2782-2791.

Stainforth,DA, T Aina, C Christensen, M Collins, N Faull, D J Frame, J A Kettleborough, S Knight, A Martin, J M Murphy, C Piani, D Sexton, L A Smith, R A Spicer, A J Thorpe, M R Allen, 2005, Uncertainty in predictions of the climate response to rising levels of greenhouse gases: Nature, v. 433, p. 403-406.

Stone,RS, E G Dutton, J M Harris, D Longenecker, 2002, Earlier spring snowmelt in northern Alaska as an indicator of climate change: Journal of Geophysical Research-Atmospheres, v. 107.

Wadhams,P, 1995, Arctic Sea-Ice Extent and Thickness: Philosophical Transactions of the Royal Society of London Series A-Mathematical Physical and Engineering Sciences, v. 352, p. 301-319.

Wadhams,P, 1999, The Odden ice tongue and Greenland Sea convection: Weather, v. 54, p. 91-97.

Wadhams,P, J C Comiso, 1999, Two modes of appearance of the Odden ice tongue in the Greenland Sea: Geophysical Research Letters, v. 26, p. 2497-2500.

Weatherly, JW, 2004, Sensitivity of Antarctic precipitation to sea ice concentrations in a general circulation model: *Journal of Climate*, v. 17, p. 3214-3223.

Weller, G, 1998, Regional impacts of climate change in the Arctic and Antarctic: *Annals of Glaciology*, Vol 27, 1998, v. 27, p. 543-552.

World Meteorological Organisation. WMO sea-ice nomenclature, terminology, codes and illustrated glossary. [259]. 1970. Geneva, World Meteorological Organisation. WMO/OMM/BMO.  
Ref Type: Serial (Book, Monograph)

Wu, XG, I Simmonds, W F Budd, 1996, Southern hemisphere climate system recovery from 'instantaneous' sea-ice removal: *Quarterly Journal of the Royal Meteorological Society*, v. 122, p. 1501-1520.



The research presented in this dissertation was carried out within the framework of the Copenhagen Global Change Initiative (COGCI), which is a co-operation among the Faculty of Science at the University of Copenhagen and a number of Danish governmental research institutions: Danish Meteorological Institute (DMI), Geological Survey of Denmark and Greenland (GEUS), and National Environmental Research Institute (NERI). The organizations involved in this work are the Institute of Geography at the University of Copenhagen and NERI, Department of Arctic Environment. The main part of the research is based on fieldwork carried out at Zackenberg in High Arctic Northeast Greenland, and is therefore a contribution to the Zackenberg Ecological Research Operations (ZERO). Further information on ZERO is available from [www.zackenberg.dk](http://www.zackenberg.dk). Additional fieldwork was done in collaboration with the Norwegian Polar Institute (NPI) at Ny-Ålesund, Svalbard, and was funded by the European Commission IHP-programme.